THE MORPHOLOGY OF THE OUTFLOW APPARATUS OF THE EYE WITH PARTICULAR REFERENCE TO ITS STRUCTURAL APPEARANCE AT VARIOUS LEVELS OF INTRAOCULAR PRESSURE.

A TWO PART THESIS PRESENTED TO THE FACULTY OF MEDICINE, UNIVERSITY OF GLASGOW FOR THE DEGREE OF DOCTOR OF PHILOSOPHY.

I. GRIERSON, B.Sc.
Tennent Institute of Ophthalmology
University of Glasgow and Western Infirmary
38 Church Street
GLASGOW G11 6NT

OCTOBER, 1976

THE MORPHOLOGY OF THE OUTFLOW APPARATUS OF THE EYE WITH PARTICULAR REFERENCE TO ITS STRUCTURAL APPEARANCE AT VARIOUS LEVELS OF INTRAOCULAR PRESSURE.

VOLUME I

CONTENTS OF VOLUME I AND II

VOLUME I

VOLUME II

ILLUSTRATIONS IN VOLUME I AND II

VOLUME I

CHAPTER I

CHAPTER 2

CHAPTER 3

CHAPTER 4

ACKNOWLEDGEMENTS

This work was supported by the Scottish Hospital Endowment Research Trust (Grant number 395) and the help is gratefully acknowledged.

The normal human ocular tissue was provided under the auspices of Dr. W. R. Lee from the West of Scotland Routine Ophthalmic Pathology Service. Normal baboon eyes came from a) control animals of investigations conducted at the Wellcome Surgical Research Institute, Glasgow and b) vitamin B_{12} deficient animals from the Wellcome Laboratories, Carshalton. Some of the normal rabbit eyes were provided by Mr. N. F. Johnson. The remaining rabbits and all the rhesus monkeys were provided through the grant allocated by the Scottish Hospital Endowment Research Trust. The benevolence of the various authorities, institutes and individuals is acknowledged.

Facilities for the experimental work were generously provided by Dr. Murray Harper of the Wellcome Surgical Research Institute. I wish to thank Professor W. S. Foulds who made the facilities of the Tennent Institute for Ophthalmology available for the period of this investigation In the main the technical work was done by myself but I am grateful to the staff of the Pathology Laboratory who prepared buffer solutions and araldite mixtures on my behalf. I am particularly indebted to my advisor and co-worker Dr. W. R. Lee for his advice, encouragement and help.

I would also like to thank Professor R. J. Scothorne and Dr. K. Carr of the Anatomy Department, Glasgow University for the use of the scanning electron microscope. The transmission electron microscope were provided by Professor J. J. Pateman of the Genetics Department, Glasgow University and Dr. J. Paul of the Royal Beatson Memorial Hospital.

The experiments conducted on rhesus monkeys at the Wellcome Surgical Research Institute were performed in conjunction with Dr. W. R. Le In addition, tissue preparation and screening with the scanning electron microscope was a joint venture. All light microscope and transmission

electron microscope investigations were conducted solely by the author. For quantitative analyses I am again grateful to Dr. W. R. Lee who acted as a second observer where this was necessary.

The script was typed by Mrs. J. Meadows and the captions to the figures by Mrs. C. E. Grierson. The Medical Illustration Department of the Western Infirmary is thanked for preparing the diagrams.

Work from the present thesis has been published in various academic journals and the relevant publications are listed below.

Grierson, I. and Lee, W.R. (1974)

Changes in the monkey outflow apparatus at graded levels of intraocular pressure: a qualitative analysis by light microscopy and scanning electron microscopy.

Exp. Eye Res. 19, 21.

Grierson, I. and Lee, W.R. (1974)

Junctions between the cells of the trabecular meshwork.

V. Graefes Arch. klin. exp. Ophth. 192, 89.

Lee, W.R. and Grierson, I. (1974)

Relationships between intraocular pressure and the morphology of the outflow apparatus

Trans. Ophth. Soc. U.K. 94, 430.

Grierson, I. and Lee, W.R. (1975)

The fine structure of the trabecular meshwork at graded levels of intraocular pressure. (1) Pressure effects within the near-physiological range (8 - 30 mm Hg)

Exp. Eye Res. 20, 505.

Grierson, I. and Lee, W.R. (1975)

The fine structure of the trabecular meshwork at graded levels of intraocular pressure. (2) Pressures outside the physiological range (0 and 50 mm Hg)

Exp. Eye Res. 20, 523 .

Grierson, I. and Lee, W.R. (1975)

Acid mucopolysaccharides in the outflow apparatus

Exp. Eye Res. 21, 417 .

Grierson, I. and Lee, W.R. (1975)

Pressure induced changes in the ultrastructure of the endothelium lining Schlemm's canal

Amer. J. Ophth. 80, 863 .

Lee, W.R. and Grierson, I. (1975)

Pressure effects on the endothelium of the trabecular wall of Schlemm's canal. A study by scanning electron microscopy

V. Graefes Arch. klin exp. Ophth. 196, 255 .

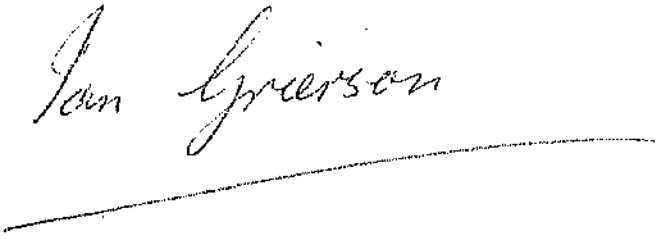

ABBREVIATIONS

In this thesis, all the thick sections were stained with toluidene blue, the majority of the thin sections were double stained with uranyl acetate and lead citrate while most of the tissue blocks for scanning electron microscopy were freeze dried (see Chapter 3). To avoid excessive repitition, only the details of special preparitory techniques or staining systems were outlined in the legends to the appropriate micrographs.

Light micrograph, transmission electron micrograph and scanning electron micrograph were abbreviated to L.M., T.E.M. and S.E.M. respectively.

SUMMARY

The morphology of the outflow apparatus, the tissues through which the bulk of the circulating aqueous humour within the eye must pass to reach the venous system, has been studied by light microscopy, transmission electron microscopy and scanning electron microscopy. The two part investigation describes the appearance of a) the normal outflow apparatus in four species (human, baboon, rhesus monkey and rabbit) and b) the rhesus monkey outflow apparatus at various maintained levels of intraocular pressure (0, 8, 15, 22, 30 and 50 mm Hg).

Cellular adhesion in the delicate meshwork tissues was enhanced by the presence of small punctate intercellular junctions one of which, a macular gap junction, has not previously been described at this site. The presence and significance of mucopolysaccharides in the drainage system has been the subject of much debate. In the present study, complex polysaccharides were consistently demonstrated in all four species. It was speculated that a prominent hydrophilic network of mucopolysaccharides, particularly in the endothelial meshwork, may have a significant influence on the rate of fluid passage through the outflow apparatus.

On anatomical grounds, the intercellular clefts of the endothelium lining the trabecular aspect of Schlemm's canal were considered to be leaky. Intercellular passage of fluid was not thought to make a significant contribution to bulk outflow. A system of large vacuolar and non-vacuolar transcellular channels were thought to be a more effective route for aqueous drainage into Schlemm's canal.

To investigate the morphology of the rhesus monkey outflow apparatus at various pressure levels, the appropriate pressures were

maintained for one hour and, thereafter, the tissue fixed at approximately the same pressure level.

At 0 mm Hg the outer meshwork was compressed and the canal endothelium contained neither vacuoles nor transcellular channels. The meshwork and the overlying canal endothelial monolayer was an effective barrier to the passage of red cells into the anterior chamber.

With progressive pressure elevation, the meshwork became more and more distended to the highest pressure in the series (50 mm Hg). That tissue disruption was found only at 50 mm Hg emphasised the effectiveness of the junctional adhesive mechanisms in binding the pliable meshwork cells together.

Associated with the progressive meshwork distension was an increase in the incidence of giant vacuoles, vacuolar transcellular channels and non-vacuolar transcellular channels up to 30 mm Hg. Within the range 8 to 30 mm Hg the relationship between vacuole numbers and intraocular pressure was linear whereas, as a result of dimensional changes to the vacuoles, the relationship between vacuolar carrying capacity and intraocular pressure was non-linear. The findings indicated that bulk outflow was accomplished by a system of temporary pressure dependent intracellular flow pathways.

At 50 mm Hg aqueous outflow was non-physiological since canal occlusion vacuole drainage and endothelial disruption was extensive.

The significance of meshwork pliability and variable porosity in the canal endothelium to ocular homeostasis, tissue function and disease processes was discussed.

CHAPTER I

GENERAL INTRODUCTION

I.1 The present investigation

The angular structures which comprise the outflow system of the vertebrate eye serve to return the bulk of the intraocular fluid, aqueous humour, to the venous system. The outflow tissues consist of the trabecular meshwork, Schlemm's canal (or its counterparts in non-primates) and a series of collector channels and aqueous veins. In the present morphological investigation the facilities afforded by light microscopy, transmission electron microscopy and scanning electron microscopy were utilised to examine a) the normal outflow apparatus in four species (human, baboon, rhesus monkey and rabbit) and b) the rhesus monkey outflow apparatus after experimental alterations to intraocular pressure.

Before outlining the aims of this research it is first of all necessary to describe the structure and function of the outflow apparatus and to review the pertinent literature which prompted the present investigation.

I.2 The intraocular circulation

I.2.1 Aqueous humour

Aqueous humour is a continuously circulating fluid contained mainly within the anterior and posterior chambers of the vertebrate eye (Fig. I.1) and is of primary importance in the maintenance of ocular tension. The volume of aqueous humour in the eye, and therefore intraocular pressure, depends on the rate of aqueous production (of which there are pressure dependent and pressure independent components) and its outflow rate from the eye (of which there are pressure dependent and virtually pressure independent pathways).

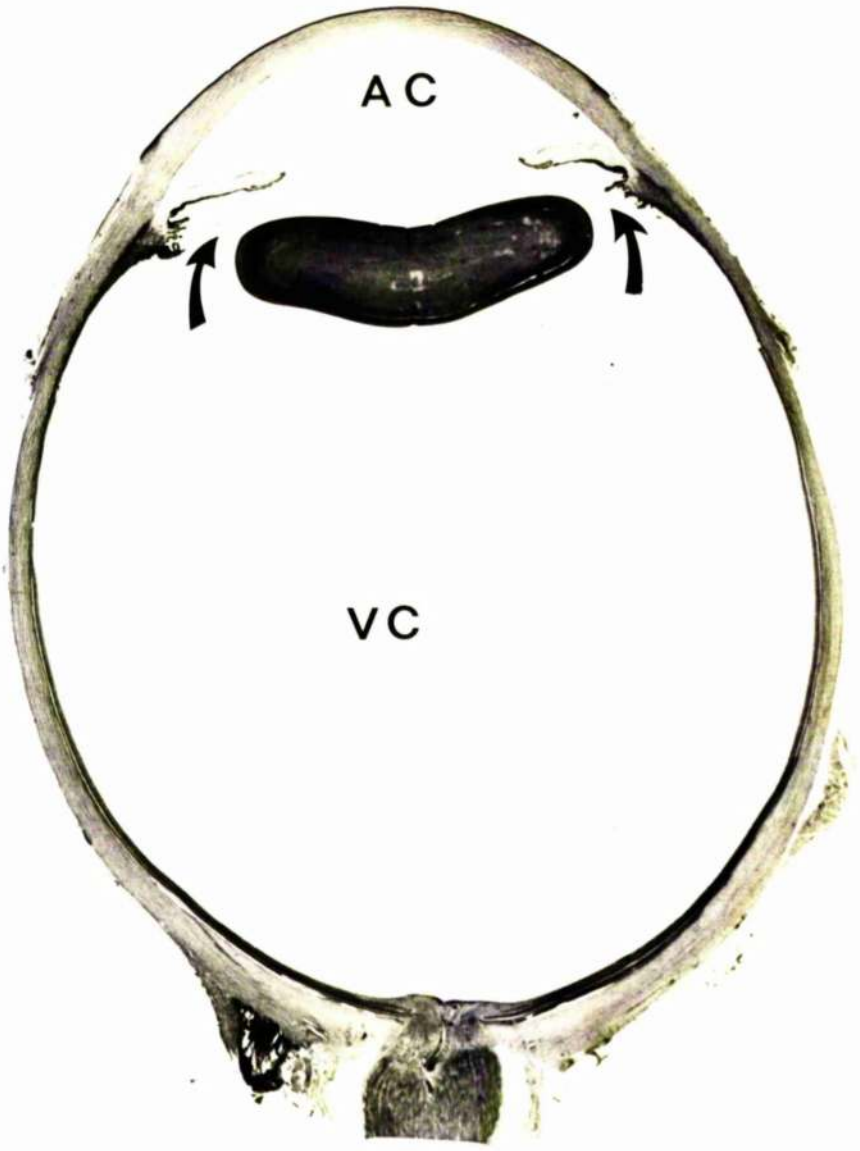

Fig.I.I Histological section through the baboon eye. The anterior chamber (AC), posterior chamber (arrows) and vitreous cavity (VC) are indicated. The lens (L) has become distorted during processing. The tissue was embedded in "paramat" wax and the section stained with haematoxylin and eosin. (x5).

I.2.2 The production of aqueous humour

The fluid is produced by the ciliary processes partly as a secretion (pressure independent) and partly as an ultrafiltrate (pressure dependent) in the eyes of primates and other vertebrates (see Cole, 1966 and 1974 for a current review of the literature) into the posterior chamber of the eye. The relative contributions made by the two components to the production of aqueous humour is still obscure. Cole (1966) considered that ultrafiltration contributed about 30% to aqueous inflow whereas Green and Pedersen (1973) thought that it made a major contribution (60-70%). On the other hand Bill (1973) found little evidence for a positive contribution from ultrafiltration to aqueous production, rather, it was suggested that it tended to cause reabsorption of fluid which had already been secreted.

However, no matter how the system operates, since ultrafiltration is pressure dependent an increase in pressure within the eye will produce a reduction of the net inflow (see Bárány, 1963; Kupfer, 1973; Masuda, 1974).

I.2.3 The outflow of aqueous humour

From the posterior chamber aqueous humour passes between the lens and the posterior surface (pigmented epithelium) of the iris, through the pupil and into the anterior chamber (Figs I.2 and I.3). The bulk outflow of aqueous from the anterior chamber is by way of modified structures, situated on the limbal side of the anterior chamber angle, which comprise the primary or conventional drainage system. Aqueous humour which exits from the eye via the conventional system first enters the trabecular meshwork. The meshwork consists of a series of

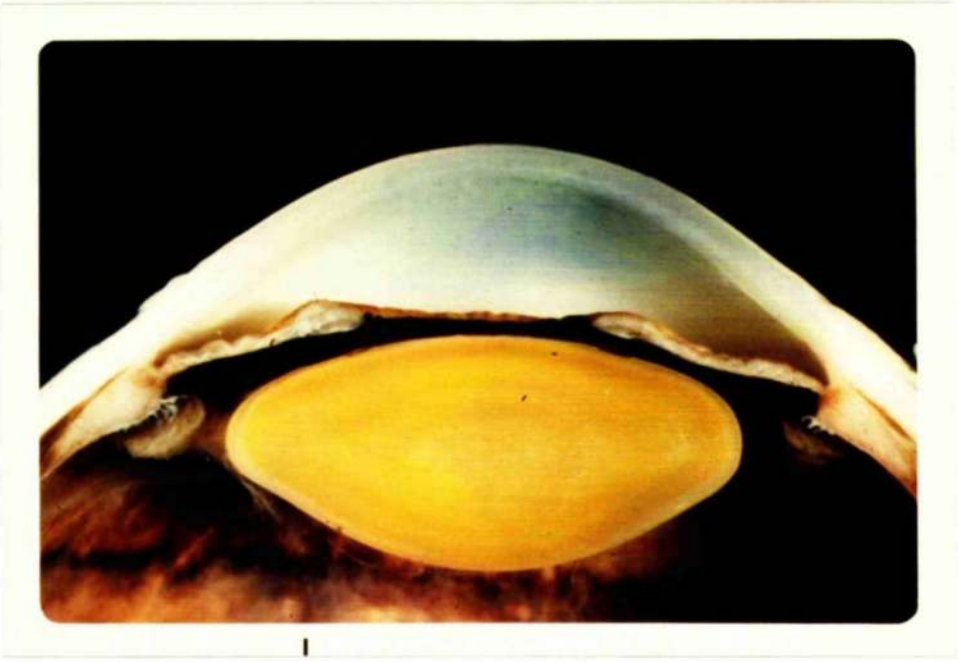

Fig.I.2 A photomicrograph of the anterior segment of the human eye. (x9)

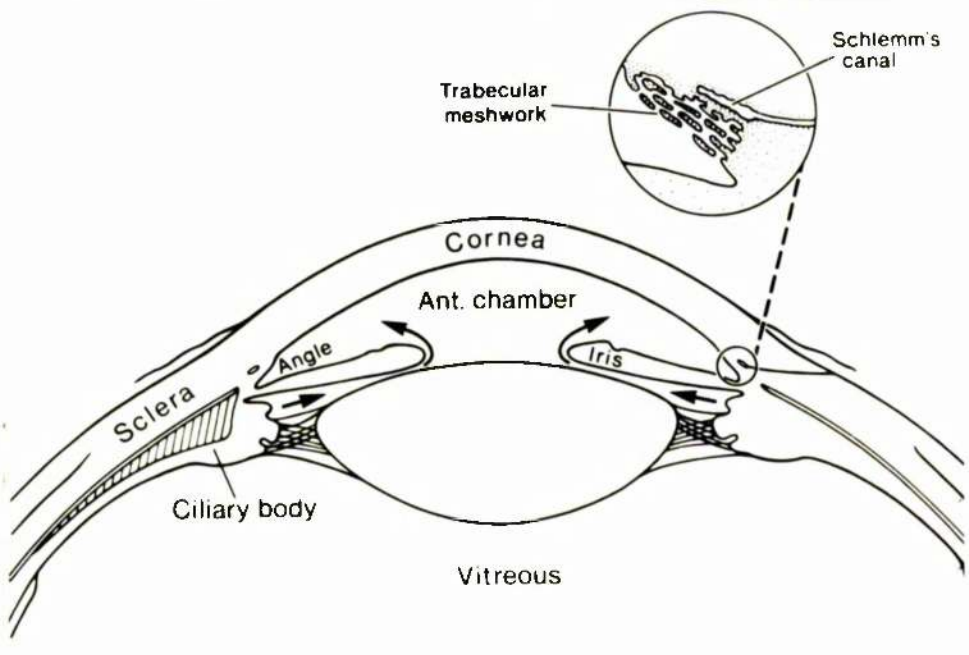

Fig.I.3 A diagram of a similar region to that shown in Fig.I.2. The arrows indicate the direction of movement of aqueous from the posterior to the anterior chamber.

endothelial covered collagenous cords and perforated sheets (trabeculae). The innermost trabeculae border the chamber angle and aqueous follows a tortuous path through and between the trabecular structures to the endothelium lining a single circular drainage vessel in primates (Schlemm's canal) or a series of drainage vessels in non-primates (referred to by a variety of names in the literature but called the angular aqueous plexi by Tripathi, 1971b). From Schlemm's canal and the aqueous plexi lead a series of collector channels, which serve either as a direct pathway (called aqueous veins by Ascher, 1942) or an indirect pathway via the deep scleral and intrascleral plexi, for the passage of aqueous into the episcleral venous system. The complex ramifications and interconnections of the various aqueous collector vessels have been demonstrated in the primate eye by the injection of neoprene (Ashton, 1951; 1952) and silicone rubber (Jocson and Grant, 1965) into the limbal vessels and the investigation of the subsequent casts. Ruskell (1961) conducted a similar investigation on neoprene casts of the system of collector vessels leading from the aqueous plexi in the rabbit eye.

The conventional drainage pathways not only function as the major exit route for aqueous humour from the vertebrate eye but also operate in a pressure sensitive manner (see Cole, 1974 for a review of the literature). As such, the rate of aqueous outflow is a function of the small but significant pressure drop from the anterior chamber angle to the episcleral vessels and the resistance offered by the structures in the drainage route. Measurements of the pressure difference between the anterior chamber angle and the superficial vessels have mainly been made in human eyes. Linnér (1955) and Grant (1958) considered that the pressure drop was about 5 mm Hg whereas Podos, Minas and Macri (1968) calculated episcleral venous pressure to be 9.0 ± 1.4 mm Hg in a series

of eyes with an average intraocular pressure of 15.9 mm Hg.

It is thought that much of the resistance to aqueous flow in the primate is located between the anterior chamber angle and Schlemm's canal because experimental removal of trabecular tissue has shown that between 60 and 80% of the total resistance can be accounted for by the trabecular meshwork plus the endothelium on the canal's trabecular aspect (Grant, 1958; 1963; Pedersen, Jocson and Sears, 1971)*. Within the meshwork the pathways for aqueous passage are particularly narrow and tortuous through the tissue immediately adjacent to the endothelium lining Schlemm's canal (the region was called the endothelial meshwork by Speakman, 1960 and Ashton, 1960). Thus the endothelial meshwork and the overlying canalicular endothelium, which together comprise the trabecular wall of the canal, have been considered to make the major contribution to trabecular resistance (Rohen, 1960; Tripathi, 1968; 1969a; 1969b; 1971a; 1974; Inomata, Bill and Smelser, 1972a; Bill and Svedbergh, 1972). Smelser (1967) summed up the concensus of scientific opinion in the statement "There is good evidence that, of the trabecular meshwork complex, that portion adjacent to the canal is the only part which offers appreciable resistance to aqueous outflow. It is this area also which is suspect in glaucoma".

---

*FOOTNOTE:- On the other hand Edwards, Hallman and Perkins (1967) failed to produce an obvious reduction in outflow resistance by a trabeculotomy procedure on the monkey meshwork.

In rabbits a similar situation probably exists. Tripathi (1971b) concluded that the morphology of the endothelium lining the aqueous plexi and the adjacent meshwork was comparable to the structural equivalents in the primate outflow system while Grant (1958) demonstrated that the experimental removal of rabbit trabecular tissue significantly reduced the resistance to aqueous outflow.

In addition to pressure-sensitive conventional drainage through the outflow system, several subsidiary drainage routes can be considered. They include a) diffusion through iris vessels, b) transcorneal flux, c) drainage via the vitreous to the retina and optic nerve and d) what has been termed uveo-scleral drainage, (Figs I.4 and I.5).

The anterior border of the iris in primates and rodents has an incomplete cover of mesothelial cells so that aqueous humour can penetrate readily into the iris stroma. In this situation the iris vessels present as a potential outflow route. Despite the permeability of iris vessels to materials of low molecular weight, and considerable interchange between aqueous and blood, there appears to be neither a reduction of, nor a positive contribution to, aqueous volume from this source (see Cole, 1974). The transcorneal movement of water from the anterior chamber to the tear film can also be considered as a drainage pathway. The rate of passage of fluid via this route will depend on the rate of water loss by evaporation at the surface of the cornea. In the normal eye, an oily layer on the corneal surface reduces the rate of fluid passage to such an extent that removal of the film produced a 20-fold increase in transcorneal flow (Mishima and Maurice, 1961). The rate of fluid loss via the transcorneal route was calculated to be about 6 ul per hour in the rabbit (Mishima and Maurice, 1961) and since aqueous flow rate in the same species approximates 4 ul per minute

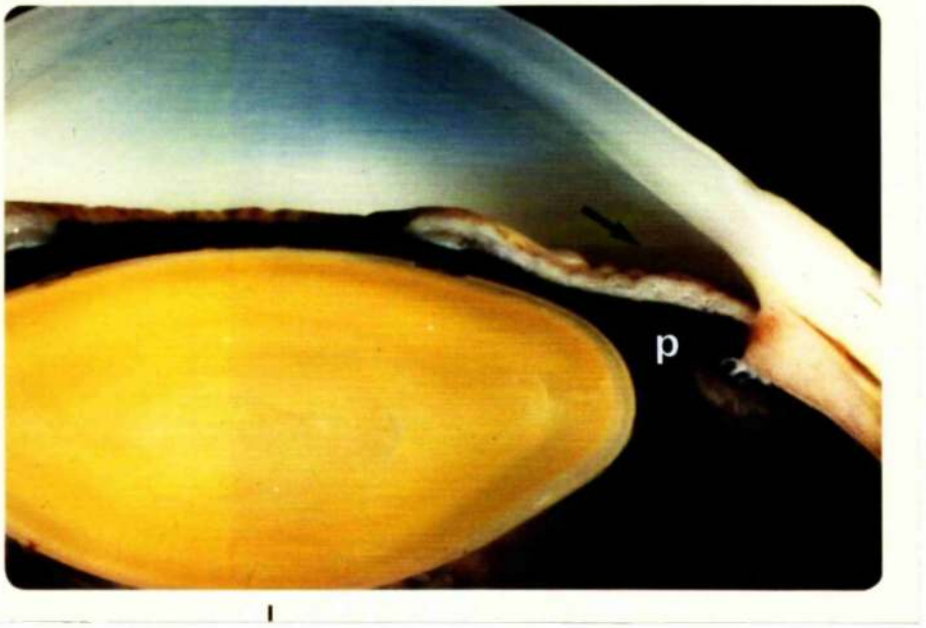

Fig.I.4 A photomicrograph which shows the posterior chamber (p) and the angle of the anterior chamber (arrow) in a human eye. (xI4).

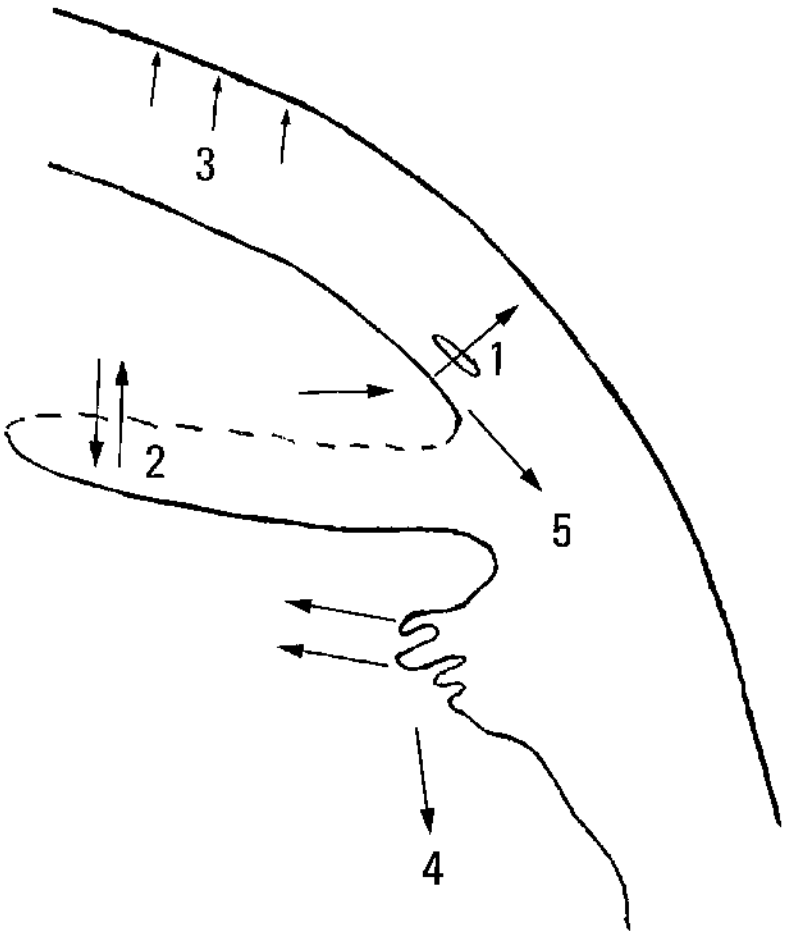

Fig.I.5 A diagram to show pathways by which aqueous humour could leave the eye.

1:- conventional drainage
2:- diffusion through iris vessels
3:- transcorneal flux
4:- posterior drainage
5:- uveo-scleral drainage

(Barány and Kinsey, 1949a and b; Kornblueth and Linnér, 1955) the corneal route is relatively unimportant to aqueous dynamics. Posterior drainage of aqueous via the retina and optic nerve appears to vary considerably between species. In the rabbit the posterior route has been shown to be of some significance whereas a similar pathway could not be demonstrated in either the human or the rhesus monkey after the injection of various colloidal materials into the vitreous (Cibis and Yamashita, 1959; Hayreh, 1966).

Of the subsidiary drainage pathways the uveo-scleral route, for primates at least, is probably the most important. A proportion of the aqueous enters the iris root and the innermost layers of the meshwork to pass between the muscle bundles in the ciliary body and reach either the suprachoroid or the episcleral tissues. The route is of greater significance in primates (Bill, 1965; 1966a and b; 1971; Bill and Hellsing, 1965; Bill and Walinder, 1966; Bill and Barány, 1966; Bill and Phillips, 1971) than in non-primates with poorly developed ciliary muscles (Bill, 1966c and d).* The description provided by Bill (1966d) for uveo-scleral drainage from the primate eye was that "These routes carry aqueous humour from the anterior chamber through the ciliary muscle, into the choroid and the suprachoroid, and out through the sclera into the episcleral tissues", and for the rabbit he said " - in rabbits, only a very small part of the aqueous humour drains by unconventional routes, which in the rabbit are restricted to the limbal region".

---

* FOOTNOTE:- Tripathi (1974) considered that Bill's findings were somewhat curious because, on purely anatomical grounds, the loose ciliary tissue of the non-primate could be expected to have a lower resistance to outflow than the more compact ciliary region of the primate.

Several successful attempts have been made to visualise the uveo-scleral pathway. After the injection of thorotrast into the anterior chamber of enucleated human eyes, Francois, Neetens and Leroux (1967) demonstrated a lateral (uveo-scleral) drainage route by microradiography. In electron microscopic investigations of the primate outflow system, Fine (1964) observed the passage of india ink particles and ferritin into the ciliary body and iris root while Inomata, Bill and Smelser (1972b) observed tracer materials in the iris root, between the muscle bundles of the ciliary body and within the suprachoroid after the infusion of a mixture of thorotrast and latex beads into the anterior chamber. The ultrastructural studies confirmed the earlier histological findings made by Rohen (1963) and Wolf (1965) in primates. Histological evidence for uveo-scleral drainage in rabbits was provided by Fowlks and Havener (1964) who followed the passage of nitro-blue tetrazolium chloride into the suprachoroid.

In contrast to the conventional drainage route, uveo-scleral drainage is relatively pressure-insensitive. The difference in pressure sensitivity was highlighted by Bill (1966a) who showed, in living cynomolgus monkeys, that for an intraocular pressure rise from 11 to 22 mm Hg conventional bulk drainage increased 5-fold, whereas unconventional uveo-scleral drainage was hardly altered.

To summarise, conventional drainage is augmented by uveo-scleral drainage and various other ancillary pathways of lesser, or even negligible, significance (Fig. I.5). The particular importance of the conventional pathway is not only that it is the major route for bulk outflow, but that it is pressure sensitive and, as such, may serve to regulate intraocular pressure in the normal eye. Cole (1974) stated " - it is clear that the low-resistance (conventional) pathways offer a means of stabilizing the intraocular pressure in the face of normal

fluctuations in the rate of formation and that this stabilizing influence will be lacking if the resistance is pathologically increased as in glaucoma".

I.3 The pathway for conventional bulk outflow

I.3.1 Introduction

Although the main outflow route for aqueous humour is via the trabecular meshwork and Schlemm's canal, the precise pathway(s) by which the fluid passes from the outer meshwork through the endothelium lining the trabecular aspect of the canal into the lumen of the vessel remains controversial.

I.3.2 Light microscopy

In the many publications which described the morphology of the primate outflow system, prior to the introduction of the electron microscope as a research tool in this field, it was generally agreed that aqueous humour flowed through the intratrabecular openings and intertrabecular spaces of the uveal and corneoscleral meshwork, but there was fundamental disagreement about the final passage of fluid through the trabecular wall of Schlemm's canal into its lumen.

A large number of authors including Asayama (1901), Henderson (1908), Seidel (1921), Sondermann (1930, 1931, 1932 and 1933), Ashton, Brini and Smith (1956) and Speakman (1959a and b, 1960 and 1961) proposed that free communication existed between the anterior chamber angle and the lumen of Schlemm's canal. As a group, the authors considered that there were relatively large openings or pores in the endothelium lining the trabecular aspect of Schlemm's canal which served as outflow pathways for aqueous humour. In a series of

publications Sondermann (1930-33) provided a particularly precise description of the flow pathways and identified endothelial lined channels (approximately 10 µm wide) which were a continuation of the intertrabecular spaces and opened directly into Schlemm's canal (internal collector channels). The so-called Sondermann's canals were subsequently identified in several light microscopic studies (Dvorak-Theobald, 1934; 1955; Lowenstein, 1951; Ashton, Brini and Smith, 1956; Carpenter, 1958; Rohen and Unger, 1959; Unger, 1959; Unger and Rohen, 1959). On the other hand, Speakman (1960 and 1961) proposed an alternative pathway via giant vacuolar structures in the endothelial lining of the trabecular wall of Schlemm's canal. He considered the vacuoles to be complex channels which made a direct communication between the canal and the underlying meshwork.

There was considerable opposition to the "free communication" theory by authors who held the view that aqueous had to seep through the canal endothelium which, at the light microscope level, had no microscopically visible openings (Virchow, 1910; Salzmann, 1912; Maggiore, 1917; Friedenwald, 1936; Troncoso, 1942; Sugar, 1951; Flocks, 1956 and many others). Frequently, the endothelium lining the canal's trabecular wall was referred to as an endothelial membrane which can be presumed to be a functional rather than an anatomical description.

By the introduction of such diverse materials as chromium phosphate, bacteria, thorotrast, angiopac and latex microspheres into the anterior chamber several investigators which include Huggert (1955, 1957a and b), François, Neetens and Colette (1955), Peter, Lyda and Krishna (1957) and Karg, Garron, Feeney and McEwen (1959) found that particles of up to 4 µm were able to pass through the meshwork into the

lumen of Schlemm's canal. In addition Hørven (1964) showed that labelled red cells passed quickly from the anterior chamber through the drainage tissues to the general circulation. Although these findings have been taken as evidence for the "free communication" theory Davson (1962) pointed out that the argument was not necessarily valid since red blood cells can pass through the walls of cutaneous lymphatics which have no visible pores. Indeed a size limit of 4 μm for inelastic particles may be taken as an argument against the patency of Sondermann's canals which can have, according to Dvorak-Theobald (1934), an internal diameter which approaches 12 μm.

Histological and perfusion studies conducted on the conventional outflow pathways in non-primates produced equally controversial findings (see Tripathi, 1974 for a review of the literature) and both "free communication" and "endothelial membrane" theories have been put forward.

I.3.3 Electron microscopy

The numerous ultrastructural (transmission electron microscopy) and topographical (scanning electron microscopy) investigations have not provided a concensus of opinion on the structural basis of aqueous movement into Schlemm's canal. Sondermann's canals have been identified both by transmission electron microscopy (Iwamoto, 1967a and b; Kayes, 1967; Tripathi, 1969a, 1974; Segawa, 1968, 1970a; Inomata, Bill and Smelser, 1972a) and scanning electron microscopy (Bill, 1970; Hoffmann and Dumitrescu, 1971). Iwamoto (1967a and b) was convinced that the channels made direct communication between the intertrabecular spaces and the canal lumen but his observations stand in isolation from those of the other morphologists who concluded that Sondermann's canals were blind invaginations which did not serve as internal collector channels.

In the first ultrastructural investigations of the drainage system (human) Garron and co-workers (Garron, Feeney, Hogan and McEwen 1958; Garron, Hogan, McEwen and Feeney, 1959; Garron and Feeney, 1959) noted giant cytoplasmic vacuoles in the endothelium lining the trabecular aspect of Schlemm's canal. Holmberg (1959, 1965) produced successful serial sections through the vacuolar structures and showed that they had openings on both their meshwork and canalicular aspects and concluded that the giant vacuoles were transcellular channels.

Subsequent reports have shown that giant vacuoles are a distinctive feature of the endothelium on the trabecular, but not the corneoscleral, aspect of the primate canal (Vegge, 1963, 1967; Feeney and Wissig, 1966; Kayes, 1967; Tripathi, 1968-74; Wulle, 1968, 1972; Hogan, Alvarado and Weddell, 1971; Agarwal, Singh, Mishra and Khosla, 1972; Inomata, Bill and Smelser, 1972a). Some investigators, despite finding giant vacuolar structures, were unable to demonstrate transcellular passageways (Vegge, 1963, 1967; Feeney and Wissig, 1966; Hogan, Alvarado and Weddell, 1971; Agarwal, Singh, Mishra and Khosla, 1972), others confirmed that a proportion of the giant vacuoles were in communication both with the canal lumen and the meshwork (Yamashita and Rosen 1965; Kayes, 1967; Tripathi, 1968-74; Wulle, 1972; Inomata, Bill and Smelser, 1972a). That giant vacuoles normally contain aqueous humour was demonstrated by Feeney and Wissig (1966), McRae and Sears (1970), Tripathi (1971) and Inomata, Bill and Smelser (1972a) who observed the accumulation of tracer materials within the lumen of giant vacuoles after the injection of the tracers into the anterior chambers of primate eyes. Vacuoles are also large enough to allow the passage of red blood cells (Bill, 1970; Inomata, Bill and Smelser, 1972a; Tripathi, 1974) wandering cells (Tripathi, 1971; Inomata, Bill and Smelser, 1972a) and bacteria (Lee, 1971)

and may be of sufficient numbers to account for the bulk of aqueous outflow (Cole and Tripathi, 1971; Tripathi, 1974).

Holmberg (1965) was of the opinion that most, if not all, of the vacuoles were transcellular channels but, by way of contrast, Kayes (1967) and Tripathi (1968) concluded that only about 2% of the giant vacuole population existed as transcellular passageways. Tripathi (1968, 1969a, 1971, 1973b, 1974) proposed that the vacuolar transcellular channel represented a stage in a cyclical process of vacuole development. It was suggested that the vacuole was initiated from an invagination on the meshwork surface of the endothelial cell, the invagination expanded, formed a transcellular channel which eventually collapsed. He acknowledged that the factors involved in endothelial vacuolation were not understood but suggested that the following factors may influence the vacuolation process*:- a) the pressure gradient across the cell, b) a peculiar property of the endothelial cells which permits vacuolation, c) the composition of the aqueous humour and d) neuronal and hormonal agents.

Inomata, Bill and Smelser (1972a) were in general agreement with Tripathi's proposal of temporary vacuolar channels formed by a cyclical process but also found non-vacuolar transcellular channels. Channels

---

*FOOTNOTE:- Giant vacuoles were shown to be a feature of the outflow apparatus in many vertebrate species (including the rabbit) (Tripathi, 1974) and Tripathi has proposed that the vacuolation process is of great phylogenetic antiquity. Recently the same author (Tripathi, 1973a; Tripathi and Tripathi, 1974) has described giant vacuoles in the endothelium lining the arachnoid granulations of the brain and proposed that vacuolar transcellular channels serve as a pathway for the bulk drainage of cerebrospinal fluid.

not associated with giant vacuoles were observed by several authors and these include Vegge (1967), Rohen and Van der Zyphen (1968, 1971), Wulle, (1968, 1972) and Fink, Felix and Fletcher (1972). In the words of Bill and Svedbergh (1972) "The formation of a large invagination does not seem to be a prerequisite for the formation of a pore however, since pores are present also in other very thin parts of the cells". The non-vacuolar channels were considered to be transcellular by Segawa (1968, 1971a), Wulle (1972), Fink, Felix and Fletcher (1972) and Inomata, Bill and Smelser (1972a), intercellular by Rohen (1969) and Van der Zyphen (1971), permanent structures by Segawa (1968, 1971a), and of temporary duration by Inomata, Bill and Smelser (1972a).

Examination of the trabecular wall of Schlemm's canal both by scanning electron microscopy (Bill, 1970; Hoffmann and Dumitrescu, 1971; Lee 1971; Bill and Svedbergh, 1972; Segawa, 1973) and by use of a surface replica technique (Segawa, 1970a) revealed pores in the endothelial cells. Several of the investigators were able to make distinction between openings which lead into vacuolar structures and non-vacuolar channels (Bill, 1970; Bill and Svedbergh, 1972; Segawa, 1973).

On the other hand, some morphologists have consistently failed to demonstrate either non-vacuolar transcellular channels or giant vacuoles in ultrastructural investigations of well fixed tissue, (Fine, 1964, 1966; Shabo and Maxwell, 1972a and b; Shabo, Reese and Gaasterland, 1973; Raviola, 1974). Shabo and co-workers (1973) concluded that giant vacuoles were preparation or post-mortem artefacts and, consistent with this conclusion, they observed increased vacuolation after delayed fixation. The findings of Fine (1966) and Segawa (1971b) who discovered more vacuolar structures in post-mortem than in "fresh" material, lent support to Shabo's proposal.

As alternatives to bulk outflow via large endothelial pores, aqueous pathways a) via the intercellular clefts between neighbouring cells (Feeney and Wissig, 1966; Shabo, Reese and Gaasterland, 1973), b) via micropinocytotic vesicles (Fine, 1964, 1966; Feeney and Wissig, 1966; Rohen, 1969; Van der Zyphen, 1971) and c) via the larger pinocytotic vesicles formed from marginal cytoplasmic folds (Fine, 1964, 1966) have been proposed (see Fig. I.6).

I.4 Primary open angle glaucoma

Aqueous humour dynamics, and the morphology of the tissues involved in aqueous production and drainage, have received considerable attention in ocular research, because only by understanding the mechanisms governing the regulation and maintenance of intraocular pressure in the normal eye can the primary processes associated with pathological increase in pressure be understood.

Primary open angle glaucoma (chronic simple glaucoma) is the most common of the group of diseases associated with a pathological increase in intraocular pressure (see Duke-Elder, 1969). In this form of glaucoma the pathological increase in intraocular pressure is considered to result from an abnormally high resistance to aqueous outflow offered by the diseased tissues of the conventional drainage pathway (see Duke-Elder, 1969). Although the primary pathology is associated with the outflow apparatus the initial changes are subtle. Identification of the early disease process is handicapped both by the lack of histopathological material from cases of early primary open angle glaucoma and the limited size and surgical trauma associated with trabeculectomy specimens. The tissue most frequently examined by the pathologist has either well established or end stage (absolute) glaucoma where the primary pathology has been obscured by secondary pressure

Route	Mechanism	Author
Intracellular	Pinocytosis involving marginal folds	Fine (1964)
	Micropinocytosis	Fine (1964, 1966), Feeney and Wissig (1966), Rohen and Van der Zyphen (1968), Rohen (1969), Van der Zyphen (1971)
	Temporary intracellular channels (non vacuolar)	Wulle (1972), Inomata, Bill and Smelser (1972)
	Permanent intracellular channels (non vacuolar)	Segawa (1968, 1971a and b), Fink, Felix and Fletcher (1972)
Intercellular	Sodermann's canals	Iwamoto (1967)
	Gaps between neighbouring cells	Vegge (1967), Rohen and Van der Zyphen (1968), Rohen (1969), Van der Zyphen (1971)
	Intercellular clefts	Feeney and Wissig (1966), Shabo, Reese and Ganesterland (1973)
Not specified	Gaps	Wulle (1968)

Fig.I.6 Non-vacuolar routes for the passage of aqueous humour through the endothelium lining the trabecular aspect of Schlemm's canal. The routes were proposed from transmission electron microscopic studies of the primate outflow system.

induced alterations to the outflow apparatus. Also, the influence of prolonged drug therapy is a complicating factor of unknown extent (among many others see Ashton, 1958, 1960; Duke-Elder, 1969; Yanoff and Fine, 1975).

Given that there is, as yet, no unified concept for the aetiology and histopathogenisis of primary open angle glaucoma recent ultrastructural investigations on the diseased outflow system by Rohen and Witmer (1972) and Tripathi (1972) are of interest. In both studies it was found that there were abnormally large amounts of ground substance in the extracellular spaces of the trabecular wall of Schlemm's canal, while Tripathi also noted a decrease in the numbers of giant vacuoles within the canal endothelium. Clearly the changes could be secondary factors in the disease process but it is possible that the increased resistance to aqueous outflow associated with open angle glaucoma may be initiated either by the development of a mechanical blockage in the trabecular wall or by progressive dysfunction of the canal endothelium. Thus, in the conventional drainage pathway, the trabecular wall of Schlemm's canal is of particular importance because a) it plays a key role in the functioning of the normal outflow system and b) it may be the site of the initial pathological changes in primary open angle glaucoma.

I.5 The aims and the approach to the current investigation

I.5.1 The normal outflow apparatus

The current investigation includes a morphological assessment of the normal outflow apparatus in three primate species (man, baboon and rhesus monkey) and the rabbit.

In the review of the literature the importance of the trabecular wall of the main drainage vessel(s) (Schlemm's canal in primates) was

emphasised and it was apparent that the nature of the ultimate pathway for the passage of aqueous through the canal endothelium was controversial. For this reason, in the present light microscopic, transmission electron microscopic and scanning electron microscopic investigation of the normal drainage tissues, the trabecular wall merited special consideration and attention was paid to the identification and structural characteristics of possible pathways for the bulk drainage through the endothelium of Schlemm's canal.

Since the delicate outflow apparatus has to maintain its integrity against a positive pressure gradient (and the action of the ciliary muscle during accommodation) particular emphasis was placed on the identification of adhesive mechanisms in the tissues. A study was made of cell-to-cell and cell-to-extracellular material attachments which enhance and maintain trabecular integrity, normal meshwork relationships and the integrity of the canal endothelium.

The extracellular elements of the outflow apparatus are of structural importance in the trabeculae. In the trabecular wall of the canal extracellular constituents are likely to have an influence on flow dynamics. Attention was therefore paid to the study of the fine structure and distribution of these materials. It has been a matter of some debate whether or not hyaluronidase-sensitive mucopolysaccharides are a significant constituent of the extracellular components in the normal outflow apparatus. Since hydrophilic complex polysaccharides would make an important contribution to trabecular resistance to aqueous outflow, an attempt was made to identify acid mucopolysaccharides and glycoproteins in the normal outflow tissues. Ultrastructural investigation of the mucopolysaccharides has been hampered because they are not visualised by conventional transmission electron microscopic staining techniques. For the present study the electron dense stains colloidal

thorium, colloidal iron and ruthenium red, which adhere to the polysaccharides, were used to identify and locate the mucins.

I.5.2 The outflow apparatus at various levels of intraocular pressure

It has been shown from physiological investigations that one of the most important properties of the conventional outflow pathways is their pressure-sensitivity. It would therefore be of some significance to undertake a morphological investigation into the effects, on the conventional drainage system, of graded change in intraocular pressure.

The second part of the current investigation describes the outflow apparatus in rhesus monkey eyes which were subjected to maintained intraocular pressure levels between 0 and 50 mm Hg for a period of one hour prior to primary fixation. It was hoped a) to discover how the delicate meshwork tissue responds both to mild and extreme pressure change and, b) to determine pressure-sensitive mechanisms for the outflow of aqueous humour through the endothelium lining the trabecular aspect of Schlemm's canal.

Although artificial pressure alteration by manometric means is an acute investigation, the experiment affords an opportunity to identify initial changes in the normal meshwork which may also develop as part of the pressure induced pathology in the course of chronic disease (primary open angle glaucoma).

In the normal outflow system transcellular channels and giant vacuole are not distributed uniformly along the canal endothelium (see Chapter 4). If pressure effects on these structures are to be assessed with any degree of accuracy then careful quantitative analysis is necessary at the various pressure levels. Light microscopy, transmission electron microscopy and scanning electron microscopy have intrinsic disadvantages which limits the amount of useful information which can be elicited from

any one technique in isolation (Fig. I.7). For this reason it was decided not to restrict the analysis to any one technique but to undertake separate quantitative studies using all three systems. In this way it was hoped that by comparison of the results of the three analyses the intrinsic disadvantages associated with each could be eliminated.

The primary vacuole quantitation was conducted by light microscopy on relatively large samples of tissue. Transmission electron microscopy was used to establish whether the vacuoles had pores and could function as flow pathways. An assessment was also made of the pressure influence on pore frequency, the significance of resolution errors in the light microscopic counts and pressure effects on other structures which may serve as flow pathways. Finally the scanning electron microscope was used to provide additional information about pore dimensions and frequency from comparatively large samples of tissue.

It was possible that changes in the drainage tissues and flow pathways, which were attributed to altered pressure, may have been produced by the toxic effects of the perfusion fluid used to maintain intraocular pressure. A preliminary study was therefore conducted to determine the influence of the mock aqueous perfusion fluid on the tissues of the outflow apparatus.

The facility of aqueous outflow was not determined in the eyes maintained at various levels of intraocular pressure. Although the physiological data would have provided useful information it was considered possible that the manipulations involved in these physiological assessments would produce alterations to the drainage tissues which could not be attributed to intraocular pressure.

At the outset of the investigation the morphological effects of intraocular pressure alteration on the drainage system was unreported but since this time several pertinent publications have appeared in the literature (Fig. I.8) and they will be discussed in the appropriate chapters

Technique	Advantages	Disadvantages
Light Microscopy (L.M.)	Relatively large tissue sample can be examined	Limited resolution adequate to identify most giant vacuoles but not vacuolar pores
Transmission Electron Microscopy (T.E.M.)	High resolving power allows the fine structure of vacuoles and their pores to be studied in detail	Only a small sample of tissue can be examined
Scanning Electron Microscopy (S.E.M.)	Very large tissue sample can be examined and the resolution is adequate to identify pores	Difficult to distinguish between true pores and artefacts formed during preparation

Fig.I.7 Advantages and disadvantages of the various microscopic systems used for the quantitative investigation of flow pathways through the canal endothelium.

Author	Species examined	Maintained pressure levels	Duration of maintained pressure
Johnstone and Grant (1973) (L.M. study)	Postmortem human eyes	Between - 2 and 50 mm Hg	2½ hrs
	One rhesus monkey	0 and 25 mm Hg	
Johnstone (1974) (L.M. study)	Rhesus monkeys	0 and 25 mm Hg	10 mins
Svedbergh (1974) (T.E.M. and S.E.M. study)	Vervet monkeys	Experimental Eyes - 33 to 48 mm Hg Control Eyes - a few mm Hg above spontaneous pressure	3 to 7 hrs
Xuyen (1975) (T.E.M. study)	Rhesus monkeys	0 and 40 cm Hg	1 hr

Fig.I.8 Previous investigations which describe the effects of pressure variation on the appearance of the outflow apparatus.

CHAPTER 2

THE GENERAL APPEARANCE AND NOMENCLATURE OF THE OUTFLOW TISSUES

2.1 The primate outflow system

2.1.1 Introduction

The angular sinus, which serves as the main drainage vessel for aqueous humour, was termed the sinus venosus sclerae and the underlying limbal tissues the spongium anguli iridocornealis (P.N.A. 1955) but the anatomic nomenclature has not been adopted by most authors. Instead, the older titles of "Schlemm's canal" (the vessel was first described by the German anatomist Friedrich S. Schlemm in 1830) and "trabecular meshwork" (a name introduced into the literature by Rochon-Duvigneaud, 1892) still carry favour.

Schlemm's canal and the trabecular meshwork occupy a position within the limbus such that the canal and the outermost portion of the trabecular meshwork are contained within the internal scleral sulcus. To quote Hogan, Alvarado and Weddell (1971) "The corneoscleral tissues are hollowed out on the internal surface to form the internal scleral sulcus. Within the sulcus are the corneoscleral meshwork and Schlemm's canal, which completely fill the cavity of the sulcus, with Schlemm's canal lying in the posterolateral part of the sulcus".

2.1.2 The general appearance of the primate trabecular meshwork

Salzmann (1912) considered that the meshwork formed a three sided prism-shaped band which, anteriorly, united with Descemet's membrane and the adjacent corneal lamellae. Posteriorly, the trabeculae merged with the scleral spur, the anterior limit of the ciliary body and the iris. The outer surface bordered directly upon the trabecular wall of Schlemm's canal while the inner surface was free and in contact with the aqueous humour of the anterior chamber (see Figs 2.1 and 2.2). The shape, location and limits outlined by Salzmann have been accepted

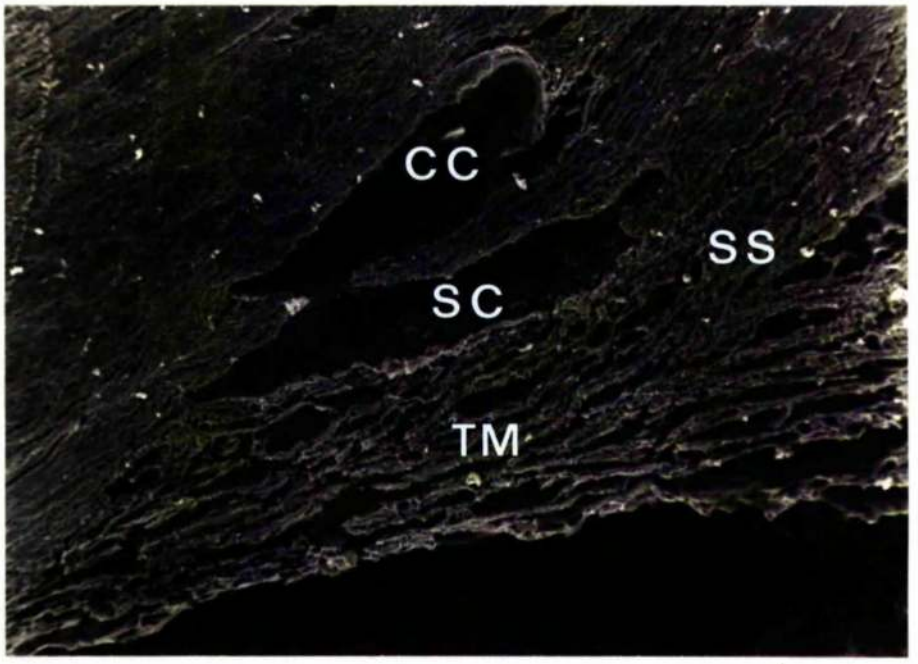

Fig.2.I The normal human outflow system as seen in meridional section by scanning electron microscopy. The outermost portion of the trabecular meshwork (TM) joins posteriorly with the scleral spur (SS). A collector channel (CC) can be seen to be in communication with Schlemm's canal (SC). S.E.M. (x200).

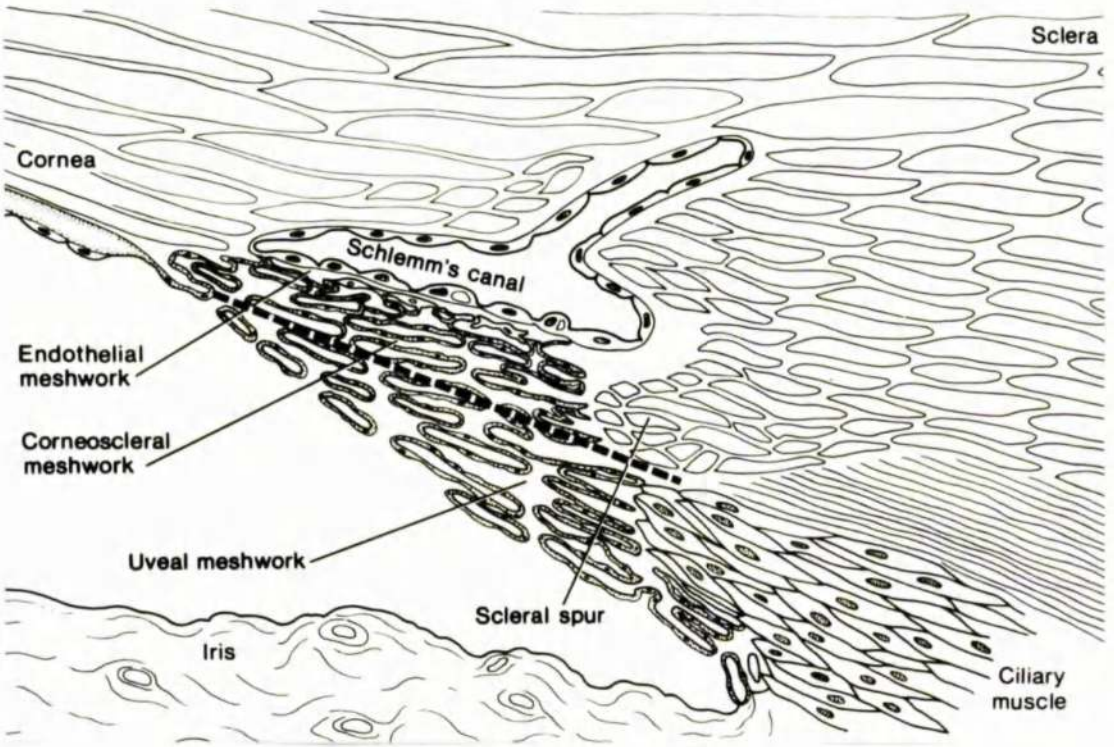

Fig.2.2 A diagram of the primate outflow apparatus.

in subsequent anatomic reviews which include those of Ashton, Brini and Smith (1956), Hogan, Alvarado and Weddell (1971), Rohen and Lütjen-Drecoll (1971), Fine and Yanoff, (1972) and Tripathi (1974).

In the meridional plane the trabeculae appear as a series of interrupted fibres or rods which are arranged loosely in layers. The spaces between the layers, the intertrabecular spaces, decrease in width towards Schlemm's canal. Each trabecula has an endothelial cover which surrounds a connective tissue core (Fig. 2.3). However, the trabeculae do not have a uniform shape throughout the meshwork. Flat preparations of the innermost portion of the trabecular meshwork, viewed either as histological preparations for light microscopy (Ashton, Brini and Smith, 1956), as surface replicas for light microscopy (Vrabec, 1974), as fresh preparations for light microscopy (Tripathi, 1969a) or as dehydrated preparations for scanning electron microscopy (Spencer, Alvarado and Hayes, 1968; Tripathi, 1969a; Anderson, 1971; Bill and Svedbergh, 1972; Segawa, 1973) show that these trabeculae are cord-like structures which branch frequently to produce an overall appearance of a network or mesh with relatively wide openings (see Chapter 4 for more details). Closer to Schlemm's canal the trabeculae are arranged as a series of flat perforated lamellae or sheets which can be appreciated by examining flat preparations under the light microscope (Ashton, Brini and Smith, 1956) but more easily with a scanning facility (Spencer, Alvarado and Hayes, 1968; Anderson, 1971; Bill and Svedbergh, 1972; see also Fig. 2.4)

2.1.3 The nomenclature of regions within the primate trabecular meshwork

Virchow (1910) made distinction between two regions within the trabecular meshwork by classifying the trabeculae which merge with the

Fig.2.3 Trabeculae from the rhesus monkey meshwork. L.M. (xI,000).

Fig.2.4 The trabecular sheets of the rhesus monkey meshwork as seen by S.E.M. (x475).

scleral spur as belonging to the scleral (corneoscleral) meshwork and those trabeculae which join with the ciliary muscle and the iris root as belonging to the uveal meshwork.

In later light microscopic investigations, Burian, Braley and Allen (1954) and Allen, Burian and Braley (1955) made further subdivisions. They accepted the corneoscleral meshwork as defined previously, but made three divisions within the uveal meshwork by distinguishing between trabecular lamellae which are associated with a) the longitudinal fibres of the ciliary muscle, b) the circular and radial fibres of the ciliary muscle and c) the iris root.

Ashton, Brini and Smith (1956) thought the previous classification to be over ambitious because there is usually no precise demarcation between longitudinal, circular and radial muscle bundles. They did, however, attribute to the uveal meshwork an outer and an inner component. The outer component was thought to extend from Descemet's membrane and adjacent corneal layers to fuse with the adventitia of the ciliary muscle whereas the cord-like trabeculae of the inner component, which also extended from Descemet's membrane and the adjacent corneal lamellae, merged with the anterior surface of the iris root.

Flocks (1956) adopted Virchow's classification of the meshwork into uveal and corneoscleral portions but he thought that the narrow zone without organised trabeculae immediately adjacent to Schlemm's canal should be called the pore area* or pore tissue to emphasise its importance in the drainage of aqueous humour. Rohen and co-workers, in a series of light and electron microscopic studies (Unger and Rohen,

---

*FOOTNOTE:- Flocks was not the first to comment on this region which had been noted previously by Rochon-Duvigneaud (1893), Asayama (1901), Salzmann (1912) and had been called the "cotton wool" tissue by Wolff (195

1959; Rohen, 1961, 1963, 1969; Rohen and Lütjen-Drecoll, 1971) preferred to call the zone the trabeculum cribriforme while Garron (1959) used a functional rather than anatomical terminology i.e. filtration tissue. Speakman (1960) was also of the opinion that the narrow band of tissue was of sufficient importance to warrant distinction. He was impressed by the cellularity of the region and called it the endothelial meshwork. Ashton (1960) considered that the endothelial meshwork was an appropriate name since it maintained uniformity with established terminology (i.e. corneoscleral and uveal meshwork). However yet another title, the juxtacanalicular connective tissue, was introduced into the literature by Fine (1964).

Hogan, Alvarado and Weddell (1971) stated that "If a title has to be applied, juxtacanalicular tissue is the most satisfactory, but we prefer to consider it as the inner wall of Schlemm's canal". Although Hogan, Alvarado and Weddell used the terms corneoscleral and uveal meshwork, their definitions of the regions were at variance with those of Burian, Braley and Allen (1954), Allen, Burian and Braley (1955), Ashton, Brini and Smith (1956) and Flocks (1956). Included within the corneoscleral meshwork were not only the trabecular fibres which made contact with the scleral spur, but also some of the underlying trabecular sheets which joined with the ciliary stroma. Thus the term uveal meshwork was restricted to those peripheral cord-like trabeculae which limited the anterior chamber angle.

Perhaps the most comprehensive classification was provided by Rohen and Lutjen-Drecoll (1971) who identified five distinct regions within the trabecular meshwork which they called:-

1) trabeculum iridis
2) trabeculum corneosclerale
3) trabeculum cribriforme

4) trabeculum corneale

5) trabeculum ciliare

The trabeculum iridis consisted of the trabecular fibres which had a posterior attachment to the iris root and the connective tissue strands in front of the ciliary muscle. They named the connective tissue strands the trabeculum ciliare. Thus the trabeculum ciliare and the trabeculum iridis comprised the uveal portion of the meshwork. The trabeculum corneosclerale consisted of the trabecular lamellae which merged with the scleral spur while the trabeculum cribriforme, as previously mentioned, was equivalent to the pore tissue of Flocks (1956). Finally, the trabeculum corneale was considered to be the region where the architecture of the trabecular meshwork altered prior to insertion at the posterior end of Descemet's membrane and the adjacent corneal lamellae.

2.1.4 The general appearance of Schlemm's canal

Schlemm's canal is an endothelial lined vessel positioned slightly anterior to the scleral spur (see Figs 2.1 and 2.2). The canal, from meridional sections, is of variable shape and has been described as being round, ellipsoid, triangular or even pyramidal (see Ashton, 1952). It is generally agreed that, in primates, Schlemm's canal is a single vessel which, from gonioscopic observations (Troncoso, 1925; Sugar, 1940; Kronfeld, 1949) and by the examination of neoprene casts (Ashton, 1951), is seen to be a continuous hoop circling the limbal region of the eye. In places, the canal is partitioned by endothelial lined septae but the septal structures are of limited extent and the bifurcations soon rejoin to form a single vessel (see Duke-Elder, 1968; Hogan, Alvarado and Weddell, 1971; Tripathi, 1974). In the human the total canalicular volume was calculated to be 0.2 cm^3 (Kronfeld, 1949)

and its length as 36 mm (Hogan, Alvarado and Weddell, 1971). Cole and Tripathi (1971) estimated the length of Schlemm's canal in the rhesus monkey to be 30 mm.

2.1.5 The nomenclature of the structural components of Schlemm's canal

Light microscopists have generally subdivided the limiting wall of Schlemm's canal into an internal or inner portion adjacent to the trabecular meshwork and an external or outer portion adjacent to the sclera (see Ashton, Brini and Smith, 1956; Holmberg, 1965; Tripathi 1969a and 1974 for reviews of the early literature).

The electron microscope made it possible to examine the canal walls in greater detail. Unfortunately there remains some inconsistency in the literature as to the limits and components of the two walls.

Initially Holmberg (1959) was of the opinion that the inner wall consisted of two layers of endothelial cells whereas the outer wall had only one. Of the two cellular layers which constituted the inner wall, that bordering the canal was a continuous lining while the other was loose and discontinuous. Later, Holmberg (Holmberg, 1965, 1966) conceded that only the endothelial monolayer which surrounded the canal should be called the canal wall, " - it seems more correct to consider the wall of Schlemm's canal as being formed by one single layer of endothelial cells." (Holmberg, 1965).

As an alternative Feeney and Wissig (1966) proposed that, in human and monkey eyes, the inner wall was not a single but a tripartite layer. The tripartite structure consisted of the endothelial monolayer on the trabecular aspect of Schlemm's canal (Holmberg's inner wall), the underlying endothelial meshwork and an incomplete layer of cells which limited the inner wall from the corneoscleral meshwork.

Tripathi (1968, 1969a and 1974) did not accept that there was an

organised layer of cells adjacent to the corneoscleral meshwork and considered that the constituents of the inner wall were a) the endothelium bordering the vessel lumen, b) its basement membrane and c) the underlying connective tissue (the endothelial meshwork). The wall on the scleral side of the canal was composed of a) the endothelial monolayer on the scleral aspect of the canal, b) the underlying basement membrane and c) a narrow zone of supporting tissue rich in extracellular material and fibroblasts. Tripathi preferred to describe the canal as having trabecular and corneoscleral (scleral) walls rather than inner and outer. As he pointed out, the anatomical position is not necessarily a good guide for a vessel which is septate, has a variable outline and whose walls become indistinguishable from each other where they merge.

2.1.6 Personal nomenclature

It is apparent that a standard nomenclature has not been adopted by either light or electron microscopists so that it is necessary to present a personal terminology for the various structural components of the drainage system.

The outflow system is considered to be those structures involved in the drainage of aqueous humour from the anterior chamber angle to the episcleral vessels whereas the term outflow apparatus will be used as a collective name for the trabecular meshwork and Schlemm's canal.

Within the trabecular meshwork four regions, the uveal, the inner corneoscleral, the outer corneoscleral and the endothelial meshwork are thought to have sufficient structural distinction to merit separate classification.

a) The uveal meshwork

The uveal meshwork is restricted to the innermost trabeculae which are

cord-like in appearance and merge with the ciliary muscle adventitia and the iris root.

b) The inner corneoscleral meshwork

The inner corneoscleral trabeculae come into contact with muscle adventitia but form flattened lamellae rather than cords.

c) The outer corneoscleral meshwork

The trabecular lamellae of the outer corneoscleral meshwork are attached to the scleral spur. The trabecular sheets are thinner and more delicate than those of the inner corneoscleral meshwork

d) The endothelial meshwork

The outermost portion of the meshwork adjacent to Schlemm's canal where there is no trabecular organisation. This network of cells and loose connective tissue elements represents the meshwork component of the canal's trabecular wall.

To ascribe trabeculae with a uveal insertion to the inner corneoscleral meshwork (the outer uveal meshwork of Ashton, Brini and Smith, 1956) may appear incongruous. Although anatomically inexact, the classification is expedient for transmission electron microscopy. Under the transmission electron microscopy, the structural differences between trabeculae are a more useful discriminatory feature than their peripheral anatomical relationships because the peripheral tissue may have been removed from the block face prior to sectioning or maybe obscured by a grid bar.

The term "endothelial meshwork" (Speakman, 1960) is chosen in preference to other possible titles (see 2.1.3) because a) it preserves descriptive uniformity, b) it highlights an easily recognisable feature i.e. cellularity (Speakman, 1960; Ashton, 1960; Tripathi, 1969a, 1974) and c) it is an anatomical rather than a functional classification.

The area of transition between the organised trabeculae of the

outer corneoscleral meshwork and the network of cells in the endothelial meshwork is termed the intermediate zone.

Schlemm's canal is considered to have a "trabecular" and "corneoscleral" rather than an "inner" and "outer" aspect. The definition of the trabecular and corneoscleral walls proposed by Tripathi (1968, 1969a, 1974) is accepted.

2.2 The rabbit

The angular region of the rabbit eye is distinguished by having a poorly developed ciliary muscle, no scleral spur and a plexus of aqueous collecting vessels which correspond to Schlemm's canal (see Tripathi, 1971b and 1974 and Chapter 4 of the thesis). Because the ciliary muscle is insubstantial, the major part of the ciliary body consists of loose connective tissue. At its anterior limit, the outer portion of the ciliary stroma is continuous with trabecular lamellae. The outermost trabeculae do not merge with ciliary elements but instead, in the absence of a scleral spur, they make contact with the sclera proper. Thus it is possible to apply primate terminology to the drainage tissues of the rabbit (see Tripathi, 1974), since trabeculae with a uveal connection, trabeculae with a scleral (corneoscleral) connection and, indeed, an endothelial network under each collecting vessel can be identified. Primate nomenclature cannot, however, be applied to the discrete drainage vessels so that, for the purpose of the present communication, the more general term of angular aqueous plexus (Tripathi, 1971b, 1974) is adopted in preference to Schlemm's canal which is a specific title for the single vessel present in the primate.

Other anatomical features of the rabbit drainage angle which are either absent from the primate system or are vestigial e.g. the ciliary cleft, the iris pillars and the spaces of Fontana are described,

defined and discussed in the more detailed account of the rabbit outflow apparatus provided in Chapter 4.

CHAPTER 3

MATERIALS AND METHODS

3.1 Normal tissue

3.1.1 Materials

The material used to investigate the morphology of the normal outflow apparatus was provided by 15 human (Homo sapiens), 17 baboon (Papio anubis), 12 rhesus monkey (Macaca mulatta) and 23 rabbit (Lepus cuniculus) eyes. Further information is listed in appendices 1 - 4 which show the species, the numbers of eyes examined, the subjects' age or weight and the modes of primary fixative penetration into the tissue. The 15 human eyes were enucleated in treatment of tumours of the posterior globe and intraocular pressure readings fell within normal limits. The baboon, rhesus monkey and rabbit eyes had no obvious ocular abnormalities and intraocular pressure was assumed to be normal. The human eyes came from patients aged between 1 and 76 years while the baboons (9-15 kilograms), the rhesus monkeys (3.0 - 5.5 kilograms) and the rabbits (1-3 kilograms) were either young or mature adults (see appendices 1 - 4).

3.1.2 Anaesthetics

Prior to primary fixation the experimental animals were anaesthetised to a level at which the corneal reflex was suppressed. The anaesthetic administered to the baboons and rhesus monkeys was pentothal (15 mg per kilogram body weight) which was introduced intravenously via a leg vein while the rabbits were anaesthetised with intravenous urethane (2 gm per kilogram body weight) via a peripheral ear vein.

3.1.3 Primary fixation

For both the human and experimental animal eyes the primary

fixative was glutaraldehyde (TAAB laboratories), either a 2 - 4% solution in 0.1M Sorenson's phosphate buffer or a 3% solution in 0.2M sodium cacodylate buffer. The working pH range for the fixative systems was 7.2 to 7.4.

a) Arterial perfusion of the primary fixative.

Arterial perfusion of the primary fixative solutions was by way of the carotid arteries in the primates and the femoral artery in the rabbits, the fixative being introduced into the circulation either while the animals were in deep anaesthesia or immediately after sacrifice (from an anaesthetic overdose). The perfusion pressure of the fixative solution was sufficient to allow easy flow of fluid with the circulation and the jugular veins were opened to serve as channels for blood and spent fixative. The eyes were left in situ for at least 30 minutes prior to enucleation and then immersion in the same fixative solution. Thereafter, the anterior segments were removed and cut into quadrants.

b) Anterior chamber perfusion of the primary fixative.

Anterior chamber perfusion of buffered glutaraldehyde was accomplished by three techniques:-

1) Two 23 gauge needles, which were each attached to a syringe (1 ml), were introduced into the anterior chamber through the peripheral cornea. Buffered glutaraldehyde was slowly introduced into the anterior chamber from one syringe and aqueous humour was carefully withdrawn with the other. The movement of the syringes was synchronous in order to maintain constant depth in the anterior chamber.

2) Two 23 gauge needles, which were attached to a continuous length of narrow bore tubing (containing buffered glutaraldehyde), were introduced into the anterior chamber. The infusion of the

fixative, and the removal of the aqueous, was achieved by the slow manual manipulation of the arms of a small peristaltic pump.

3) A 23 gauge needle, which was attached to a manometer system containing buffered glutaraldehyde, was introduced into the anterior chamber. The height of the reservoir was set to maintain an intraocular pressure of between 15 and 20 mm Hg and fixative was allowed to infuse into the anterior chamber.

With each of the three intracameral perfusion techniques the infusion of fixative occurred in vivo and the animals were not sacrificed until fixative penetration was well established (frequently fluorescein dye was added to the primary fixative solution to serve as a marker). After 30 minutes the eyes were enucleated and immersed in the same fixative solution. The anterior segments were cut into quadrants while immersed in fixative solution.

c) Immersion fixation.

With the baboons, rhesus monkeys and rabbits, the eyes were enucleated in vivo or immediately after sacrifice. As rapidly as possible the eyes were then immersed in buffered glutaraldehyde, opened, the lenses removed and the anterior segments divided by horizontal and vertical slices into quadrants.

Calottes of suitable human anterior segment material were provided by the West of Scotland Routine Pathology Service from pathology specimens which had reached the laboratory either as intact globes or globes with corneal trephines.

Thin slices containing limbal tissue were cut from both the perfusion and immersion fixed material and these were left in the primary fixative solution for not less than four hours. After this period the tissue blocks from each eye were separated into batches prior to subsequent processing for either light microscopy and

transmission electron microscopy, special staining techniques for transmission electron microscopy or scanning electron microscopy.

3.2 Experiments to study the effects of intraocular pressure variation on the outflow system

3.2.1 Materials and anaesthetics

A total of 17 young adult rhesus monkeys weighing between 3 and 5 kilograms were used in this part of the investigation (appendix 6). The animals were tranquilised with intramuscular phencyclidine (1.5 mg/Kg), anaesthetised with intravenous pentothal (15 mg/Kg) and, thereafter, kept at a suitable level of anaesthesia (as indicated by an absence of the corneal reflex) by regular intravenous injection of the same anaesthetic. The animals were sacrificed at the termination of the experiments by an overdose of Euthetal.

3.2.2 Barány's solution

The infusion fluid adopted for the pressure experiments was a phosphate buffered salt solution, isotonic with aqueous humour (Barány, 1964) which was carefully filtered through a "millex" disposable filter (Millipore S.A. France) before use. The buffered mock aqueous was thought to be particularly suitable because in two reports (Barány, 1964; Ellingson and Grant, 1971) better consistency was found in repeated facility determinations from the same eye with Barány's solution than with isotonic saline.

Before the pressure experiments were performed however, it was necessary to exclude the possibility that the Barány's solution had any significant effect on the ultrastructure of the outflow apparatus. In a preliminary experiment on three monkeys, the right eye of each

animal was cannulated by hand with two 23 gauge needles and the aqueous replaced by the slow infusion of Bárány's solution. The infusion fluid was introduced by the manual manipulation of a peristaltic pump which caused the fluid to flow into and out of the anterior chamber via the intracameral needles. When the anterior chamber contents had been replaced, the infusion was halted and the eye was left in situ for one hour. After this period the left eye was cannulated in a similar manner to the right eye and the fluid in both eyes was replaced by 2 - 4% phosphate buffered glutaraldehyde by means of the peristaltic pump. Ten minutes later the animals were sacrificed and the eyes enucleated. Thereafter the anterior segments were removed and immersed in fixative of the same concentration to that used for anterior chamber infusion.

3.2.3 Experimental procedures for the intraocular pressure study

In the 14 rhesus monkeys, which were the subjects of the intraocular pressure investigation, pressure was controlled by an intracameral 25 guage needle attached to a monometer system containing Bárány's solution (Fig. 3.1). The needle was introduced into the anterior chamber, through the cornea, using a needle gun (Edwards and Yerlett, 1972) which was found to be a more satisfactory method than introducing the needle by hand.

In the first 9 monkeys, the experiments were arranged so that the experimental eyes were maintained at either 8, 22 or 30 mm Hg (three at each pressure level) in the control eye of each animal, the reservoir maintained an intraocular pressure of 15 mm Hg which was approximately 2 mm Hg higher than the mean value for spontaneous pressure obtained from 9 eyes (13 ± 3 mm Hg). Intraocular pressures were measured with a Bell and Howell pressure transducer attached to

a Devices pen recorder.

After one hour, a second needle from a duplicate reservoir system was inserted into each eye. The fluid in this second pressure system was 2 - 4% phosphate buffered glutaraldehyde and the eyes were fixed in vivo by clamping the reservoir containing mock aqueous and allowing fixative to enter the anterior chamber from the second reservoir (fluorescein dye served as a marker and provided visual confirmation of the rapid distribution of the fixative solution in the anterior chamber) (Fig. 3.1). Since the fixative reservoir was set at the same height as the mock aqueous reservoir, intraocular pressure was considered to be constant throughout the experiment. An exception was made in the three eyes maintained at 8 mm Hg because fixative entry was slow. In each of the experimental 8 mm Hg eyes, infusion was assisted by gently withdrawing a small quantity of fluid from the anterior chamber through the mock aqueous infusion needle, after which the intraocular pressure was allowed to return to 8 mm Hg. In each pressure experiment, 10 minutes were allowed for fixative penetration before the animals were killed and 30 minutes after death the anterior segments were excised and stored in fixative.

In two animals, the experimental eyes were maintained at 30 mm Hg intraocular pressure and the controls at 15 mm Hg intraocular pressure. The regime was similar to that described above except that fixation was achieved by in vivo carotid perfusion and severed jugular veins functioned as exit channels.

Finally, three animals were studied at pressures far outside the physiological range. One eye was maintained at 0 mm Hg intraocular pressure and the other at 50 mm Hg intraocular pressure. One hour later, the high pressure eye was fixed in a similar manner to that described previously. The zero pressure eye was enucleated while

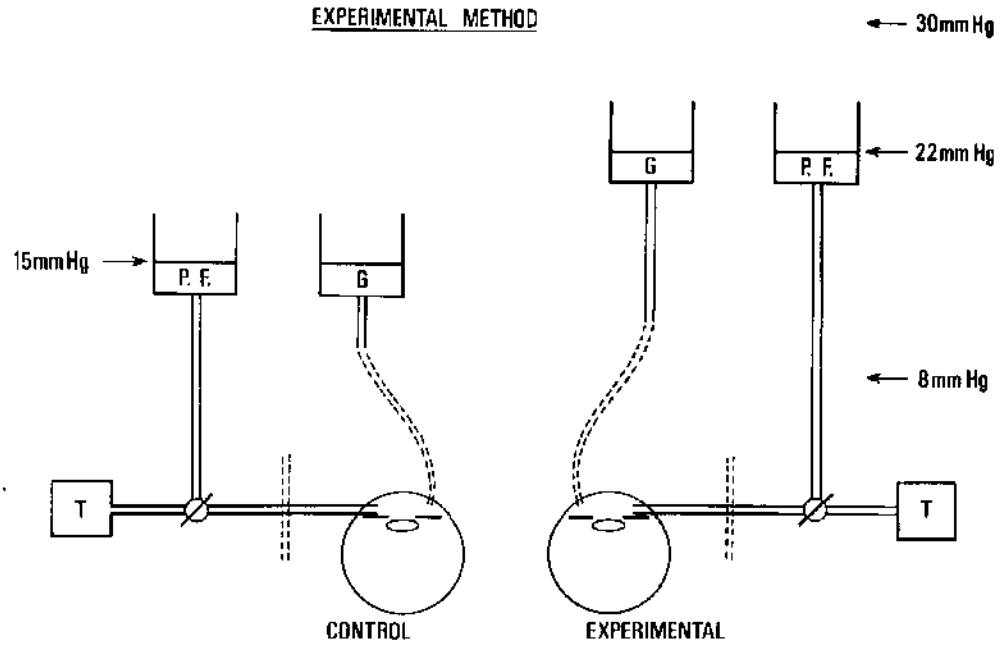

Fig.3.I The experimental system used to control intraocular pressure in the rhesus monkey. Intraocular pressure was maintained by reservoirs containing perfusion fluid (P.F.) and determined by pressure transducers (T). Fixation with glutaraldehyde (G) was accomplished from auxilliary reservoir systems which duplicated the appropriate maintained pressure levels.

attached to the manometer system and immediately immersed in 2 - 4% phosphate buffered glutaraldehyde. The immersed globe was opened and the anterior segment removed so that fixative penetration of limbal structures could be more rapid (Fig. 3.2).

3.2.4 Subsequent treatment

Hereafter, the procedure was identical for all the eyes which were part of the intraocular pressure investigation. The anterior segments were divided horizontally and vertically and left in fixative for 24 hours after which at least 6 blocks of limbal tissue were removed from each quadrant and processed conventionally for transmission electron microscopy (Fig. 3.3). The remaining tissue was used either for scanning electron microscopy or for special staining for transmission electron microscopy.

3.3 Conventional (routine) tissue preparation for light microscopy and transmission electron microscopy

Following primary fixation in buffered glutaraldehyde, the tissue blocks were washed in the appropriate buffer for at least two hours (frequently overnight) after which the tissue was post-fixed in 1% buffered osmium tetroxide (TAAB laboratories) for one hour. Subsequently the post-fixed material was rewashed in buffer then dehydrated through graded alcohols, cleared in propylene oxide and embedded in araldite (TAAB laboratories). Thick (1, 1.5 and 2 μm) and ultrathin (500 - 800Å) sections were usually cut in the meridional plane on an LKB ultrotome III but tangential sections of the outflow system were also examined. The ultrathin sections of the outflow system were cut in ribbons, mounted on copper grids (100 and 200 mesh) and, after staining, viewed in either

Experiment	No. of Animals	Intraocular Pressure (mm. Hg)		Mode of Fixation
		Experimental Eye	Control Eye	
a) To assess the suitability of Burnny's solution	3	NOT REGULATED		Anterior Chamber Infusion
b) To investigate the effects of pressures within the near physiological range	3 3 3	30 22 8	15 15 15	Anterior Chamber Infusion Anterior Chamber Infusion Anterior Chamber Infusion
c) To asses the mode of fixative penetration	2	30	15	Carotid Perfusion
d) To investigate the effects of pressures outside the physiological range	3	50	0	Anterior Chamber Infusion

Fig.3.2 A table showing the numbers of animals used, the maintained pressure levels and the mode of primary fixation for the intraocular pressure study.

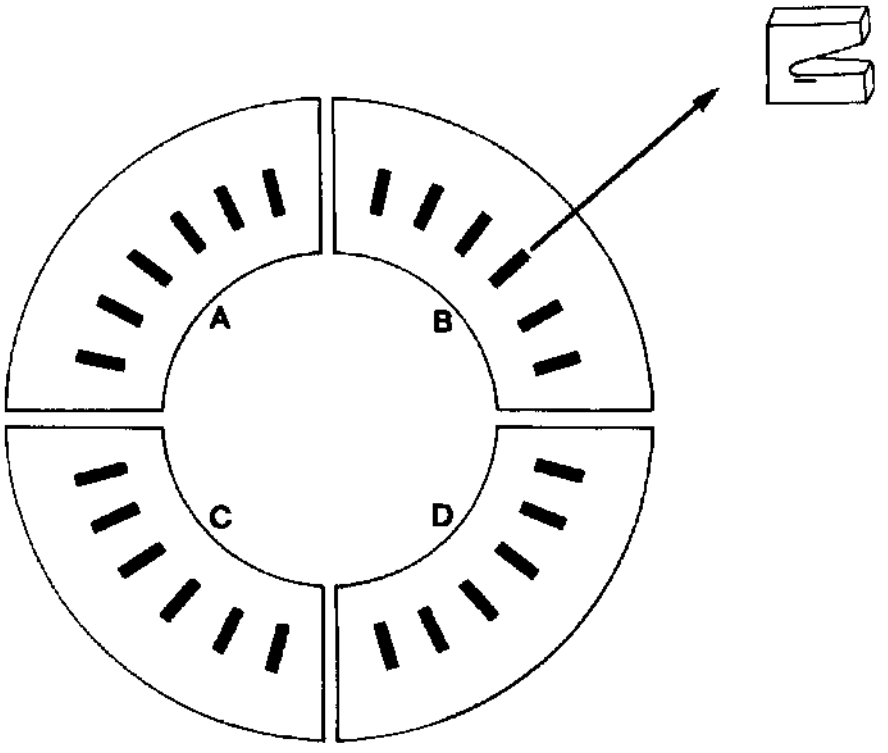

Fig.3.3 A diagram to show the position and location of the tissue blocks taken for electron microscopy. Six segments of limbal tissue were removed from each quadrant.

a Phillips 300 or a Siemens Elmiskop 1A electron microscope.

Thick sections were stained with a filtered solution of toluidine blue in 2.5% sodium carbonate solution which required gentle heating on a hot plate for the optimum staining reaction. Ultrathin sections were either double stained with a saturated solution of uranyl acetate in 50% alcohol (10 - 20 minutes) and subsequent exposure to Reynold's lead citrate solution (5 minutes) or stained in the alcoholic uranyl acetate solution alone (20 - 30 minutes).

3.4 Specific staining techniques for transmission electron microscopy

3.4.1 Introduction

Some blocks of limbal tissue, both from "normal" eyes and each of the eyes which were subjected to experimental pressure alteration, were treated by special staining techniques (see appendices 1 - 6) to provide additional information concerning:-

a) the nature of the cell-to-cell attachments and the extracellular materials in the normal outflow apparatus and,

b) the effects of experimental pressure alteration on the cellular relationships and the distribution of the extracellular materials.

3.4.2 Uranyl acetate "en bloc" staining

A uranyl acetate "en bloc" staining procedure was used by Farquar and Palade (1965) and Karnovsky (1967) to emphasise the trilaminar nature of the cell plasmalemmae and therefore to allow better resolution of junctional modifications in the intercellular clefts between adjoining cells. The procedures used in the present study were based on those provided by the previous authors.

For the "en bloc" treatment, segments of limbal tissue were given repeated washes in either distilled water or 25% alcohol in

distilled water and then subjected to a 1% uranyl acetate solution for varying time periods between 2 and 24 hours. The uranyl acetate solution was made up in either veronal acetate buffer (pH 5.0) as used by Farquar and Palade (1965), 0.05M sodium hydrogen maleate - NaOH buffer (pH 6.0) as used by Karnovsky (1967) or distilled water. Thereafter the tissue blocks were dehydrated and embedded in the conventional manner.

Exposure of the tissue blocks to uranyl acetate solutions for longer than 2 hours did not improve the definition of the various constituents of the plasmalemma or the junctional modifications and since, particularly when aqueous uranyl acetate was used, there was evidence of ultrastructural damage after the longest exposures (12 - 24 hours), short exposures (2 - 4 hours) were favoured. Sections treated "en bloc" with uranyl acetate were examined with subsequent uranyl acetate section staining and uranyl acetate staining followed by a 2 or 10 minute exposure to lead citrate. Sections without further staining were also examined.

3.4.3 Colloidal "en bloc" staining

The cationic electron dense dyes, colloidal thorium and colloidal iron (with and without conversion to Prussian blue) were used to demonstrate the presence and distribution of acid mucopolysaccharides in the outflow apparatus (appendices 1, 2, 3, 4 and 6 show the numbers of eyes investigated). The stains react with the charged end groups of the carbohydrate moieties (e.g. hyaluronic acid, sialic acid and chondroitin sulphate) of long chain mucins. The staining procedures are outlined in Fig. 3.4 and were conducted on post-fixed buffer washed tissue prior to dehydration. The method used for thorium staining was outlined by Revel and Leblond (1967) and that for colloidal

a) Colloidal Thorium

1. buffer wash
2. rinse in 3% acetic acid, pH 2.6
3. expose to a 1% solution of thorium hydroxide in 3% acetic acid, pH 2.6, at room temperature (24 hrs)
4. wash in 3% acetic acid to remove non-specific stain

b) Colloidal Iron

1. buffer wash
2. rewash in 12% acetic acid
3. expose to dialysed colloidal iron in 12% acetic acid, pH 1.1 to 1.3, at room temperature (60 - 90 mins)
4. wash carefully in 12% acetic acid

Conversion to Prussian blue (optional)

5. expose to a mixture of 2% potassium ferrocyanide and 2% hydrochloric acid (about 20 mins)
6. wash in distilled water

Fig.3.4 The procedures for colloidal thorium and colloidal iron staining.

iron, with optional conversion to Prussian blue, by Gasic and Berwick (1964). Both procedures demand, for a specific staining reaction, the reduction of tissue pH to non-physiologically low levels. Thin sections were examined after exposure to alcoholic uranyl acetate solution for various time periods, after double staining with uranyl acetate and lead citrate solutions or without section staining.

3.4.4 Ruthenium red staining

Ruthenium red, an inorganic dye, was shown to stain extracellular materials which were probably acid mucopolysaccharides (Luft, 1964, 1971). Because of the fine grain, high resolution and good contrast of the ruthenium reaction product, this stain was used both as an indicator of complex glyco-substances and as an intercellular marker. Since, for optimum staining, ruthenium red must be present in the initial fixative fluid, only baboon and rabbit eyes were available for this part of the investigation (appendix 5). The staining procedure, which was adapted from that outlined by Luft (1964), is shown in Fig. 3.5. When a less intense staining reaction was required (see Chapter 6 section 6.5) the ruthenium concentration was reduced to between 300 and 400 ppm and osmication was restricted to 4 hours. Thin sections were viewed either without subsequent treatment or after 10 minutes exposure to uranyl acetate.

For consistent results it was found necessary to have ruthenium red in each of the tissue processing solutions prior to alcoholic dehydration and the absence of ruthenium red from either fixative solution eliminated the electron dense reaction product from the tissue.

Ruthenium red treatment

1) Fix fresh tissue blocks by immersion in cold ($4^{o}C$) sodium cacodylate buffered glutaraldehyde (2.5% glutaraldehyde in 0.2M sodium cacodylate buffer) containing between 300 and 1,000 ppM ruthenium red. Fixation time can be between 2 and 24 hrs.

2) Wash tissue in 0.2M cacodylate buffer to which has been added the appropriate concentration of ruthenium red.

3) Post fix in a 5% solution of osmium tetroxide and cacodylate buffer containing ruthenium red (4 to 15 hrs).

4) Wash in 0.2M cacodylate buffer containing ruthenium red prior to dehydration and conventional processing.

Fig.3.5 The procedure for staining with ruthenium red.

3.5 Preparation of tissue for scanning electron microscopy

3.5.1 Secondary fixation and storage

The blocks of glutaraldehyde fixed tissue set aside for scanning electron microscopy were buffer washed, post-fixed in 1% buffered osmium tetroxide and then again washed in the appropriate buffer. The tissue which was not dissected and processed immediately was either stored, without prior treatment, in the appropriate buffer or stored in 5% neutral formal saline.

3.5.2 Tissue dissection

Slices of limbal tissue, without further dissection, were used to investigate the cut surface appearance of the outflow apparatus in the meridional plane. With some tissue blocks the inner (uveal) meshwork was examined by dissecting off the iris. To expose the uveal trabeculae a clean cut was made from the iris root to the supraciliary space. Finally, to observe the endothelium which lines Schlemm's canal, the walls of the canal were exposed by cutting towards the corneal endothelium from the anterior portion of the canal and into the supraciliary space from the posterior portion with a razor blade knife ground to the appropriate size. From Fig. 3.6 it can be seen that the dissection leaves two pieces of tissue, one with the endothelium on the corneoscleral aspect of the canal and the other with the endothelium on the trabecular aspect (see Lee, 1971).

3.5.3 Tissue drying

The tissue was dehydrated either by air or freeze drying. Air drying took place in a dessicator at atmospheric pressure and room temperature after the water in the tissue had been replaced by a

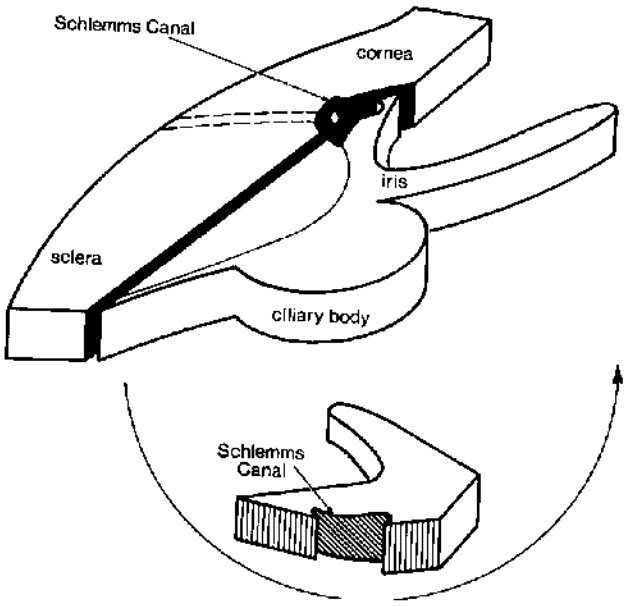

Fig.3.6 Dissection of Schlemm's canal for scanning electron microscopy.

volatile solvent. Water replacement by a volatile solvent was necessary to lower surface tension forces which tend to flatten soft biological tissue and clump structural components together as the gas/solvent phase passes through the material during the drying procedure. Several volatile solvents were used for air drying, each with a lower surface tension than water including ethyl alcohol, acetone, chloroform, amyl acetate and diethyl-ether and of these the latter solvent was used most frequently.

The tissue blocks, after double fixation and a buffer wash were rewashed in distilled water to remove the salts. If the solvent was water soluble e.g. ethyl alcohol and acetone tissue water was gradually replaced through increasing solvent concentrations in water to 100% solvent (30 minutes in each concentration). If the solvent was water insoluble e.g. diethyl-ether and amyl acetate the tissue water was gradually replaced to 100% ethyl alcohol and thereafter the alcohol was replaced from the tissue in increasing concentrations of the water insoluble solvent to 100%. With diethyl-ether, for example, after washing the fixed tissue in distilled water the material was passed through ethyl alcohol/water mixtures of 25%, 50%, 75%, 90% to 100% ethyl alcohol and then passed through ethyl alcohol/diethyl-ether mixtures of 25%, 50%, 75%, to 100% ether.

It was found, however, that all the techniques of air drying which were employed produced varying degrees of flattening and shrinkage to such an extent that the vast majority of the "normal" tissue and all the tissue which was part of the intraocular pressure investigation was freeze dried.

The freeze drying procedure adopted in this study was an adaption from the methods outlined by Boyde and Wood (1969). Fixed tissue blocks were rinsed in distilled water and the superficial

fluid removed on lint free absorbent paper. As quickly as possible the specimens were quenched in liquid arcton 12 (boiling point -39°C, melting point -155°C) which had melted after first being solidified over liquid nitrogen. From here, the tissue was rapidly transferred to a tinfoil boat submerged in liquid nitrogen. Subsequently the boat was placed on the cold plate (precooled with liquid nitrogen) in the vacuum chanber of a Balzars Micro BA 3 freeze drying apparatus. A pressure of less than 1×10^{-5} Torr was obtained as quickly as possible, the tissue was allowed to warm up and, after 24 hours, the specimens were removed. Because the tissue was allowed to warm up, the tissue dried both by sublimination (gas/solid phase) and probably by evaporation (gas/liquid phase). Although this process involves the risk of tissue distortion and the formation of ice crystal artefacts (these artefacts are discussed in more detail in Chapter 11) the process was relatively quick and the final topographical appearance, generally, was satisfactory. A tissue block 1 - 3 mm thick can take in excess of 72 hours to dry purely by sublimation (Boyde and Wood, 1969).

3.5.4 Coating and viewing of the dried tissue

The dried specimens were removed from the vacuum system and mounted on standard viewing stubs (as recommended by Cambridge Instruments) with silver conducting paint (Acheson Colloids Company) care being taken to mask out excess tissue with the same conductive paint. Finally, before viewing, the mounted tissue was coated with either gold - palladium in an A.E.I. vacuum chamber or with gold in a Polaron splutter coater E 5,000. The specimens were examined at tilts between 0 and 45° in a Cambridge Stereoscan S600. The machine was capable of an optimum resolution between 200 and 300Å and was operated at accelerating voltages between 7.5 and 25KV.

CHAPTER 4

THE MORPHOLOGY OF THE NORMAL PRIMATE AND RABBIT OUTFLOW SYSTEMS

4.1 Introduction

In this chapter, the morphology of the outflow apparatus in the four species (human, baboon, rhesus monkey and rabbit) is described. An assessment and discussion of the findings of previous authors runs concurrent with the description of the normal outflow apparatus.

4.2 Materials and methods

The details of the animals used and the mode of primary fixative entry into the tissue can be seen in appendices 1 - 4. The processing and preparation techniques for light microscopy, transmission electron microscopy and scanning electron microscopy are outlined in Chapter 3.

4.3 The primate outflow apparatus

4.3.1 Species comparison

The light micrographs in Fig. 4.1 show meridional sections through the trabecular meshwork and Schlemm's canal in the human, baboon and rhesus monkey eye. From Fig. 4.2 it can be seen that the most obvious interspecies variation occurred in the topography and prominence of the uveal meshwork, the presence or absence of an operculum (Rohen, Lütjen and Barány, 1967), the prominence of the scleral spur, the thickness and composition of the endothelial meshwork and the frequency of septae which bridge Schlemm's canal.

Iris processes were seen occasionally in thick sections but were more easily identified by scanning electron microscopy. The structures were infrequent in all three species but they were particularly rare in the rhesus monkey anterior chamber angle.

In the human and baboon meshwork the uveal cords were delicate and criss-crossed to form a network of interconnecting strands (Fig. 4.3).

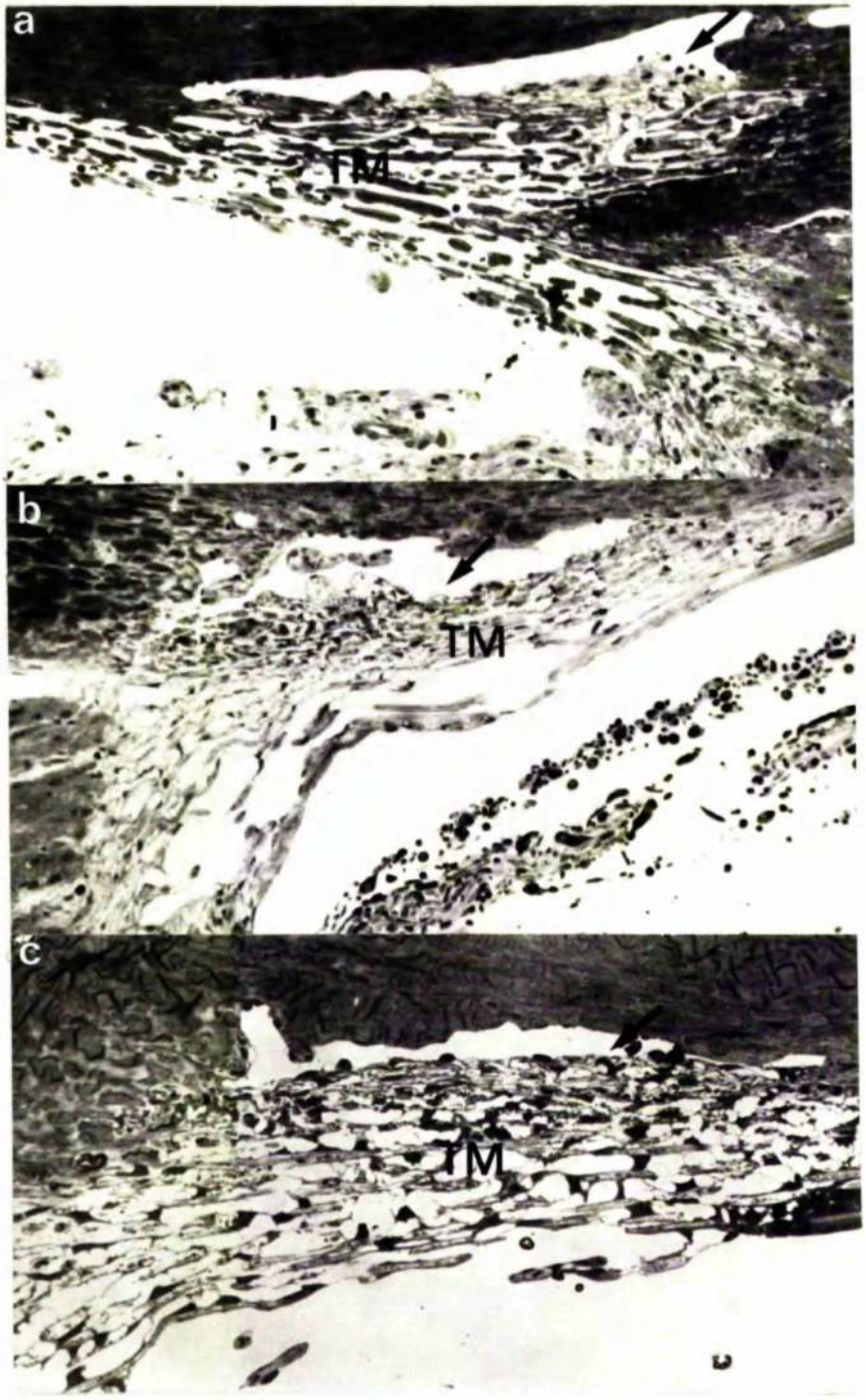

Fig.4.I Schlemm's canal (arrow) and the trabecular meshwork (TM) in a) the human, b) the baboon and c) the rhesus monkey. L.M. (a and b xI50; c x300).

Structure		Species	
	Human	Baboon	Rhesus Monkey
Iris processus	Occasional	Occasional	Rare
Uveal meshwork	Delicate cord-like trabeculae	Delicate cord-like trabeculae	Flatter and thicker trabeculae
Operculum trabeculi	None	Present in some eyes	Present in some eyes
Scleral spur	Prominent	Less prominent	Poorly developed
Outer corneo-scleral meshwork	Substantial	Substantial	Less substantial
Intermedinte zone	Not obvious	Obvious	Relatively extensive
Endothelial meshwork	Significant	Significant	Moderate
Giant vacuoles	Variable sometimes prolific	Variable sometimes prolific	Variable sometimes prolific
Bridging septae	Relatively infrequent	Relatively infrequent	Frequent

Fig.4.2 A table to show interspecies variation in the appearance of the drainage tissues for the 3 primate species.

Fig.4.3 An S.E.M. which shows the cord-like trabeculae which comprise the uveal meshwork of the baboon. (x450).

The holes, formed by the crossing over of the various trabecular cords, were wide in the posterior portion but became progressively narrower towards the anterior insertion at the cornea. Where the innermost layers of the uveal meshwork merge with the corneal endothelium and Descemet's membrane, topographical differences were noted between the human and the baboon. In the human, the cord-like trabeculae became flattened in the transition zone but in the baboon, cord-like elements persisted although these became progressively more scarse and isolated (Figs 4.4 a and b).

Rhesus monkey uveal cords were generally flatter and thicker than their counterparts in the human and baboon. The openings through the trabecular layers were wide but there were fewer than in the other two species (see Chapter 7 Fig. 7.4).

Rohen, Lütjen and Bárány (1967) described a "fibrous membrane" (operculum trabeculi), in the two primate species Macaca irus and Cercopithecus aethiops, which extended from the corneal lamellae to cover the anterior portion of the meshwork. In the present investigation an operculum of variable size was identified in some baboon and rhesus monkey eyes whereas in others there was either a vestigial remnant or it was totally absent. An analogous structure was not observed in the human meshwork (Figs 4.1 and 4.5).

The scleral spur was more prominent in the human than in the rhesus monkey and baboon, therefore the outer corneoscleral meshwork was a relatively more significant and the inner corneoscleral meshwork a less significant portion of the human outflow system than in the other two species (Figs 4.6 a and b).

The endothelial meshwork was a fairly narrow zone of tissue in all three species. In the human, there was a fairly sharp demarcation between the endothelial network of cells and the organised trabeculae

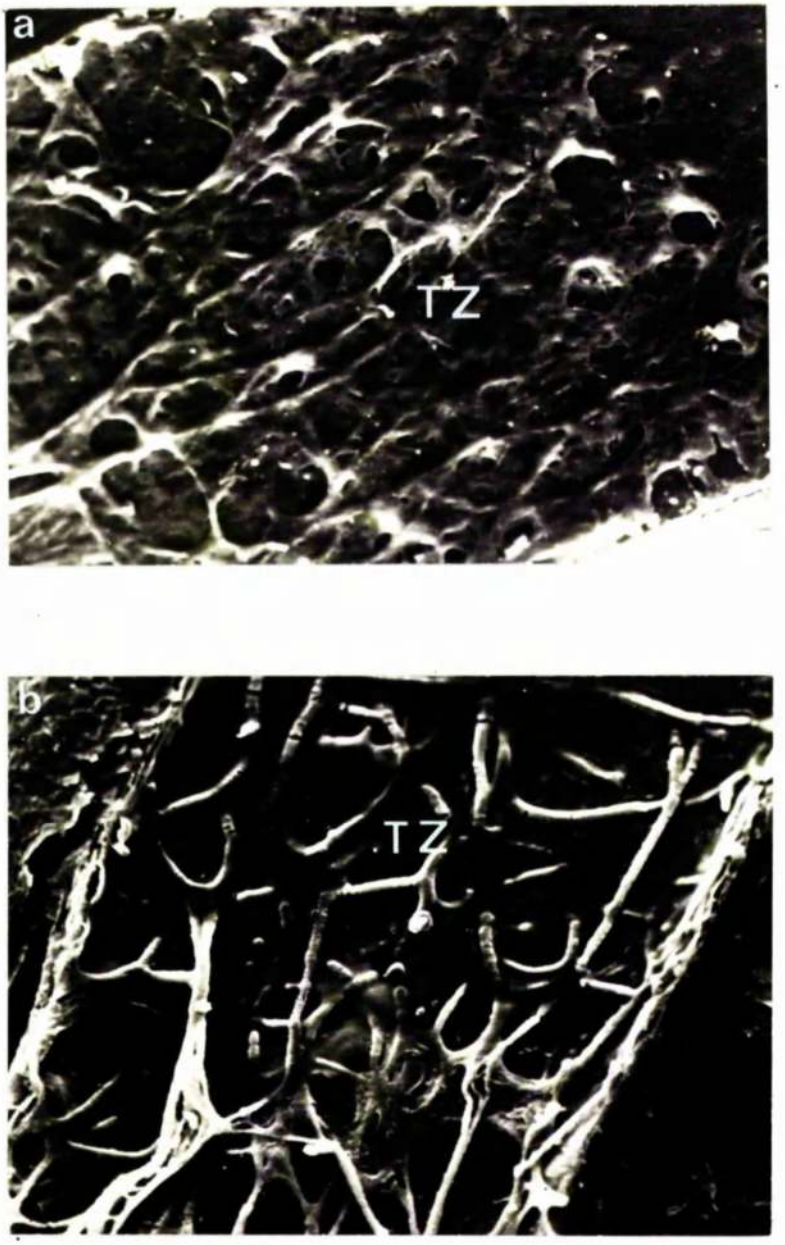

Fig.4.4 The transitional zone (TZ) between the meshwork and the cornea as seen from the anterior chamber angle in a) the human and b) the baboon. S.E.M. (x200).

Fig.4.5 Schlemm's canal and the trabecular meshwork of the baboon. The small arrows indicate the operculum trabeculi. L.M. (x300).

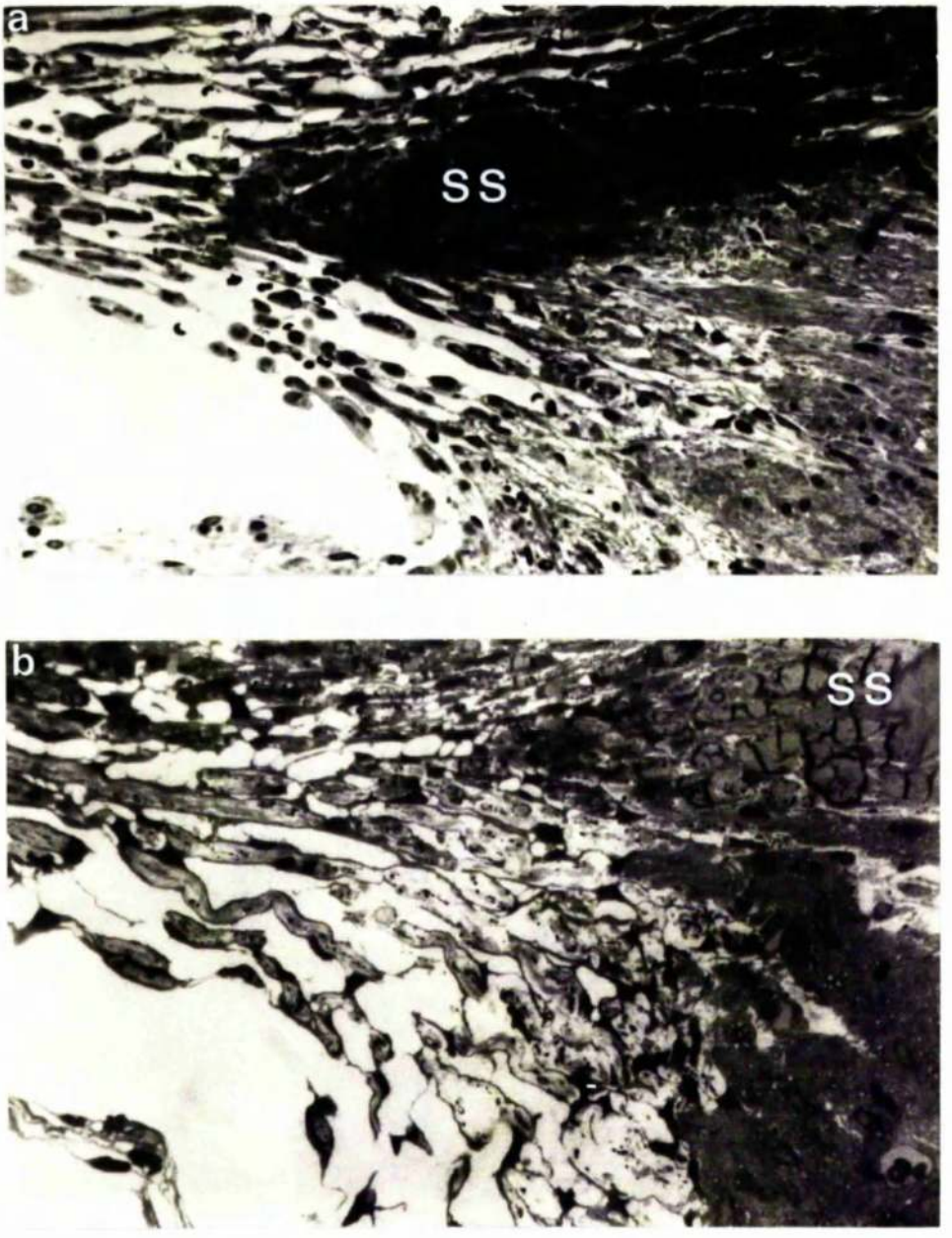

Fig.4.6 The posterior meshwork, scleral spur (SS) and part of the ciliary muscle in a) the human and b) the rhesus monkey. L.M. (a x450; b x550).

of the outer corneoscleral meshwork (Fig. 4.7 a) to the extent that several authors (see Holmberg, 1965; Feeney and Wissig, 1966; Vegge, 1967; Hogan, Alvarado and Weddell, 1971) have described an irregular endothelial border separating the endothelial meshwork from the first intertrabecular space. By way of contrast in the rhesus monkey, there was a gradual transition from the non-trabecular network of the endothelial meshwork to trabeculae with a complete endothelial cover. I have called the region of transition, which consists of trabeculae with poorly organised cores and an incomplete cellular cover, the intermediate zone (Fig. 4.7b). The baboon meshwork had a recognisable but narrow intermediate zone.

In all three primate species, the numbers and size of the giant vacuoles in the endothelium lining the trabecular aspect of Schlemm's canal (Fig. 4.7) varied quite considerably from eye to eye and even within an individual eye at different levels of section. The mode of primary fixation adopted appeared to have some influence on vacuolar frequency. Vacuoles were always present in eyes which were fixed by anterior chamber or arterial infusion but after immersion fixation their numbers were less consistent (giant vacuoles were absent from 2 rhesus monkey, 1 baboon and 1 human eye but their numbers were prolific in other preparations).

The septae which bridge Schlemm's canal were a distinctive feature of the rhesus monkey outflow apparatus but were less frequent in the human and the baboon canal.

Curly collagen and clumps of elastic-like material (see section 4.3.2 for more details) were more prevalent in the extracellular component of the human outflow apparatus than they were in the other two species. These features, plus the greater prevalence of melanin granules in human trabecular meshwork cells were thought to be age

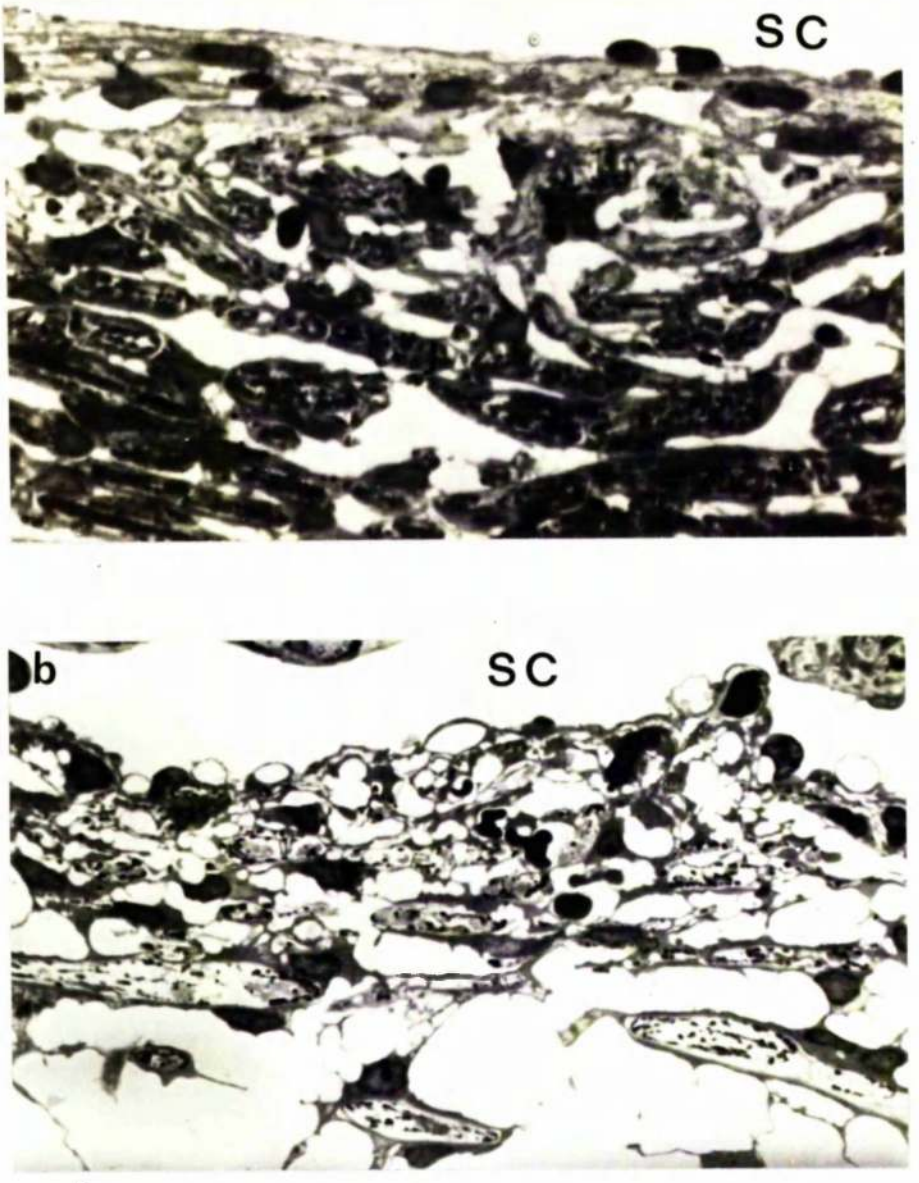

Fig.4.7 Schlemm's canal (SC) and the underlying meshwork in a) the human and b) the rhesus monkey. L.M. (x900).

dependent changes rather than specific species characteristics (Rohen and Lütjen-Drecoll, 1971; Tripathi, 1974). It must be remembered that most of the human eyes came from patients in the sixth and seventh decade whereas the monkey eyes were from young adults. That more non-native cells (e.g. polymorphonuclear, leukocytes, plasma cells, macrophages and lymphocytes) were present in the human tissue than in the other primates could be accounted for by the fact that there was some form of ocular pathology associated with each of the human specimens.

4.3.2 A common description of the architecture and ultrastructure of the outflow apparatus in the three primate species.

Apart from the differences outlined in the previous section there was sufficient conformity between the three species to allow a generalised account of the architecture and ultrastructure of the outflow apparatus. The appearance of the tissue as seen in this investigation differed little from that described by previous authors (see Hogan, Alvarado and Weddell, 1971; Tripathi, 1969a and 1974 for general reviews).

The trabecular endothelial cells had an ovoid nucleus, a moderate number of small mitochondria with dense matrices, a prominent Golgi apparatus and relatively large amounts of rough endoplasmic reticulum*. In addition, cisternae of smooth endoplasmic reticulum, primary lysosomes, lysosomal complexes, multivesicular bodies, cilia, centrioles, lipid vesicles, melanin granules, glycogen deposits, free ribosomes and

---

*FOOTNOTE:- The prominent Golgi apparatus and the large amounts of rough endoplasmic reticulum were taken by Tripathi (1974) to be an indication of high metabolic activity. Hogan, Alvarado and Weddell (1971) thought that the endothelium may be involved in active synthesis of extracellular materials.

microtubules were observed on occasion (Figs 4.8 to 4.11). Both smooth and coated micropinosomes were numerous but were particularly obvious close to the cell plasmalemma. Microfilaments (50-70 Å in diameter and of indeterminate length) were a distinctive feature of the trabecular endothelial cells. The filaments were arranged in bundles and, except in cytoplasmic processes, their orientation was such that most bundles were cut transversely in meridional sections and longitudinally in tilted frontal sections (Fig. 4.14).

The endothelial cells generally formed a complete trabecular cover, however the trabecular organisation was lost prior to the fusion of trabecular elements with corneal lamellae and Descemet's membrane. An incomplete cellular cover on the trabeculae was a feature of the intermediate zone between the outer corneoscleral and endothelial meshwork and also at the posterior insertion of the inner corneoscleral and uveal meshwork with the connective tissue lamellae from the ciliary muscle.

Neighbouring trabecular endothelial cells sometimes had tortuous zones of apposition (Figs 4.8 and 4.10) but a simple overlap or tongue-in-groove association was more common. The intercellular spaces were modified by two types of macular junction (described in detail in Chapter 5). Cellular contact between adjacent trabeculae was established either by process-to-process apposition or by apposition between the more substantial perinuclear cytoplasmic bulges on adjacent trabeculae. On other occasions one endothelial cell was incorporated into the cellular cover of two neighbouring trabecular beams. The various cytoplasmic projections had the effect of creating an extremely tortuous route for the passage of aqueous humour through the intertrabecular spaces.

Tripathi (1969a, 1974) considered that attachment of the endothelial cover to the extracellular component of the trabeculae was enhanced by

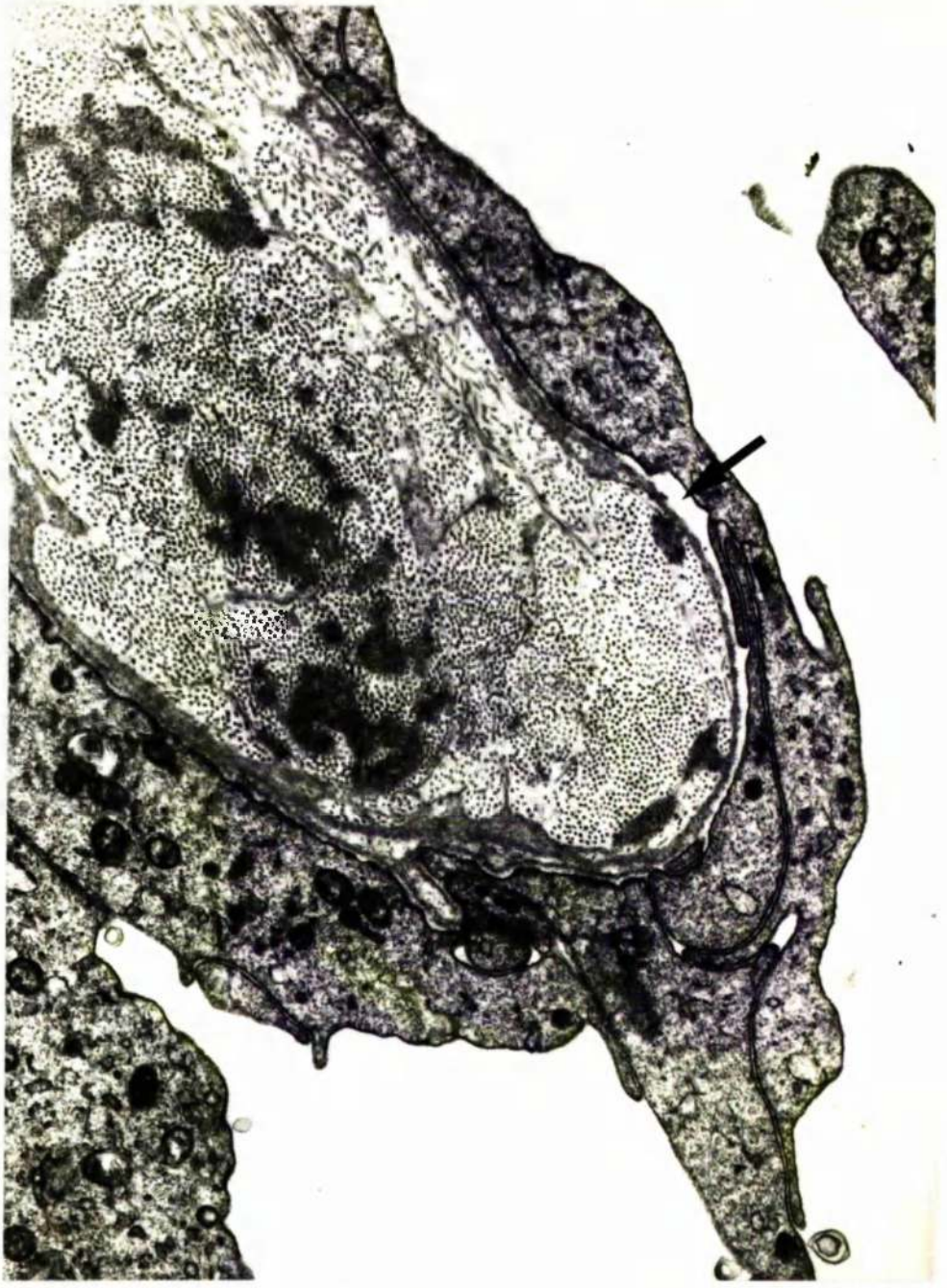

Fig.4.8 Part of a uveal trabecula from the baboon trabecular meshwork. The arrow indicates a region where the cellular cover is not in contact with the basement material. T.E.M. (xI8,000).

Fig.4.9 A node formed by two uveal cords in contact. One cord is sectioned longitudinally (A) while the other appears in cross section (B). Elastic-like material is indicated (arrow). Human tissue, T.E.M. (x36,000).

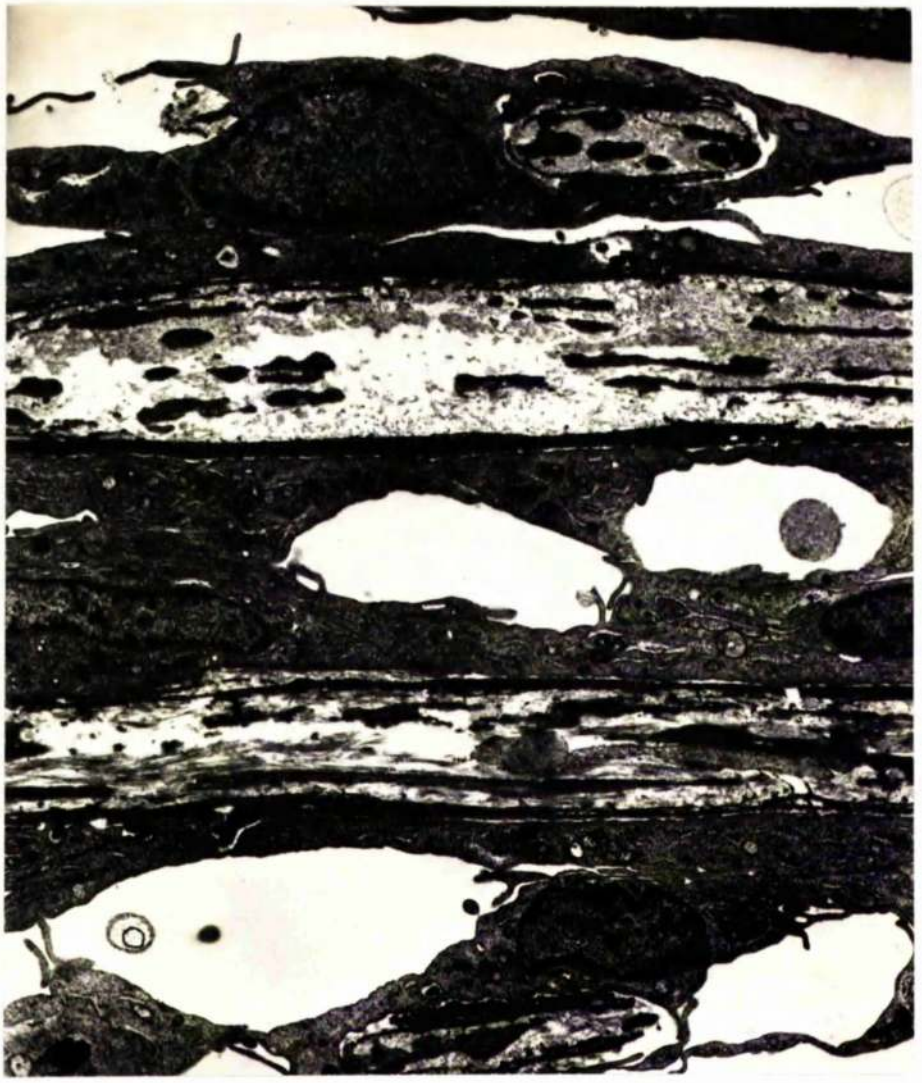

Fig.4.IO Corneoscleral trabeculae from the baboon meshwork. T.E.M. (x6,500).

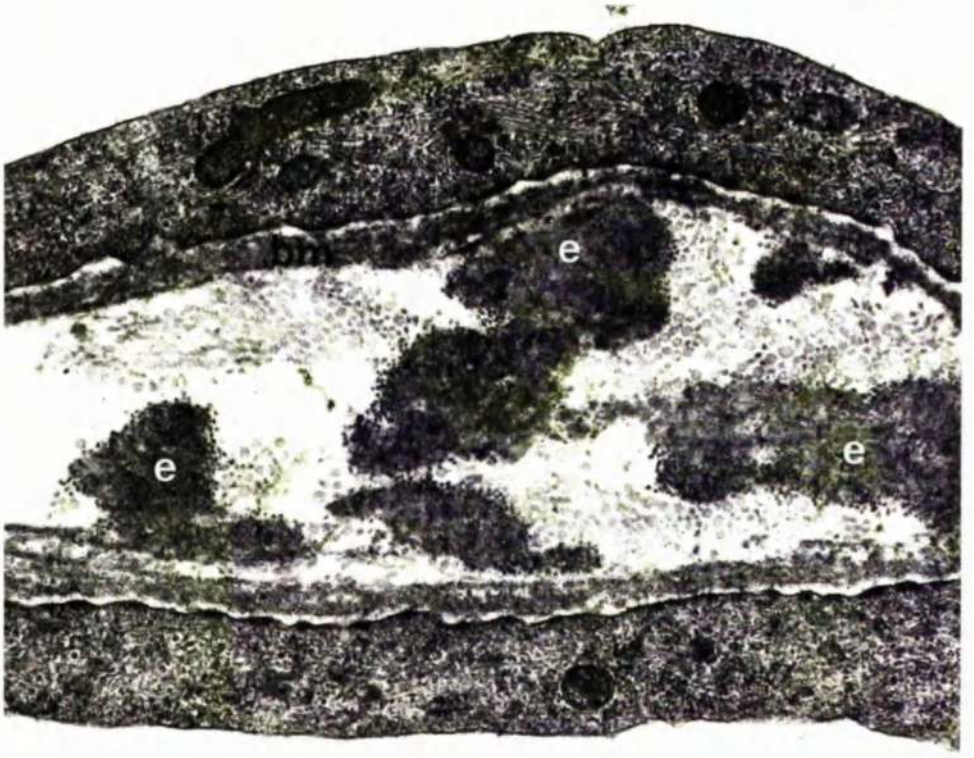

Fig.4.II Part of a rhesus monkey corneoscleral trabecula, clumps of elastic-like material (e) and basement material (bm) are indicated. T.E.M. (x25,000).

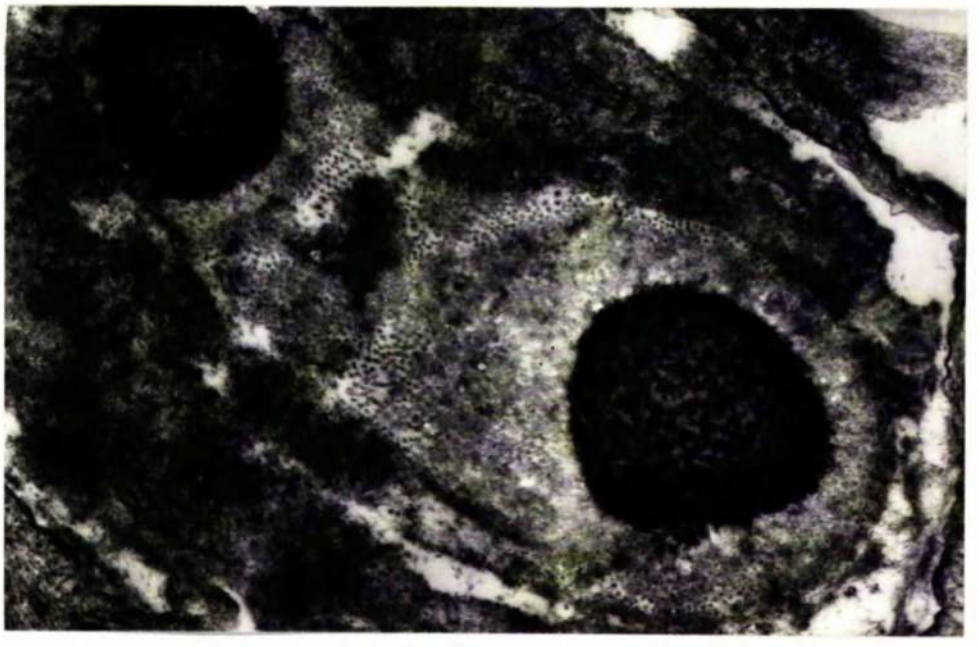

Fig.4.I2 Clumps of elastic-like material, after uranyl acetate "en bloc" treatment and subsequent uranyl acetate section staining, from a human corneoscleral trabecula. T.E.M. (x43,000).

rather insignificant hemidesmosomes. In the present study small densifications were seen on the trabecular surface of the endothelial cells (Fig. 4.13) and these appeared to be associated with a rather indistinct web of fine fibrils present in the superficial cytoplasm (Figs 4.13 and 4.15). Although the densifications could be rather poorly developed hemidesmosomes, a similar arrangement of superficial fibrils and surface densifications has been described in fibroblasts (see Curran, 1967) where the fibrils were thought to be strands of tropocollagen and the densifications were the sites for their extrusion into the extracellular space.

A much more effective adhesive device was the cytoplasmic projections or "pegs" which extended from the endothelial cells into the intracellular materials of the trabecular cores. The pegs have been mentioned by previous authors (Spelsberg and Chapman, 1962; Tripathi, 1969a, 1974) but, as yet, they have not been described in detail. They contained few cytoplasmic organelles but did have a prominent fibril content which appeared to be an extension of the superficial web. The cytoplasmic pegs could be subdivided into four arbitrary groupings:-

a) Small projections (0.1 to 0.5 μm long) which terminated within the basement material (see Chapter 6 Fig. 6.4a). This type was prevalent in the inner corneoscleral meshwork where the basement layer was thick.

b) Pegs (0.3 to 1.0 μm) which frequently had a swollen apex with a narrow stalk (collar stud shaped) and penetrated through the basement material (Fig. 4.15). They were common in uveal and outer corneoscleral trabeculae.

c) Pegs (up to 2.0 μm) which came into association with cellular elements within the connective tissue cores in the larger trabeculae (see Chapter 6 Fig. 6.4b).

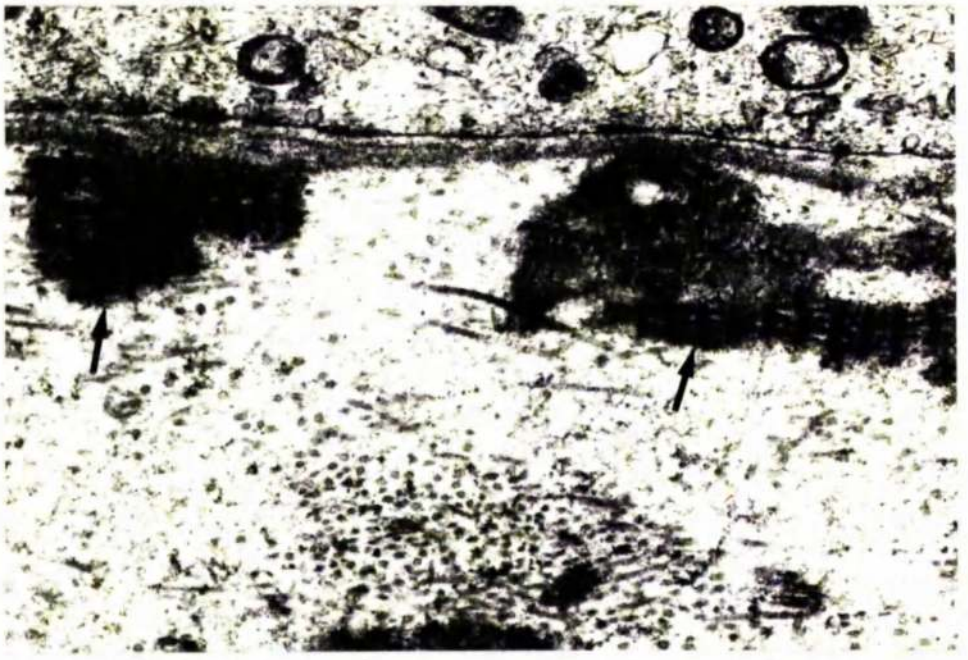

Fig.4.I3 Curly collagen (arrows) in association with basement membrane material in a baboon corneoscleral trabecula. T.E.M. (x45,000).

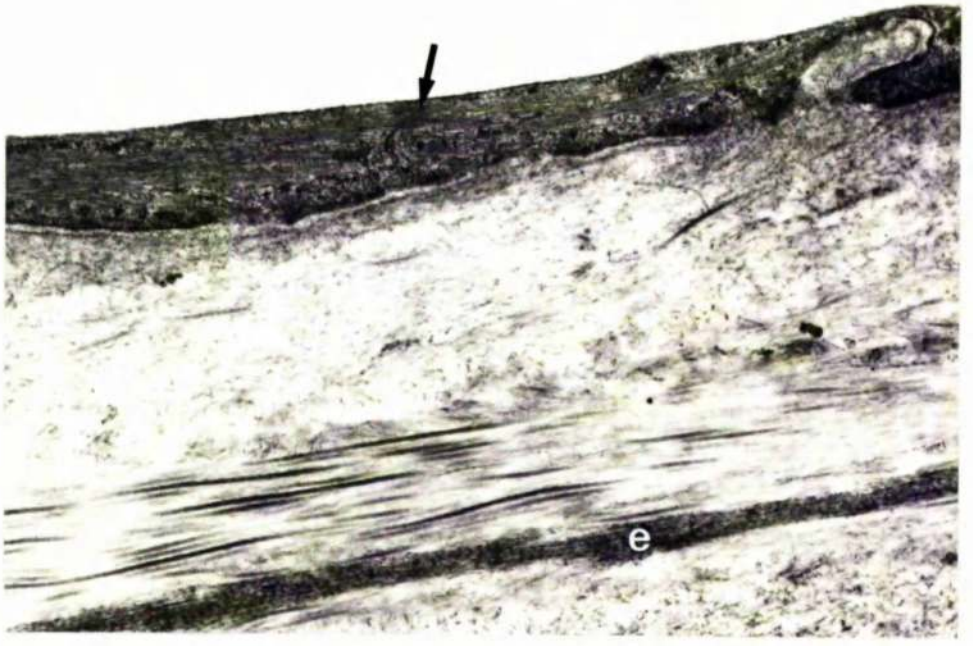

Fig.4.I4 A tilted frontal section through part of a human corneoscleral trabecula. Endothelial microfilaments (arrow) and elastic-like material (e) are indicated. T.E.M. (x22,000).

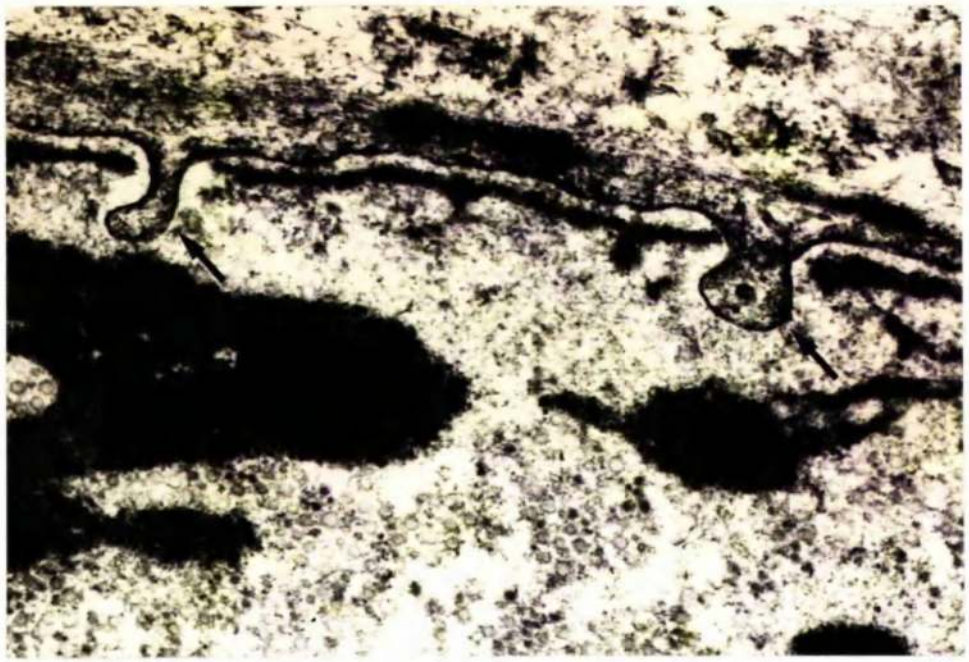

Fig.4.I5 Part of a baboon corneoscleral trabecula to show cytoplasmic pegs (arrows). T.E.M. (x50,000).

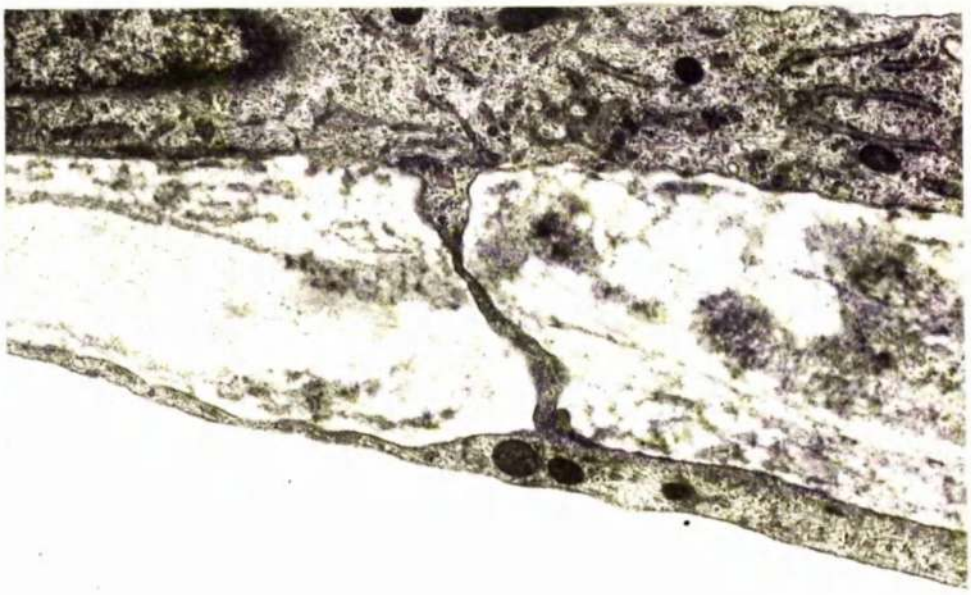

Fig.4.I6 A cytoplasmic process which passes through the trabecular core to make contact with the adjacent endothelial cell. Human corneoscleral trabecula, T.E.M. (x2I,000).

d) Larger cytoplasmic projections (often over 2.0 μm in length) which extended across the trabeculae and made contact with adjacent endothelial cells (Fig. 4.16).

Within the basement material, the two components described by Tripathi (1974), a relatively dense, narrow basement membrane and an underlying, frequently diffuse, basement substance could be distinguished in some regions (Figs 4.8 and 4.14) but not in others (Figs 4.11 and 4.15) As a general rule, the basement zone was thicker in the inner corneoscleral meshwork (Fig. 4.10) than in either the uveal (Figs 4.8 and 4.9) or the outer corneoscleral (Figs 4.11, 4.13 to 16) meshwork. Variation in the width and the closeness of the association between the basement material and the endothelium could be quite considerable within an individual trabecula. Usually the basement materials were more scanty and more loosely associated with the endothelium in regions where the cellular cover was incomplete (e.g. the intermediate zone and the posterior portion of the inner corneoscleral and uveal meshwork) however a similar situation could be found in some trabeculae where, in isolated sections, the cellular cover was apparently intact (Fig. 4.8).

Beneath the trabecular basement material and often within the central collagenous core, there were foci of electron dense material which appeared as plaques in cross section (Figs 4.8 and 4.10 to 4.13) but in longitudinal section were seen as elongated bands (Figs 4.9 and 4.14). The plaques were most prominent in the broad trabeculae of the inner corneoscleral meshwork and, with conventional staining, were either homogenous or had two distinct components - an electron dense amorphous core and a less dense but granular periphery. With uranyl acetate "en bloc" staining, differentiation between the two components was enhanced and the central core no longer appeared amorphous but was seen to consist of a coarse granular material (Fig. 4.12).

Yamashita and Rosen (1964) and Iwamoto (1969) found that the plaques had an affinity for stains which demonstrated elastin. Since the specificity of the staining system was less than ideal, other investigators have been less convinced that there were true elastic fibres in the trabeculae (Garron and Feeney, 1959; Vegge and Ringvold, 1971; Hogan, Alvarado and Weddell, 1971; Agarwal, Singh, Mishra and Khosla 1972). However, it must be considered probable that the plaques do contain elastic elements because Tripathi (1969a) has shown that the material was sensitive to elastase. Tripathi (1969a, 1974), in agreement with Yamashita and Rosen (1964) and Iwamoto (1964), speculated that the elastic tissue was a component of the central electron dense core rather than the peripheral zone.

The collagen fibrils in the trabeculae had a regular 640Å periodicity and measured approximately 150 to 400Å in diameter. Within the uveal cords the fibrils were aligned parallel to the long axis of the trabeculae, so that in meridional sections the collagen was cut either longitudinally or in cross-section and this depended on the orientation of the trabecular beam. To amplify the point, Fig. 4.9 shows a trabecular "node" where two uveal cords cross and are oriented at right angles to each other. In the corneoscleral trabeculae, the fibrils once again were arranged parallel to the long axis of the sheets so that in true meridional sections, the collagen was cut transversely (Figs 4.10, 4.11 and 4.13) and in tilted frontal sections cut longitudinally (Fig. 4.14).

Associated with the collagen fibrils, the elastic-like material and the basement substance were clumps of banded material which was called curly collagen by Garron and Feeney (1959). The material had a regular pattern of alternating light and dense zones with a periodicity of 1000Å. The substance has been referred to by a multiplicity of

names which include "1000 Å banded collagen", "kollagenoid", "long-spacing collagen" and "sheath collagen". Each name implies that the material is collagenous for which, as has been pointed out be Vegge and Ringvold (1971), there is no direct evidence.

In the endothelial meshwork the native cells formed a network by process-to-process connections (Figs 4.17 and 4.18) The cells* compartmentalised the region into a series of interconnecting extracellular spaces which narrowed as Schlemm's canal was approached. The spaces contained a variety of extracellular materials the abundance of which varied both within the same eye at different levels of section and between different eyes of the same species.

The extracellular materials consisted of collagen fibres with a regular 640 Å periodicity, plaques and bands of elastic-like material, curly collagen, aggregates of fine fibrils with diameters which approached 100 Å, deposits of amorphous ground substance and granular material which, in its most organised form, could be seen as a network or web of interconnecting strands (Figs 4.17 - 21, 4.25 and 4.26). In most preparations the distribution of extracellular materials in the spaces of the endothelial meshwork was erratic. Since the various ground elements were retained by a loose framework of cells (for example see Fig. 4.18) the possibility of selective washout during processing must be considered.

Golgi vesicles, rough endoplasmic reticulum, mitochondria and melanin were more abundant in the endothelial meshwork cells (Fig. 4.17) than in the trabecular endothelial cells. Also cilia were more frequently

---

*FOOTNOTE:- Outside the plasmalemmae of the endothelial meshwork cells focal deposits of basement substance were occasionally observed.

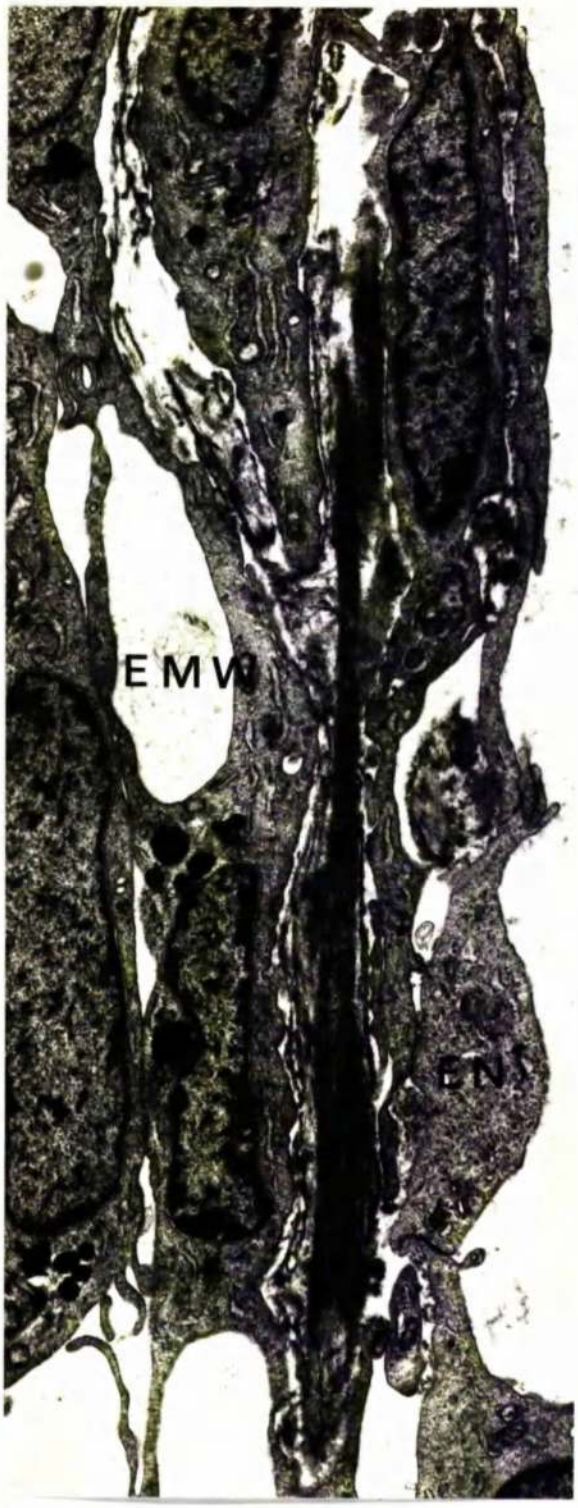

Fig.4.I7 The endothelium (EN) lining Schlemm's canal and the underlying endothelial meshwork (EMW). Baboon tissue, T.E.M. (xII,500).

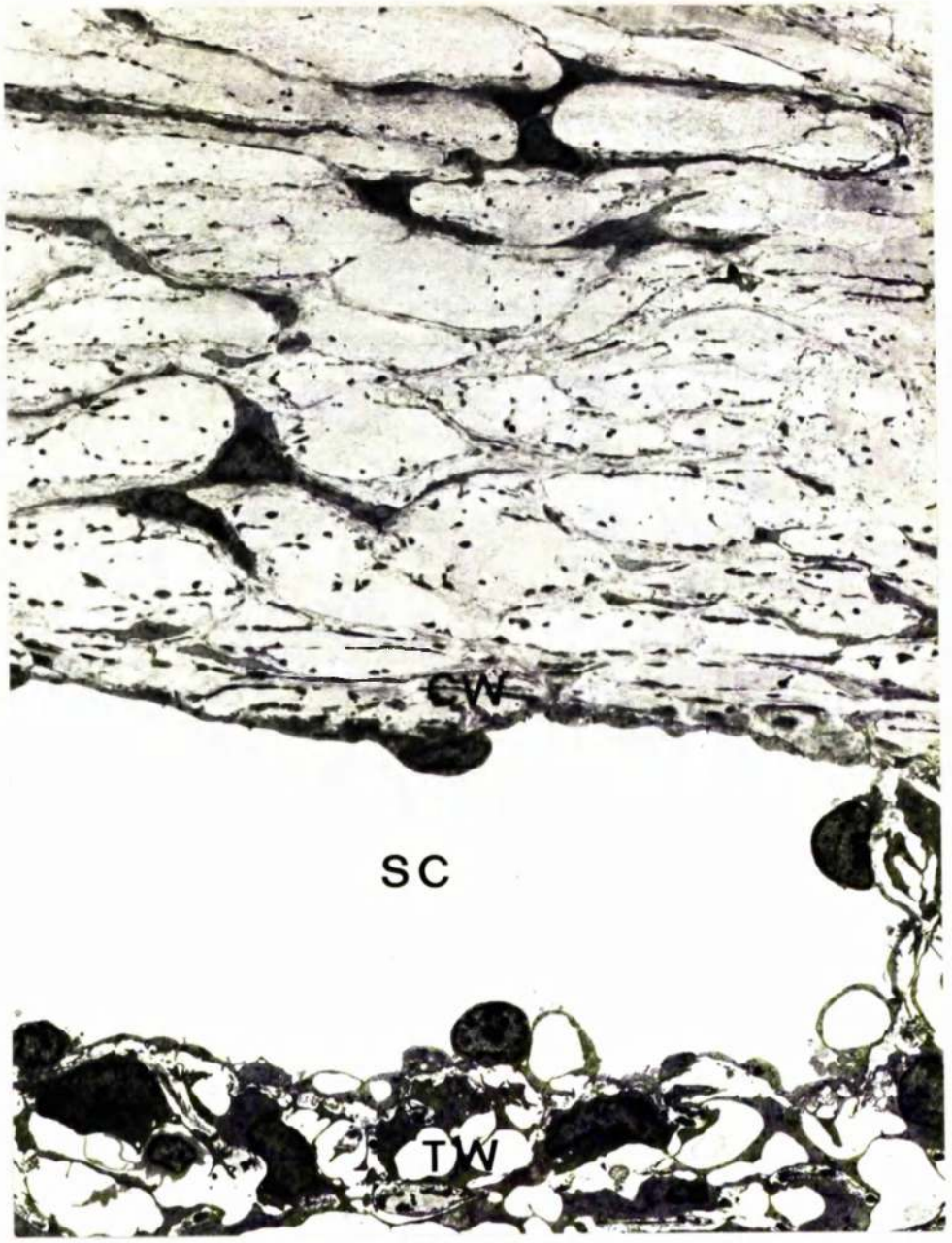

Fig.4.I8 Part of Schlemm's canal (SC) in the rhesus monkey. The canal's trabecular wall (TW) and corneoscleral wall (CW) can be compared. T.E.M. (x2,I00).

Fig.4.I9 Part of the trabecular wall of Schlemm's canal from the human is shown in a). There are 2 openings through the endothelial monolayer (arrows) one opening is empty and the other contains a cell in transit. The opening which contains a cell is shown at higher magnification in b). A minipore c) and a crystalline inclusion body d) from elsewhere in the endothelium are also shown. Human tissue, T.E.M. (a x5,000; b x50,000; c x50,000; d xI00,000).

Fig.4.20 Fibrillar material interspersed with collagen in the rhesus monkey endothelial meshwork. T.E.M. (x28,500).

Fig.4.2I Beneath the endothelium (EN) on the trabecular aspect of Schlemm's canal a network of granular material may be found. Rhesus monkey tissue, T.E.M. (x45,000).

identified in the former than the latter cell type (Fig. 4.22). Typically the cilium was located in a deep groove or depression of the cell surface and the base of the organelle came into close association with a basal body situated close to the plasmalemma (Fig. 4.22a). Cross-sections through the cilia revealed the typical axial arrangement of nine doublets surrounding two solitary microtubules (Fig. 4.22b).

The endothelial meshwork cells contained a modified form of rough endoplasmic reticulum (described previously by Inomata, Bill and Smelser, 1972a and Raviola, 1974) which was not found elsewhere in the outflow system and was therefore a characteristic of the cell type. The cisternae, in cross-section, had a rod-like appearance* and they measured up to 3.0 μm in length by less than 0.1 μm in width. Each rod was limited by a single membrane which had a regular array of polyribosomes on its cytoplasmic aspect. In fortuitous sections the modified reticulum was seen to be in continuity with the membranes of unmodified rough endoplasmic reticulum (Fig. 4.23a). Most rods had an internal pentalaminar substructure which consisted of two electron dense layers separated from each other by an electron lucent core and from the limiting membranes by irregular lucent zones (Fig. 4.23). In oblique section the electron dense layers within the rods had a striated appearance (Fig. 4.23b) indicating a regular periodicity. The rods did occur in isolation but parallel arrays of up to six structures were more typical (Fig. 4.23b).

---

*FOOTNOTE:- Although the cisternae were rod-like in cross-section, they were probably sheet or plate-like in three dimensions which would be consistent with the established three dimensional appearance of unmodified rough endoplasmic reticulum.

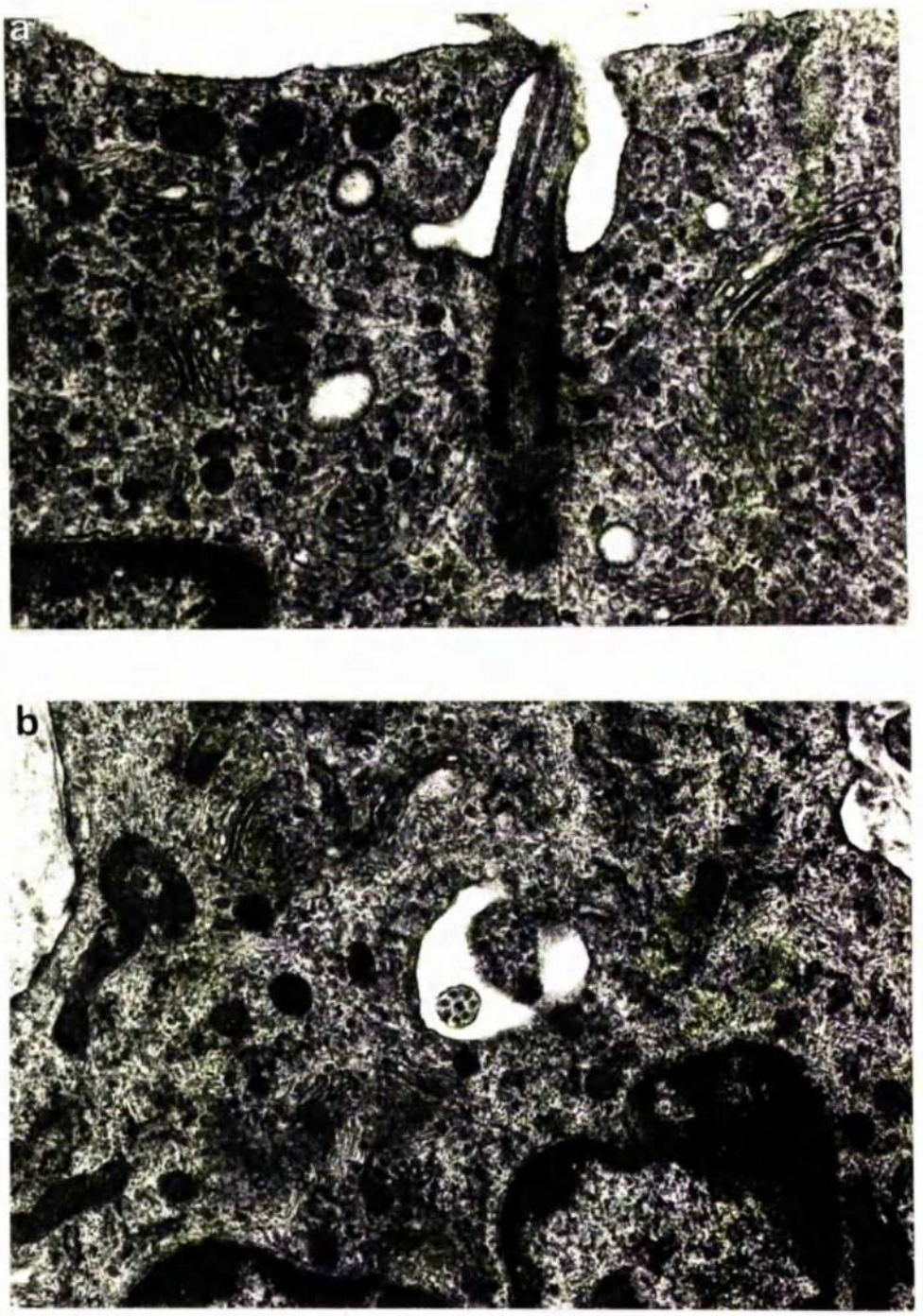

Fig.4.22 Endothelial meshwork cells with cilia. The organelle is cut transversely in a) (human) and in cross-section in b) (rhesus monkey). T.E.M. (a x4I,000; b x27,000).

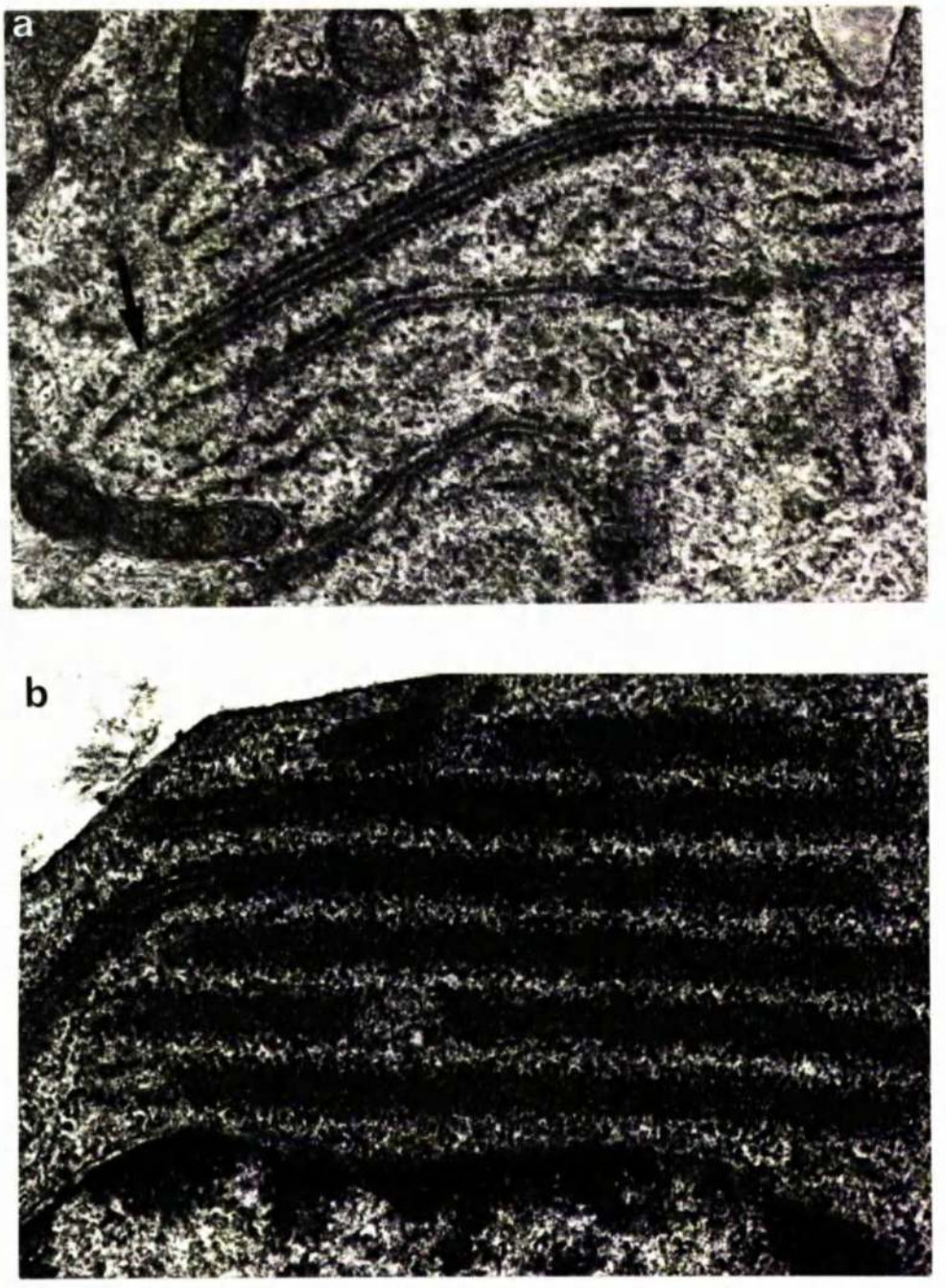

Fig.4.23 The modified rough endoplasmic reticulum found in endothelial meshwork cells cut in a) cross-section and b) oblique section. The arrow in a) indicates continuity between modified and normal rough endoplasmic reticulum. Rhesus monkey tissue, T.E.M. (x50,000).

Cytoplasmic microfilaments abounded in the endothelial meshwork cell cytoplasm (Fig. 4.24) and filaments could, on occasion, be seen to insert into the plasmalemmae. They were present not only in the main cell bodies but also in the cytoplasmic processes which made contact with adjacent meshwork cells (the possible function of the filaments is discussed in Chapter 9).

Where the endothelial meshwork was distended, the cells had a stellate appearance with elongated processes (Fig. 4.18). Elsewhere the cells tended to be aligned with their long axes parallel to the endothelial monolayer bordering Schlemm's canal (Figs 4.17 and 4.19). Junctional modifications (see Chapter 5) were observed sporadically in the regions of process and cellular apposition within the network.

The endothelium lining the trabecular aspect of Schlemm's canal was a continuous monolayer of abutting endothelial cells (Figs 4.17 to 4.19, 4.28 and 4.29). In the lateral borders between neighbouring cells, junctional modifications of the occluding type were usually present (see Chapter 5 for more details).

The endothelial cells were narrow except at the perinuclear zone which produced a prominent bulge into the canal lumen. Vesicles and saccules of the Golgi apparatus, mitochondria and cisternae of rough endoplasmic reticulum were aggregated in the perinuclear cytoplasm but were rare elsewhere in the cells. Lysosomes, multivesicular bodies, lysosome complexes, tubules of smooth endoplasmic reticulum, microtubules, glycogen, lipid vesicles, dense bodies, centrioles, cilia and crystal-like inclusions could, on occasion, be seen in the endothelial monolayer. The crystal-like structures were infrequent but when found on each occasion they had a lattice structure and in cross-section were either rectangular or trapezoid in shape (Fig. 4.19d). The cells were

Fig.4.24 Microfilaments in an endothelial meshwork cell. Human tissue, T.E.M. (x50,000).

engaged in micropinocytotic activity and both coated and uncoated vesicles were recognised. The vesicles were in greater abundance at the luminal than the trabecular aspect of the endothelium (Figs 4.25 and 4.26). Fawcett (1963, 1965) described a form of pinocytosis in capillary endothelia by which fluid was taken into the cells as a result of the folding over of surface cytoplasmic projections (marginal folds) to form intracytoplasmic vesicles. These larger vesicles were noted in the endothelial monolayer but their distribution was sporadic. Microfilaments were abundant throughout the cell cytoplasm and were of comparable diamete (50 - 70 Å) to those found in the cells of the underlying meshwork.

As has previously been mentioned (section 4.3.1) the incidence of giant vacuoles in the endothelium on the canal's trabecular aspect was variable both within the same eye and between different eyes. On occasion the giant vacuoles could be extremely large, up to 14 µm in diameter, (in the investigation conducted by Inomata, Bill and Smelser, 1971a the authors found that some vacuoles were as long as 13 to 15 µm whereas, Tripathi, 1974 stated that some vacuoles may reach 25 µm) but in this study they were usually between 2 and 6 µm in diameter. Each giant vacuole was surrounded by the cytoplasm of a solitary endothelial cell, was membrane limited and usually had an apparently empty lumen (Figs 4.18, 4.26, 4.27a and 4.28). However, there were some vacuoles in whose concavity were flocculent material similar to basement substance (Figs 4.26, 4.27b and 4.28), red cells or wandering cells.

Although, in isolated sections, most giant vacuoles appeared to be intracytoplasmic, a significant percentage had openings on their meshwork aspect (Figs 4.26 and 4.27b) and less frequently on their luminal aspect (Fig. 4.27a). Both types of opening or pore were membrane lined and, typically, the lumen pores were smaller than the meshwork pores. Serial reconstructions showed that giant vacuoles

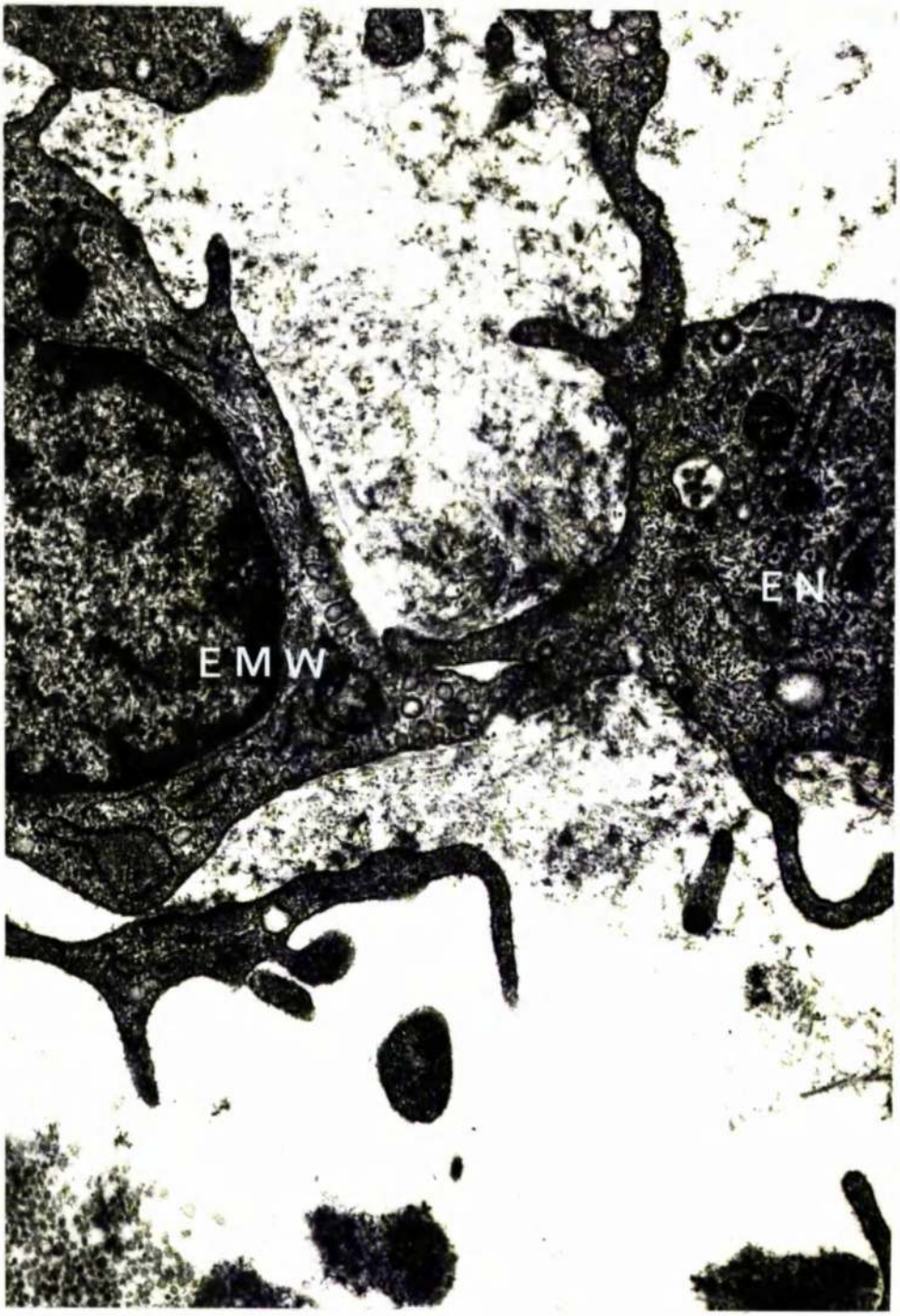

Fig.4.25 Attachment between an endothelial meshwork cell (EMW) and an endothelial cell (EN) in the lining of Schlemm's canal. Rhesus monkey tissue, T.E.M. (x32,000).

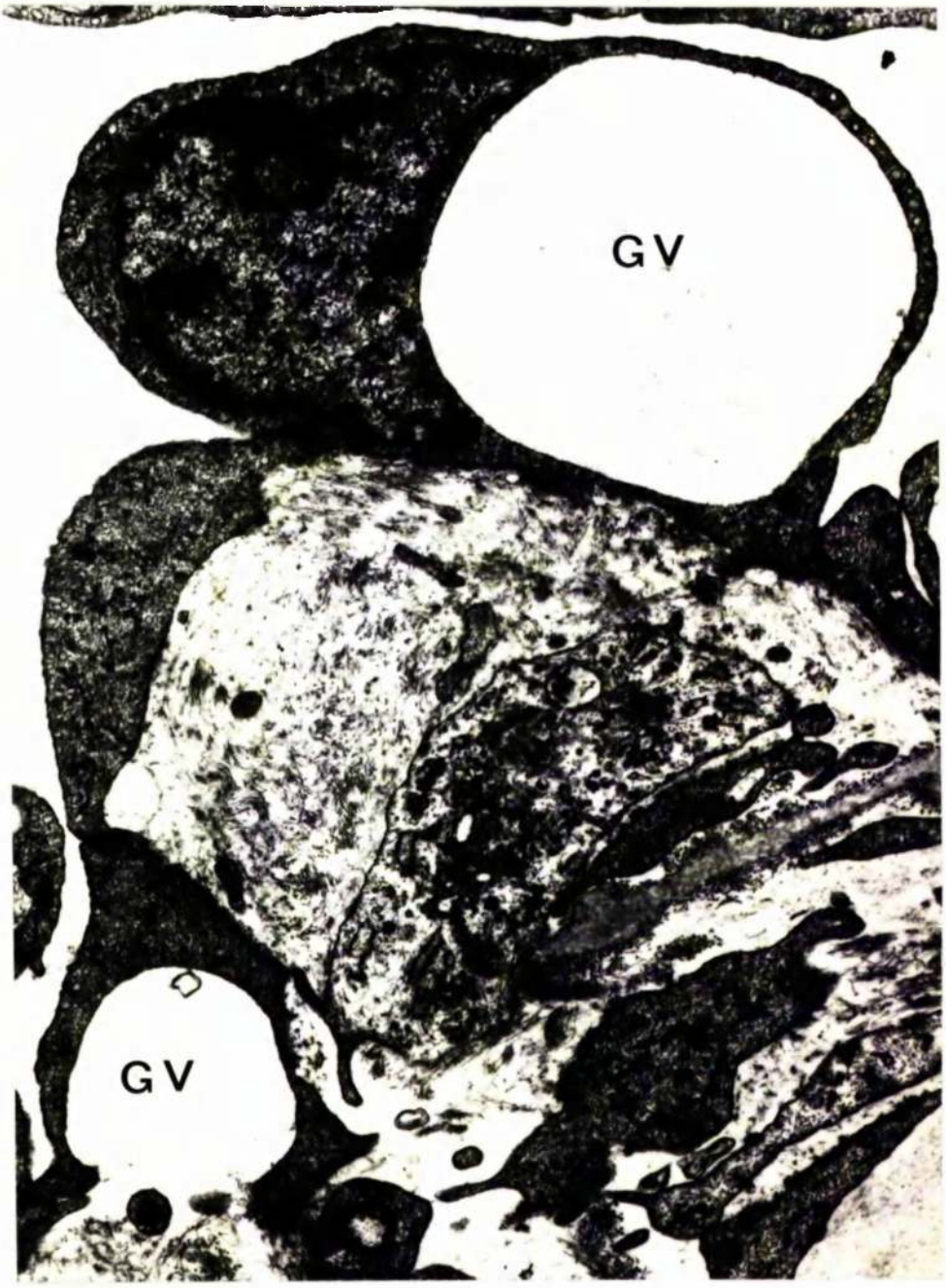

Fig.4.26 Giant vacuoles (GV) in the endothelium lining the trabecular aspect of Schlemm's canal. Human tissue, T.E.M. (xI6,000).

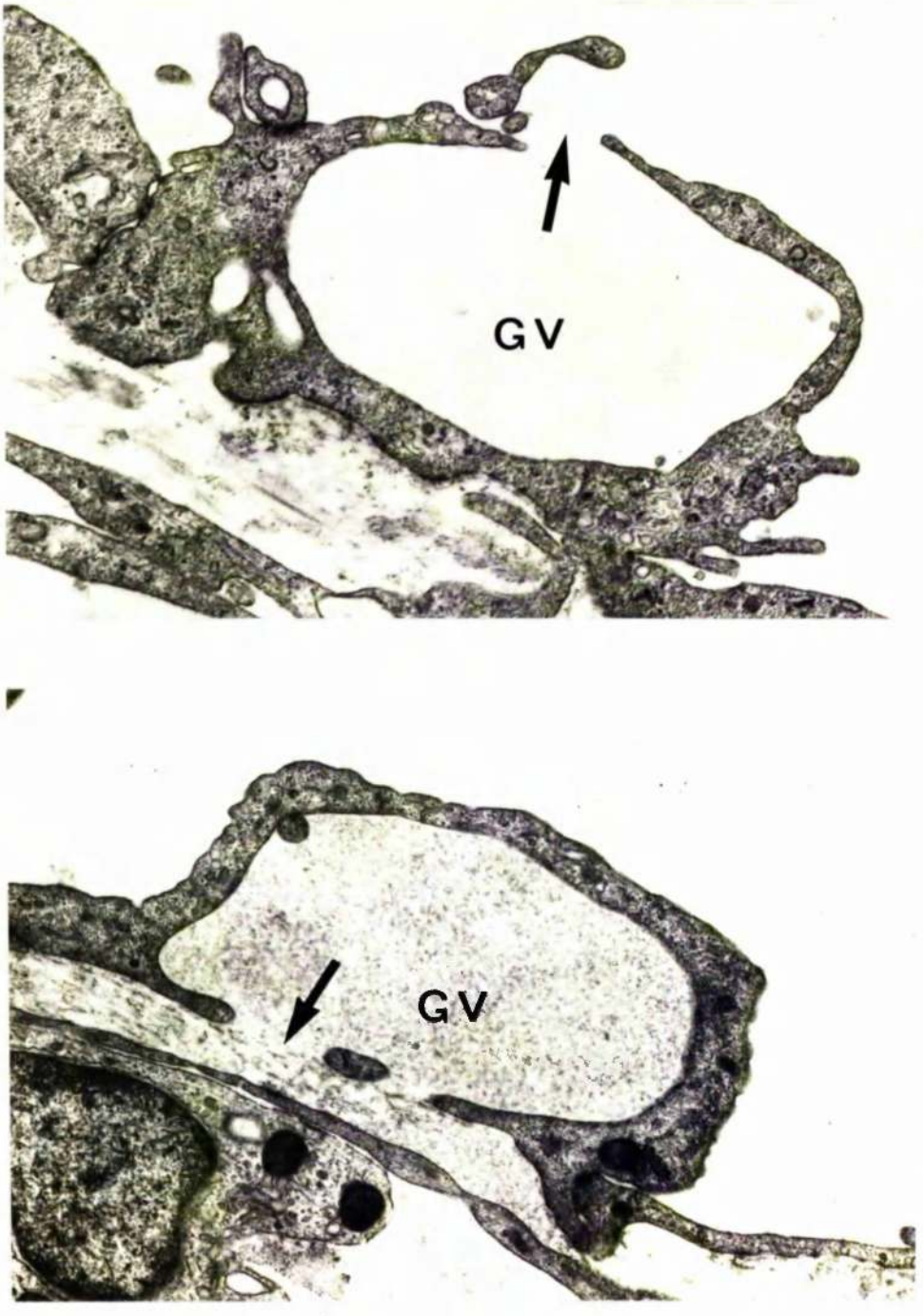

Fig.4.27 Giant vacuoles (GV) in endothelial cells on the trabecular aspect of Schlemm's canal. The arrow indicates in a) a lumen pore and in b) a meshwork pore. Human tissue, T.E.M. (x2I,000).

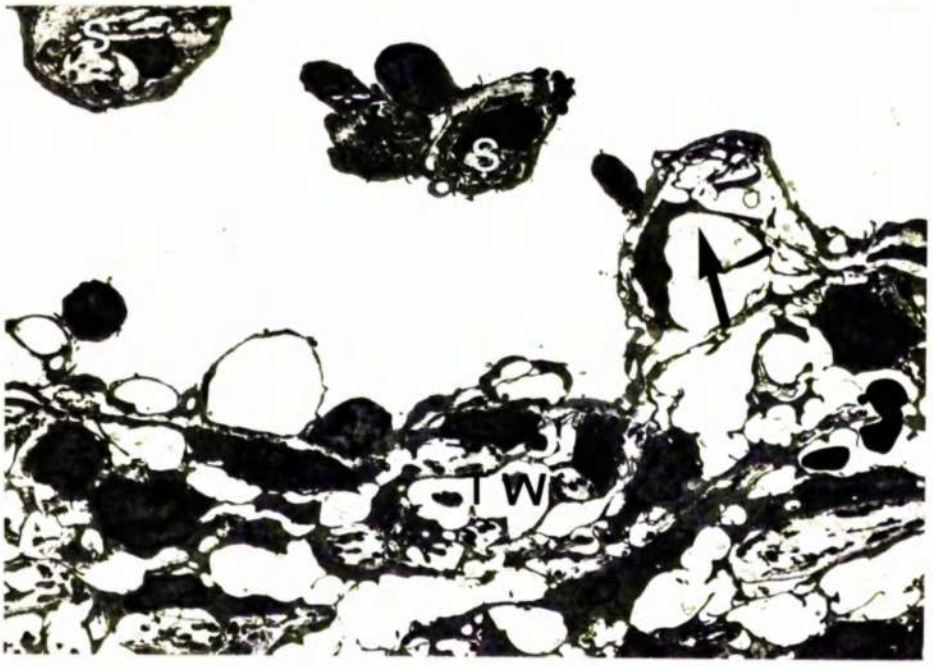

Fig.4.28 A partly sectioned septum appears as islands of tissue (S) within Schlemm's canal. The bulge (arrow) in the trabecular wall (TW) probably represents the trabecular termination of the septum. Rhesus monkey tissue, T.E.M. (xI,600).

were not intracellular vesicles but were invaginations. Most had pores on their meshwork aspect only, but a few were transcellular channels with pores on both surfaces. As such, the ultrastructural description of the vacuolar structures is in good agreement with that provided by previous morphologists (see Kayes, 1967; Inomata, Bill and Smelser, 1972a and Tripathi, 1974) who considered that the vacuolar transcellular channel may serve as an outflow pathway for aqueous humour (see Chapter I). Fink, Felix and Fletcher (1972) were of the opinion that many vacuoles represented dilatations of the intercellular cleft, this is not borne out by the present study. Some vacuole-like intercellular swellings were noted but they were rare and at the fine structural level could easily be distinguished from "true" giant vacuoles.

Openings were sometimes found in the narrower portions of the endothelial cells* and were either empty (Fig. 4.19a) or contained a wandering cell in transit (Figs 4.19a and b).

An occasional feature of the narrow marginal regions of the endothelial cells (and the attenuated cytoplasmic shell surrounding the larger giant vacuoles) were small fenestrations (Fig. 4.19c) (called minipores by Inomata, Bill and Smelser, 1972a). The pores measured approximately 0.1 μm at their maximum width and were included in not more than 5 - 6 serial thin sections. The minipores were intracellular and their diaphragm consisted of a single unit membrane in continuity with the plasmalemma of the endothelial cell.

Deep infolds of the endothelial monolayer were thought to correspond to the Sondermann's canals of light histology (see Chapter I).

---

*FOOTNOTE:- Giant vacuoles were generally associated with the perinuclear cytoplasm.

They did not communicate with the intertrabecular spaces and therefore were considered to be invaginations of the canal endothelium into the meshwork (Holmberg, 1965; Vegge, 1967; Tripathi, 1969a, 1974; Inomata, Bill and Smelser, 1972a and others) and not internal collector channels (Iwamoto, 1967a and b).

Small villi or diverticulae projected from the trabecular aspect of the canal into the lumen. In isolated sections the villi appeared as "islands", were roughly circular with a covering of 2 - 5 endothelial cells and contained cellular and extracellular elements similar to those found in the endothelial meshwork (Fig. 4.30).

The endothelial monolayer on the canal's trabecular aspect did not have a distinctive or even a continuous basement membrane but focal deposits of basement material could be found (Fig. 4.20). In the absence of a substantial basement membrane, sub-endothelial deposits of extracellular material and cellular contacts with the underlying meshwork probably served as adhesive mechanisms (Inomata, Bill and Smelser, 1972a; Tripathi, 1974). Inomata and co-workers drew attention to small cytoplasmic processes from the canal endothelium into the sub-endothelial zone which they thought may be important anchoring devices. Processes of this type were a common feature of all the preparations examined in the present study (Fig. 4.25). Cellular contact between the monolayer and the endothelial meshwork will be described in detail in Chapter 9.

The endothelial cells lining the corneoscleral aspect of Schlemm's canal had a similar organelle content to those on the trabecular aspect except that giant vacuoles, non-vacuolar pores, minipores and crystalline inclusions were not present. The cells were more elongated and the nuclei more ovoid than those of the opposing endothelium (Figs 4.18, 4.29 and 4.31). Occluding junctional modifications were present in the lateral borders between the adjacent cells (see Chapter 5). The corneo-

scleral endothelial monolayer did not have the distinctive basal processes which were such an obvious feature of the trabecular monolayer but instead rested on a fairly thick basement membrane (Fig. 4.31). The basement material separated the endothelium from a connective tissue zone, structurally distinct from the deeper corneosclera. The region consisted of 1 to 5 layers of elongated fibroblasts embedded in a compact extracellular matrix (Fig. 4.31). The predominant component of the matrix was closely packed collagen fibrils but varying amounts of elastic-like substance, curly collagen, fine filamentous elements and amorphous material were identified. The three components, endothelium, basement membrane and underlying fibroblast zone, together constituted the corneoscleral wall of Schlemm's canal (see Chapter 2 and Tripathi, 1969a, 1974).

The ultrastructural characteristics of the septae which bridged Schlemm's canal varied according to their proximity to the trabecular and corneoscleral walls. Close to the trabecular aspect, the endothelium encasing the septae had prominent nuclei and occasional giant vacuoles while the core had a similar structure to the endothelial meshwork (Fig. 4.28). By way of contrast, close to the corneoscleral aspect, the endothelium had ovoid nuclei and no giant vacuoles and encased a dense extracellular matrix in which an occasional fibroblast was embedded (Fig. 4.29). Between the two extremes was a zone of gradual transition. Frequently the whole septum was not included in one isolated section so that portions were seen either as islands of tissue in Schlemm's canal or as projections from the canal wall (Figs 4.28 and 4.29).

After dissection, the endothelium on both aspects of the canal were examined by scanning electron microscopy. In all three species the endothelium on the canal's trabecular surface consisted of a mosaic

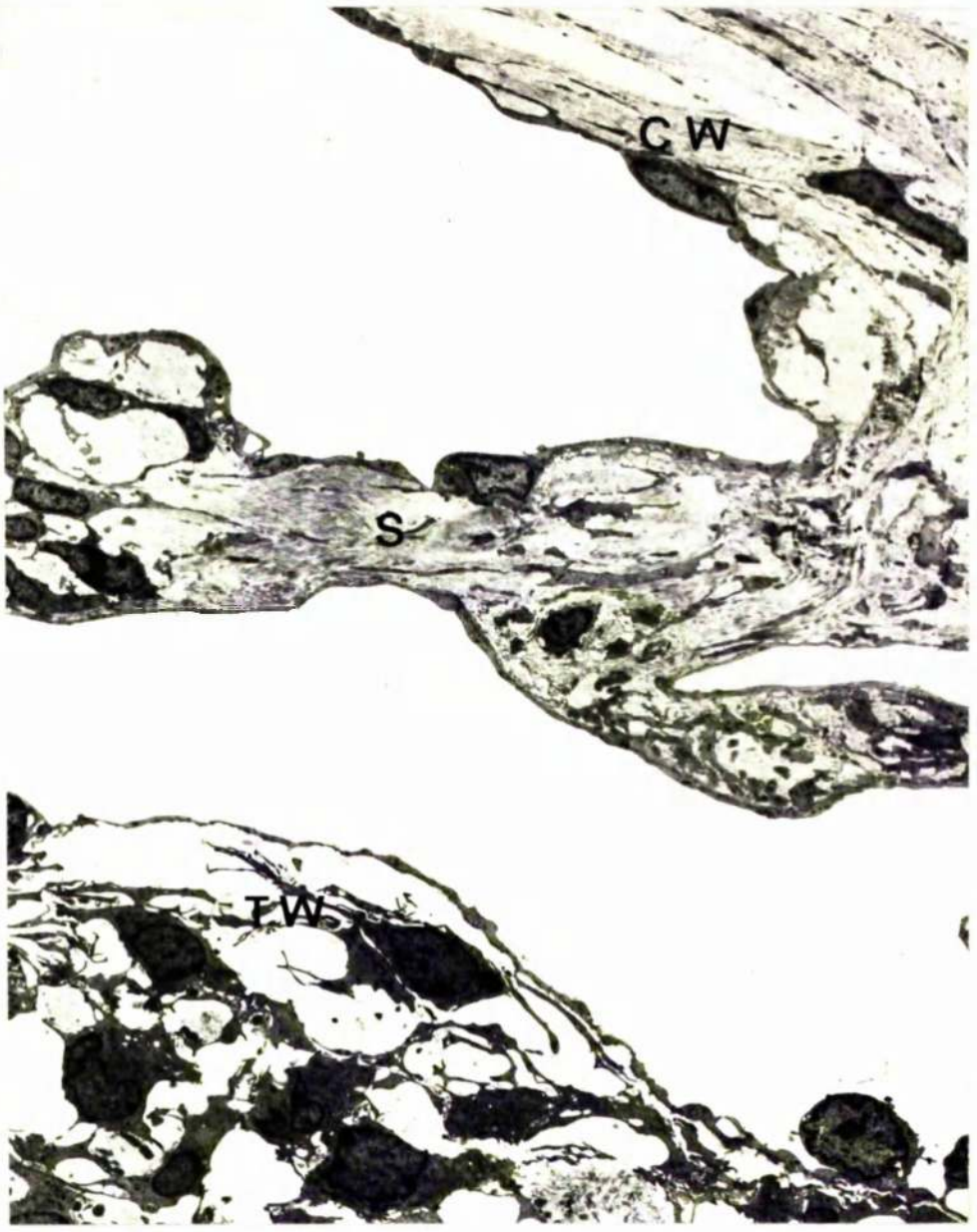

Fig.4.29 Part of a septum (S) projecting from the corneoscleral wall into Schlemm's canal. The tissue of the septum has the characteristics of the corneoscleral (CW) rather than the trabecular (TW) wall. Rhesus monkey tissue, T.E.M. (x2,000).

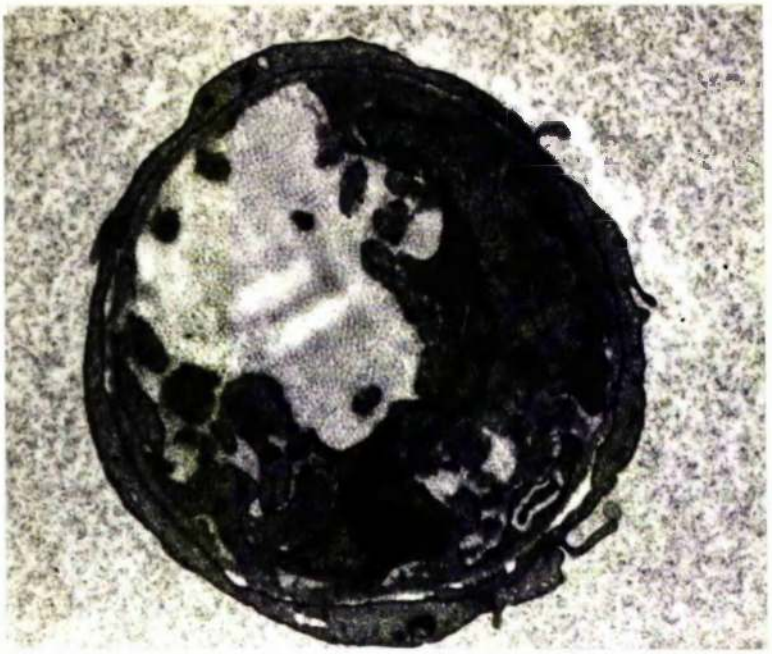

Fig.4.30 A cross-section through a villus-like projection extending from the trabecular wall of Schlemm's canal. Rhesus monkey tissue, T.E.M. (xII,000).

Fig.4.3I Part of the corneoscleral wall of Schlemm's canal (SC) in the baboon. The continuous endothelial basement membrane is indicated by arrows. T.E.M. (x9,500).

of spindle-shaped cells each of which had a central ovoid bulge. The cells were arranged with their long axes in the coronal plane (Fig. 4.32). Two distinct components could be recognised in some of the ovoid bulges, one was a region resistant to surface tension forces while the other was much less sturdy and prone to collapse particularly during air drying (Fig. 4.33). It seemed reasonable to conclude, as others have done (Bill, 1970; Bill and Svedbergh, 1972; Lee, 1971; Segawa, 1973), that the resistant zone was the protrusion of the cell nucleus and the more delicate portion was the location of a giant vacuole. Careful freeze drying reduced the effects of surface tension forces so that vacuolar collapse was, to some extent, prevented. This made the identification of giant vacuoles difficult except where the delicate vacuolar shell was mechanically disrupted by the dissection technique to reveal its hollow interior (Fig. 4.34).

Even after optimum fixation and drying procedures openings with a smooth outline were found in a proportion of the ovoid bulges and also in positions which were remote from the perinuclear bulge (Fig. 4.35). The conclusion made by Bill (1970), Bill and Svedbergh (1972) and Segawa (1974) was that the former were lumen pores in giant vacuoles and the latter were the openings of non-vacuolar transcellular channels.

The endothelium on the corneoscleral aspect of the canal also had a characteristic mosaic of spindle-shaped cells but here the individual units were longer and their ovoid bulges were less prominent. Pores of a similar nature to those described in the trabecular monolayer, were not found in any of the dissections examined.

Both light microscopic and transmission electron microscopic investigations have revealed the presence of nerve fibres in the trabecular meshwork (see Hogan, Alvarado and Weddell, 1971; Tripathi, 1974 for reviews). Although early investigators considered that the

Fig.4.32 The endothelial monolayer (EM) on the trabecular side of Schlemm's canal. The underlying meshwork (arrow) and iris (I) can be seen. Human tissue, S.E.M. (x200).

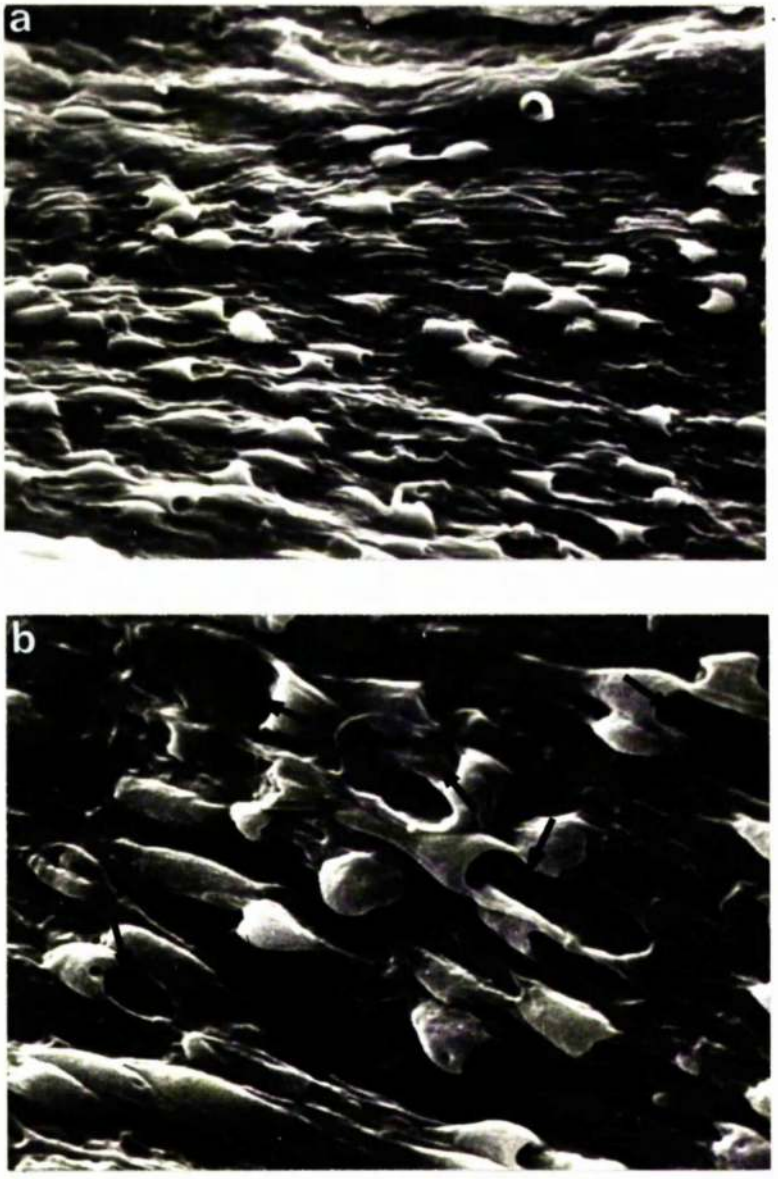

Fig.4.33 The endothelial monolayer on the trabecular aspect of Schlemm's canal after air drying from ethyl alcohol. Low a) and b) high power views of endothelial bulges are show. In b) arrows indicate collapsed (vacuolar) portions of the bulges. Baboon tissue, S.E.M. (a x800; b xI,600).

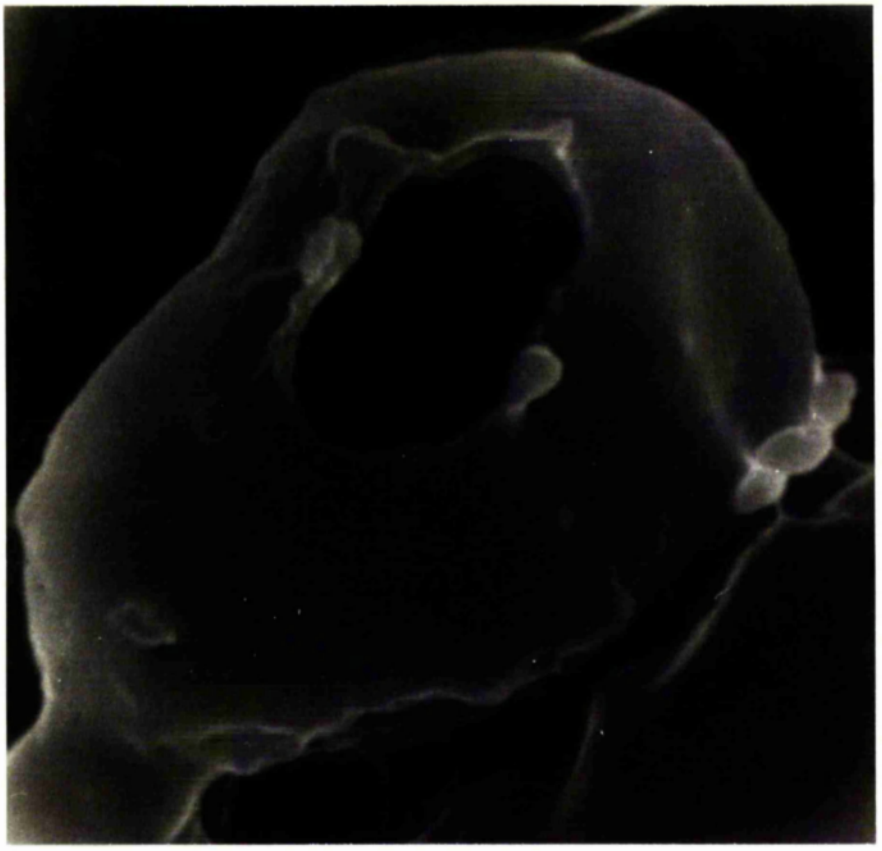

Fig.4.34 An endothelial bulge on the trabecular side of Schlemm's canal which, from an artefactual opening, can be seen to have a hollow interior. Human tissue, S.E.M. (xI2,000).

Fig.4.35 A smooth rimmed pore in an endothelial bulge from the trabecular wall of Schlemm's canal. Rhesus monkey tissue, T.E.M. (x20,000).

fibres merely passed through the meshwork, ultrastructural studies have revealed both specialised and unspecialised terminations within the drainage tissue (Feeney, 1962; Hogan, Alvarado and Weddell, 1971; Inomata, Bill and Smelser, 1972a; Tripathi, 1974; Nomura and Smelser, 1974).

Consistent with the previous studies, both myelinated and non-myelinated fibres were observed in the tissues of the present investigation. The myelinated fibres predominated in the scleral spur but sometimes these fibres were identified in the connective tissue cores of uveal and inner corneoscleral trabeculae (Fig. 4.36). Non-myelinated fibres were more common and were found throughout the outflow system:- in uveal and corneoscleral trabeculae (Fig. 4.37a), in the endothelial meshwork (Fig. 4.37b) and beneath the endothelium lining the corneo-scleral aspect of Schlemm's canal (Fig. 4.38). However the scleral spur and the region prior to the insertion of the trabeculae into the ciliary muscle were particularly rich in non-myelinated fibres and, in these regions, terminals were identified with relative ease (Fig. 4.39). Elsewhere terminals were found only on occasion* and although nerve fibres often followed a route immediately beneath the endothelium lining the trabecular aspect of Schlemm's canal, terminals were not found in intimate contact with the endothelium (a finding which concurs with the more extensive and specific investigations of Tripathi, 1974 and Nomura and Smelser, 1974).

The role of nervous elements in normal meshwork function remains obscure but the possibility that they have some regulatory or influencing action on aqueous drainage must be considered (see Feeney, 1962; Tripathi,

---

*FOOTNOTE:- In a general morphological investigation small and indistinct terminals can be easily missed. This can result in a misleading impression of their frequency.

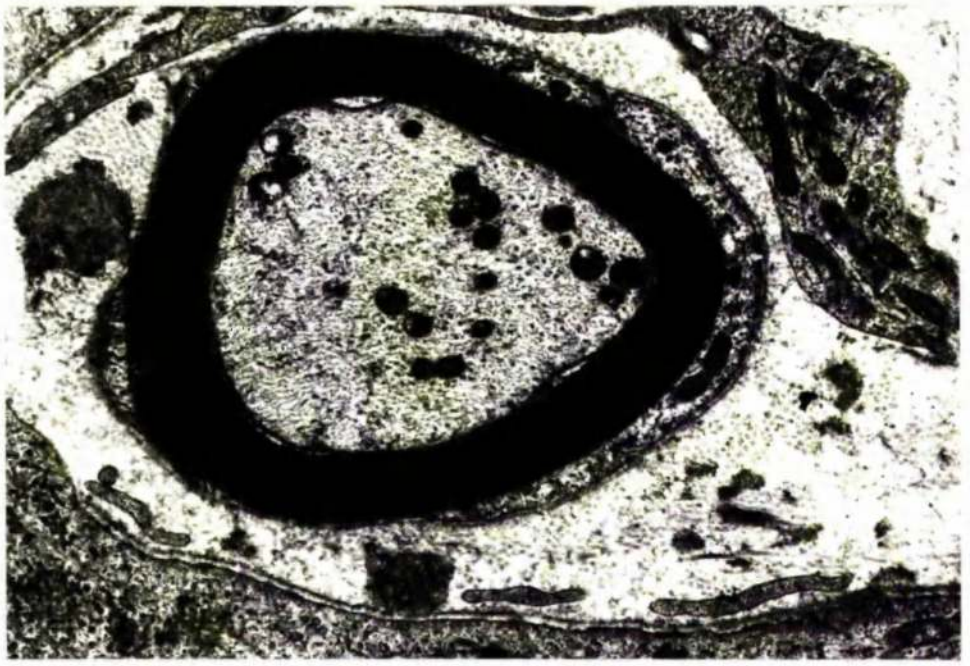

Fig.4.36 A myelinated nerve fibre in the core of an inner corneoscleral trabecula. Rhesus monkey tissue, T.E.M. (xI6,000).

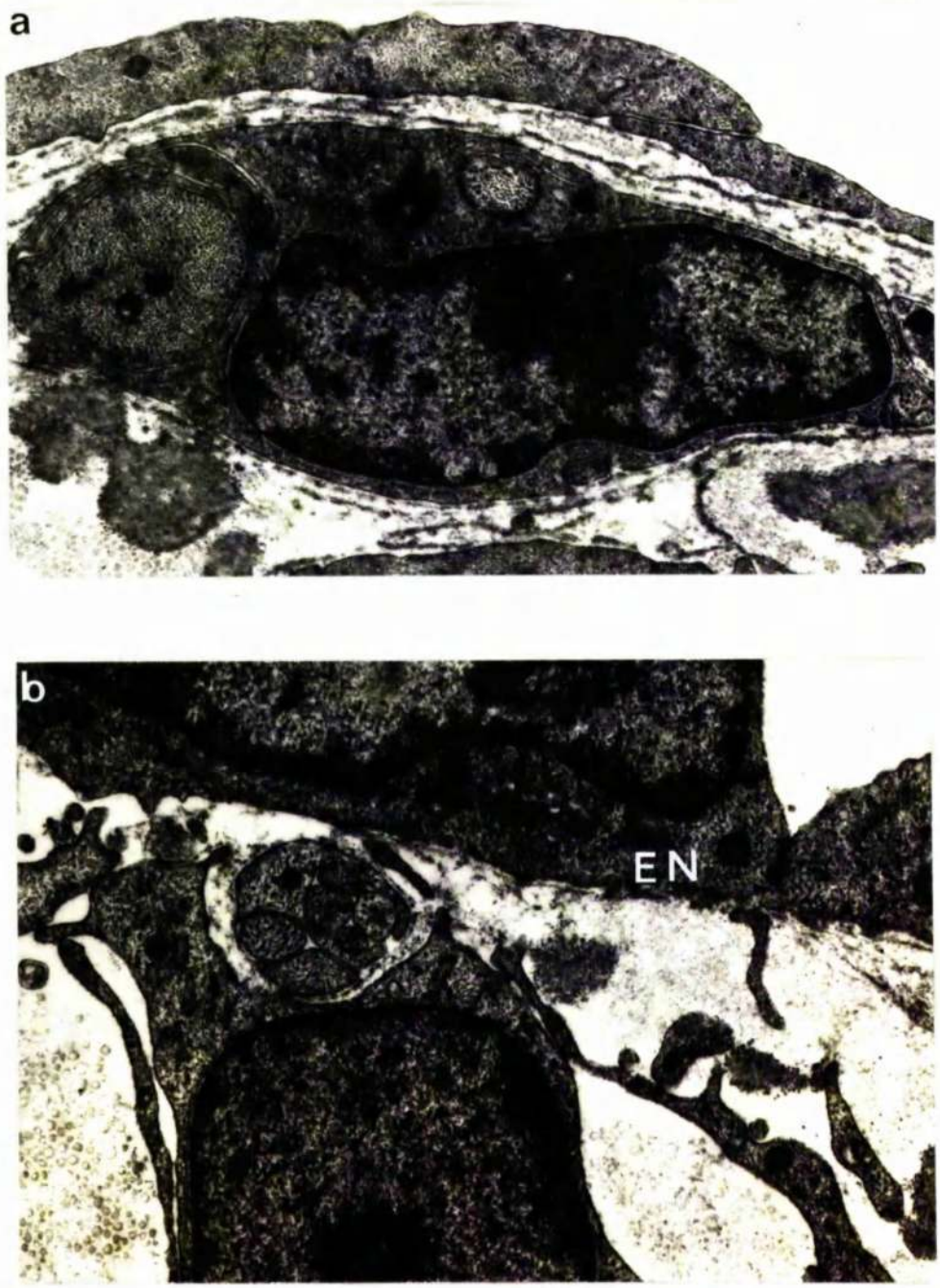

Fig.4.37 Non-myelinated nerve fibres in the rhesus monkey meshwork. a) Shows a fibre within an outer corneoscleral trabecula and b) shows several axons from the endothelial meshwork in close proximity to the canal endothelium (EN). T.E.M. (a x24,000; b x20,000).

Fig.4.38 A small nerve bundle containing two non-myelinated fibres. The bundle lies immediately beneath the basement material of the endothelium lining the corneoscleral aspect of Schlemm's canal. Human tissue, T.E.M. (x22,500).

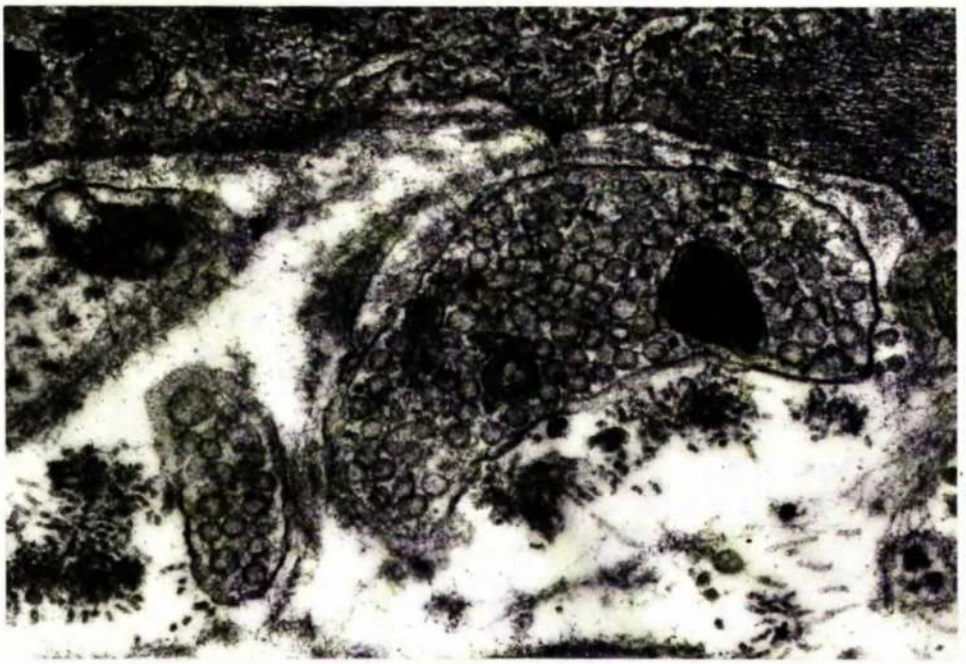

Fig.4.39 Nerve endings, containing numerous electron lucent synaptic vesicles, beneath a meshwork cell. Baboon tissue, T.E.M. (x55,000).

1974; Nomura and Smelser, 1974).

4.4 The rabbit outflow apparatus

The limbal zone of the rabbit eye (Figs 4.40 and 4.41) was characterised by a poorly developed ciliary muscle and a posterior extension of the anterior chamber angle. As such, the angular region was similar to that of other herbivores in which the ciliary muscle is composed of a limited number of meridional fibres. The space which penetrates the fibrous or adventitial component of the ciliary body has been termed the ciliary cleft (see Tripathi, 1974).

In the rabbit eye the corneal endothelium and Descemet's membrane extended over the inner surface of the trabecular meshwork (Fig. 4.40). Thus, the bulk of the aqueous humour in the anterior chamber must first pass into the ciliary cleft and the ciliary adventitia before reaching the trabecular meshes and the drainage vessels. With the absence of substantial ciliary musclature, the patency of the ciliary cleft and the anterior chamber angle was maintained by supporting connective tissue struts (Figs 4.40, 4.41 and 4.42) called pectinate ligaments by Hueck (1839). Under the light microscope the pectinate ligaments were seen as endothelial lined, heavily pigmented structures which originated from the iris and appeared to merge with the corneal endothelium and Descemet's membrane (Fig. 4.40). However, Tripathi (1974) has shown that the connective tissue ligaments penetrated both the endothelium and its membrane to merge with the underlying tissues. By scanning electron microscopy, the ligaments had a conical appearance with a wide base on the iris aspect narrowing to a thin zone of insertion on the limbal aspect (Fig. 4.42). The spaces delineated by the ligaments have been called the spaces of Fontana by various authorities (see Tripathi, 1974) and serve as passageways for the flow of aqueous humour into the

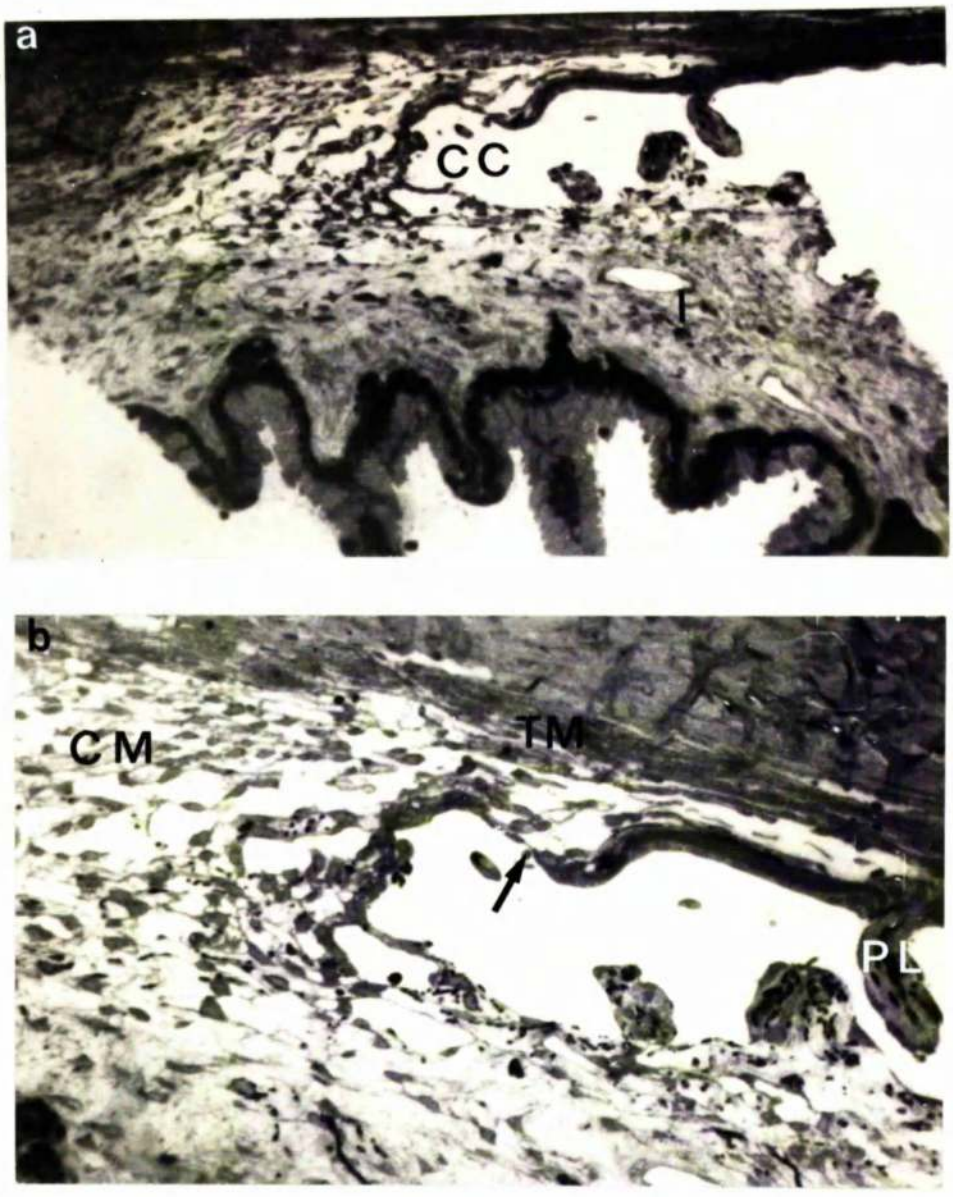

Fig.4.40 The rabbit drainage angle by L.M. at a) low and b) higher magnification. In a) the ciliary cleft (CC) and iris (I) are indicated. In b) the ciliary meshwork (CM) and the trabecular meshwork (TM) can be seen more clearly. An arrow indicates the limit of extension of the corneal endothelium. A partially sectioned pectinate ligament (PL) is seen to penetrate the corneal endothelium. (a x150; b x275).

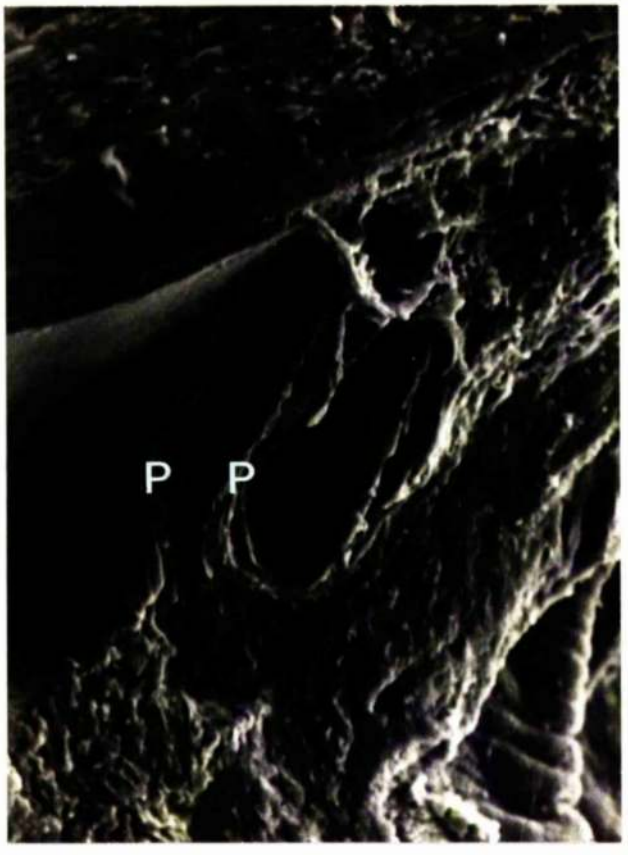

Fig.4.4I The rabbit drainage angle. Pectinate ligaments (P) and an aqueous collecting vessel (arrow) are indicated. S.E.M. (x200).

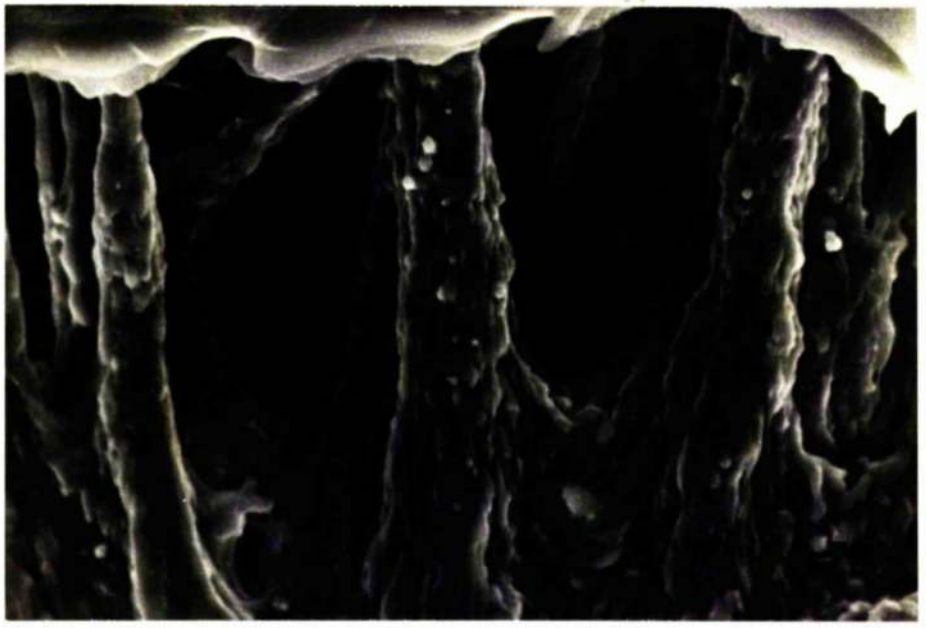

Fig.4.42 Rabbit pectinate ligaments. They have a conical appearance, wide at the iris then narrowing towards their insertion through the corneal endothelium. S.E.M. (x600).

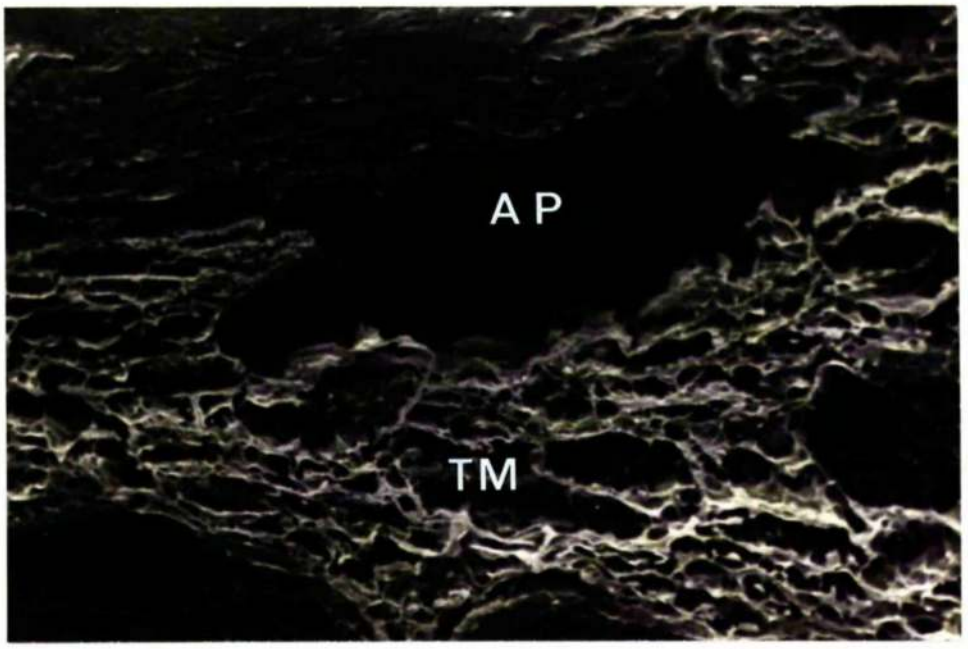

Fig.4.43 A vessel of the rabbit angular plexus (AP) and the underlying trabecular meshwork (TM). S.E.M. (x900).

depths of the ciliary cleft.

Bordering the ciliary cleft was a stroma or adventitia which made up the bulk of the ciliary body (Figs 4.40 and 4.44). Primarily it consisted of layers of adventitial cells between which were occasional smooth muscle cells (absent from the more anterior portion), melanocytes, an occasional blood monocyte, scattered collagen fibrils, clumps of elastic-like material and other extracellular components.

Within the trabecular meshwork, complete encasement of the trabeculae by an endothelial cover was rare. Generally the endothelial cells were arranged in parallel layers which were continuous with the ciliary adventitial cells, but vertical processes from the cells partially limited what loosely could be termed trabeculae. Macular junctional modifications (see Chapter 5) were present in the intercellular clefts of adjoining meshwork cells and adventitial cells. In the meshwork the connective tissue cores of the trabeculae contained the same extracellular components found in primate trabeculae but they were lacking both in organisation and quantity (Fig. 4.45).

Close to each aqueous vessel of the angular plexus there was a narrow zone where the cells formed a network similar to that seen in the primate endothelial meshwork (Fig. 4.46). The aqueous vessels were lined by a continuous endothelial investment and the cells had the ultrastructural characteristics of primate endothelial cells. In agreement with the original findings of Tripathi (1971b) giant vacuoles were observed in some endothelial cells (Fig. 4.46).

The similarity between the aqueous vessels which serve the rabbit, and Schlemm's canal was highlighted with the scanning facility (Fig. 4.43) Although dissection of rabbit vessels was impractical the ovoid bulges of the spindle-shaped endothelial cells could be seen by oblique viewing. Occasionally pores were noted both on the ovoid bulges and in peripheral

Fig.4.44 Layers of rabbit ciliary adventitial cells prior to their merger with the trabeculae. T.E.M. (x4,500).

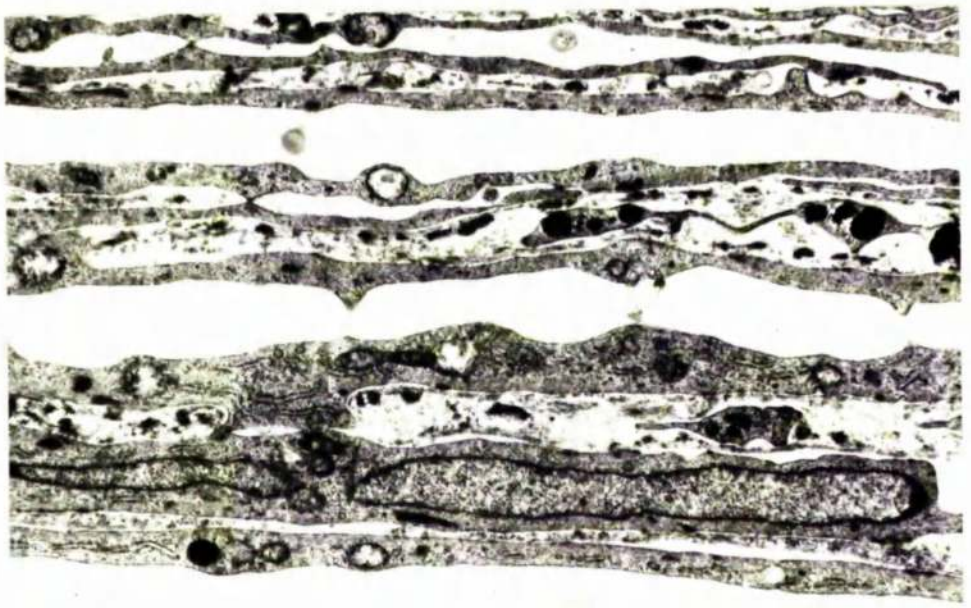

Fig.4.45 Trabeculae in the rabbit meshwork. T.E.M. (xIO,000).

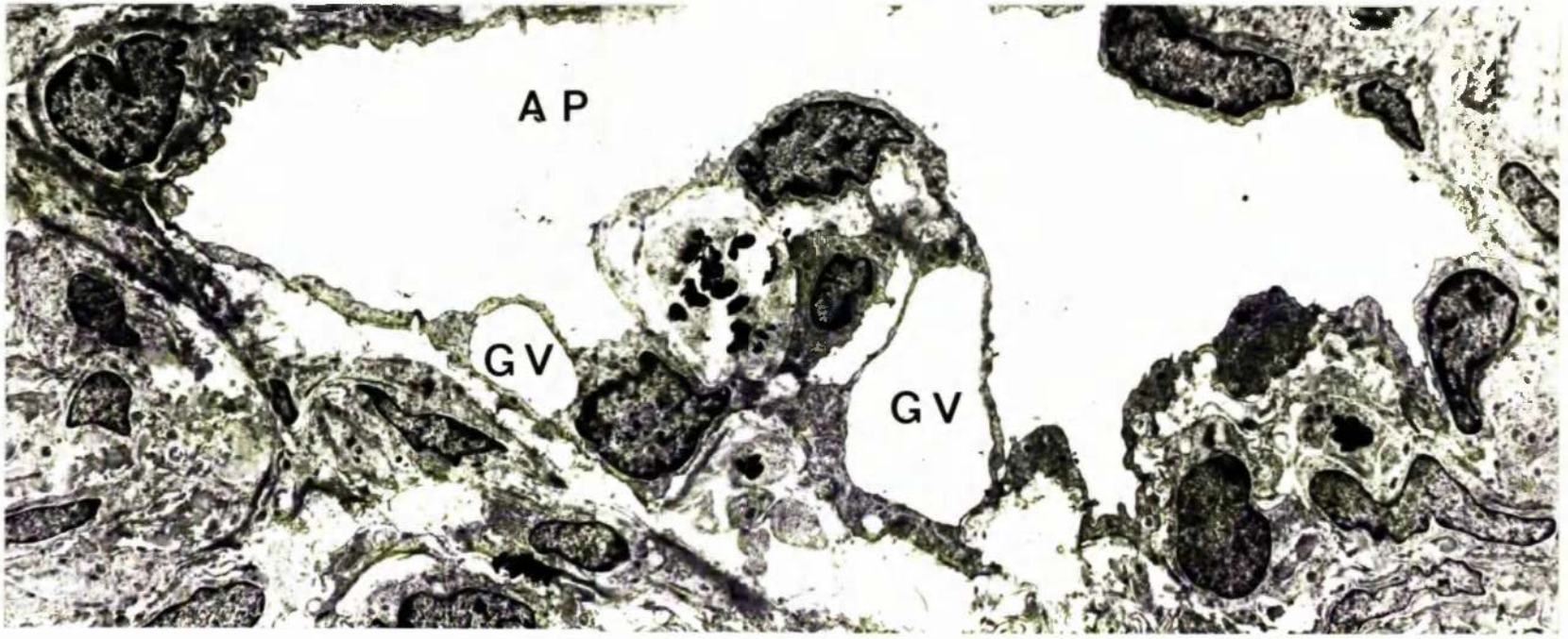

Fig.4.46 A vessel of the rabbit aqueous plexus (AP), some endothelial cells contain giant vacuoles (GV). T.E.M. (x5,000).

parts of the endothelial cells.

Both myelinated and non-myelinated nerve fibres abounded throughout the meshwork and sometimes terminals were identified. A characteristic feature of the posterior meshwork was the presence of relatively large nerve bundles. These nerve bundles contained mainly non-myelinated fibres but an occasional myelinated fibre could be recognised (Fig. 4.47).

Fig.4.47 Part of a relatively large nerve bundle in the rabbit meshwork. Only one myelinated axon is present (arrow). Tissue treated "en bloc" with uranyl acetate and the section stained with uranyl acetate and lead citrate. T.E.M. (xII,000).

CHAPTER 5

JUNCTIONS BETWEEN THE CELLS OF THE OUTFLOW APPARATUS

5.1 Introduction

This chapter is concerned with a detailed ultrastructural investigation of the junctions between the cells in the primate and rabbit outflow system. Junctional modifications between meshwork cells have received little attention in the literature which is surprising since they may contribute to the maintenance of tissue integrity. On the other hand cell-to-cell adhesion in the endothelium lining Schlemm's canal and the non-primate angular aqueous plexus has stimulated more interest.

Authorities have failed to agree either on the structural characteristics of the canalicular endothelial junctions or their effectiveness as an intercellular barrier to fluid and particle penetration from the underlying meshwork. When horseradish peroxidase was introduced into the primate anterior chamber (MacRae and Sears, 1970; Shabo and Maxwell, 1972b) the small particles entered the intercellular clefts between the cells of the endothelium lining the trabecular aspect of Schlemm's canal but failed to penetrate the junctional barrier. The findings lent support to morphologists, including Feeney and Wissig (1967), Tripathi (1968, 1971a, 1974) and Inomata, Bill and Smelser (1972a), who considered that the junctions were zonulae occludentes which surrounded the endothelial cells as continuous bands of membrane fusion. Tripathi (1971b and 1974), from his investigations of the endothelium lining the non-primate aqueous plexus, concluded that here the junctions between the neighbouring cells were also zonulae occludentes. However Shabo, Reese and Gaasterland (1974), in their study of the monkey outflow apparatus, stated that the junctions between the cells of the canalicular endothelium were a series of focal membrane fusions rather than continuous zonular belts.

As discontinuities in the junctional system could serve as an important route for aqueous outflow, the present study was undertaken in an attempt to resolve the controversy and to assess the role of intercellular passage in the bulk outflow of aqueous humour. In addition the structure, distribution and frequency of junctions between meshwork cells was investigated to determine their potential significance in tissue adhesion.

5.2 Materials and methods

The material came from normal primate and rabbit eyes. The animals used and the mode of primary fixation are provided in appendices 1 to 5. The special techniques of "en bloc" staining with uranyl acetate and ruthenium red impregnation are outlined in Chapter 3.

All measurements of junctional dimensions quoted in the following text were made directly from prints with a x7 magnifier which incorporated a graticule. Print and plate magnifications were standardised with the aid of a line grating (2,160 lines per mm).

5.3 Effects of fixation

A structure was found in the meshwork cell processes of some eyes which consisted of a zone (up to 0.6 μm in width) where the cytoplasm was extruded to the extent that the plasmalemmae were in close apposition (Fig. 5.1). These intracellular regions were pentalaminar and therefore resembled the occluding type of cell-to-cell junctioning. Unlike "true" cellular junctions, which were common to all the eyes examined and were unaffected by either the mode of primary fixative penetration or the range of fixative concentrations used in this study, the intracellular "pseudojunctions" were observed in only a few eyes. The pseudojunctions were restricted to 2 human and 2 baboon eyes fixed by immersion in

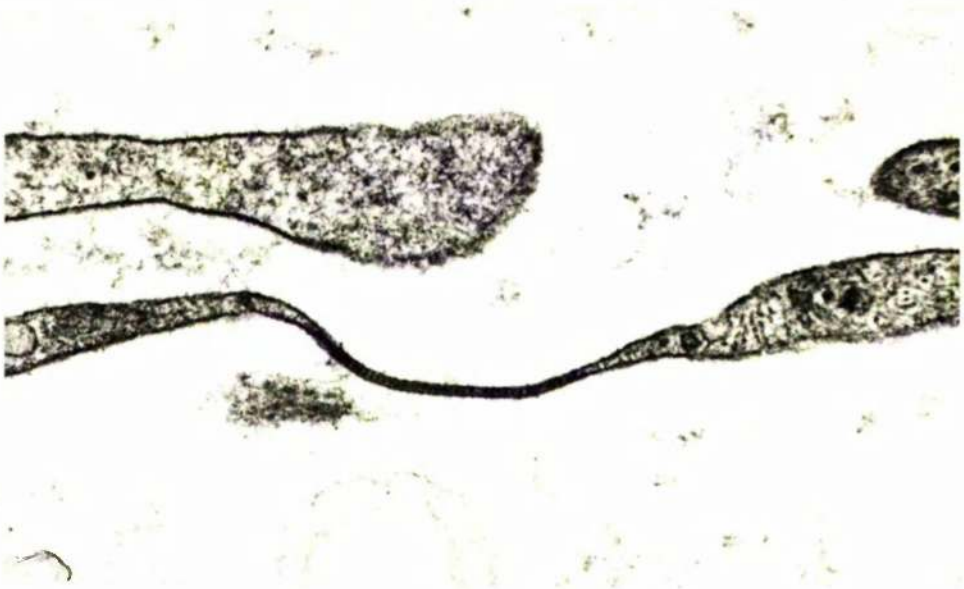

Fig.5.I A structure in a human endothelial meshwork cell in which the cell cytoplasm is absent and opposing plasmalemmae are in contact. T.E.M. (x50,000).

hypertonic primary fixative solution (4% gluteraldehyde in an 0.1M phosphate buffer solution).

5.4 Junctions between meshwork cells

5.4.I Conventional staining

Two types of junctional modification were identified in the intercellular spaces between neighbouring meshwork cells.

After uranyl acetate and lead citrate section staining on conventionally processed tissue, the first type was distinguished by a slight narrowing of the intercellular space, a densification of the cytoplasm in the junctional zone and a slightly increased electron density in the interspace between the opposing plasma membranes (Fig. 5.2) At high magnification narrow strands of particularly dense staining material were seen to cross between the opposing plasma membranes in some of the junctional zones. With uranyl acetate, but without lead citrate staining, the cytoplasmic densifications associated with the junction were less prominent and intermembranous strands could not be resolved. The junctions involved approximately 0.1 to 0.4 μm of the interspace and, by serial sections, were shown to be focal "button" or "plaque-like" structures. They were classified as maculae adhaerentes after the system proposed by Farquar and Palade (1963) and their appearance was identical i all four species.

The second type of junction was characterised by an extreme narrowing of the intercellular space to the extent that, with uranyl acetate and lead citrate staining, it had the distinctive pentalaminar appearance indicative of fusion between the opposing membranes (Fig. 5.3). After uranyl acetate staining without subsequent exposure to lead citrate, the mid-line was considerably less electron dense i.e. the junction had a trilaminar rather than a pentalaminar appearance (Fig. 5.15a). In all

Fig.5.2 A macula adhaerens which modifies the intercellular space between two cells in the baboon trabecular meshwork. T.E.M. (x216,000).

Fig.5.3 A region of close apposition between two meshwork cells. Rhesus monkey tissue. T.E.M. (x216,000).

four species the second type was also a "button" junction but the modification was considerably more extensive in the rabbit than the primate meshwork (Fig. 5.8). The junctions were of comparable size in the rhesus monkey (Figs 5.3 and 5.5) and baboon (Figs 5.4, 5.6 and 5.9) but involved a particularly small portion of the zone of apposition between adjoining cells in the human meshwork (Figs 5.7 and 5.12).

With conventional staining the second junctional type appeared to represent a total obliteration of the intercellular space and, on this basis, could be classified as a macula occludens (Farquar and Palade, 1965 However some of the characteristics of the junction made the classificatio suspect. In true cross section, junctional thickness was not less than 180 Å and therefore thicker than would be expected for a true occluding junction which, by definition, represents the fusion of two plasma membranes. From some sections it was evident that the mid-line of the junction, which should have been a continuous line of intimate contact between the outer leaflets of the opposing membranes, had a distinct periodicity (Figs 5.3, 5.7 and 5.8). When oblique sections through the membrane associations were examined, the junctions had a striated appearance at low magnification (Fig. 5.9a) and at increased magnification circular structures (subunits) with a dense core and lucent periphery were distinguished. The subunits were usually ill defined (Fig. 5.9b).

5.4.2 "En bloc" treatment

The classification of the macula adhaerens was confirmed using the "en bloc" staining method. It was difficult to identify the adhering junction when the sections were left unstained because the cytoplasmic densifications were no longer obvious. The junction was seen as a circular area of slightly increased electron density which also involved the intercellular space. Two obviously separate trilaminar plasma membranes passed through the junctional region (Fig. 5.10).

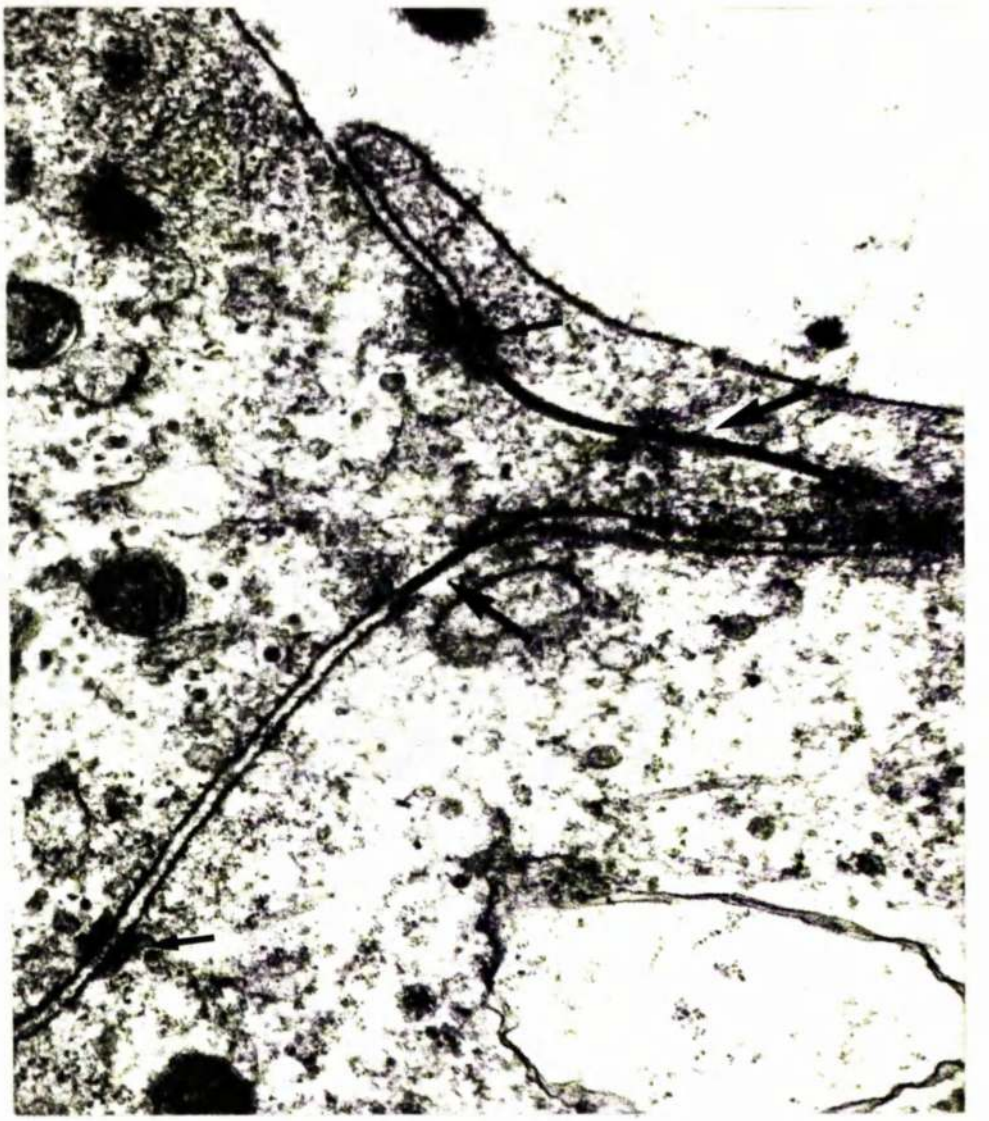

Fig.5.4 A lateral border between two endothelial cells from a baboon uveal trabecula. The intercellular space is modified by a junctional complex of maculae adhaerentes (small arrows) and regions of close apposition (large arrows). T.E.M. (x64,000).

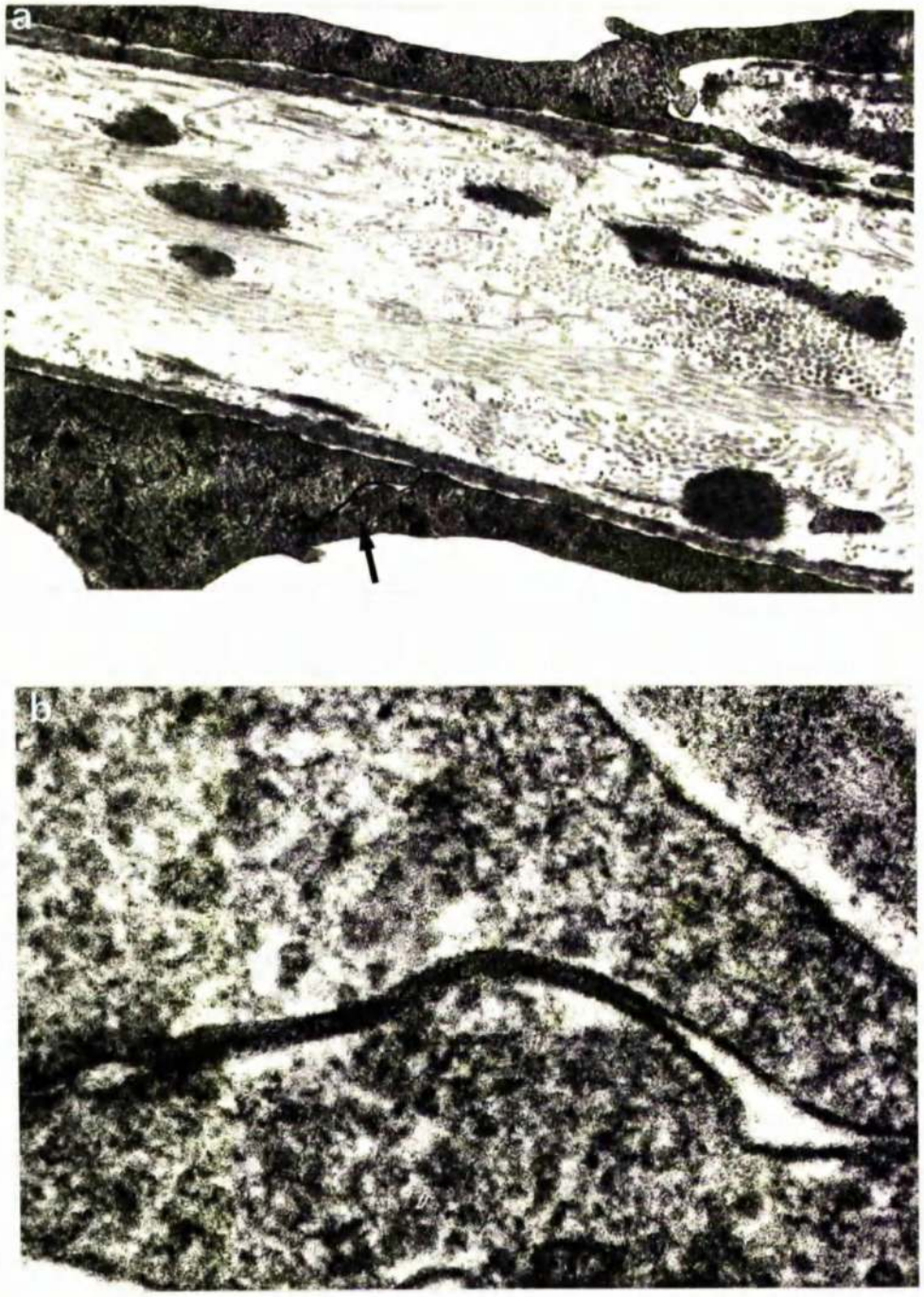

Fig.5.5 a) Part of a corneoscleral trabecula from the rhesus monkey meshwork. The arrow indicates an intercellular cleft shown at higher power in b). The intercellular cleft is modified by a junction in which the membranes are closely apposed. T.E.M. (a x20,000; b xI70,000).

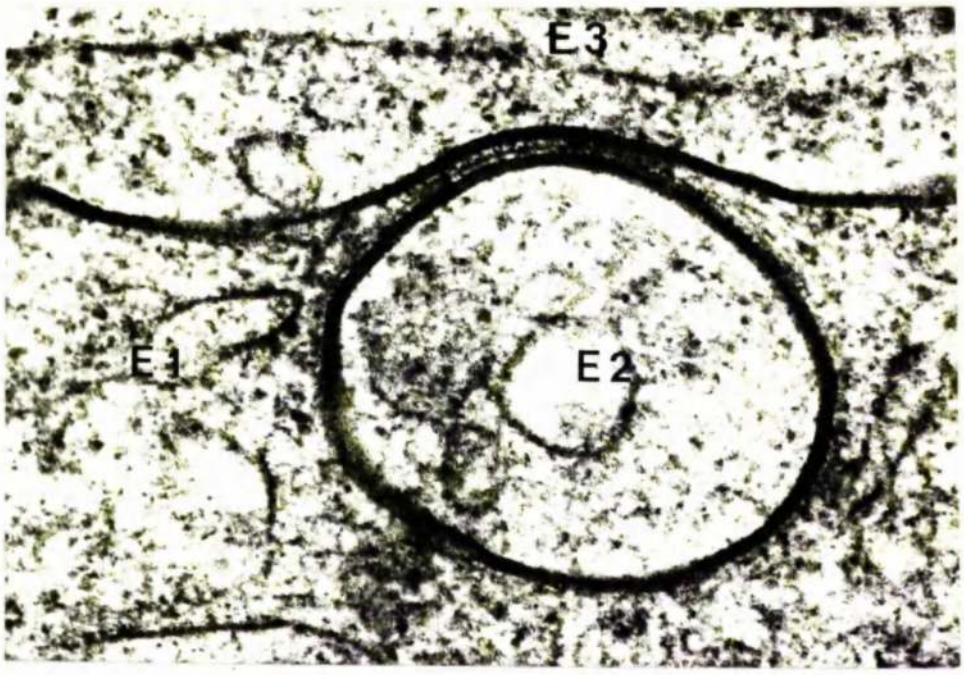

Fig.5.6 Zones of apposition between three endothelial cells EI, E2 and E3 in the baboon corneoscleral meshwork. The intercellular space between the finger-like process E2 and the cell EI is completely modified, in this level of section, by a region of close membrane apposition. T.E.M. (xI00,000).

Fig.5.7 A region of close apposition between endothelial meshwork cells (arrow) in the human meshwork. T.E.M. (x50,000).

Fig.5.8 A region of close apposition between rabbit meshwork cells. T.E.M. (x200,000).

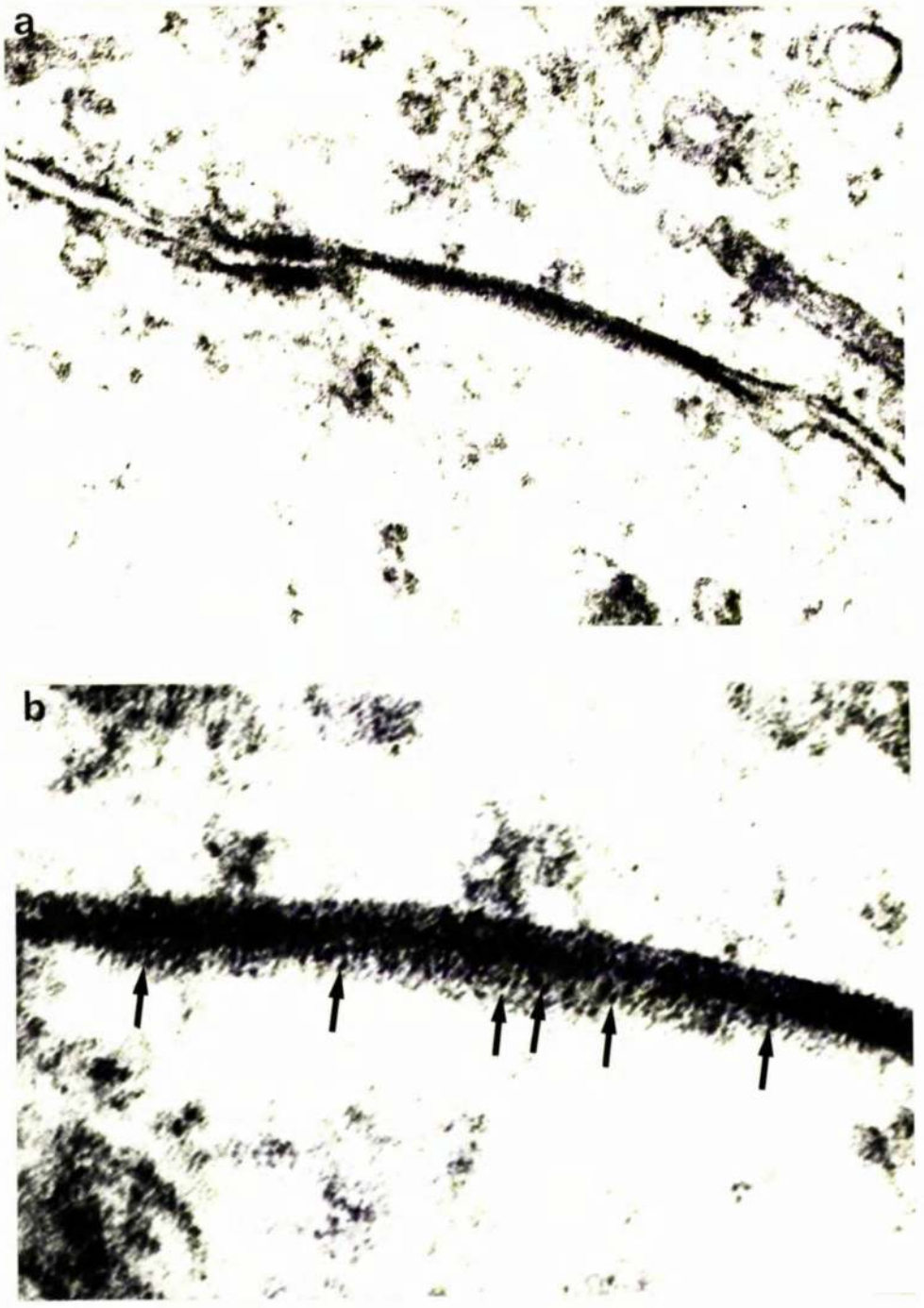

Fig.5.9 A region of close apposition between baboon meshwork cells which has been cut obliquely. At low power a) the junction has a striated appearance whereas at higher magnification b) subunits (arrows) can be seen. T.E.M. (a x110,000; b x300,000).

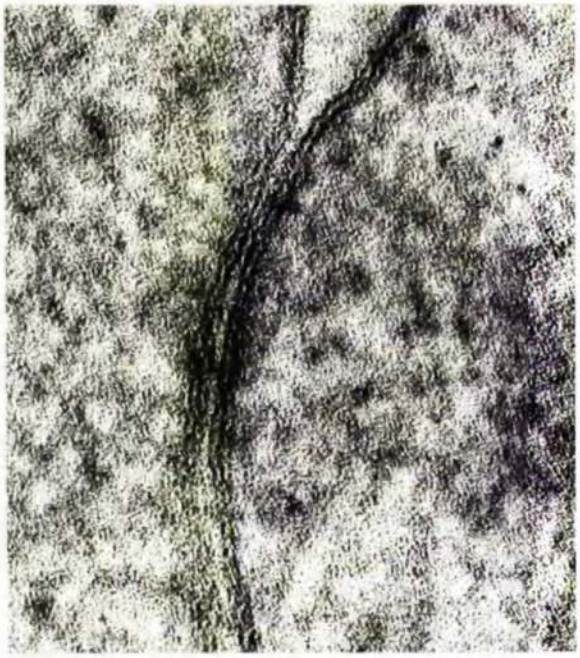

Fig.5.IO A macula adhaerens between rabbit meshwork cells treated "en bloc" with uranyl acetate and no subsequent section staining. T.E.M. (x280,000).

After "en bloc" treatment and subsequent double staining of the sections with uranyl acetate and lead citrate, the modification which resembled an occluding junction was of similar thickness (180Å) to that found with conventional treatment. The junction was still pentalaminar but the mid-line was much thicker (80 - 90Å) than would have been expected for the fusion line of the outer membrane leaflets in an occluding junctio (Figs 5.11 to 5.13a). Reducing the exposure time to lead citrate from 10 to 2 minutes decreased the electron density of the central region so that, in places, the outer leaflets of the opposing plasma membranes could be seen to be separate (Fig. 5.13b).

Without section staining, the separation of the outer leaflets was further emphasised (Fig. 5.14) and the distance between the two membrane leaflets was calculated to be between 30 and 40Å. Subunits could be identified more easily between the two membrane leaflets than had been possible with conventional staining because their electron lucent periphery was more clearly defined (Fig. 5.14).

Junctions which appear septilaminar in cross section and contain an array of subunits have been identified in various tissues of the body and were called gap junctions by Revel and Karnovsky (1967).

5.4.3 Ruthenium red treatment

After ruthenium red treatment electron dense deposits were located within the intercellular spaces of adjoining meshwork cells. With high concentrations (1,000 p.p.m.) of ruthenium in the fixative solutions the deposit was seen as a continuous electron dense layer whereas with low concentrations ($\leqslant$ 400 p.p.m.) the material had reduced density and was restricted to focal, sporadically distributed clumps within the interspace. Although the distribution was patchy in unmodified intercellular space, there was usually a particularly prominent electron density associated with the adhering junctions indicating that the interspace at the site of

Fig.5.II An extensive region of close association between rabbit meshwork cells. "En bloc" staining plus uranyl acetate and lead citrate section staining. T.E.M. (x240,000).

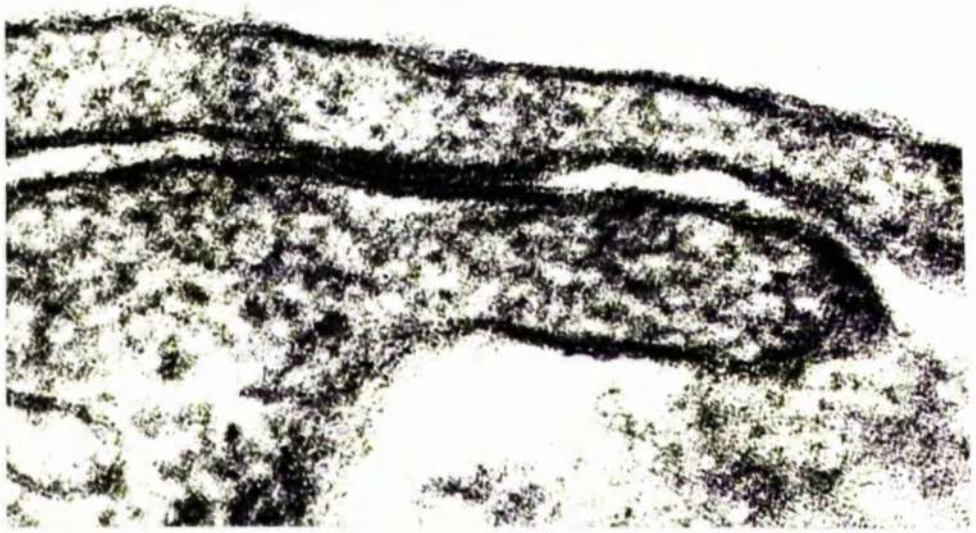

Fig.5.I2 A more limited region of membrane association in the human meshwork. "En bloc" treatment with uranyl acetate and lead citrate section staining. T.E.M. (x240,000).

Fig.5.I3 Regions of close membrane apposition in the rabbit meshwork after "en bloc" treatment plus uranyl acetate and lead citrate section staining. a) The junction is pentalaminar after I0 minutes in lead but b) septilaminar when exposure is reduced to 2 minutes. T.E.M. (x560,000).

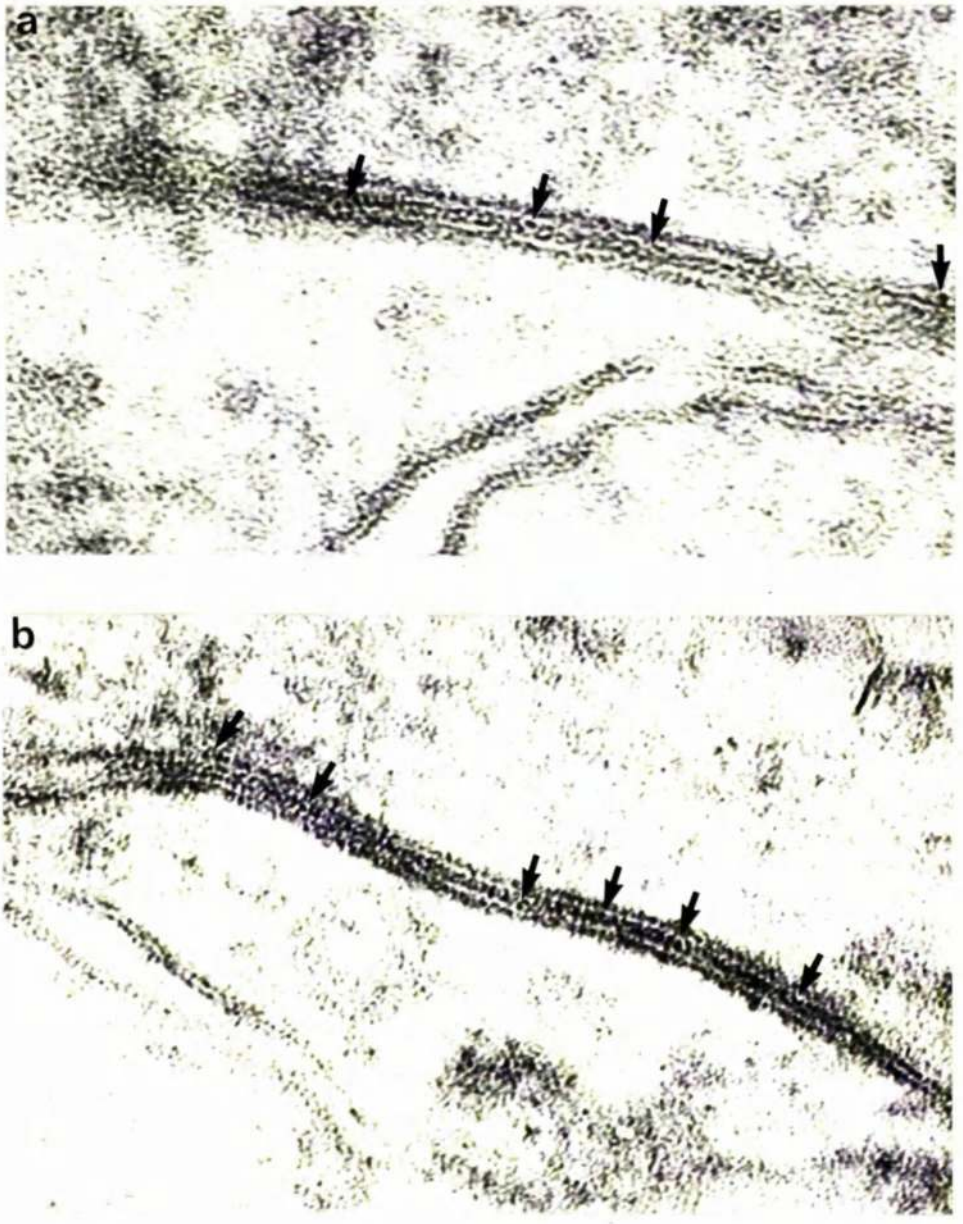

Fig.5.I4 Regions of close membrane association in a) the rabbit and b) the rhesus monkey meshwork. With "en bloc" treatment and no subsequent section staining the junctions have the characteristics of gap junctions i.e. they are septilaminar and have subunits (arrows) in the interspaces. T.E.M. (a x425,000; b x350,000).

a macula adhaerens had an affinity for ruthenium red.

The ruthenium red material penetrated the 30 to 40Å space between the opposing leaflets of the gap junction (Figs 5.15b and 16) and thus provided further evidence that the junction was not of the occluding type. In cross-sections the electron dense ruthenium deposit was seen, at low magnification, to be an apparently uniform line through the junctional zon (Figs 5.15b and 16a) but at higher magnification small discontinuities were noted (Fig. 5.16b). The discontinuities were narrow electron lucent bridges across the 30 to 40Å gap which probably corresponded to the characteristic subunits identified in oblique sections.

5.4.4 Distribution and frequency

In the three primate species the adhering and gap junctions were present between the covering cells on the uveal (Fig 5.4) and the corneoscleral (Fig. 5.5) trabeculae, where endothelial processes made contact in both regions (Fig. 5.6), at zones of cellular and process apposition in the endothelial meshwork (Fig. 5.7) and at the sites of cellular association between endothelial meshwork cells and the canal endothelium. Maculae adhaerentes and gap junctions were also found between the adventitial cells which were associated with the posterior meshwork and the ciliary muscle bundles. Junctional attachments were not identified between muscle fibres and adventitial cells. Gap and adhering button junctions were distributed throughout the rabbit outflow tissues, viz, between the cells of the trabecular portions of the meshwork (Fig. 5.8), adjoining adventitial cells in the extensive ciliary stroma and at attachment points between the network of cells beneath the vessels of the angular aqueous plexus.

It must be remembered however that both types of junction were focal structures so that their distribution was intermittent at the various site in all four species. The macula adhaerens was of similar dimensions in

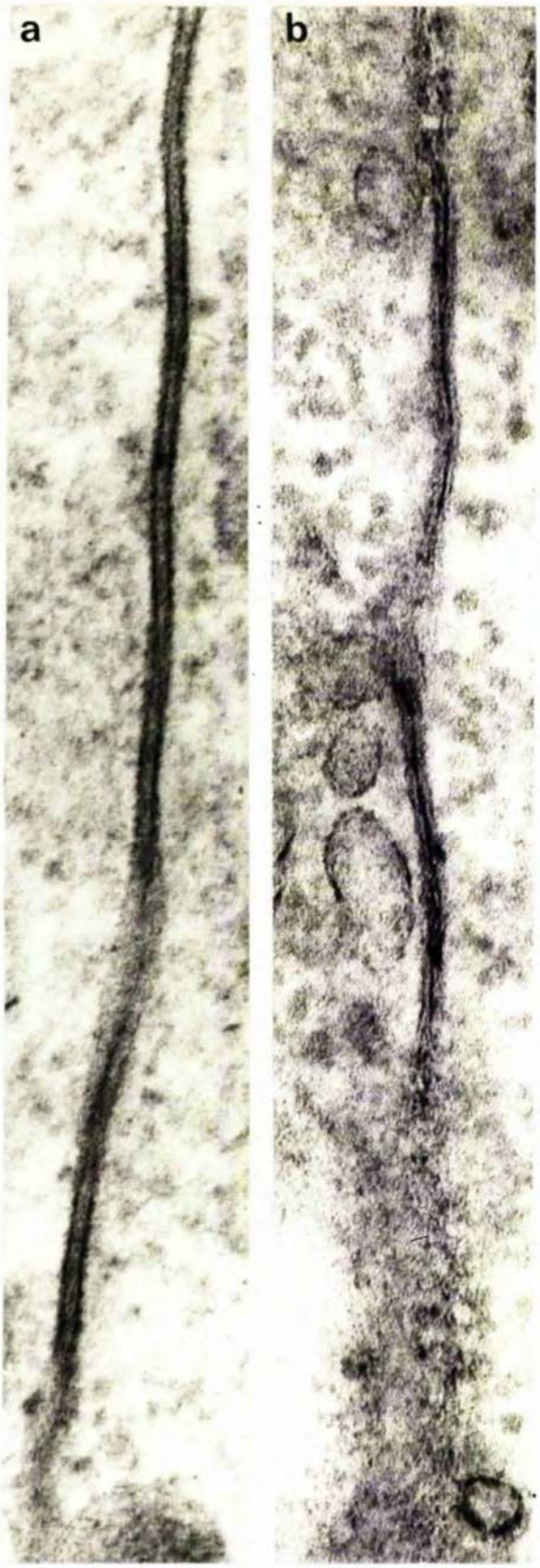

Fig.5.I5 Gap junctions between rabbit meshwork cells after uranyl acetate section staining. In a) the junction is trilaminar whereas in b) ruthenium red (400 ppm) has penetrated the interspace of the gap junction. T.E.M. (xI80,000).

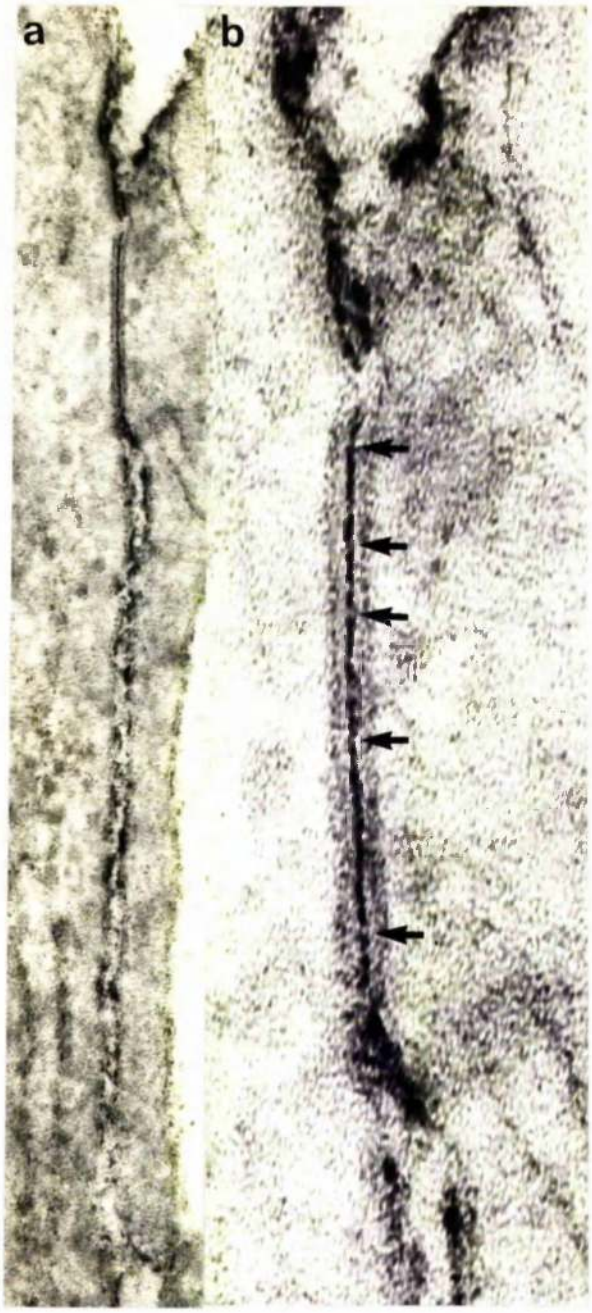

Fig.5.I6 A gap junction in the baboon meshwork which has been penetrated by ruthenium red (400 ppm). a) At low magnification the ruthenium deposit appeared to be continuous within the junctional zone. b) At higher magnification small lucent bridges were noted (arrows). No section staining, T.E.M. (a xII0,000; b x350,000).

the rabbit and primate as was its relative frequency, but because the gap junction was a more extensive structure in the rabbit, i.e. it involved a larger portion of the intercellular space, this junction was identified far more frequently in the rabbit than the primate meshwork.

5.5 Junctions between the endothelial cells lining Schlemm's canal and the angular aqueous plexus

5.5.1 Conventional staining

Both the primates and the rabbit had from one to five junctional modifications in the lateral borders between neighbouring endothelial cells. The junctions were characteristically narrow areas of membrane modification with a region of cytoplasmic densification immediately adjacent to the junctional zone (Fig. 5.17). Although there were often several junctional modifications within each intercellular cleft, most were sectioned obliquely so that the important details of membrane association were obscured. True cross sections through the junctional zone sometimes revealed a membrane-to-membrane contact (Fig. 5.17a) but in others the intercellular gap was narrowed but not closed (Fig. 5.17b).

5.5.2 "En bloc" treatment

Uranyl acetate "en bloc" staining emphasised the trilaminar structure of the plasma membrane allowing the membrane associations in the junctional region to be studied more easily. Attempts were made to trace individual cell junctions through different levels of section but this exercise was of limited value. Each junction had a tortuous path, becoming reorientated as it bent or tilted along its course, so that a true cross section was usually followed by many oblique views.

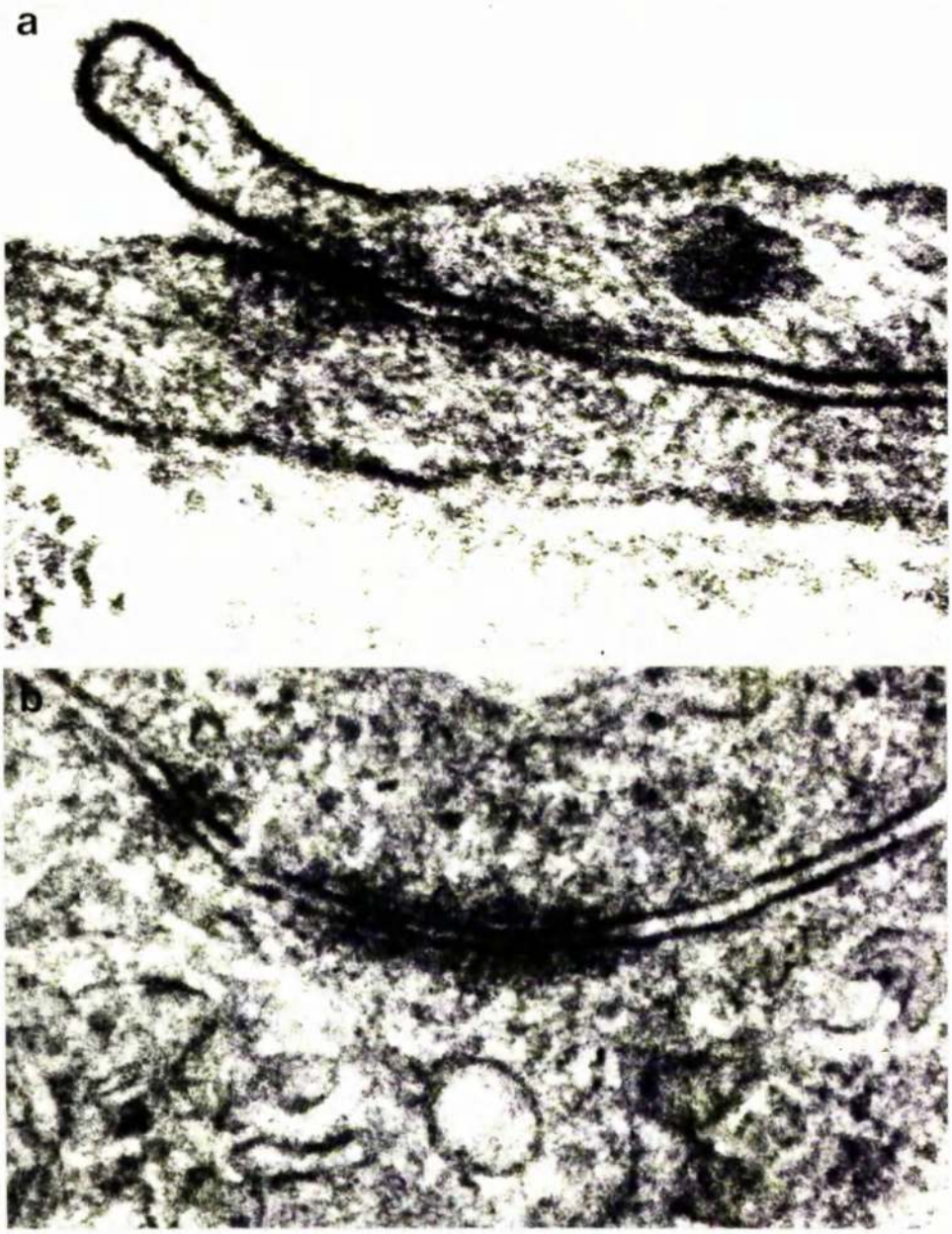

Fig.5.I7 Junctional modifications in the lateral borders between neighbouring endothelial cells on the trabecular aspect of Schlemm's canal. In a) there appears to be membrane-to-membrane contact but in b) the intercellular cleft is narrowed but not closed. Human tissue, T.E.M. (xI90,000).

In the primates and the rabbit three distinct junctional forms were identified between the neighbouring endothelial cells.

a) The most common junctional type was distinguished, both with (Figs 5.18 and 5.19) and without (Figs 5.20 and 5.22) subsequent section staining, as a punctate fusion between the associated plasma membranes. Where the two plasma membranes were in close proximity, the junction had a pentalaminar appearance and measurements of junction thickness gave values of 130 and 140 Å. The junctional width was less than the thickness of two plasma membranes (where n = plasma membrane thickness, the junctional thickness was between 2.0 and 1.8n) and, on this basis, was considered to represent a total occlusion of the intercellular space (see Reese and Karnovsky, 1967). The zone of membrane fusion extended for less than 200 Å in the vertical plane and it seemed probable that the junction circumscribed the cell in the form of a zonula or belt.

b) The second type of junction had dimensions outside those of the punctate occluding junctions. With "en bloc" treatment, plus uranyl acetate and lead citrate section staining, it appeared pentalaminar but differed from the occluding junctions in that the junctional region extended over 0.1 µm in the vertical plane. Total junctional thickness was approximately 180Å and the electron dense mid-line measured 80 to 90Å (Fig. 5.21). Without section staining, a 30 to 40Å space was seen to separate the outer leaflets of the apposing membranes (Fig. 5.22) and, as could be expected, the ratio of junction to membrane width was greater than 2. Indeed, a favourable structural comparison could be made between this second type of junction and the gap junctions between meshwork cells. When it was possible to get sufficient information from sequential sections, it appeared that the 180Å thick junction was a focal modificatio contained within the zonular belt of the 130 to 140Å thick occluding junction.

Fig.5.I8 Two adjoining cells from a vessel in the rabbit angular plexus. Punctate occluding junctions are indicated by arrows. T.E.M., "en bloc" treatment and uranyl acetate section staining. (x300,000).

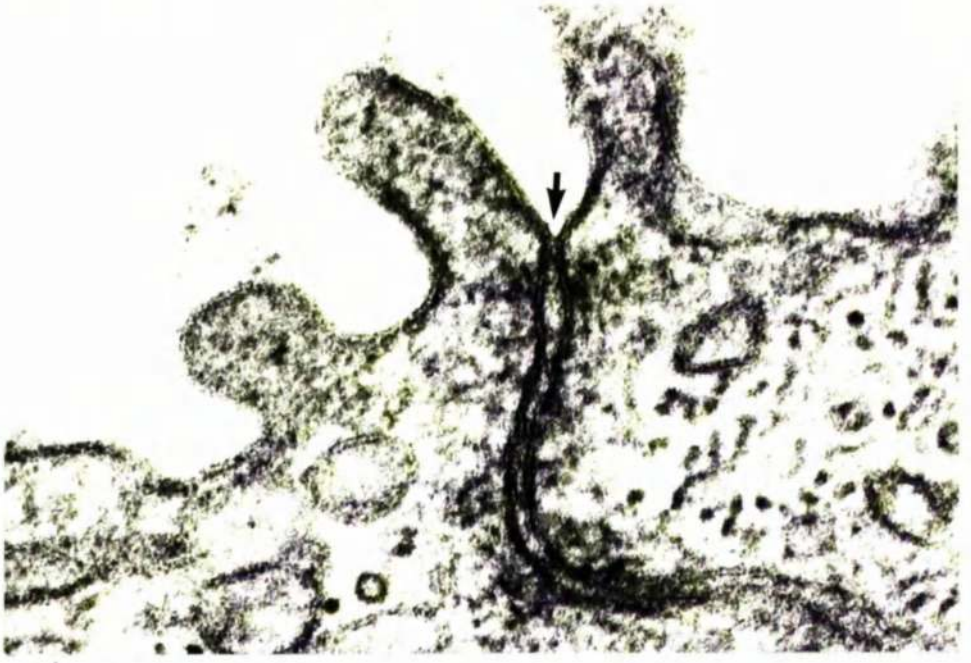

Fig.5.I9 A puntate fusion is indicated by an arrow. Human tissue, "en bloc" treated with subsequent uranyl acetate and lead citrate section staining. T.E.M. (x200,000).

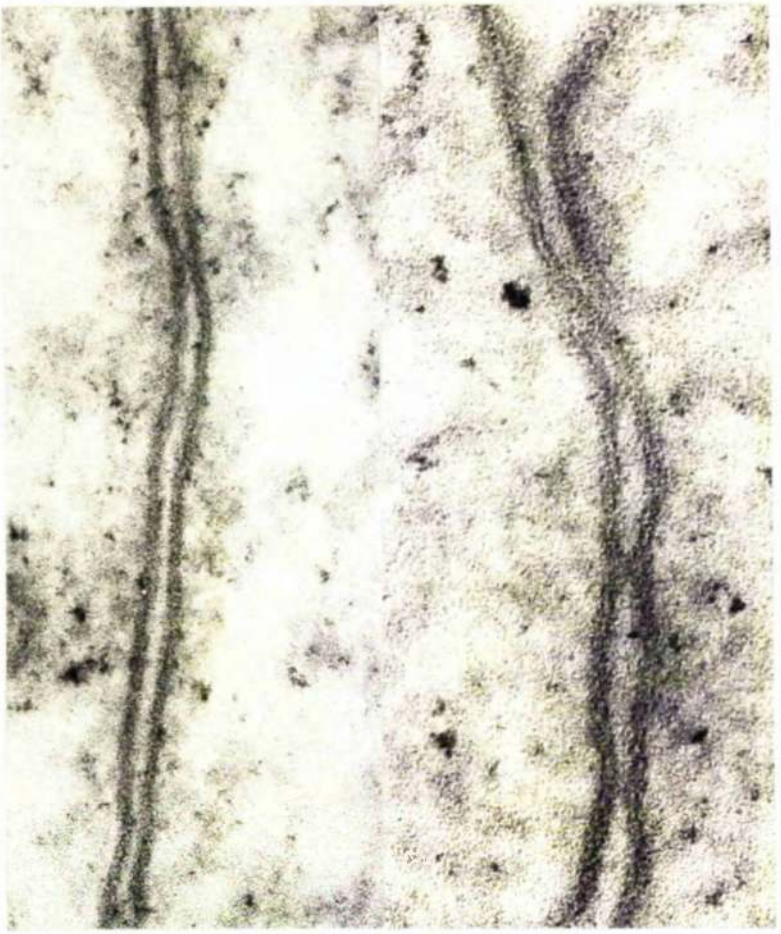

Fig.5.20 The arrows indicate occluding junctions between endothelial cells on the trabecular aspect of Schlemm's canal. Baboon tissue, "en bloc" treatment with no section staining. T.E.M. (a x280,000; b x350,000).

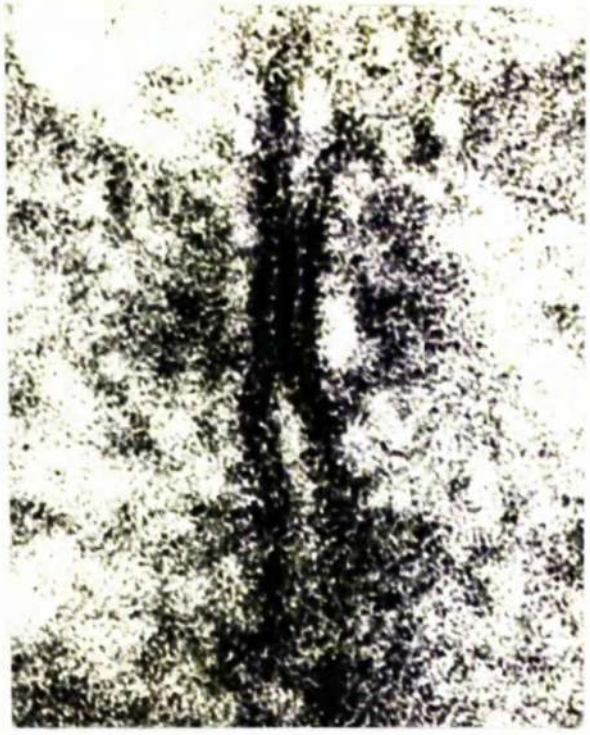

Fig.5.21 A gap junction between cells in the human canalicular endothelium. "En bloc" treatment plus uranyl acetate and lead citrate section staining. T.E.M. (x610,000).

Fig.5.22 An occluding (small arrow) and gap (large arrow) junction in the baboon canalicular endothelium. "En bloc" treatment and no section staining. T.E.M. (x340,000).

c) At the site of the third type of modification, the apposing plasma membranes were separated by a distinct though variable space which could be as narrow as 45Å and as wide as 90Å. After "en bloc" treatment plus uranyl acetate and lead citrate section staining, the space at the junctional region was seen to contain amorphous material of high electron density (Fig. 5.23). Without section staining the amorphous material was not readily visualised. It was not possible to determine whether this type of modification was discrete or, like the gap junction, represented a region of membrane separation within the zonular belt of occluding junction.

5.5.3 Ruthenium red treatment

Electron dense ruthenium red deposits penetrated the intercellular clefts but did not provide useful information about the permiability characteristics of the endothelial junctioning because the material was free to enter from both the luminal and the meshwork (or scleral) aspects of the cleft. Unidirectional tracer studies (introducing tracer exclusively into either Schlemm's canal or the trabecular meshwork), which were not performed in the present investigation, would have been more informative.

5.5.4 Distribution and frequency

The occluding junctions were by far the most common type of modification and were present between endothelial cells on both the trabecular and corneoscleral aspects of Schlemm's canal and between the endothelial cells which bordered the vessels of the rabbit aqueous plexus. The gap junctions were identified in intercellular clefts on both sides of Schlemm's canal and between the endothelial cells of the rabbit aqueous plexus. Their infrequency has handicapped structural and serial

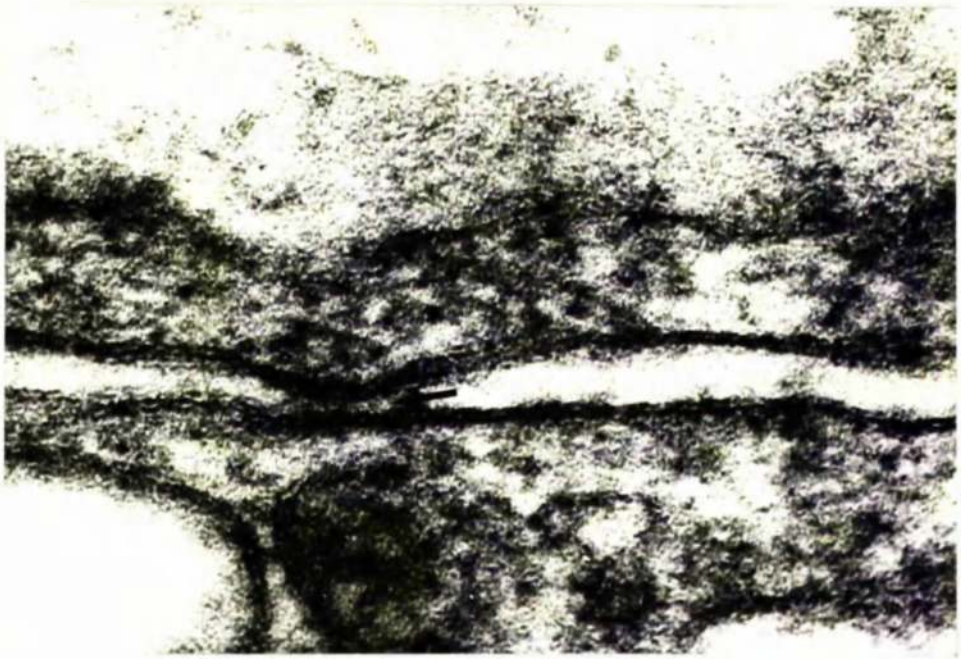

Fig.5.23 The intercellular cleft between two canalicular endothelial cells contains a junctional modification (arrow). At the site of the junction the opposing plasma membranes are separate. The space between the membranes is in excess of 75Å wide and contains electron dense material. Human tissue, "en bloc" treatment with subsequent uranyl acetate and lead citrate section staining. T.E.M. (x310,000).

investigations and, although they were thought to be focal or macular junctions within the occluding zonular belts, their extent remains undetermined. Undoubtedly they represented only a very small proportion of the junctional bands in which they occurred.

The third group of modifications, those in which the membrane separation was between 45 and 90Å, were absent from the endothelium on the corneoscleral aspect of Schlemm's canal and also, in rabbit vessels, from the endothelia adjacent to sclera. Generally, these junctions were infrequent but their incidence varied quite considerably from specimen to specimen.

5.6 Conclusions

5.6.1 Junctions between meshwork cells

Intracellular pentalaminar membrane associations, similar to those mentioned in the present text, have been described in the processes of glial cells and the choroidal plexus epithelium of the vertebrate brain (Brightman and Reese, 1969) and in cultured Schwannoma cells (Conley and Herman, 1973). Brightman and Reese (1969) found the intracellular membran associations in brain tissue only after their tissue blocks had been immersed in hypertonic solutions from which they concluded that the associations were an artefact produced by cellular shrinkage. As intracellular appositions in meshwork cell processes were present only after the tissue had been exposed to hypertonic fixative, my own findings concur with those of the previous authors.

Of the two types of "real" junctional attachment in the trabecular meshwork, one was a simple adhering junction (macula adhaerens) while the other had the characteristics of a macular gap junction. Their strategic positioning at the lateral borders between trabecular endothelial cells and at the sites of process apposition in the uveal, corneoscleral and endothelial meshwork would suggest that they have an adhesive function.

Strong cellular cohesion is important to a loosely organised tissue like the trabecular meshwork where cellular associations can be taxed by changes in intraocular pressure (see volume II of this thesis) and, probably, also by altered ciliary muscle tone (Rohen, Lütjen and Barány, 1967).

Rohen and Lütjen-Drecoll (1971) described junctions they called zonulae occludentes between the endothelial cells on human trabeculae, while Smelser and Ozanics (1971) identified tight junctions in the developing monkey meshwork. In the light of the present findings, it would seem reasonable to conclude that the previous authors observed gap rather than tight junctions but, with conventional staining, were unable to make the distinction. Gap junctions have been reported at many other sites within the eye including, for example, between retinal pigment epithelial cells (Hudspeth and Yee, 1973), photoreceptors (Raviola and Gilula, 1973), corneal endothelial cells (Leuenberger, 1973), non-pigmente and pigmented ciliary epithelium (Raviola, 1971 and 1974), lens fibres (Wakeley, 1974), iris smooth muscle fibres (Hogan, Alvarado and Weddell, 1971), iris fibroblasts (Ringvold, 1975) and choriocapillary endothelial cells (Spitznas and Reale, 1975).

The presence of subunits in the space between the apposing plasma membranes is a characteristic feature of the gap junction (Revel and Karnovsky, 1967; Brightman and Reese, 1969; Revel, Yee and Hudspeth, 1971; Friend and Gilula, 1972 amongst many authors), which can be seen to their best advantage from freeze-etched or freeze-fractured preparations (Chalcroft and Bullivant, 1970; Goodenough and Revel, 1970; Revel, Yee and Hudspeth, 1971; Friend and Gilula, 1972; Hudspeth and Yee, 1973; Spitznas and Reale, 1975 and many others). The intramembranous subunits are thought to be tubes which function as low resistance passageways between the associated cells (Lowenstein, 1973) through which ions

(Payton, Bennett and Pappas, 1969; Pappas, Asada and Bennett, 1971; Johnson and Sheridan, 1971; Rose, 1971; Revel, Yee and Hudspeth, 1971; Sheridan, 1971; Gilula, Reeves and Steinbach, 1972) or metabolites (Gilula Reeves and Steinbach, 1972) can pass from one cell to the other with relative ease.

Whether or not gap junctions have such a role in the meshwork is speculative. However, the presence of gap junctions between meshwork cells introduces the possiblity that these cells are in much closer physiological association than has been suspected previously.

5.6.2 Junctions between canal endothelial cells

"En bloc" staining with uranyl acetate has confirmed that there are regions of membrane fusion in the junctional modifications between the endothelial cells lining Schlemm's canal (and the vessels of the rabbit aqueous plexus). In at least some of the junctional belts small focal gap junctions can be found. The fact that gap junctions are also present between endothelial meshwork cells and where endothelial meshwork cells and canal endothelial cells meet, indicates that the cells in the trabecular wall of Schlemm's canal form a synchronised system. The value of cell coupling at this site is obscure, but it is conceivable that coupling may have significance in the regulation of aqueous outflow. Somewhat similar junctional organisations have been reported between the choriocapillary endothelial cells (Spitznas and Reale, 1975) and between the approximation of the underlying pericytes with these endothelial cells (Matsusaka, 1970) Again it has been suggested that the endothelial cells and pericytes form a coherent system but, as in the outflow apparatus, neither the importance of nor the mechanism for the operation of such a system has been elaborated.

The significance of the junctions with the 45 to 90Å openings is also difficult to assess, Shabo, Reese and Gaasterland (1974) were the

first to describe this form of junctioning in the endothelium of Schlemm's canal and proposed that the small openings could serve as a major route for the passage of aqueous humour into Schlemm's canal.

The case for the in vivo existence of such wide regions of membrane separation is difficult to prove since they may be produced either as a processing artefact or result from tissue manipulation prior to fixation. Certainly the junctions between the endothelial cells are readily disrupted by massage to the eyeball (Tripathi, 1971a) and paracentesis (Raviola, 197- and are therefore relatively fragile. In the present study the fact that the junctional openings were of variable size (between 45 and 90Å), that their frequency was not constant from specimen to specimen and that they were absent from the endothelium on the more robust scleral wall, could be interpreted as evidence that they were traumatic disruptions to occluding zonules rather than junctional entities in their own right.

On the other hand, open junctions rather similar to those in the endothelium of Schlemm's canal have been shown to modify the intercellular clefts between peripheral capillary endothelial cells (Reese and Karnovsky 1967; Karnovsky, 1967). Although the open junctions may play a role in capillary permeability (Reese and Karnovsky, 1967; Karnovsky, 1967) their significance as a major intercellular pathway for the passage of aqueous humour into Schlemm's canal is more dubious. Quantitative calculations by Bill (1975) indicate that even when a most generous allowance is made for their frequency and extent, such a system could account for only a small proportion of the bulk drainage of aqueous humour.

CHAPTER 6

MUCOPOLYSACCHARIDES IN THE OUTFLOW APPARATUS

6.1 Introduction

An important constituent of the extracellular component of connectiv tissue is the group of compounds called acid mucopolysaccharides or glycosaminoglyans. The complex polysaccharides are synthesised within the connective tissue cells mainly at the Golgi apparatus (Revel, 1970; François, 1975), although glycosylation of glycosaminoglycans and glycoproteins may begin while the nascent polypeptides are still associate with the ribosomes (Revel, 1970). Mucopolysaccharides are released from the cells in a soluble (depolimerised) form and polymerisation occurs outside the cells. The extremely long chain polymers are immobilised in connective tissues by entanglement with each other and with the coarse open network formed by collagen and elastic fibres (Fessler, 1957). Within the connective tissues the fine polysaccharide mesh is thought to have a selective filtration effect on the passage of solute molecules and, because the polymers are strongly hydrophilic, they bind water into the tissues (see Ogston, 1970).

The complex polysaccharides are not restricted to the extracellular framework of connective tissues but they also form a coating on all cell surfaces. The cell coat has been implicated in such diverse functions as metabolite transport (the charged end groups of the macromolecules serve as receptor sites), intercellular communication and cellular adhesion (see Revel and Goodenough, 1970).

If there was an extensive hydrophilic polysaccharide network in the outflow system, it would offer resistance to fluid conductance and therefore have a considerable influence on outflow dynamics.

The initial investigations conducted by Bárány and co-workers (Bárány, 1953, 1956; Bárány and Scotchbrook, 1954) showed that the resistance to aqueous outflow in enucleated non-primate eyes could be

halved by the introduction of hyaluronidase into the perfusion fluid. However the findings of subsequent perfusion and histological studies have been variable so that the significance of mucopolysaccharides in the outflow system remains controversial (see Ashton, 1959, 1960; Tripathi, 1969a, 1974 and the discussion to this chapter).

Although the polysaccharides are not visualised by conventional staining systems for transmission electron microscopy, recent investigators have made positive identification of hyaluronidase sensitive material in the trabecular meshwork using a modification of the Hale reaction for acid mucopolysaccharides with (Segawa, 1970b) and without (Armaly and Wang, 197[illegible] conversion to Prussian blue.

In this chapter the results of an ultrastructural investigation into the distribution of mucopolysaccharides in the normal outflow apparatus of four species (man, baboon, rhesus monkey and rabbit) are presented. The polysaccharide complexes were visualised by means of the two cationic electron dense dyes colloidal thorium and colloidal iron (with and without conversion to Prussian blue) and the electron dense stain ruthenium red.

Colloidal thorium and iron react at low pH with the polysaccharide moieties e.g. chondroitin sulphate, sialic acid and hyaluronic acid in the macromolecular complexes and have been used for the ultrastructural localisation of these polymers in a variety of tissue and cell types (Gasic and Berwick, 1963; Revel, 1964; Clark and Curran, 1964; Ito, 1965; Curran, Clark and Lovell, 1965; Yardley and Brown, 1965; Wetzel, Wetzel and Spicer, 1966; Rambourg and Leblond, 1967; Groniowski, Biczyskwa and Walski, 1969 and many others). It has been proposed that ruthenium red stains carbohydrate containing complexes including acid mucopolysaccharides, however the evidence is somewhat circumstantial (see Luft, 1971) and the nature of the reaction remains obscure.

6.2 Materials and methods

6.2.1 Colloidal thorium and colloidal iron

The staining procedures which were adopted are outlined in chapter 3 Fig. 3.4, while the animals used are listed in appendices 1 - 4. Prior to colloidal thorium and colloidal iron treatment but after primary fixation, meridional blocks of limbal tissue were given a buffer wash and then they were incubated for periods of 1 to 48 hours at 37° C in either:-

a) buffered testicular hyaluronidase (B.D.H. laboratories) of various activities between 10 and 2,500 W.H.O. units per ml. of phosphate buffer (pH 6.9 or 7.2).

b) hyaluronidase in the same range of concentrations but which had been inactivated by boiling.

c) in buffer alone.

or d) not incubated but stored in buffer at 4° C.

Thereafter the tissue was again washed in buffer prior to secondary fixation in 1% osmium tetroxide and subsequent staining in the colloidal solutions.

6.2.2 Ruthenium red

Fresh tissue, from rabbit and baboon eyes (see appendix 6), was eith immersed in fixative containing ruthenium red or subjected to a buffered solution containing active or inactivated hyaluronidase prior to fixation and staining (see chapter 3 Fig. 3.5 for the staining procedure). The enzyme concentrations were the same as with colloidal thorium and iron staining but exposure was not longer than 3 hours.

6.3 The appearance of the stains

Both colloidal thorium and iron showed a similar staining pattern in

the outflow apparatus of the four species examined and the distribution of the staining materials was not influenced by the mode of primary fixative penetration into the tissue. The thorium particles were of variable size (50 - 400Å in diameter) and of irregular shape, whereas the iron particles were regular finger-like crystals (50Å wide and over 100Å in length). Usually the iron and thorium particles were not found in the cytoplasm of the meshwork cells unless the cell plasma membrane was mechanically disrupted. When acid ferrocyanide was used in conjunction with colloidal iron, the meshwork appeared blue under the light microscope and under the transmission electron microscope the Prussian blue crystals presented as coarse electron dense irregularly distributed deposits.

Although there was not a quantitative investigation into time - enzyme concentration effects (due to limitations in the staining techniques), in general it was found that at least 2 hours incubation in an enzyme solution of not less than 100 W.H.O. units per ml. was required to produce a significant reduction in staining.

Ruthenium red was identified as an electron dense homogenous material and its distribution was similar in both the baboon and rabbit outflow systems. Adequate staining occurred only when "fresh" tissue was immersed in primary fixative containing ruthenium red. The staining reaction was poor in tissue preincubated in either active or boiled hyaluronidase. Therefore the nature of the ruthenium staining reaction remained unresolved

6.4 Colloidal thorium and iron

6.4.1 The primates

The three primate species were considered collectively, since species differences were minimal. It should be added, however, that the staining reactions in the humans were more variable than in the other primates. From the limited sample of human eye examined, differences in staining

intensity could not be related to either the age of the patient or the siz of the intraocular tumour.

Within the uveal and corneoscleral meshwork, the colloidal thorium and iron formed a continuous cover over the apical surface of the trabecular endothelial cells. The cover was also present on the trabecula surface of the endothelial cells but only where the basement material was thin or separated from the endothelial cover (Figs 6.1 and 6.2). Stain penetration into the intercellular clefts was poor and was easily missed i uranyl acetate and lead citrate stained sections. When the sections were left unstained, the scanty deposits of colloidal material in the intercellular spaces could be seen more easily because the cellular profiles ha little contrast (see chapter 9 Fig. 9.17). Prussian blue crystals also formed an apical and basal layer on the trabecular endothelial cells, but with this coarse stain there was a certain amount of intracellular penetration (Fig. 6.5a).

In the trabecular cores, the Prussian blue deposits were numerous and were distributed haphazardly (Fig. 6.5a). By way of comparison, the smaller thorium and iron particles were deposited in a reproducable and specific pattern. Usually there was only limited penetration of thorium and iron into the basement substance but there was always a distinct and continuous layer of particles on the internal surface of the basement material (Fig. 6.1 and 6.2). Cytoplasmic pegs, which terminated within (Fig. 6.4a) or penetrated through (Fig. 6.4b) the basement material, had a surface layer of stain particles which was usually more prominent on the former than the latter type of peg.

Towards the centre of the trabecular core, the thorium and iron particles were adherent to and dispersed between the collagen fibrils. Colloidal material was prominent around, but not usually within, the clusters of curly collagen and the clumps of elastic-like substance (Figs 6.1 and 6.2). Iron micelles tended to penetrate into the dense

Fig.6.I Part of a corneoscleral trabecula from the baboon meshwork stained with colloidal iron. T.E.M., uranyl acetate counterstain (x28,000).

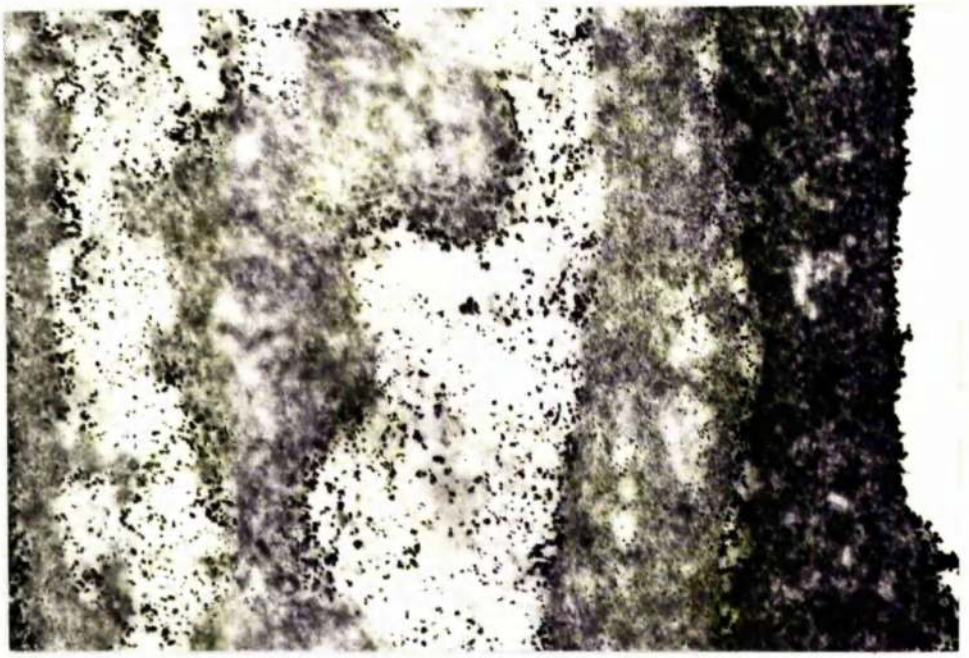

Fig.6.2 Part of a corneoscleral trabecula from the rhesus monkey meshwork stained with colloidal thorium. T.E.M., uranyl acetate counterstain (x65,000).

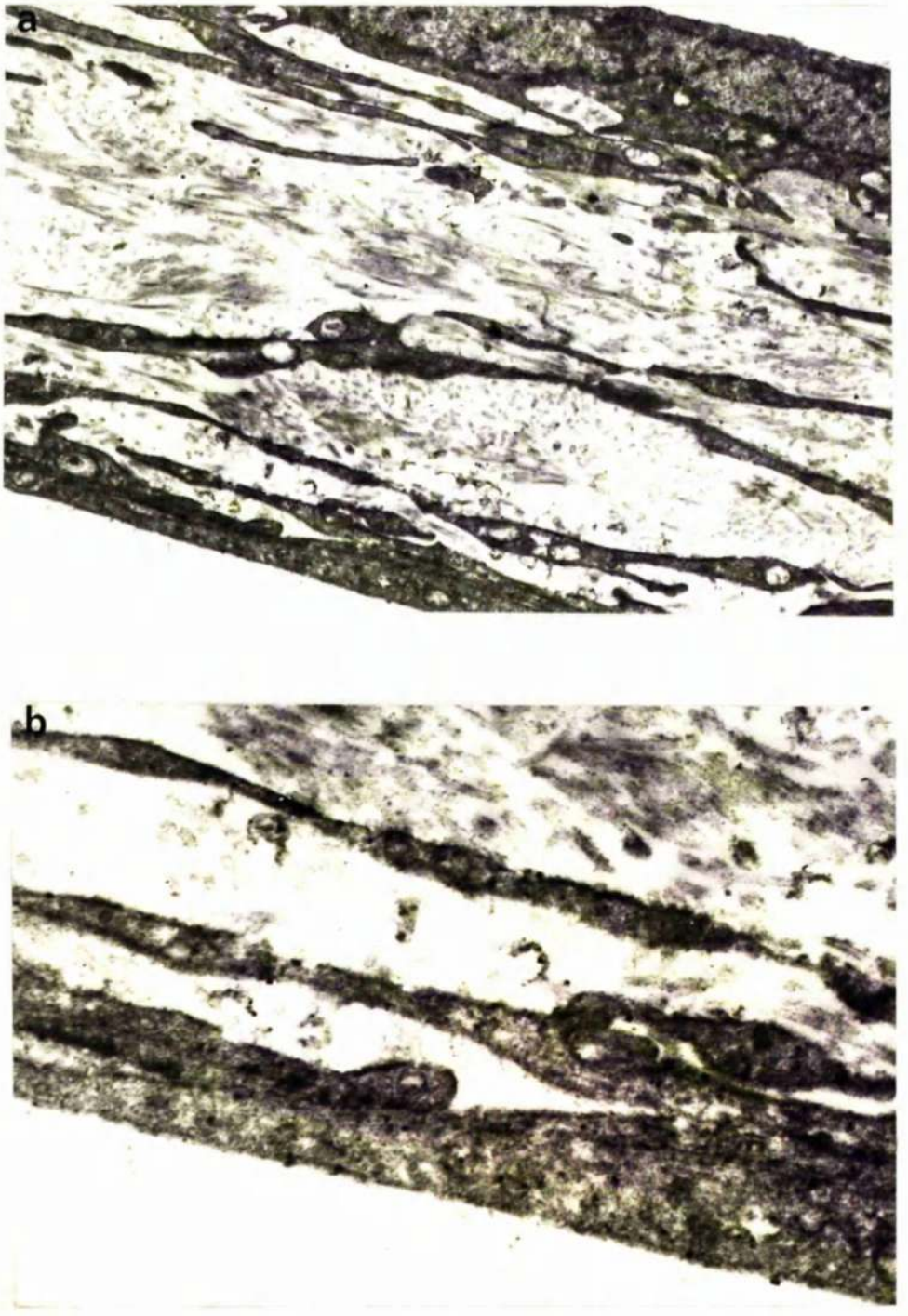

Fig.6.3 A corneoscleral trabecula from the baboon meshwork after 24 hours exposure to I,800 W.H.O. units of hyaluronidase and subsequent iron staining a) at low and b) at higher magnification. T.E.M., uranyl acetate counterstain (a xI0,000; b x 28,000).

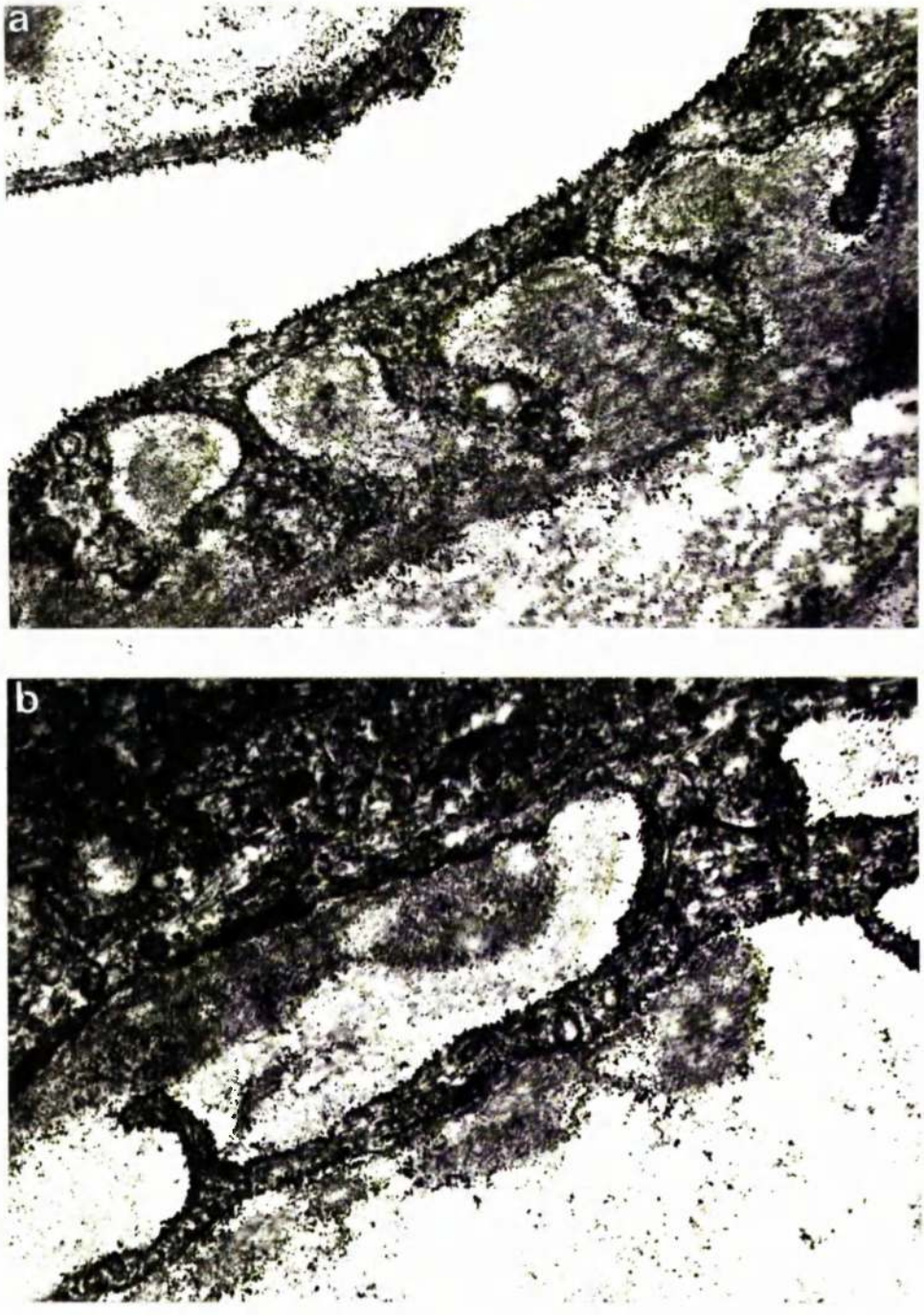

Fig.6.4 Cytoplasmic pegs from the cellular cover on corneoscleral trabeculae a) in the human and b) in the baboon meshwork. T.E.M., colloidal thorium and uranyl acetate counterstain (x38,000).

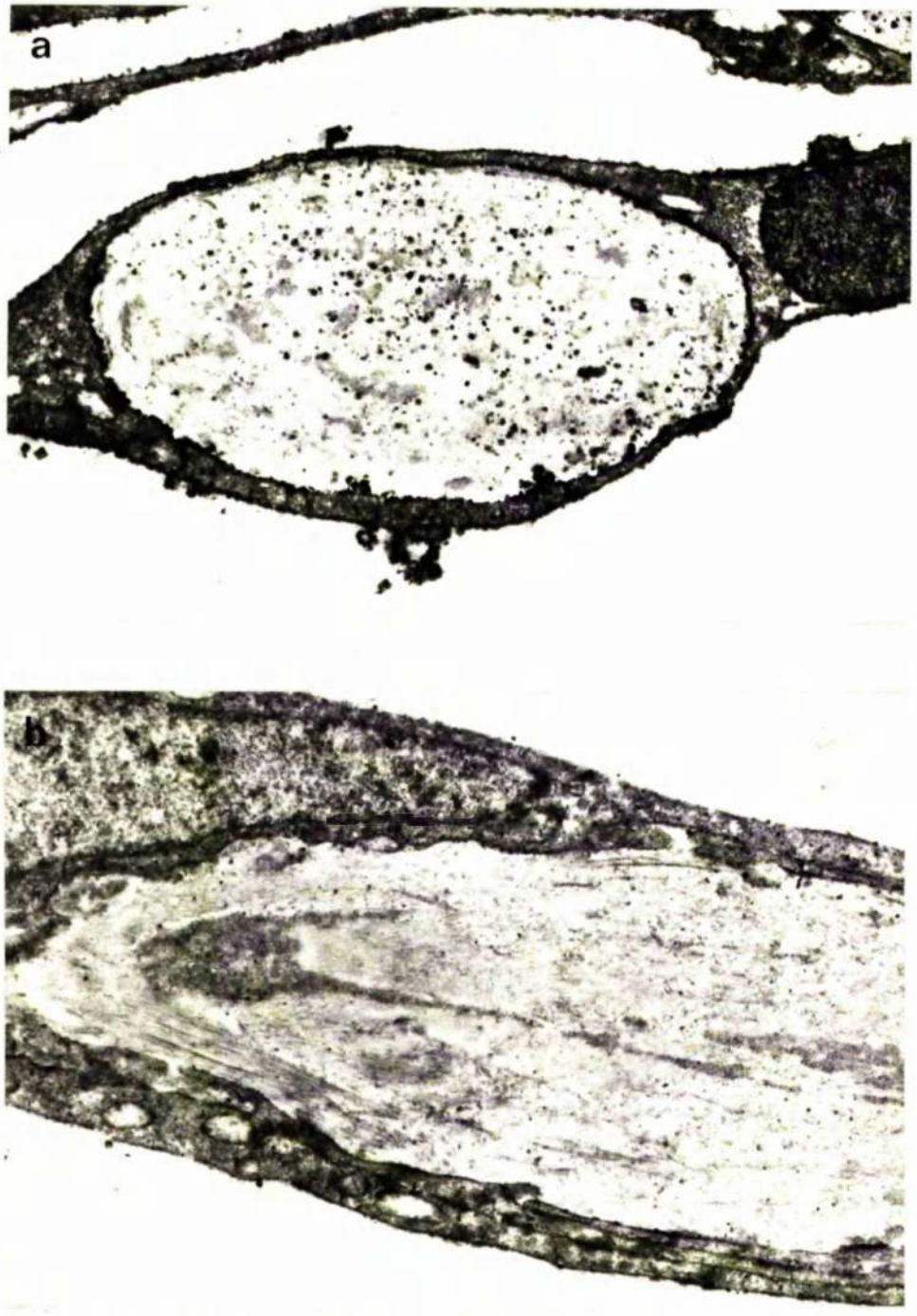

Fig.6.5 Uveal trabeculae from the human meshwork after colloidal iron conversion to Prussian blue a) without and b) with hyaluronidase (I,000 W.H.O. units per ml for 6 hours) pretreatment. T.E.M., uranyl acetate counterstain (xI3,000).

extracellular masses to a greater extent than the larger thorium particles. In general, the intertrabecular spaces were free from staining material except where occasional strands, demarcated by thorium, crossed the spaces and linked the covering layer of two endothelial cells on adjacent trabeculae. Strands were not prominent after iron staining.

Hyaluronidase pretreatment removed most of the colloidal thorium and iron staining from the trabeculae (Fig. 6.3), but even after a 48 hour incubation some residual stain was found in localised regions on the endothelial cells (particularly on the apical surface). The Prussian blue reaction was eliminated almost entirely (Fig. 6.5b).

In the endothelial meshwork the deposition of thorium and iron stain was intense (Figs. 6.6 and 6.7). The native cells were lined by a regular and even coating which was interrupted only by the length zones of apposition between the neighbouring cells. Large concentrations of stain were associated with the extracellular elements and were dense at the periphery of the clumps of collagen, curly collagen and elastic-like material. The stains did not reach the centre of the tight aggregates of extracellular material, whereas heavy deposition of colloidal thorium and iron occurred throughout the loose collections of fibrillar material and the patchy basement membrane beneath the endothelium lining Schlemm's cana Stain particles were also apparent in the spaces which, by conventional treatment, would be optically empty. Thorium deposits were often arranged in a network of fine strands of particles which connected neighbouring clumps of extracellular material (Fig. 6.7). The iron particles were less frequently seen as chains, but even this diffuse staining pattern often served to bring a certain continuity to adjacent clumps of extracellular material which would otherwise have appeared to be isolated.

The endothelium lining the trabecular aspect of Schlemm's canal had, on its abluminal surface, a particle coat which was in close

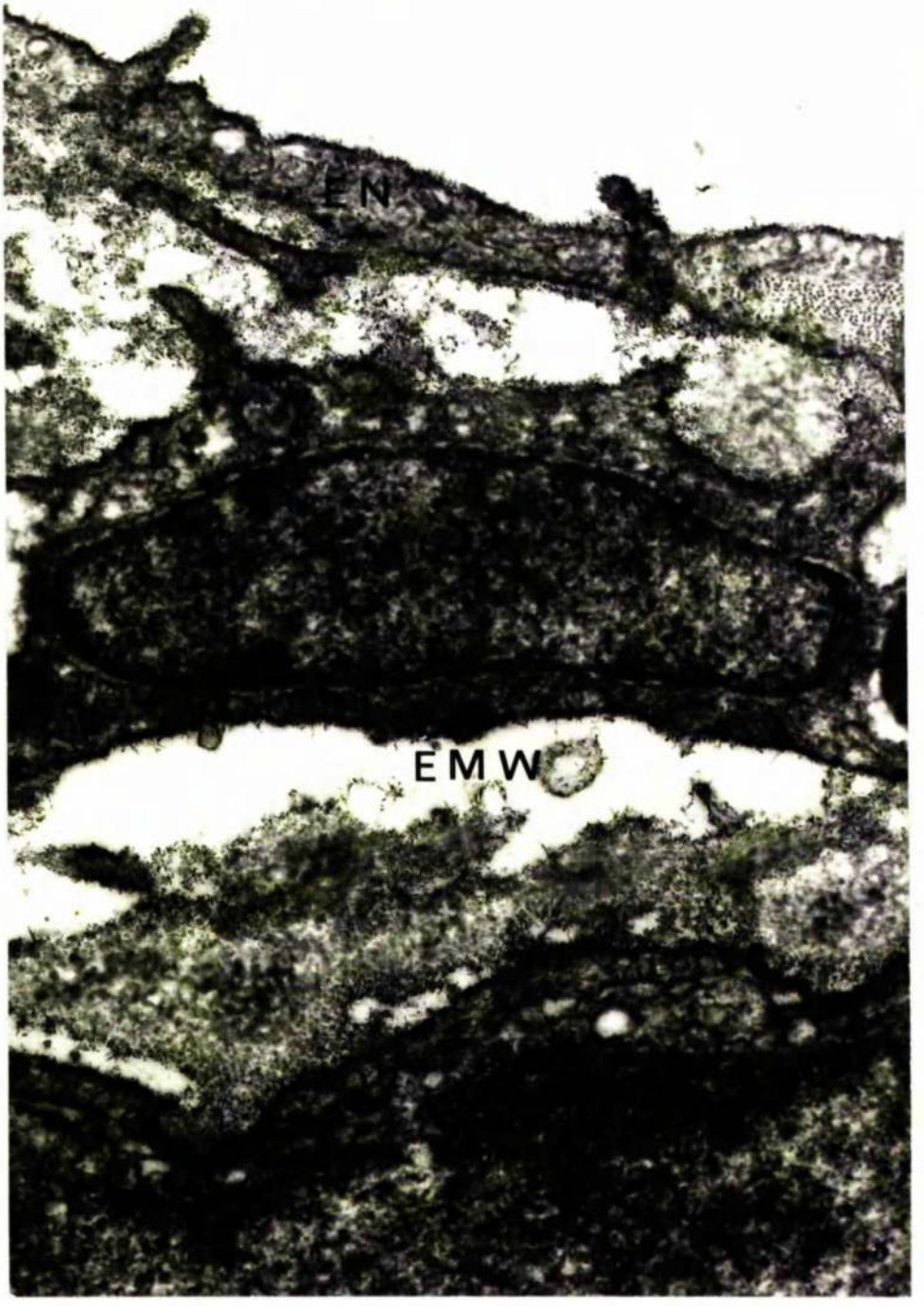

Fig.6.6 Part of the endothelium lining Schlemm's canal (EN) and the endothelial meshwork (EMW) from a baboon after colloidal iron treatment. T.E.M., uranyl acetate counterstain (x40,000).

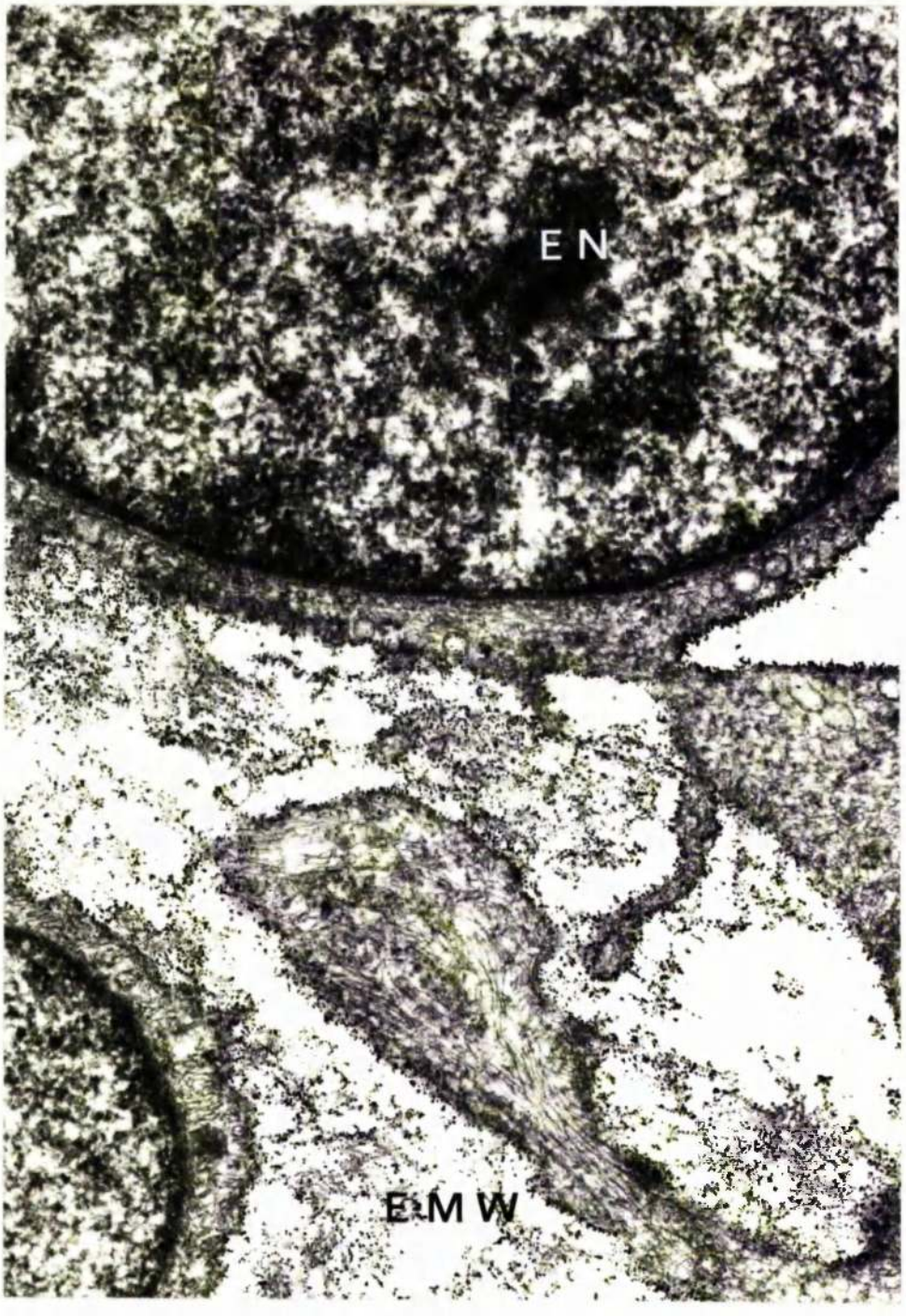

Fig.6.7 Part of the endothelium lining Schlemm's canal (EN) and the endothelial meshwork (EMW) of a human after colloidal thorium treatment. T.E.M., uranyl acetate counterstain (x39,000).

association with the plasma membrane. A similar, although thicker, coat formed a continuous layer on the luminal surface of the lining endothelium of the trabecular wall, the corneoscleral wall, the bridging septae and the collector channels. Except for a few of the small particles the stain deposit did not penetrate, to any great extent, the 200Å clefts between the neighbouring cells. Intracytoplasmic iron and thorium particles were identified within the micropinosomes at the cell surface and in this situation the smaller particles penetrated more easily than the larger (Fig. 6.8).

The giant vacuoles in the endothelium lining the trabecular aspect of Schlemm's canal had, invariably, a continuous lining of stain on the luminal aspect of their limiting membranes (Figs. 6.9 and 6.10). When meshwork and canal pores were found in the vacuoles it could be seen that the stain coat on the vacuolar membranes was in continuity with that on the plasmalemmae. In association with the meshwork pores, there were aggregates of particulate staining material both within and immediately beneath the pores (Fig. 6.10). On occasion, colloidal particles were identified within the vacuolar lumen either as dense aggregates or in association with loosely dispersed flocculent material (Fig. 6.9).

When the colloidal iron was converted to Prussian blue the reaction product was prevalent in the extracellular spaces of the endothelial meshwork and was found as an irregular deposit on the surfaces of the endothelial meshwork cells and the cells lining Schlemm's canal. Precipitate was frequently observed within the cytoplasm of both cell type

Pretreatment with hyaluronidase removed much of the colloidal thoriu and iron from the outer meshwork and abolished the Prussian blue reaction. Residual colloidal particles, which were present even after the longest exposures to the maximum concentration of enzyme, were more in evidence on the cell surfaces than in the extracellular spaces. The coating on the

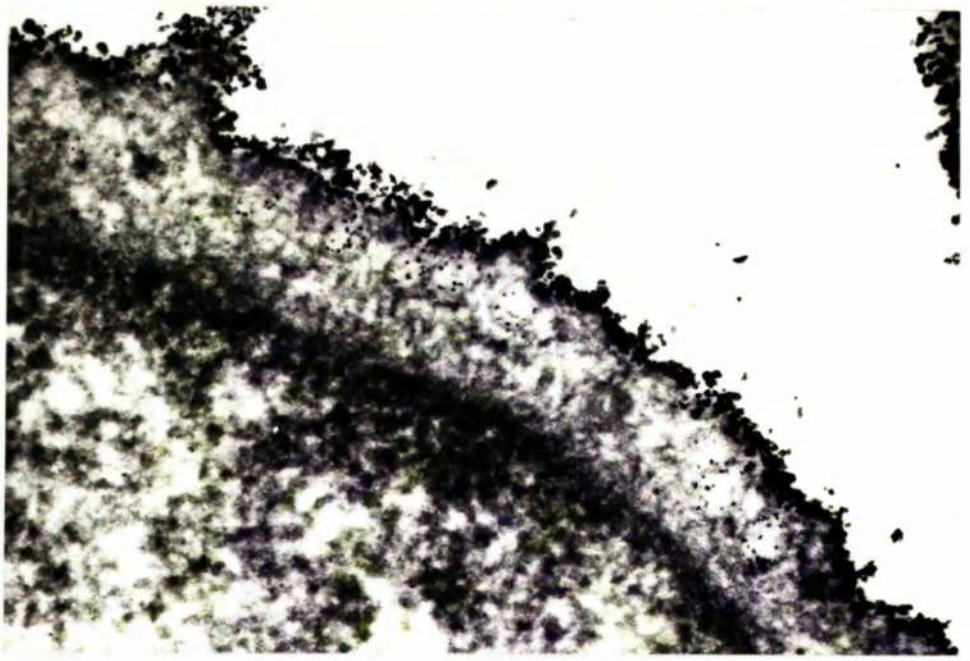

Fig.6.8 The particularly dense coat on the luminal surface of the endothelium lining the trabecular aspect of Schlemm's canal. Only the smallest particles have entered the surface micropinosomes. Thorium treated human tissue with no counterstain. T.E.M. (x90,000).

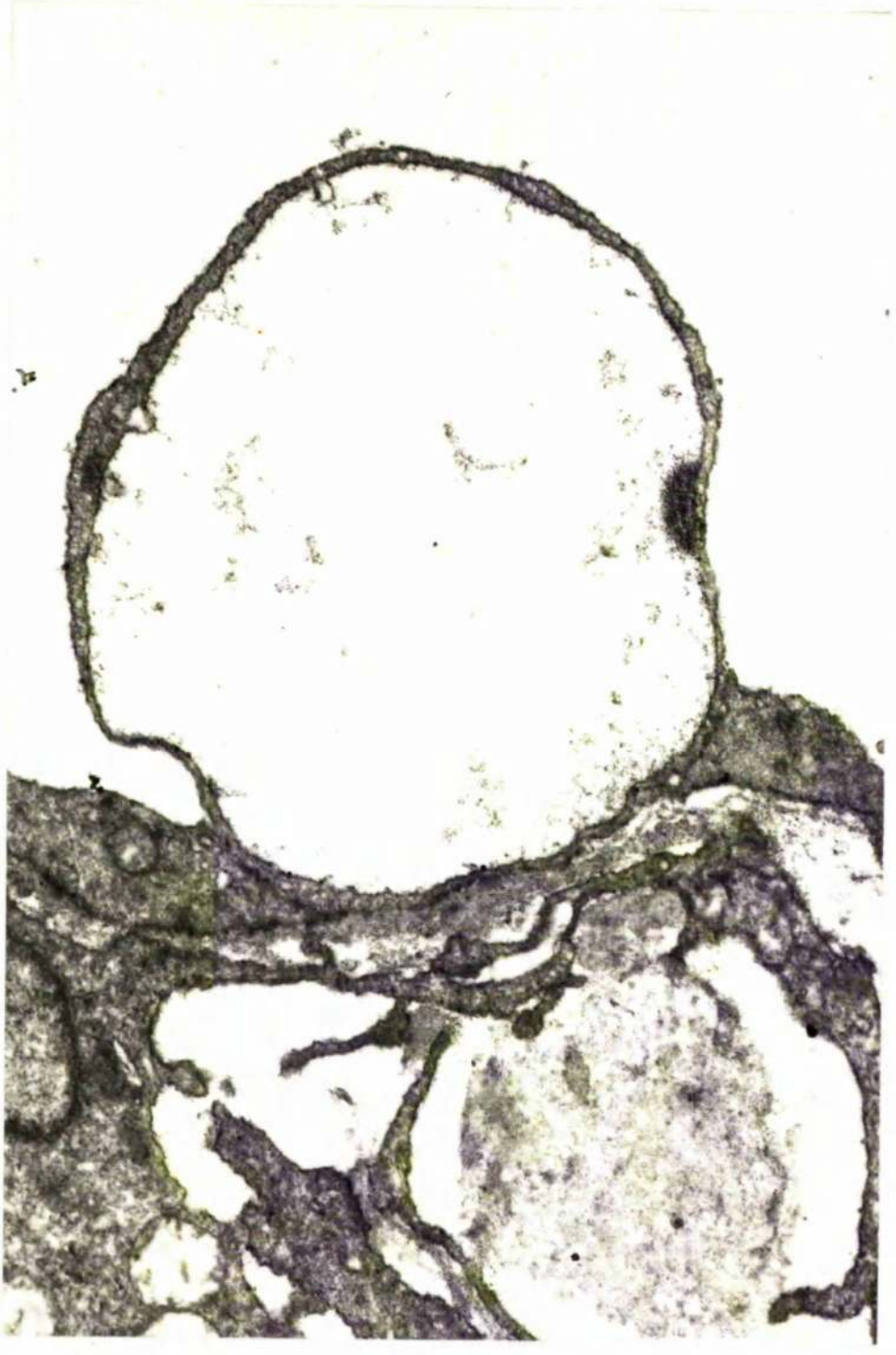

Fig.6.9 A giant vacuole in the endothelium lining the trabecular aspect of Schlemm's canal from baboon tissue stained with colloidal iron. Electron dense iron deposits are present within the vacuole lumen. T.E.M., uranyl acetate counterstain (xI7,000).

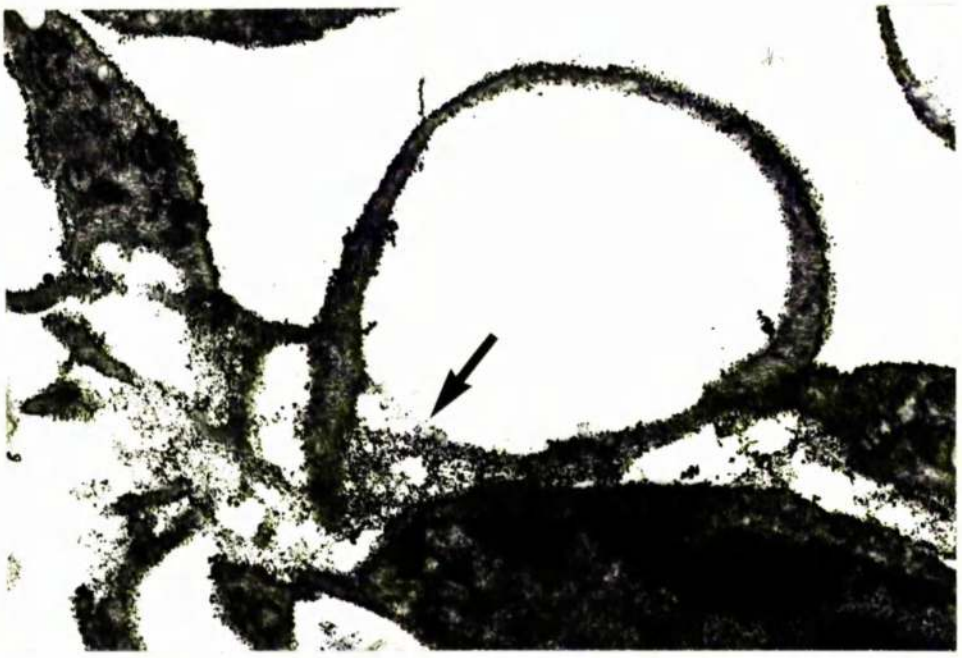

Fig.6.IO A giant vacuole with a meshwork pore (arrow) in the endothelium lining the trabecular aspect of Schlemm's canal from rhesus monkey tissue stained with colloidal thorium. Stain particles are concentrated in and around the pore opening. T.E.M., uranyl acetate counterstain (x23,000).

luminal aspect of the endothelium lining Schlemm's canal was particularly resistant to hyaluronidase action.

6.4.2 The rabbit

The pattern of colloidal thorium and iron deposition was similar to that seen in the meshwork of the three primate species. A coating of colloidal particles was present on the plasma membrane of each meshwork cell and concentrations of particles were in close association with the extracellular connective tissue elements but were absent from the intertrabecular spaces. Staining was particularly obvious in the meshwork adjacent to the endothelium lining the vessels of the aqueous plexus (Fig. 6.11) and the vessel endothelium had a layer of staining material on both its meshwork and lumen surfaces (Fig. 6.12a). Invariably, vacuole had a layer of colloidal particles around their limiting membranes. Pretreatment with hyaluronidase produced a similar reduction in the amount of stain deposit to that observed in the primates (Fig. 6.12b).

After iron treatment with conversion to Prussian blue, deposits of hyaluronidase-sensitive reaction product were found in the trabeculae, the endothelial meshwork and on the endothelial cells which lined the vessels of the angular aqueous plexus.

6.5 Ruthenium red

Although the ruthenium red staining reaction is poorly understood and, in the present investigation hyaluronidase pretreatment was unhelpful, essentially the staining pattern was similar to that found with the cationic dyes.

An electron-dense coating of ruthenium red covered the surface of meshwork cells and canalicular endothelial cells in both the baboon and the rabbit. As well as forming a deposit on "free" cell surfaces,

Fig.6.II Colloidal iron staining of the grouhd substance in the rabbit endothelial meshwork. T.E.M., uranyl acetate counterstain (x49,000).

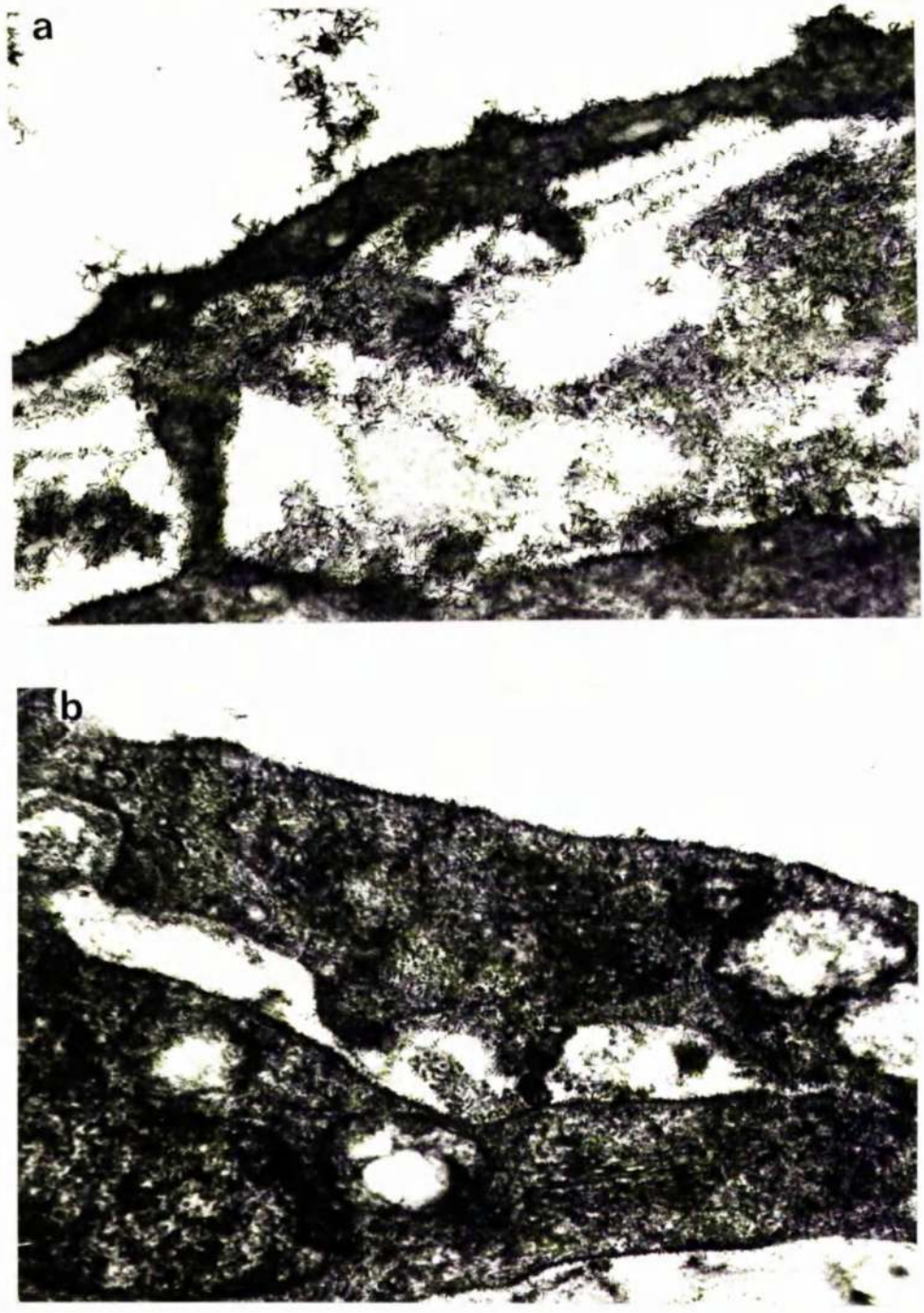

Fig.6.I2 Part of the endothelium lining a vessel of the rabbit aqueous plexus and the underlying endothelial meshwork. A demonstration of iron deposition a) without and b) after preincubation in hyaluronidase (500 W.H.O. units per ml for 24 hours). T.E.M., uranyl acetate counterstain (x4I,000).

ruthenium red penetrated intercellular spaces much more readily than the coarser cationic colloidal dye particles (Fig. 6.14). With high concentrations of ruthenium in the fixative solutions (600 to 1,000 p.p.m. a thick and continuous deposit was present on the cell surfaces and in the intercellular spaces (Figs. 6.13 and 6.14) but at low concentrations (400 p.p.m. and less) the stain distribution was more patchy (Fig. 6.15). With low concentrations of ruthenium red in the fixative solutions there was preferential staining for the interspaces of gap junctions (chapter 5, Fig. 5.16), maculae adhaerentes and the luminal surfaces of micropinosomes which opened onto the cell surface (Fig. 6.15).

Ruthenium red increased the electron density of the connective tissue elements in the trabeculae (Fig. 6.13). The trabecular basement substance showed intense staining, whereas ruthenium helped to emphasise the banding patterns in both the clumps of elastic-like material and the collagen fibrils.

The extracellular spaces of the endothelial meshwork had a particular affinity for ruthenium and the fine grain deposit demarcated a delicate network of interconnecting filaments which extended between neighbouring cells and surrounded aggregates of collagen, curly collagen and elastic-like material (Fig. 6.16). To see the network to its best effect the ruthenium concentration in the fixative had to be low (400 p.p.m. and less) otherwise the fine filaments were masked by electron dense stain deposits.

6.6 Discussion

This investigation has provided evidence to indicate that complex polysaccharides are constituents of the normal primate and rabbit outflow apparatus. The findings therefore furnish support for the more limited ultrastructural investigations conducted by Segawa (1970b) and Armaly and

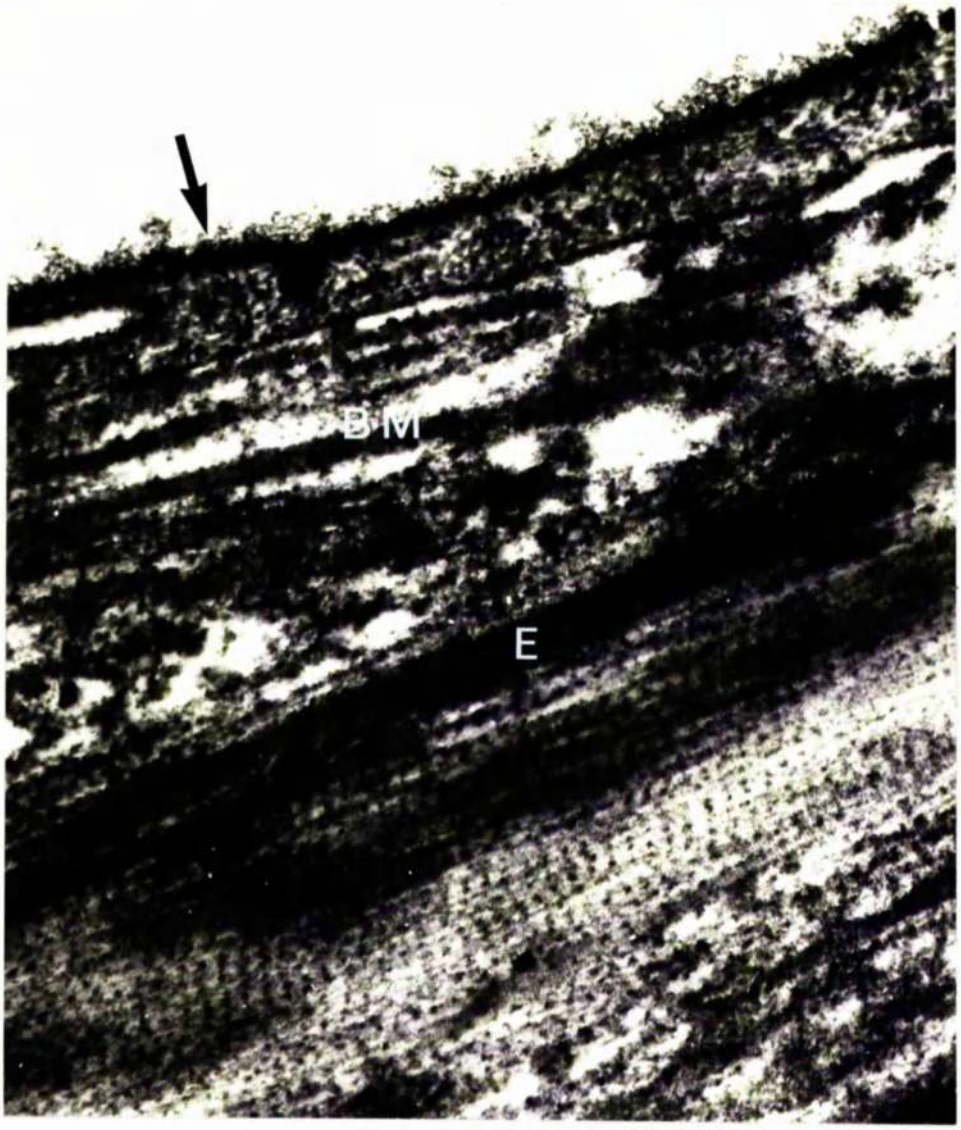

Fig.6.I3 Part of a baboon corneoscleral trabecula stained with ruthenium red (I,000 ppm). The apical surface of the endothelium (arrow), the basement material (BM), elastic-like substance (E) and the collagen are electron dense. T.E.M., no subsequent section staining (x54,000).

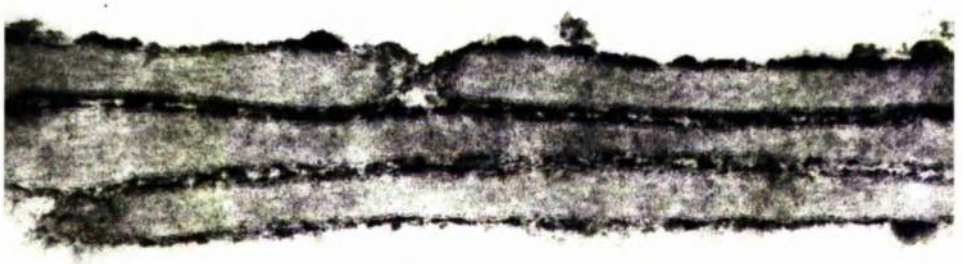

Fig.6.I4 Ruthenium deposit in the intercellular spaces of process connections in the baboon meshwork. T.E.M., no section staining, ruthenium concentration 800 ppm (xI00,000).

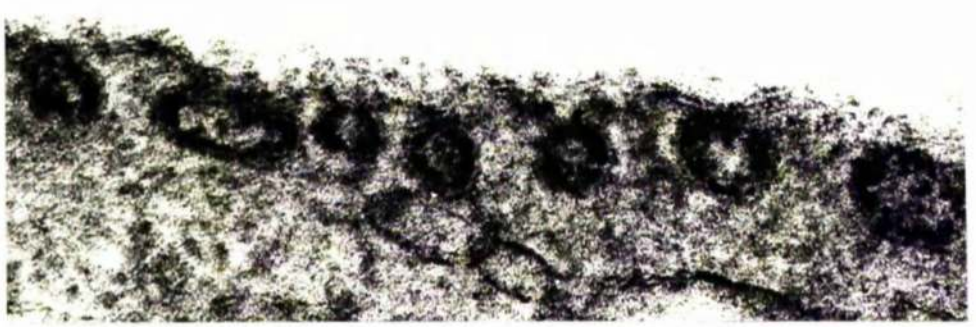

Fig.6.I5 Micropinosomes on the apical surface of the baboon canal endothelium. T.E.M., no section staining, ruthenium concentration 400 ppm (x350,000).

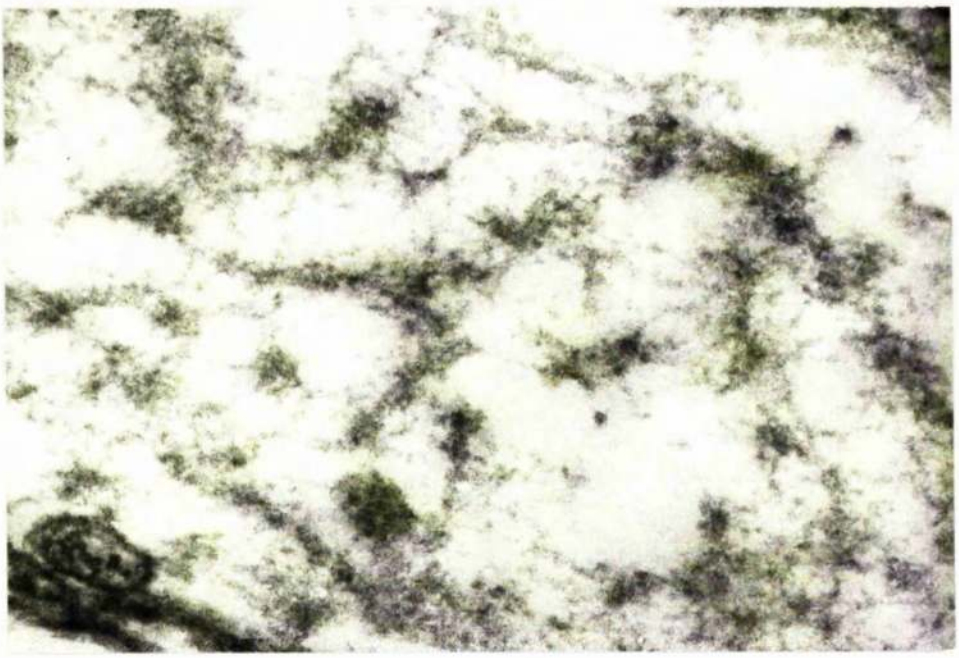

Fig.6.I6 Mucopolysaccharide network in the baboon endothelial meshwork after ruthenium red treatment (400 ppm). T.E.M., no counterstain (xI00,000).

Wang (1975). It has been shown that a major constituent of this meshwork mucopolysaccharide is sensitive to testicular hyaluronidase and, as such, is probably hyaluronic acid containing mucopolysaccharides and/or acidic sulphomucins which contain condroitin sulphate a and c (Pearse, 1972). On the other hand, to promote enzyme penetration into the tissue blocks, a wide range of time exposure is necessary (1 to 48 hours) so that at the longer exposures the possible proteolytic action of the enzyme may account for a proportion of the reduced staining.

The persistance of residual stain, particularly on cell surfaces, even after prolonged exposure to hyaluronidase may be due to insufficient enzyme penetration but it could also be explained by the presence of other hyaluronidase-resistant complex polysaccharides in the tissue. The most likely candidates are the sialic acid containing polymers which are though to be constituents of the extracellular coat on most cell types (Rambourg and Leblond, 1967).

Direct evidence for the reaction of ruthenium red with the polysaccharide moieties of mucopolysaccharides has not been provided in this study but the similarity of its staining pattern with that of the other staining systems, in conjunction with the conclusions of Luft (1971) makes the proposal a reasonable one.

The importance of acid mucopolysaccharides in the meshwork does not necessarily depend on the amount present (which is unknown) but their strategic positioning in relation to the pathways for aqueous flow. Colloidal thorium and iron staining indicates that the heaviest concentrations are to be found in the extracellular spaces of the endothelial meshwork of both the primates and the rabbit. After ruthenium red treatment the complex polysaccharides are seen to be organised into a delicate network of filaments. The hydrophilic mucopolysaccharide network, situated in the narrow and intricate flow pathways of the endothelial

meshwork may have a significant influence on fluid conductance. In addition, if the distribution of mucopolysaccharides is patchy, the network could create regions of preferential flow. The concept, that fluid may pass more easily through certain functionally discrete pathways in the meshwork (Rohen, Lütjen and Barány, 1967; see Chapters 7 and 9), is supported by the observation that clusters of giant vacuoles are often particularly prominent where the underlying extracellular spaces are distended and positive staining for extracellular mucins is sparse. If giant vacuoles are involved in the transfer of aqueous across the endothelial monolayer lining Schlemm's canal (see Chapters I, 4, 7, 8, 10 and 12) then mucopolysaccharides, by reducing the effective diameter of the vacuolar channel, may also influence aqueous outflow at this site (Fig. 6.17). Indeed the fact that all the giant vacuoles have stain deposit on their limiting membranes, is indirect evidence to show that most vacuoles must have at least one opening through which the stain can enter.

Extrapolation from the morphological evidence provided by electron microscopy to in vivo and in vitro facility measurements of the effects of hyaluronidase on the drainage route is tenuous. In this experiment an obvious reduction in colloidal thorium and iron staining is seen only after 2 hours of incubation of fixed tissue blocks in hyaluronidase. It is possible that there is considerable enzyme action with short exposure, but that the staining systems are not sufficiently sensitive to detect the change. Certainly, previous attempts to demonstrate a hyaluronidase-sensitive barrier by facility measurements, although they have provided variable results, have shown a quite rapid hyaluronidase effect which was more convincing in non-primates (Barány, 1953; Barány and Scotchbrook, 195 Berggren and Vrabec, 1957) than in primates (Pedler, 1956; Grant, 1963;

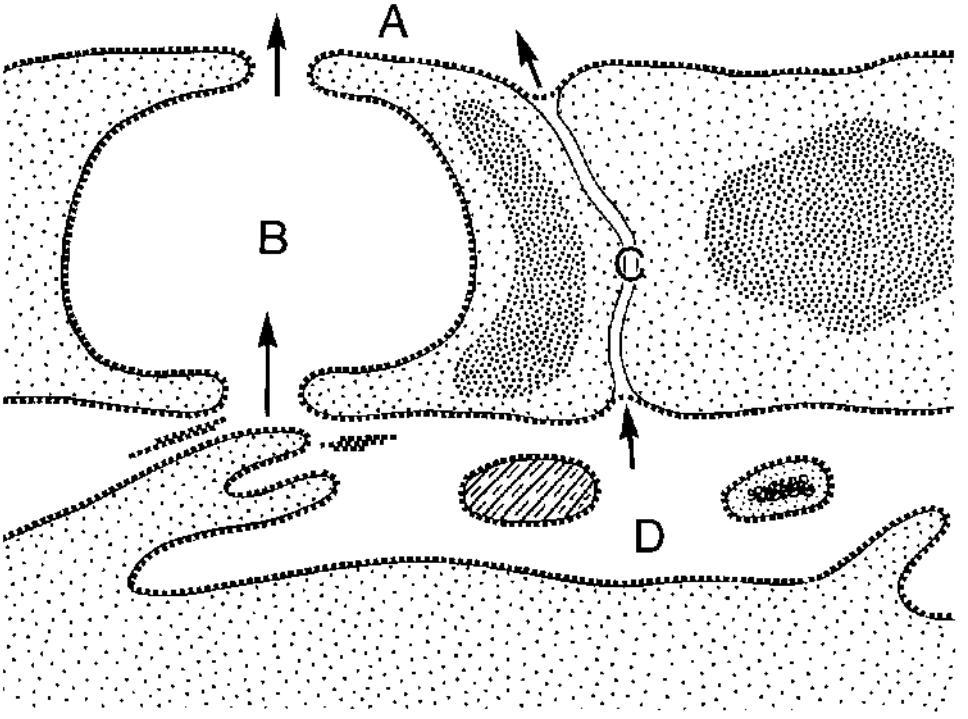

Fig.6.17 The transendothelial passage of aqueous from the endothelial meshwork (D) into Schlemm's canal (A) whether transcellular (B) or intercellular (C) will be influenced by the presence of mucopolysaccharides. In the diagram mucopolysaccharides are indicated by a dotted line.

Petersen and Jocson, 1974). It would appear that a valid correlation between facility determinations and morphological appearances requires a staining technique of fine resolution, which will permit quantitation, so that subtle changes in the acid mucopolysaccharide content (produced by short exposures to hyaluronidase) can be determined.

THE MORPHOLOGY OF THE OUTFLOW APPARATUS OF THE EYE WITH PARTICULAR REFERENCE TO ITS STRUCTURAL APPEARANCE AT VARIOUS LEVELS OF INTRAOCULAR PRESSURE

VOLUME II

CONTENTS OF VOLUME II

VOLUME II

ILLUSTRATIONS IN VOLUME II

VOLUME II

CHAPTER 7

CHAPTER 8

CHAPTER 9

SUMMARY TO VOLUME II

Volume II of this thesis describes the appearance of the aqueous humour outflow system of rhesus monkey eyes maintained, for one hour, at various intraocular pressure levels (0, 8, 15, 22, 30 and 50 mm Hg).

The meshwork was compressed at 0 mm Hg and became progressively distended as intraocular pressure was elevated so that at 50 mm Hg, much of the canal lumen was occluded. Up to 30 mm Hg, tissue integrity was preserved but at 50 mm Hg, the endothelium lining the trabecular aspect of Schlemm's canal was perforated and the architecture of the underlying meshwork was disrupted.

Giant vacuoles were absent from the canal endothelium at 0 mm Hg but there was a linear increase in vacuole numbers from 8 to 30 mm Hg. Because the average size of the vacuoles also increased with pressure elevation, the relationship between intraocular pressure and the aqueous carrying capacity of the vacuole population was non-linear. At 50 mm Hg there were fewer vacuoles than at either 30 or 22 mm Hg.

Most of the vacuolar structures were blind invaginations from the meshwork surface of the endothelial cells but a small proportion were transcellular channels. It was considered that the transcellular channels may serve as pathways for the passage of aqueous humour into Schlemm's canal. As the channels became progressively more prevalent up to 30 mm Hg, the vacuole/transcellular channel system was a pressure dependent outflow route. Non-vacuolar transcellular channels, associated with marginal regions of the canal endothelial cells, were thought to be an auxilliary pathway for aqueous passage through the trabecular wall of Schlemm's canal. The non-vacuolar channels were also temporary pressure-sensitive structures and were probably similar in nature to the vacuolar channels.

It was considered that pressure maintenance during fixation was necessary for future morphological studies on the drainage system otherwise the appearance of the tissue may not reflect the in vivo situation.

CHAPTER 7

A QUALITATIVE ANALYSIS OF THE CHANGES INDUCED IN THE RHESUS MONKEY OUTFLOW APPARATUS BY INTRAOCULAR PRESSURE ALTERATION (AS SEEN BY LIGHT MICROSCOPY AND SCANNING ELECTRON MICROSCOPY)

7.1 Introduction

This chapter describes the gross morphological appearance of the outflow apparatus at graded levels of intraocular pressure. To this end, the tissue was examined both by light microscopy and scanning electron microscopy.

7.2 Materials and methods

Fourteen rhesus monkeys were the subjects of the investigation into pressure effects on the outflow apparatus (appendix 6) and the details of the experimental procedures were outlined in Chapter 3. Thick sections for light microscopy were usually cut in the meridional plane but tilted-frontal sections were also examined. Meridional slices of limbal tissue and flat preparations of the innermost uveal lamellae were screened in the scanning electron microscope.

7.3 Pressure effects within the near physiological range

7.3.1 15 mm Hg (control tissue)

The outflow apparatus in the 2 eyes fixed by carotid perfusion were indistinguishable from those fixed by anterior chamber perfusion. There was some variation in the gross appearance of the outflow apparatus in the 15 mm Hg control series but this was far less than that seen in the group of normal rhesus monkey eyes where intraocular pressure was not regulated (the subjects of Chapter 4). A common description could, therefore, be provided.

Schlemm's canal was open in all quadrants of each eye but the canal lumen was more enlarged in some eyes than others. The nuclei of the endothelial cells on the trabecular aspect of the canal were rounded and produced prominent cytoplasmic bulges. Those on the corneoscleral

aspect of the canal were more elongated and ellipsoid so that their perinuclear projections were less distinctive. Moderate numbers of irregularly distributed giant vacuoles were a feature of the endothelium on the trabecular aspect of the canal, were rare in the endothelium lining the septae and were absent from the endothelium on the canal's corneoscleral aspect (Fig. 7.1). Generally the endothelial meshwork was compact but it became more distended where a collector channel drained the canal lumen. Intertrabecular spaces were narrow but distinct between the trabecular lamellae of the outer corneoscleral meshwork, were wider in the inner corneoscleral meshwork and were widest between the trabecular layers which comprised the uveal meshwork (Figs 7.1 and 7.2).

Under the scanning electron microscope the canal endothelium above the meshwork was seen as a monolayer from which discrete fusiform bulges projected into the canal lumen. Where sectioned, the bulges were either solid (nuclei) or hollow (giant vacuoles) (Fig. 7.3). Endothelial cell processes, seen to cross the intertrabecular spaces from thick sections (Fig 7.2), were visualised in three dimensions as either pillars or strands. Cell bodies which linked adjacent trabeculae were identified as flat sheets of tissue (Fig. 7.3). The pillars, strands and sheets compartmentalised the intertrabecular spaces and, particularly in the outer meshwork where spaces were narrow, created a maze of tortuous passageways through which aqueous must pass to reach the canal endothelium. The intertrabecular spaces were narrow in the outer corneoscleral meshwork and the intratrabecular openings were small. On the other hand, the openings through the uveal trabecular lamellae were extremely large with diameters of approximately 60 μm in the posterior portion close to the iris root and 30 to 40 μm through the more compressed anterior

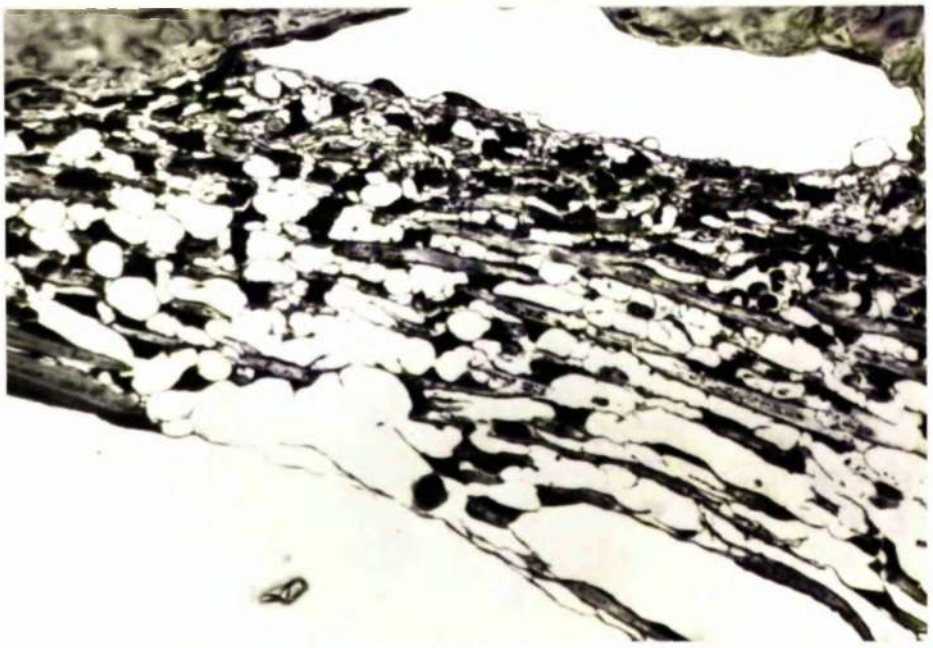

Fig.7.I Part of the outflow system at I5 mm Hg. The canal lumen is open and giant vacuoles of various sizes are present in the endothelium lining the canal's trabecular aspect. L.M. (x350).

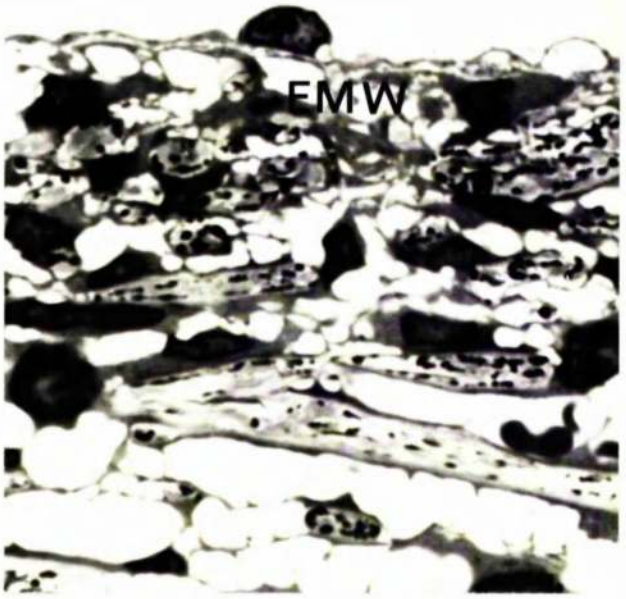

Fig.7.2 Part of the outer meshwork including the endothelial meshwork (EMW) at I5 mm Hg. L.M. (xI,200).

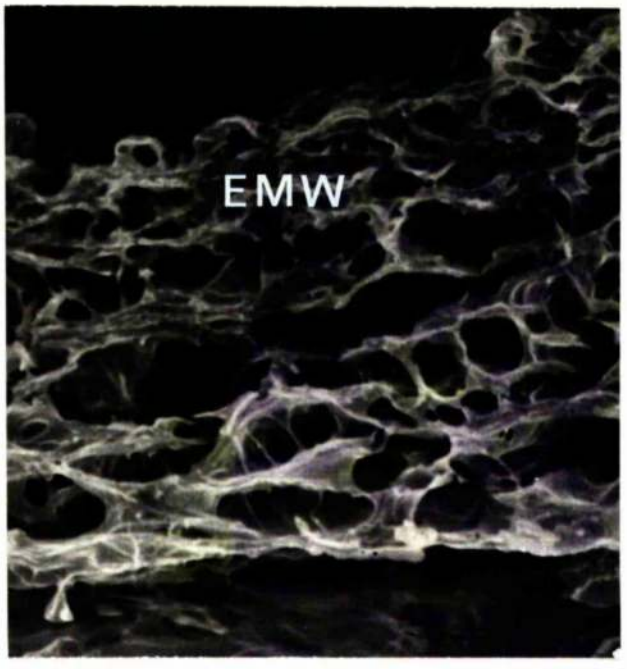

Fig.7.3 S.E.M. showing a similar region to that in 7.2. The endothelial meshwork (EMW) is indicated. (xI,200).

portion close to the corneal endothelium (Fig. 7.4).

7.3.2 8 mm Hg

The lumen of Schlemm's canal was usually wide and both the canal and adjacent collector vessels contained scattered clumps of red cells (Fig. 7.5). In the endothelium lining the canal, nuclear protrusions were obvious on the trabecular aspect but giant vacuoles were small and infrequent. Vacuoles were absent from the endothelium lining the septae (Figs 7.5 and 7.7). Under the canal endothelium, the endothelial and outer corneoscleral meshwork were compressed and showed a distinctive inward bowing towards the anterior chamber angle which could be seen to the best effect under the scanning electron microscope (Fig. 7.6). It was appreciated that the "flow pathways" for aqueous through the outermost corneoscleral trabecular lamellae and the endothelial meshwork were flattened and more tortuous as a result of the tissue compression.

Although cell and tissue relationships were altered in the outer meshwork, the intertrabecular spaces between the trabeculae of the inner corneoscleral and the uveal meshwork were of a similar width to those in the 15 mm Hg control group (Figs 7.5 and 7.6). Equally, the intratrabecular openings through the uveal trabecular layers were indistinguishable from those seen in the control group.

7.3.3 22 mm Hg

At 22 mm Hg, the endothelial and outer corneoscleral meshwork were more distended and giant vacuoles were more in evidence in the canal endothelium than at 15 mm Hg. A particular feature was the prominence of focal bulges (occasionally observed in the control tissue) in the canal's trabecular wall (Fig. 7.8). The bulges were formed by

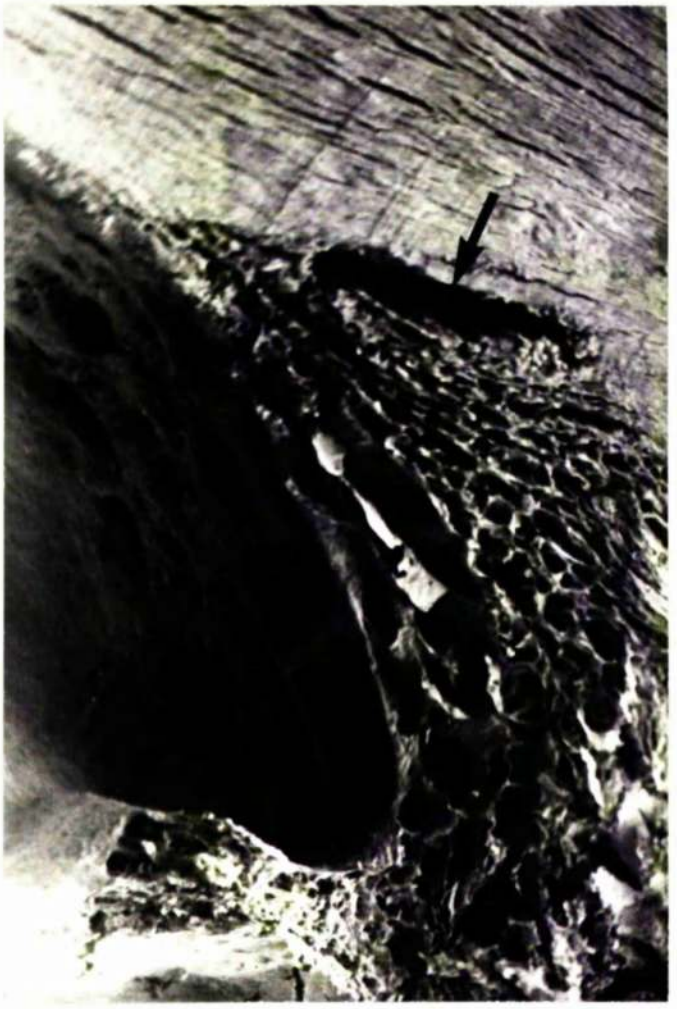

Fig.7.4 S.E.M. which shows the wide spaces of the uveal meshwork. Schlemm's canal is indicated by an arrow. I5 mm Hg (xI70).

Fig.7.5 The outflow system at 8 mm Hg. The canal lumen is wide and contains some red cells. L.M. (x350).

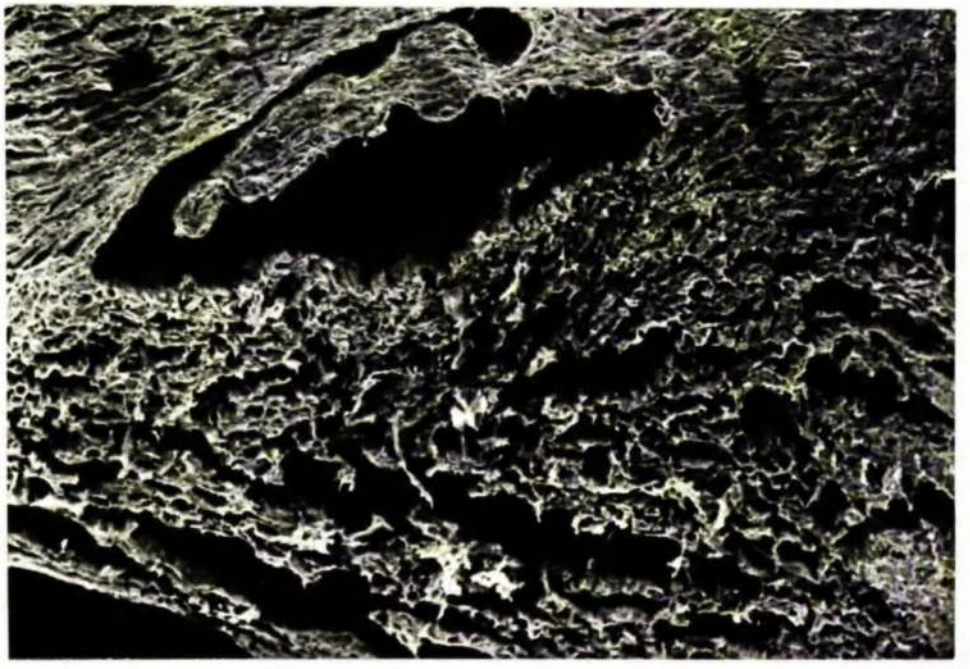

Fig.7.6 The wide canal and compressed endothelial meshwork at 8 mm Hg is particularly obvious by S.E.M. (x350).

Fig.7.7 An L.M. in which the compressed endothelial meshwork and the narrow intertrabecular spaces of the outer corneoscleral meshwork at 8 mm Hg can be seen. Giant vacuoles in the endothelium lining the canal are rare. (xI,000).

Fig.7.8 At 22 mm Hg there are focal bulges in the endothelial meshwork. L.M. (x3IO).

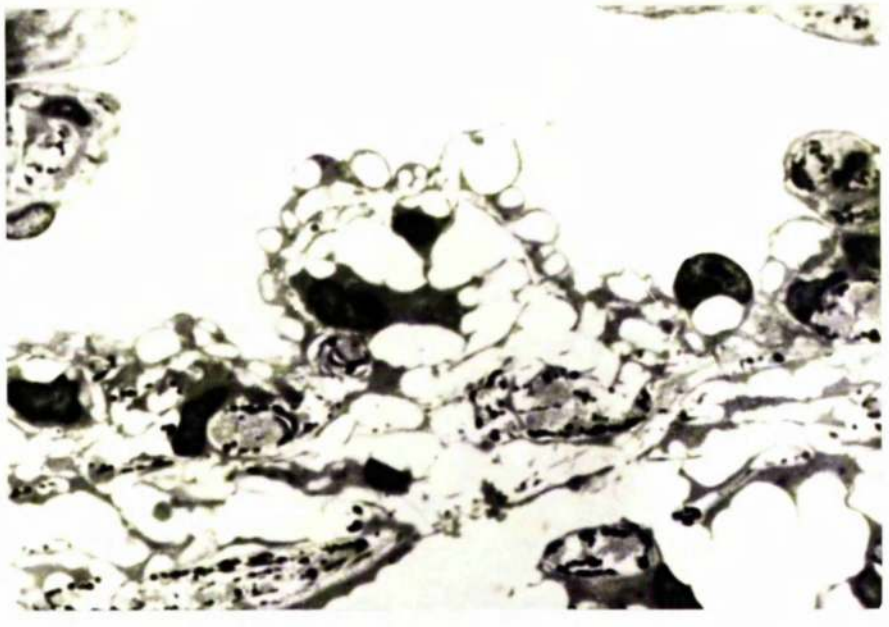

Fig.7.9 A concentration of vacuoles in the canal endothelium above a focal bulge in the endothelial meshwork at 22 mm Hg. L.M. (xI,300).

focal dilatations of the extracellular spaces and giant vacuoles were often aggregated into clusters within the overlying endothelial monolayer (Fig. 7.9). The bulging of the outer meshwork caused focal constriction of the canal lumen.

7.3.4 30 mm Hg

At 30 mm Hg, the appearance of the outflow apparatus was similar in the anterior chamber and carotid perfused tissue.

Each specimen had a narrow canal the patency of which was maintained where a septum crossed from one wall to the other (Fig. 7.10) but extreme constriction occurred where a collector channel joined the canal lumen (Fig. 7.11). Vacuolation was prolific along the whole length of the endothelial monolayer above the meshwork and vacuole size appeared to be increased. Vacuole-like structures were also abundant in the endothelium lining the septae and were, on occasion, associated with endothelial cells on the corneoscleral aspect of the canal (Figs 7.10 and 7.11). The endothelium on the trabecular aspect of Schlemm's canal was highly convoluted and the cells were thin and attenuated. Beneath the monolayer, the outer meshwork was extremely distended. Intertrabecular spaces in the outer corneoscleral meshwork were wider than at lower pressures while the extracellular spaces of the endothelial meshwork were swollen. Despite the substantial alterations to tissue configuration, associations between meshwork cells and cellular contacts between adjacent trabeculae appeared to be maintained by thin extended cell processes (Figs 7.10 and 7.11).

Three dimensional viewing revealed that there was little or no alteration to intratrabecular spatial relationships or to the large translamellar apertures within the inner corneoscleral and uveal meshwork. On the other hand, closer to Schlemm's canal dilatation of

Fig.7.10 At 30 mm Hg giant vacuoles are prominent in the endothelium lining the trabecular aspect of Schlemm's canal and the septae. L.M. (xI,100).

Fig.7.II The extreme distension of the endothelial and outer corneoscleral meshwork at 30 mm Hg. L.M. (x500).

the intertrabecular spaces was associated with enlargement of the intratrabecular openings through the outer corneoscleral lamellae.

7.4 Pressure effects outside the near physiological range

7.4.1 0 mm Hg

At this pressure, Schlemm's canal was extremely dilated and gorged with red cells. Red cells also filled the lumina of collector channels and aqueous veins. The refluxed blood contained only a few polymorphonuclear leukocytes, blood monocytes and platelets. Platelets were absent from most of the sections which were examined. The few which were found showed no evidence of degranulation or lysis, were not aggregated and none were attached to the vessel walls.

The endothelium lining the trabecular aspect of Schlemm's canal was thin but intact and was devoid of giant vacuoles. The endothelial and outer corneoscleral meshwork were indistinguishable from each other and together formed a compact zone of compressed cells and trabeculae in which few spaces were observed (Fig. 7.12). The intact canal endothelium and the compressed underlying meshwork afforded a reasonably effective barrier to blood cell penetration so that only the occasional red cell was present within the trabecular tissue.

In the inner corneoscleral and uveal parts of the meshwork the intertrabecular spaces were of similar width to those seen at higher pressures but, even at the level of light microscopy, there was detectable trabecular pathology. Some of the trabecular cores appeared thickened, the endothelium on the trabeculae was vesiculated and a proportion of the cells were either swollen or disrupted (Figs 7.12 and 7.13).

With the scanning electron microscope structural interpretation

Fig.7.I2 At 0 mm Hg the outer meshwork forms a compact zone and giant vacuoles are absent from the endothelium lining the canal. L.M. (xI,400).

Fig.7.I3 Degenerate trabeculae and wide intertrabecular spaces in the inner meshwork at 0 mm Hg. L.M. (xI,400).

was made difficult by the extrusion, during the drying process, of coagulated proteins from the blood in Schlemm's canal onto the cut surface of the compressed outer meshwork.

7.4.2 50 mm Hg

Although the uveal meshwork was little altered from that at 0 mm Hg (or, for that matter, any of the intermediate pressures), changes in the outer meshwork were quite dramatic. The tendency at 30 mm Hg for meshwork tissue to prolapse into collector channels was much more pronounced at 50 mm Hg. With the aid of the scanning electron microscope, meshwork bulges were seen to project as far as 100 µm up collector channels. In these situations, the meshwork demonstrated a remarkable ability to undergo extreme deformation without total disintegration (Fig. 7.14). The pronounced distension of the outer meshwork brought about occlusion of much of the canal lumen so that the flattened endothelium on the canal's trabecular aspect was brought into contact with the endothelium on the canal's corneoscleral aspect. Occlusion was particularly evident in the anterior portion of the canal and here only a few distorted vacuoles were distinguished. The posterior portion of the canal, supported by the scleral spur, was less prone to closure and well developed giant vacuoles were prominent in the endothelium lining the trabecular aspect of the canal. Despite the presence of vacuolar structures in the endothelium of the septae and, more occasionally, the corneoscleral endothelium, overall there appeared to be fewer vacuoles than at either 22 or 30 mm Hg intraocular pressure (Fig. 7.15).

7.5 Conclusions

This light microscopic and scanning electron microscopic

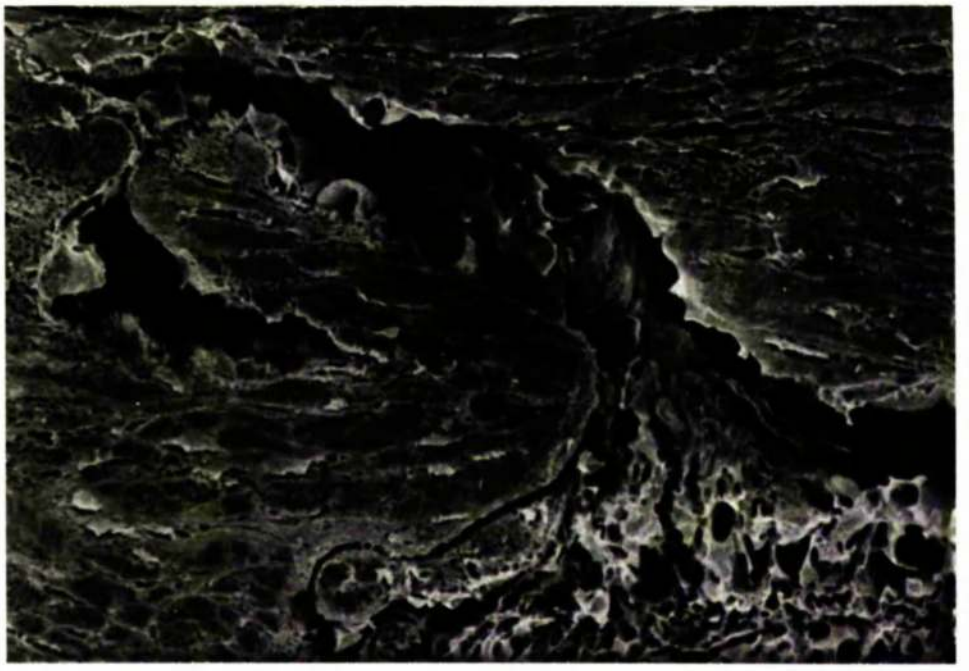

Fig.7.I4 Prolapse of outer meshwork tissue into a collector channel at 50 mm Hg. L.M. (x600).

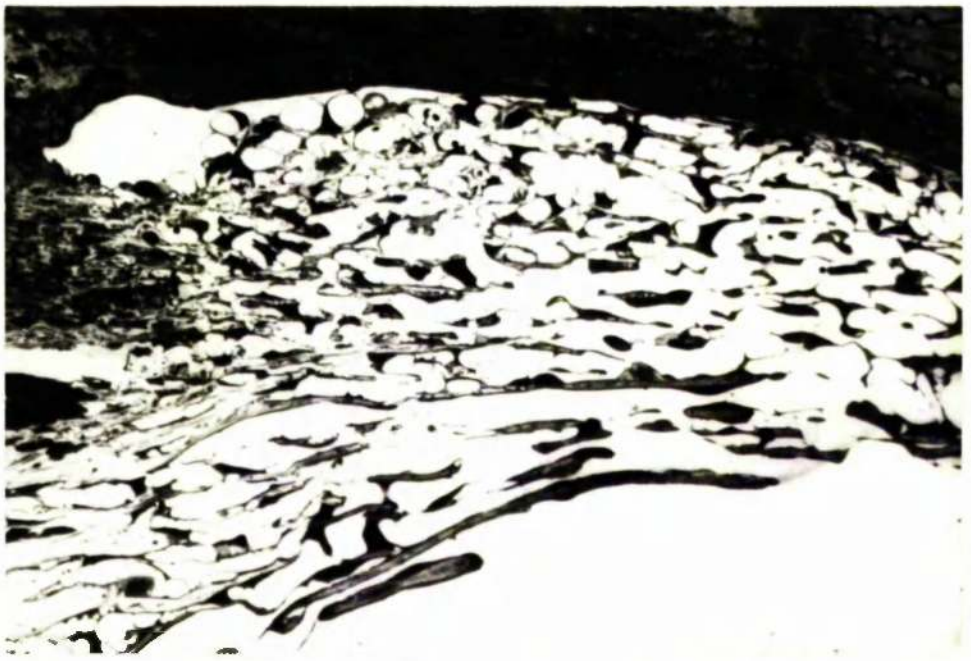

Fig.7.I5 The extreme distension of the outer meshwork at 50 mm Hg. Much of the canal lumen is occluded and giant vacuoles are restricted to regions where the canal is patent. L.M. (x350).

investigation has demonstrated that changes to intraocular pressure in vivo induce substantial alterations to the tissues of the outflow apparatus. The spatial relationships in the uveal and inner corneoscleral meshwork remained unaltered throughout the pressure range. The most marked pressure effects were on the outer corneoscleral meshwork, the endothelial meshwork and the endothelium lining the trabecular aspect of Schlemm's canal.

The delicate tissues of the outer meshwork and the trabecular wall of Schlemm's canal were remarkably pliable. At 0 mm Hg the trabecular and cellular elements were collapsed together but as intraocular pressure was increased to and passed normal (8 to 50 mm Hg) the intertrabecular spaces and intratrabecular openings became progressively wider, endothelial meshwork cells were separated and the overlying canal endothelium became convoluted and attenuated. As a result of the generalised distension of the outer meshwork at the highest intraocular pressures, the endothelium on the trabecular aspect approached and even came into contact with that on the corneoscleral aspect of the canal. Relatively rigid structures within and around the meshwork tended to oppose the distortion and displacement of the loose meshwork tissue. The outer trabeculae were strengthened by insertion into the cornea and the scleral spur; this attachment and the struts formed by the septae within the canal, prevented total occlusion even at the excessively high intraocular pressure of 50 mm Hg.

It would seem that spatial relationships in the meshwork were dependent on hydrostatic pressure and not on inherent rigidity. However, the distension of the outer meshwork produced by hypertension should not be considered solely in terms of tissue pliability since the trabeculae of the inner meshwork were likely to be equally

malleable. The fanning out of the tissue elements in the outer meshwork was probably the result of greater interference with fluid flow through this region where the openings (fluid pathways) were smaller than those in the uveal and inner corneoscleral meshwork.

Remarkably similar findings to those outlined in this chapter were reported by Johnstone and Grant (1973) from a study of enucleated human eyes. It is interesting that the property of the meshwork to distend but still maintain its integrity is a feature not only of viable tissue but also of tissue whose viability is questionable. On this basis it could be argued that changes in meshwork configuration are produced as a passive response to pressure variation and the nature of the change is dependent upon physical or mechanical properties of the meshwork cells and the architectural arrangement of the tissues.

The absence of giant vacuoles in the endothelium of Schlemm's canal at 0 mm Hg and their progressive increase with stepwise pressure increase within the near physiological range (8 to 30 mm Hg) is evidence that vacuoles are temporary pressure sensitive structures. Vacuolar pressure sensitivity has recently been demonstrated by other investigators (Johnstone and Grant, 1973; Kayes, 1975a). At the non-physiological pressure of 50 mm Hg, vacuolation was reduced and partial closure of Schlemm's canal must have been, to some extent, responsible for this reduction by severely limiting the amount of endothelium available for vacuolation. The pressure effects on the giant vacuoles merits special attention and careful consideration since these structures have been implicated in the transendothelial transfer of aqueous humour (see Chapter I). More detailed investigations of the pressure/vacuolation relationship are presented in later chapters (Chapter 8 and 10) therefore further comment on the vacuolar structures in the present chapter is unnecessary.

Although Schlemm's canal was filled with red cells at 0 mm Hg, they were absent from the inner meshwork and found only on occasion within the endothelial meshwork. This observation was consistant with the findings of Johnstone and Grant (1973), who suggested that the collapsed outer meshwork was an effective barrier to the reflux of blood cells into the anterior chamber, but was at variance with the paracentesis investigation conducted by Raviola (1974). Raviola found that, after the removal of primary aqueous humour, platelets abounded in the lumen of Schlemm's canal, the integrity of the endothelial monolayer was lost and blood penetrated the meshwork. In the present investigation (and that of Johnstone and Grant, 1973) obvious deficits in the canal endothelium were not found and there was no evidence of platelet accumulation. The findings indicate that the effectiveness of the meshwork as a blood aqueous barrier may depend on the vigour by which artefical reversal of the normal pressure gradient is achieved.

When Johnstone (1974) investigated pressure dependent changes in the rhesus monkey outflow system he described villus-like structures projecting from the meshwork into the lumen of Schlemm's canal. The villi were thought to be open ended endothelial lined tubules which established free communication between the meshwork and Schlemm's canal. It was suggested that, at physiological pressures the tubules were distended but at low pressures they were compact, thus they functioned as one way valves by permitting aqueous outflow in the former situation but not the reflux of blood in the latter.

Johnstone's demonstration was not entirely convincing because he was unable to show the actual canalicular openings of the so-called tubules. The existence of endothelial tubules was not confirmed during the present study. At physiological pressures, structures

remarkably similar to Johnstone's tubules were noted from isolated thick sections but examination of a sequence of serial sections revealed that they were either the trabecular portion of a septum or blind focal bulges from the canal's trabecular wall.

CHAPTER 8

A QUANTITATIVE ASSESSMENT BY LIGHT MICROSCOPY OF PRESSURE EFFECTS ON THE GIANT VACUOLE POPULATION

8.1 Introduction

A quantitative analysis by light microscopy was attempted to determine in a more precise manner the effects of intraocular pressure alteration on the giant vacuole population in the endothelium lining Schlemm's canal.

8.2 Materials and methods

This part of the investigation was restricted to the 9 rhesus monkeys used for investigations of pressure change within the near physiological range and which were fixed by anterior chamber infusion, plus the 3 animals in which intraocular pressure was maintained at 0 and 50 mm Hg.

8.2.1 Vacuole counts; nucleus counts (0 - 50 mm Hg tissue)

Four blocks of tissue from each quadrant were taken for this part of the analysis. One hundred serial sections (1.5 µm) were cut from each block and every tenth section was used for a "vacuole count" (Fig. 8.1) in which the giant vacuoles were counted in the following regions of the canal lining endothelium:-

a) the trabecular aspect

b) the corneoscleral aspect

c) the septae and the endothelium connecting the trabecular and the corneoscleral aspects of Schlemm's canal.

The vacuole counts were made with x 10 and x 100 (oil immersion) lenses on coded sections and personal repeatability tests gave a variation of less than 8%. The results were expressed as either a total vacuole count from the 160 serial sections from each eye or as a mean value per section which was calculated from the series of counts

ANALYSIS	4 blocks per quadrant	100 sections per block	150/um per block (approximately)
TOTAL	16 blocks per EYE	1,600 sections per EYE	2,500/um sample per EYE (approximately)

Fig.8.I The tissue sampled from each eye for the vacuole counts.

done on each eye.

The nuclei in the endothelium lining the trabecular aspect of Schlemm's canal were counted in one thick section from each of eight tissue blocks (two from each quadrant) in the nine 15 mm Hg control eyes. This analysis was performed to determine whether or not there was a significant variation in the numbers of nuclei, and therefore the endothelial cells, between individual animals.

8.2.2 Vacuolar dimensions (8 - 30 mm Hg tissue)

The length and maximum width of the individual vacuoles at the various pressure levels was determined from photomicrographic enlargements (at a print magnification of x 1,000) of the lining endothelium in 100 serial thick sections from one randomly chosen block of tissue from each eye.

The total numbers of complete and incomplete vacuoles within the 150 μm length of the lining endothelium were separately recorded and from the vacuole reconstruction data, an average value for vacuolar length and maximum width was obtained.

The vacuolar length was expressed in terms of the number of sections which included the individual complete vacuole. Values for maximum vacuolar width (μm) were obtained from the complete vacuoles with the aid of a x 7 magnifying lens which incorporated a graticule.

8.2.3 Estimated vacuolar numbers, volume and capacity

For the purpose of these estimations (derived from the information provided by the quantitative analysis) it was necessary to assume that the vacuolar dimensions obtained from serial reconstruction were representative of the total vacuole population

in a given eye.

8.3 Results

It was necessary to provide a working definition of what constituted a giant vacuole because these structures had such a variable shape. As seen by light microscopy, giant vacuoles appeared as smooth walled, round, ovoid or reniform vesicles within the cytoplasm of the endothelial cells lining the canal. The vacuoles frequently projected into the lumen of Schlemm's canal and were in general empty, but occasionally wandering cells or red cells were identified within the vacuole (Fig. 8.2). Structures which were considered to simulate vacuoles included:-

a) localised bulges which involved more than one endothelial cell and were possibly the pseudovacuoles described by Rohen (1969).

b) small areas of lucency at the limits of optical resolution which could have been either spaces between adjacent cells or spaces between processes from the lining endothelium and the underlying meshwork cells.

Using the above criteria the differences in sample vacuole counts between two observers was less than 5% when vacuoles were numerous but was slightly higher when vacuoles were infrequent (the average interobserver error was approximately 8%).

8.3.1 Vacuole counts

The results obtained for the vacuole counts for the three animals in each pressure group 30, 22 and 8 mm Hg are shown with their corresponding controls in Figs 8.3, 8.4, 8.5. The mean value for the vacuole counts per thick section at 30 mm Hg was approximately four

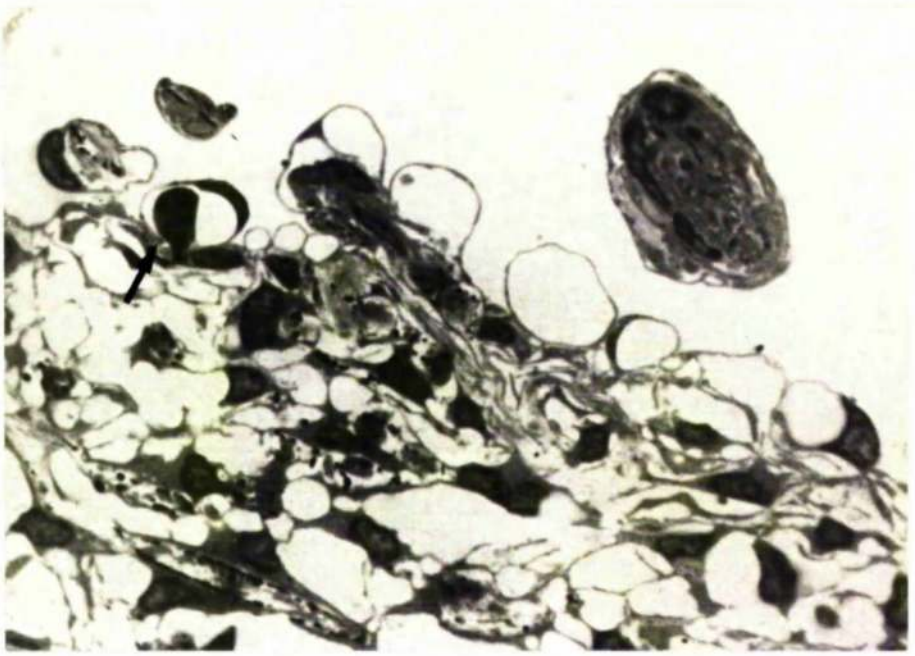

Fig.8.2 Giant vacuoles in the endothelium on the trabecular aspect of Schlemm's canal at 30 mm Hg. The lumen of one vacuole contains part of a wandering cell (arrow).L.M.(xI,300)

times that in the corresponding 15 mm Hg controls (Fig. 8.3). At 22 mm Hg the mean vacuole counts were also larger than the control values but the difference, although significant for each of the three animals ($P<0.001$), was less striking (Fig. 8.4). By way of contrast, at 8 mm Hg the mean vacuole counts were significantly lower than the control counts ($P<0.001$) (Fig. 8.5). The variation in the vacuole count at different levels of section, both within the same tissue block and between different blocks from each eye, was substantial. However when the values obtained from the opposite halves of each eye were compared no overall trend to sectorial difference was apparent in either the 15 mm Hg control eyes (Fig. 8.7) or in the experimental eyes.

The total vacuole counts (i.e. the total count from 160 sections for each eye) were plotted in the form of a scatter diagram of vacuole counts against the intraocular pressure levels of 8, 22 and 30 mm Hg (the 15 mm Hg control values were not included because of the statistical considerations involved in dependency between the right and left eyes of each animal). The derived equation for the regression line was:-

$$\text{TOTAL VACUOLE COUNT} = 264 \times \text{I.O.P.} - 1744$$

and this was used to predict vacuoles counts outside the 8 - 30 mm Hg intraocular pressure range. Since the intercept with the x axis was close to 7 mm Hg, it was to be expected that vacuoles would not be found at 0 mm Hg and if linearity remained "true" the total vacuole count at 50 mm Hg would be approximately 11,500 and the mean vacuole count would be greater than 70 counts per section. Certainly, no vacuoles were observed at 0 mm Hg but at 50 mm Hg the mean value for the vacuole count per section in each of the three animals was considerably lower than 70 (Fig. 8.6) and, indeed, was less than the

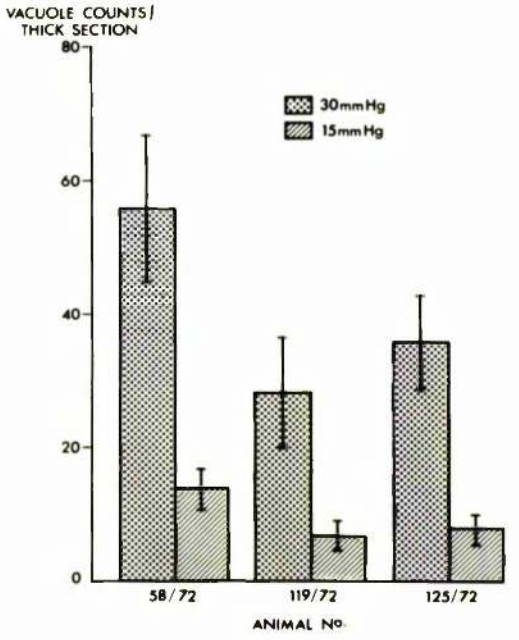

Fig.8.3 The mean number of vacuole counts per thick section and standard deviations at 30 and 15 mm Hg.

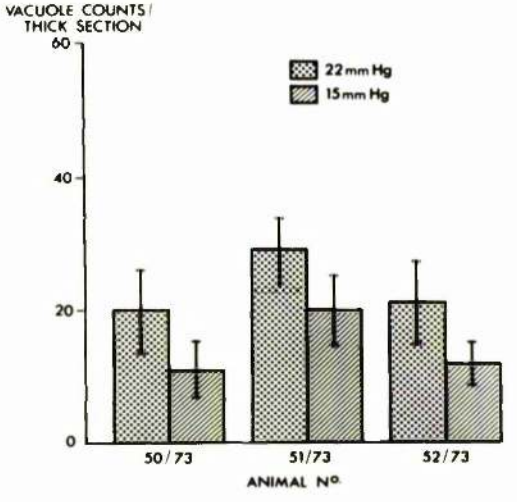

Fig.8.4 The mean number of vacuole counts per thick section and standard deviations at 22 and 15 mm Hg.

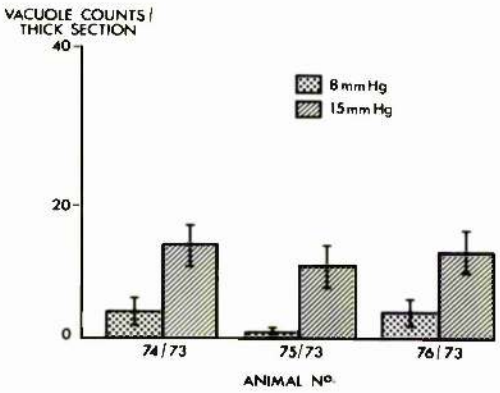

Fig.8.5 The mean number of vacuole counts per thick section and standard deviations at 8 and 15 mm Hg.

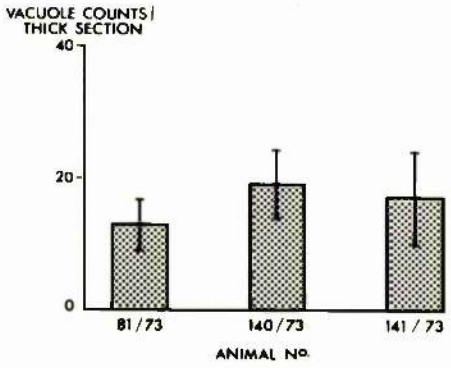

Fig.8.6 The mean number of vacuole counts per thick section and standard deviations at 50 mm Hg.

vacuole counts at 22 and 30 mm Hg (Fig 8.7). It would seem reasonable to suggest that at a pressure somewhat greater than 30 mm Hg, factors come into play which produce a levelling off in the vacuole count leading to the decrease seen at 50 mm Hg (Fig. 8.8).

In addition, it was evident that a large proportion of the counts at 50 mm Hg included vacuoles present in the endothelium lining the septae (which bridge the canal) and in the endothelium of the connecting wall between the trabecular and corneoscleral aspects of the canal. From Fig 8.9 it can be seen that the vacuoles in the endothelium lining the bridging septae and connecting wall form less than 10% of the total count up to 30 mm Hg, but at 50 mm Hg the proportion is higher than 30%. Vacuoles were also observed in the endothelium on the corneoscleral aspect of Schlemm's canal in the three 50 mm Hg eyes and in one eye maintained at 30 mm Hg (animal no. 58/72) but these vacuoles constituted less than 5% of the total count in each case.

8.3.2 Nucleus counts

The variation in the mean nucleus count between the nine 15 mm Hg control eyes was minor (range:- maximum 10.3 $\pm$ 4.4, minimum 7.9 $\pm$ 2.4) with an average value (a grand mean) of 8.9 nuclei per section for the group of eyes examined (Fig. 8.10). When the counts from each eye were compared statistically by the "student T test" the differences were not significant.

8.3.3 Changes in vacuolar dimensions (8 - 30 mm Hg)

The change in the vacuole count obtained from isolated single thick sections could have represented a change in vacuole numbers or could have been related to alterations in vacuolar size (i.e. changes

Animal Number	SEGMENT			
	Superior	Inferior	Temporal	Nasal
58/72	14.2 ± 1.7	13.4 ± 0.7	13.9 ± 1.5	13.7 ± 1.2
119/72	6.4 ± 0.8	6.6 ± 0.8	6.2 ± 0.6	6.8 ± 0.6
125/72	7.5 ± 0.5	7.8 ± 2.0	6.9 ± 0.8	8.3 ± 1.7
50/73	9.5 ± 2.3	11.7 ± 4.1	8.7 ± 2.2	* 12.5 ± 3.6
51/73	21.9 ± 3.2 *	17.7 ± 3.4	19.9 ± 3.7	19.7 ± 4.2
52/73	11.9 ± 2.1	12.1 ± 2.8	11.8 ± 2.1	12.2 ± 2.8
74/73	14.3 ± 1.6	14.3 ± 3.6	12.5 ± 1.9	** 16.1 ± 2.4
75/73	13.5 ± 2.0 ***	8.9 ± 1.9	12.1 ± 3.0	10.3 ± 2.7
76/73	10.7 ± 1.9 ***	14.5 ± 2.2	12.7 ± 3.6	12.5 ± 1.5

Fig.8.7 Comparison between the mean vacuole count per thick section (under the x100 lens) and the standard deviation from the superior and inferior, temporal and nasal halves of each of the 15 mm Hg control eyes. * $P < 0.05$
** $P < 0.01$
*** $P < 0.001$

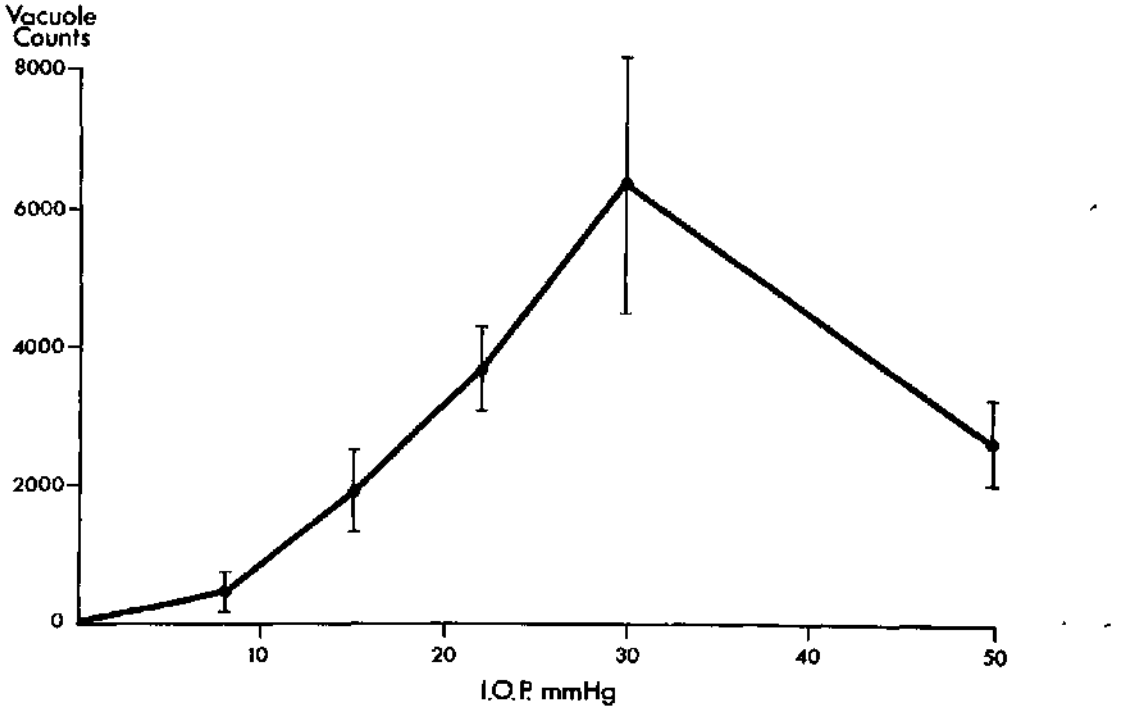

Fig.8.8 The mean and standard deviation of the total vacuole counts under the x100 lens (160 sections counted per eye) of the various eyes at each pressure level between 0 and 50 mm Hg.

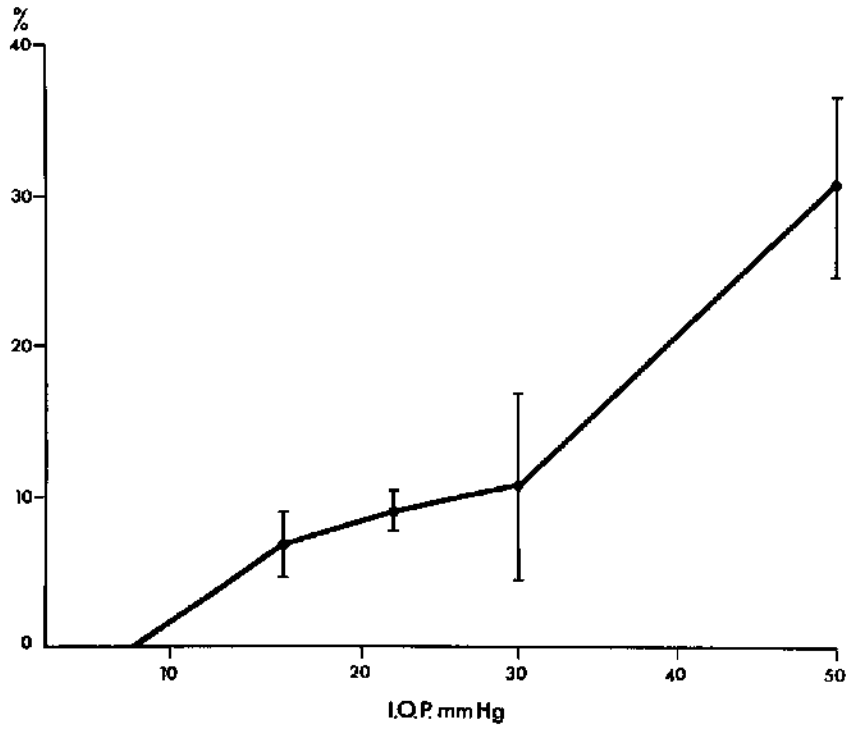

Fig.8.9 The mean and standard deviation of the percentage incidence of septum and connecting wall vacuoles in the total vacuole counts under the xIOO lens for the eyes at each pressure level between 0 and 50 mm Hg.

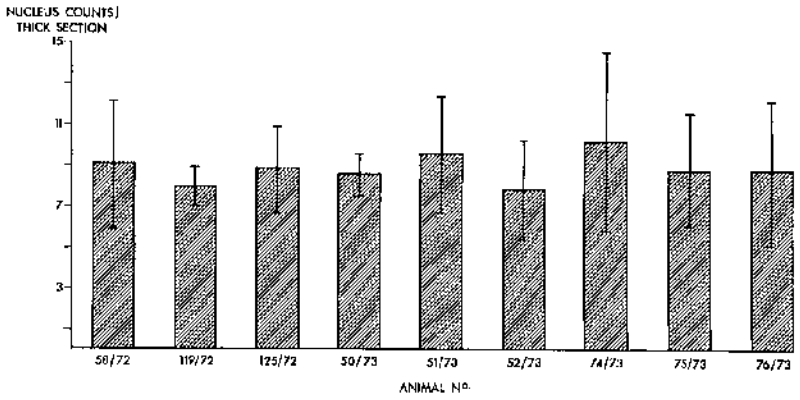

Fig.8.10 The mean number of nucleus counts per thick section (under the x100 lens) and standard deviations for each of the 15 mm Hg control eyes.

in axial length of vacuoles with the plane of section). Therefore, an attempt was made to separate the effects of change in vacuole morphology from the apparent numerical increase in vacuole numbers.

Evidence that there were vacuolar size differences at the various pressure levels was obtained by counting with a x 10 and a x 100 lens. The results (Fig. 8.11) show that at the higher pressures a greater proportion of vacuoles could be counted with the low power lens. The combined ratios of giant vacuoles counted under the x 10 lens and those smaller vacuoles not distinguished under the x 10 lens but counted under the x 100 lens in the experimental and the corresponding 15 mm Hg control eye for each animal was calculated. The complex ratios (the experimental over the control ratio for each animal) from each of the three groups 30, 22 and 8 mm Hg were compared. The ratios in the 30 mm Hg group were significantly different from those in both the 22 and 8 mm Hg groups ($P < 0.05$) while the 22 mm Hg ratios were significantly different from the 8 mm Hg ratios, again at the $P < 0.05$ level.

Reconstruction of the vacuole population from the 100 serial photomicrographs of Schlemm's canal in one tissue block from each eye confirmed that there was an increase in vacuole dimensions with increase in pressure (Fig. 8.12). When the values for maximum vacuolar length (in sections) and width (in μm) were plotted in histogram form, it was seen that the histograms tended to have a skew distribution so that the bulk of the vacuole populations, regardless of pressure, consisted of small vacuoles (see appendix 7a - f).

Comparison of the three 30 mm Hg vacuole populations with their corresponding controls showed that despite the increase in average vacuolar dimensions at the higher pressure (Fig. 8.12), only a small proportion of the 30 mm Hg vacuole populations were outwith the range

Animal No.	IOP	X100 count	X10 count	IOP	X100 count	X10 count
58/72	30	8,910	3,826	15	2,208	354
119/72	30	4,464	2,000	15	1,040	192
125/72	30	5,781	3,003	15	1,222	240
50/73	22	3,219	1,664	15	1,701	777
51/73	22	4,571	2,558	15	3,163	1,833
52/73	22	3,341	1,745	15	1,914	724
74/73	8	670	252	15	1,794	810
75/73	8	181	34	15	2,286	1,026
76/73	8	622	191	15	2,022	936

Fig.8.II The total vacuole counts for each experimental eye and its corresponding control eye within the pressure range 8 - 30 mm Hg under the x100 and x10 lenses.

Animal No.	EXPERIMENTAL				CONTROL			
	I.O.P. (mm Hg)	Vacuole Numbers (incomplete)	Average Width (µm)	Average Length (µm)	I.O.P. (mm Hg)	Vacuole Numbers (incomplete)	Average Width (µm)	Average Length (µm)
58/72	30	1,024 (88)	5.4	8.4	15	330 (24)	2.6	5.6
119/72	30	602 (56)	4.7	6.5	15	224 (14)	2.5	4.7
125/72	30	667 (60)	5.1	6.9	15	201 (12)	2.1	5.0
50/73	22	391 (43)	3.5	6.9	15	204 (14)	2.1	5.2
51/73	22	534 (47)	3.0	6.0	15	228 (29)	2.8	5.4
52/73	22	453 (36)	3.5	6.2	15	252 (18)	2.3	5.7
74/73	8	78 (6)	1.6	4.2	15	272 (24)	2.0	4.8
75/73	8	39 (1)	1.5	3.3	15	262 (21)	2.7	5.3
76/73	8	90 (4)	1.8	3.8	15	240 (24)	2.6	5.4

Fig.8.12 The number of vacuoles and their average maximum width and length in a 100 serial section sample for each eye within the pressure range 8 - 30 mm Hg.

of values found in the 15 mm Hg vacuole populations (appendix 7a and b). In the example shown in Fig. 8.13 (animal number 58/72) only about 6% of the 30 mm Hg vacuole population occurred in more than 14 serial sections (the longest control vacuole) (Fig. 8.13a) and only about 10% had a greater maximum width than 10.1 μm (Fig. 8.13b). At 22 mm Hg the vacuole populations extended over a similar range of length (appendix 7c) and width (appendix 7d) as the control populations. From appendix 7e, it can be seen that only about 7% of the 15 mm Hg control vacuoles lie outside the range of length in the 8 mm Hg vacuole population and from appendix 7f only about 12% of the control vacuoles have a width outside the 8 mm Hg range.

8.3.4 Estimates of changes in vacuole numbers, volume and capacity (8 - 30 mm Hg).

With the information available, the changes in vacuole numbers, volume and capacity could be estimated (Fig. 8.14). A total vacuole number was calculated for each animal by dividing the mean vacuole count per section (under the x 100 lens) by the average vacuole length in sections for each eye and the results were expressed in numbers of giant vacuoles per mm length of canal. When the value obtained were plotted against the corresponding pressure level, it was evident that vacuole numbers increased in an almost linear fashion (Fig. 8.15). The three 30, 22 and 8 mm Hg experimental values were plotted in the form of a scatter diagram (ignoring the 15 mm Hg values) and the "best fit" line had a positive slope and satisfied the equation:-

$$\text{VACUOLE NUMBERS} = 209 \times \text{I.O.P.} - 891$$

To confirm the significance of the relationship between estimated vacuole numbers and pressure, the ratios of the experimental and

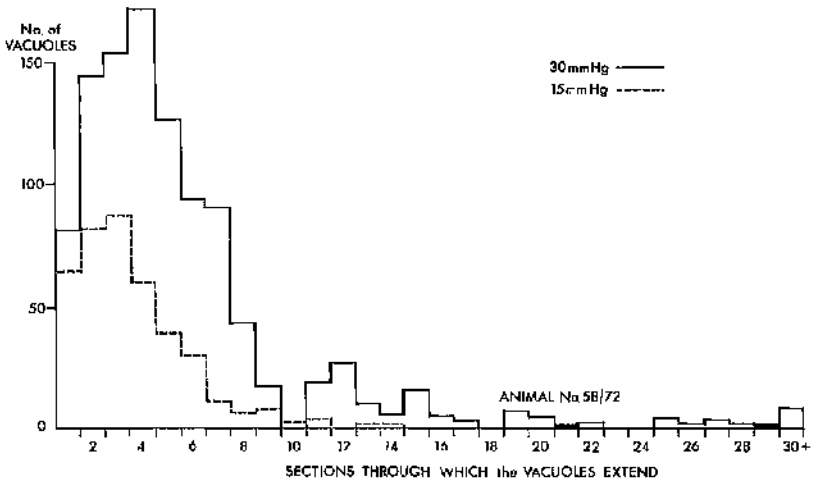

Fig.8.13a The distribution of giant vacuoles (in a 100 serial section sample) according to maximum length.

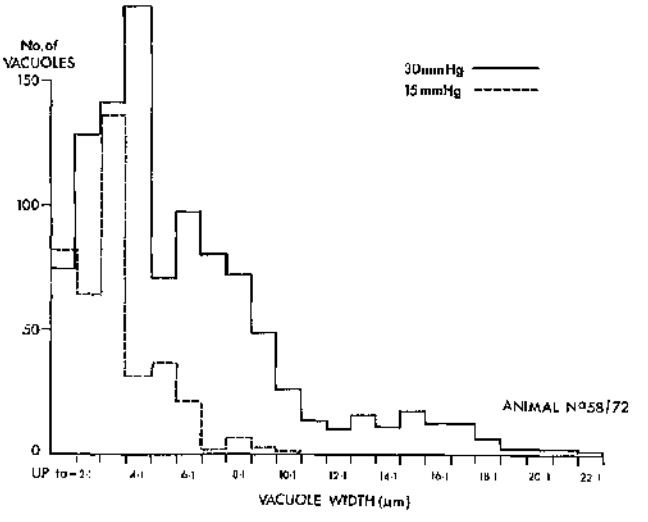

Fig.8.13b The distribution of giant vacuoles (in a 100 serial section sample) according to maximum width.

Animal No.	I.O.P.	Estimated Vacuole Numbers per mm length of canal	Estimated Average Vacuole Volume (μm^3)	Estimated Vacuolar Capacity per mm length of canal (μm^3)	I.O.P. (mm Hg)	Estimated Vacuole Numbers per mm length of canal	Estimated Average Vacuolar Volume (μm^3)	Estimated Vacuolar Capacity per mm length of canal (μm^3)
58/72	30	6,630	128.3	846,780	15	2,460	19.8	48,782
119/72	30	4,290	75.2	322,608	15	1,360	15.4	21,252
125/72	30	5,232	94.0	491,808	15	1,520	11.6	17,556
50/73	22	2,900	44.3	128,470	15	2,000	12.0	24,000
51/73	22	4,757	28.3	134,897	15	3,667	22.2	81,407
52/73	22	3,370	39.8	134,126	15	2,105	15.8	33,263
74/73	8	1,000	5.6	5,600	15	2,979	10.1	30,090
75/73	8	389	3.9	1,299	15	2,113	20.2	42,764
76/73	8	1,026	6.4	6,586	15	2,333	19.1	44,610

Fig.8.14 The average vacuolar volume from a 100 serial section sample and the estimates of vacuolar numbers and total vacuolar capacity per mm length of canal for each of the eyes within the pressure range 8 - 30 mm Hg.

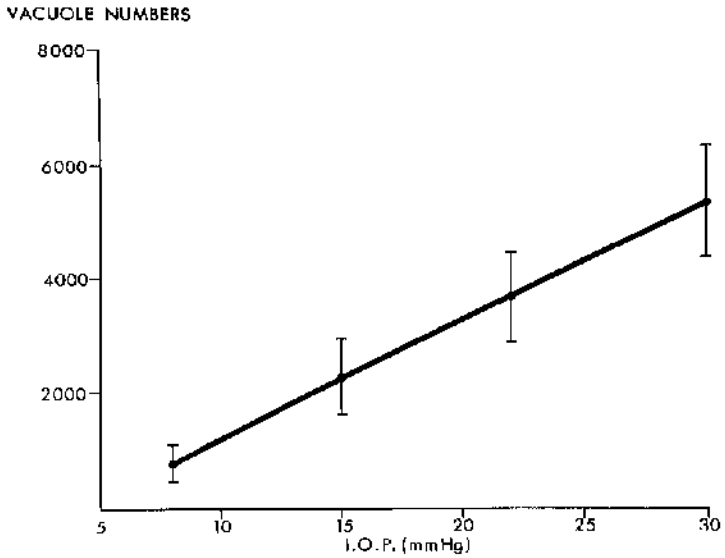

Fig.8.15 The mean number of giant vacuoles per mm length of canal and standard deviations from the estimates of vacuolar numbers.

control values for each animal were plotted against intraocular pressure (thus allowing control values to be used without "dependency" problems). The slope of the subsequent regression line was significantly greater than zero ($P < 0.001$).

To assess the pressure-induced changes in average vacuolar volume, it was necessary to assume that the vacuoles had a regular geometric shape and it was considered from the study of serial photomicrographs that a regular spheroid was closest to the shape of these somewhat variable and irregular structures. An estimate of mean vacuolar volume at the various pressures between 8 and 30 mm Hg was calculated therefore, from the values of average maximum vacuolar length and width for each eye, using the formula $4/3\,\pi\,6^2a$ (Figs 8.14 and 8.16). The results showed that the mean vacuolar volume (the mean of the average vacuolar volumes for each of the eyes at the various pressure levels) increased quite dramatically with increase in pressure (Figs 8.16 and 8.17). Since the mean vacuolar volume increased in progressively greater increments as the intraocular pressure increased, the relationship between the two factors was likely to be non-linear (Fig. 8.17). An estimate of total vacuolar capacity per mm length of canal endothelium was made by multiplying the average vacuolar volume by the estimated number of vacuoles per mm length of canal endothelium in each eye (Fig. 8.14) these values also showed a dramatic, non-linear increase with increase in pressure (Fig. 8.18)*.

---

*FOOTNOTE:- The regression equations derived from the values of average vacuolar volume and total vacuole capacity per mm length of canal for the experimental eyes were:-

a) AVERAGE VACUOLAR VOLUME = $1.82e^{0.12 \times I.O.P.}$

b) AVERAGE VACUOLAR CAPACITY PER MM LENGTH OF CANAL = $647.79e^{0.23 \times I.O.P.}$

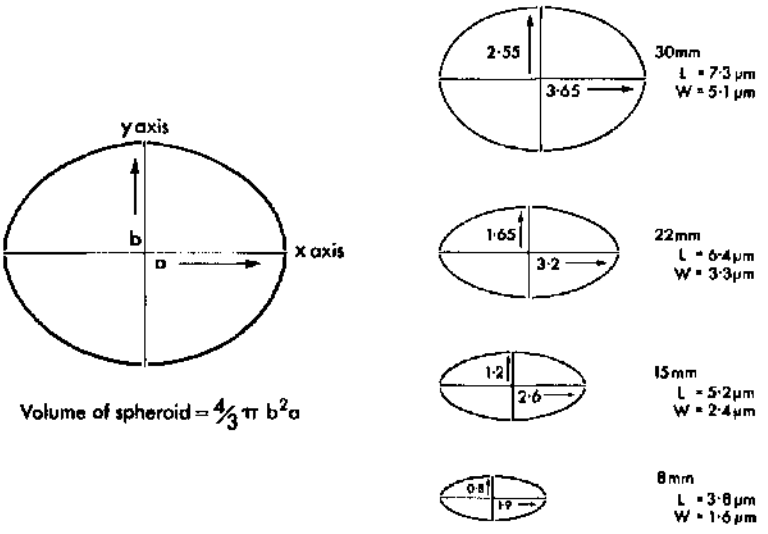

Fig.8.16 The geometry of a regular spheroid and estimated changes in average vacuolar dimensions assuming this regular shape.

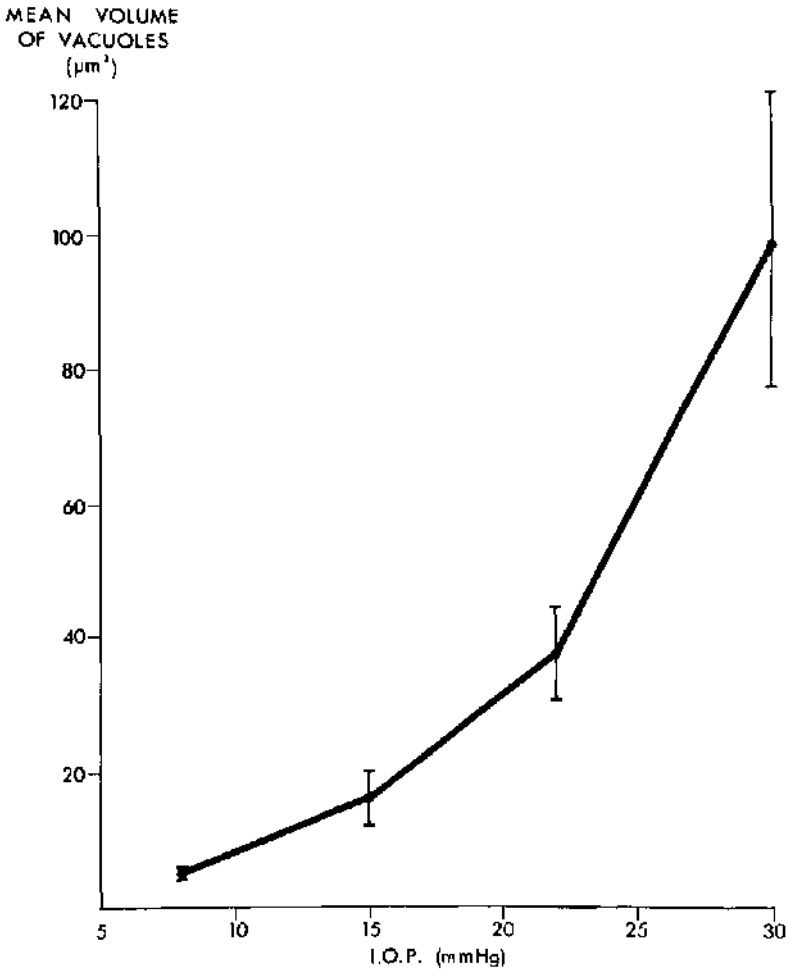

Fig.8.17 The mean vacuolar volume and standard deviations at each pressure level within the range 8 to 30 mm Hg.

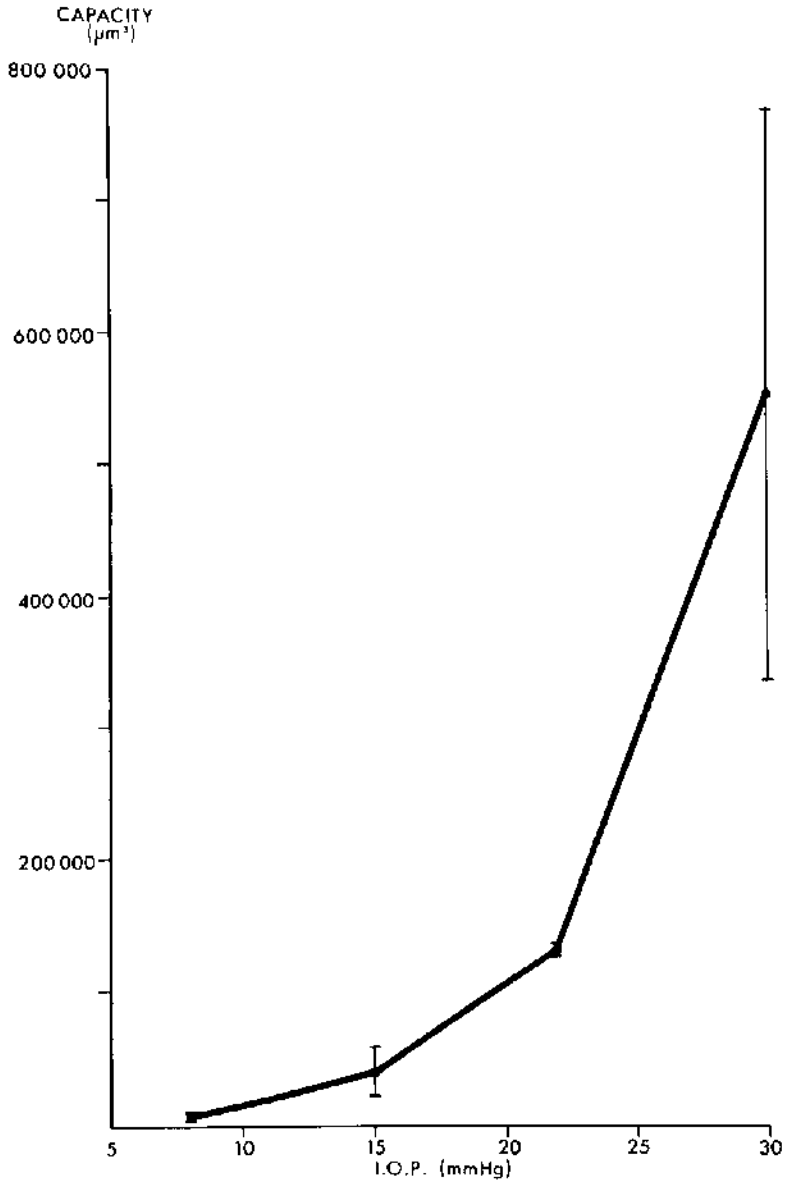

Fig.8.18 The mean total vacuolar capacity per mm length of canal and standard deviations at each pressure level within the range 8 to 30 mm Hg.

8.4 Discussion

The findings from the present quantitative analysis confirmed and extended the light microscopic observations described in the previous chapter. Since at 0 mm Hg there were no giant vacuoles and from 8 - 30 mm Hg there was an apparently linear increase in the vacuole counts within this pressure range, then clearly vacuole formation was pressure dependent. At 50 mm Hg, the vacuole counts were lower than at 22 and 30 mm Hg and this reduction could, to some extent, be explained by the partial closure of Schlemm's canal at 50 mm Hg which was described in the previous chapter.

Essentially, the increase in vacuole counts between 8 and 30 mm Hg was due to both a numerical increase in vacuole numbers and to an increase in the size (particularly the axial length in the direction of the plane of section) of the individual vacuoles. Although the increase in vacuole numbers appeared to be linear within this pressure range the estimates of change in average vacuolar volume indicated that an exponential relationship with pressure may exist. In turn, the association between total vacuolar capacity (the amount of vacuolar aqueous within the endothelium lining Schlemm's canal) and pressure also seemed to be exponential. Calculations from the appropriate regression equations highlighted the significance of pressure induced alterations to vacuolar morphology. Although there were only about 2.5 times as many vacuoles at 30 mm Hg than there were at 15 mm Hg, because there was a 6 fold increase in average vacuolar volume over the same pressure range, the vacuolar aqueous carrying capacity of the endothelium at the higher pressure was almost 15 times greater than that of the lower pressure.

However since, at best, the calculations were only a rough

estimation of the changes occurring in the vacuole population it would be unwise to extrapolate too far from the present findings which indicated trends and were not intended to provide absolute values. The assumption that vacuoles were of regular shape was an oversimplification, whereas the limited sample (150 μm) of the total canal endothelium (approximately 30 mm) used for the determination of vacuolar dimensions, may have been inadequate to achieve an accurate assessment. Equally important was that errors, of unknown extent, existed in the vacuole counts as a result of limited optical resolution. Structures which only superficially resembled giant vacuoles (e.g. pseudovacuoles, see Chapter 10) may have been included within the counts and a proportion of the smaller vacuoles may have been omitted.

There is little published light microscopic data in the literature on quantitative estimates of giant vacuole numbers and distribution. Inomata, Bill and Smelser (1972) concluded from reconstructions of 110 serial light micrographs that, in the cynomolgus monkey, approximately 3,200 giant vacuoles were to be found per mm length of canal at a maintained pressure of 18 cm of water. The estimate was somewhat higher than the value obtained from the prediction curve for vacuole numbers in the present investigation for that pressure (approximately 1,900) but taking into consideration species difference, possible differences in what was considered to be a vacuole and the small samples of tissue examined, the difference between the estimates is not too discouraging. Wickham and Worthen (1974) found statistically significant differences ($P < 0.05$) in vacuole counts between quadrants in each of two eyes - one maintained at 50 mm Hg and the other at 15 mm Hg. The finding is not supported by the present study in which consistent differences were not found when halves rather than quadrants

were compared for each eye.

From their quantitative analysis Inomata, Bill and Smelser (1972a) concluded that the total number of nuclei per mm length of canal was about 1,600. The average value for nucleus counts per section in the present investigation was 8.9 and since the nuclei measured about 6 µm in the direction of the length of the canal (they occupied approximately 4 serial sections) their incidence per mm length of canal was about 1,500 which was remarkably close to the value obtained by the previous authors. In the rhesus monkey, Schlemm's canal measured approximately 30 mm in circumference (personal observation), therefore the total number of nuclei (and cells) in the endothelium lining the trabecular aspect of the canal was in the order of 40 - 50,000. This was below the range (57,000 - 200,000 cells calculated by Cole and Tripathi (1971) but was higher than the value obtained in human eyes by Bill and Svedbergh (1972) from scanning electron microscopy (23,000 cells). An interesting conclusion could be drawn from the present results when vacuole and cell incidences were compared. At 30 mm Hg vacuole numbers were between 3 and 4 times greater than the estimated numbers of endothelial cells in the endothelium on the trabecular aspect of the canal while at 15 mm Hg there were still slightly more vacuoles than endothelial cells (the vacuole numbers were reduced by 10% to allow for vacuoles on the septae). Therefore, it would seem that in the hypertensive outflow system, many of the endothelial cells have several discrete vacuoles incorporated in their cytoplasm.

If giant vacuoles serve as a mechanism for the bulk transfer of aqueous through the lining endothelium into Schlemm's canal, as has been suggested by several authors (see Chapter I), then the changes in vacuolar numbers and dimensions with increased and decreased

intraocular pressure are consistent with the operation of a homeostatic mechanism. At an increased pressure the vacuolation process could accommodate increased transcellular fluid flow which would tend to lower the pressure in the anterior chamber while at a decreased pressure the reverse would happen. On the other hand, the demonstration of changes in vacuole numbers and their aqueous carrying capacity (e.g. the 15 fold increase in vacuolar aqueous from 15 to 30 mm Hg) was not in itself evidence that these particular vesicles were involved in the transfer of aqueous across the canal endothelium*. Only those vacuoles which had openings on both their meshwork and lumen aspects were transcellular channels which could have served as flow pathways (Holmberg, 1965; Kayes, 1967; Tripathi, 1968, 1969a, 1971a, 1972, 1974 ; Inomata, Bill and Smelser, 1972a). It therefore remains to be determined whether a) the vacuoles described here had pores and b) the influence of intraocular pressure alterations on pore incidence.

---

*FOOTNOTE:- Indeed, although both Johnstone and Grant (1973) and Kayes (1975a and b) demonstrated vacuolar pressure sensitivity they were non-committal about the role of giant vacuoles in aqueous outflow.

CHAPTER 9

PRESSURE EFFECTS ON THE FINE STRUCTURE OF THE OUTFLOW APPARATUS

9.1 Introduction

In this chapter particular attention is paid to a) those properties of the meshwork which permit distension without disruption, b) the pressure effects on cell ultrastructure and extracellular materials (including mucopolysaccharides) and c) the pathological changes produced at the non-physiological pressure levels.

9.2 Materials and methods

Limbal tissue from the eyes of 17 rhesus monkeys (which were used for the investigation of pressure effects on the outflow system, appendix 6) was examined in the transmission electron microscope after a) conventional preparation and sections staining, b) uranyl acetate "en bloc" staining and c) colloidal thorium and iron treatment (see Chapter 3).

Uranyl acetate "en bloc" staining was used to investigate cell-to-cell junctions while the colloidal stains were utilised to determine the distribution of charged mucins at the various pressure levels.

9.2.1 Quantitative assessment of organelle content

Preliminary qualitative examination of the meshwork cells indicated that the cytoplasmic content of lysosomes, lysosomal complexes, multivesicular bodies and lipid vesicles was increased at the higher pressures. Therefore, a quantitative analysis was undertaken to compare the incidence of these organelles at the pressures of 15 and 30 mm Hg. Since the area of the individual meshwork cells was non-uniform in random ultrathin sections, the analysis could have been influenced by observer selection and regional variation. To achieve

comparable measurements, 10 of the largest endothelial cells were chosen from good quality coded sections cut from each of 20 coded blocks (five from each quadrant) and for this purpose five experimental and five control eyes provided the tissue.

The organelle counts were made directly in the electron microscope and distinction was made between the cells of the endothelial meshwork and the cells lining the trabeculae. The findings were expressed as organelle counts per 100 cells examined and paired t-tests were used for the statistical analyses.

9.3 Results

The initial experiment showed that the exposure of the outflow apparatus to the mock aqueous solution for one hour had no recognisable effect on the cell ultrastructure. Although significant differences in tissue appearances were not found when the two fixation techniques of carotid perfusion and anterior chamber infusion were compared, the ultrastructural preservation was better with the latter technique.

9.3.1 15 mm Hg

The 15 mm Hg intraocular pressure control group conformed to a general pattern and the examination was concentrated on the outer regions of the meshwork where, in the experimental eyes, the most significant pressure induced changes occurred (see Chapter 7).

In the outer corneoscleral meshwork, the adjacent trabeculae were separated by narrow intertrabecular spaces and cellular contact across the spaces was maintained either by process connections or by apposition between the perinuclear bulges of endothelial cells on adjacent trabeculae (Fig. 9.1).

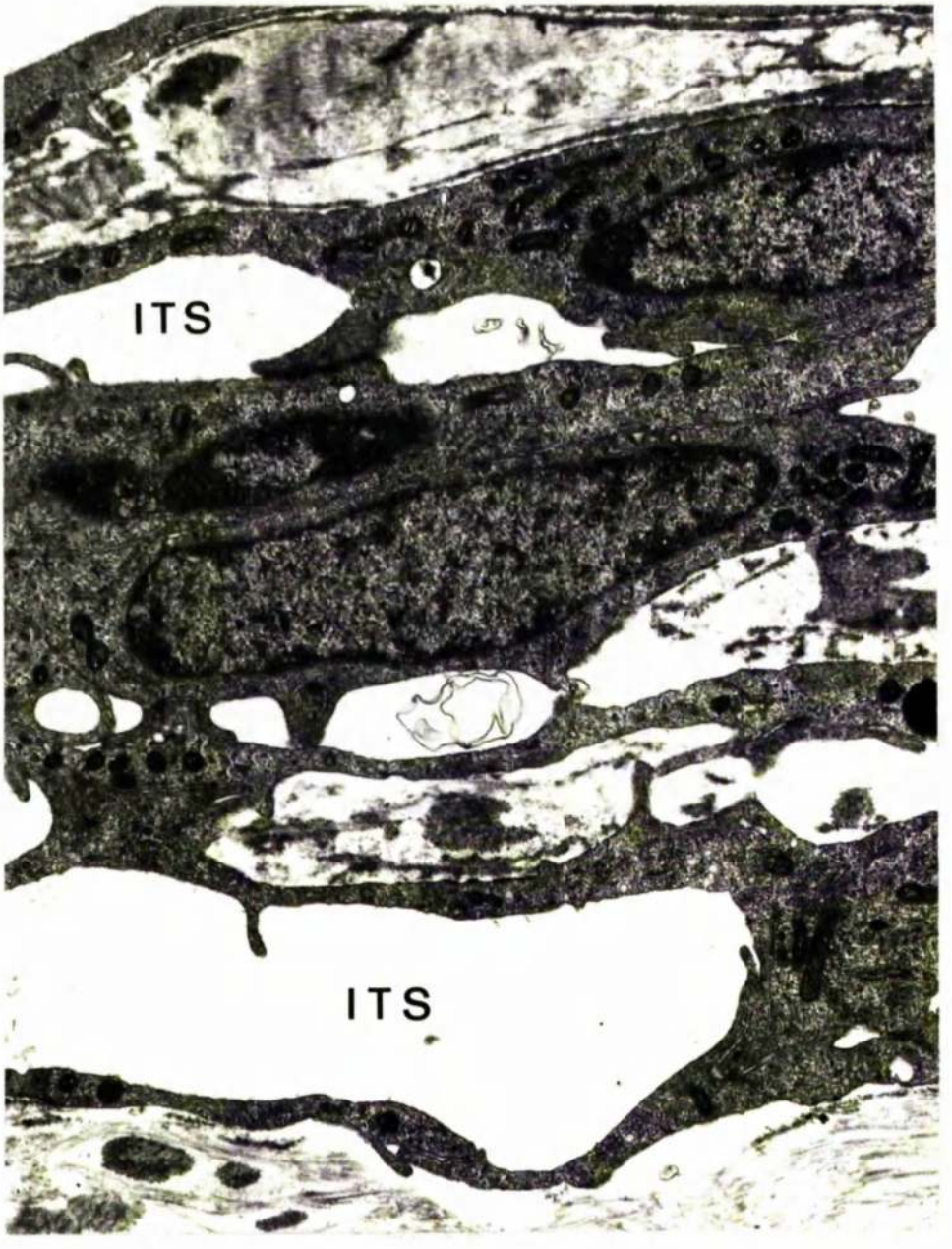

Fig.9.I Part of the corneoscleral meshwork at I5 mm Hg. The intertrabecular spaces (ITS) are narrow. T.E.M. (xI4,000).

The endothelial meshwork was a variable though narrow region (8 - 16 μm thick). Within this zone the native cells were generally orientated with their long axes parallel to the endothelium lining the canal (Fig. 9.2) but in some areas the cell orientation was more random (Fig. 9.3). The cells formed a network by process contacts between neighbouring cells, the processes were usually short, but could extend up to 2 μm in length. Extracellular material was identified in the spaces between the native cells and primarily it consisted of fibrils, ground substance, collagen fibres and elastic-like material (Figs 9.2, 9.3, 9.4).

In both the corneoscleral and endothelial parts of the meshwork, cytoplasmic microfilaments (100Å in diameter) were prominent in all the cells and ran in bundles parallel to the long axes of the cells (this feature was mentioned in detail in Chapter 4). Also the adhering and gap junctions, which were considered in chapter 5, were frequently seen in the zones of apposition between neighbouring cells.

The endothelium lining the trabecular aspect of Schlemm's canal was a continuous monolayer of cells whose lateral borders met either in a narrow zone of apposition or in a tongue-in-groove insertion. Within the intercellular clefts the junctional modifications described in chapter 5 were identified. Uranyl acetate "en bloc" staining revealed regions of occlusion and, on rare occasions, junctional zones where there was no membrane fusion. The endothelial cells contained cytoplasmic microfilaments. These structures were found throughout the cell cytoplasm but were prominent in the short stumpy processes which projected through the patchy basement membrane. These processes came into contact with either extracellular materials, endothelial meshwork cells or meshwork cell processes (Figs 9.4 and 9.5). In all, five types of canal endothelium/meshwork cell apposition were identified

Fig. 9. 2. Generally at I5 mm Hg the endothelial meshwork cells (EMC) are orientated with their long axes parallel to the canalicular endothelium (EN). The native cells are in contact with each other by short processes (arrows). T.E.M. (xII,000).

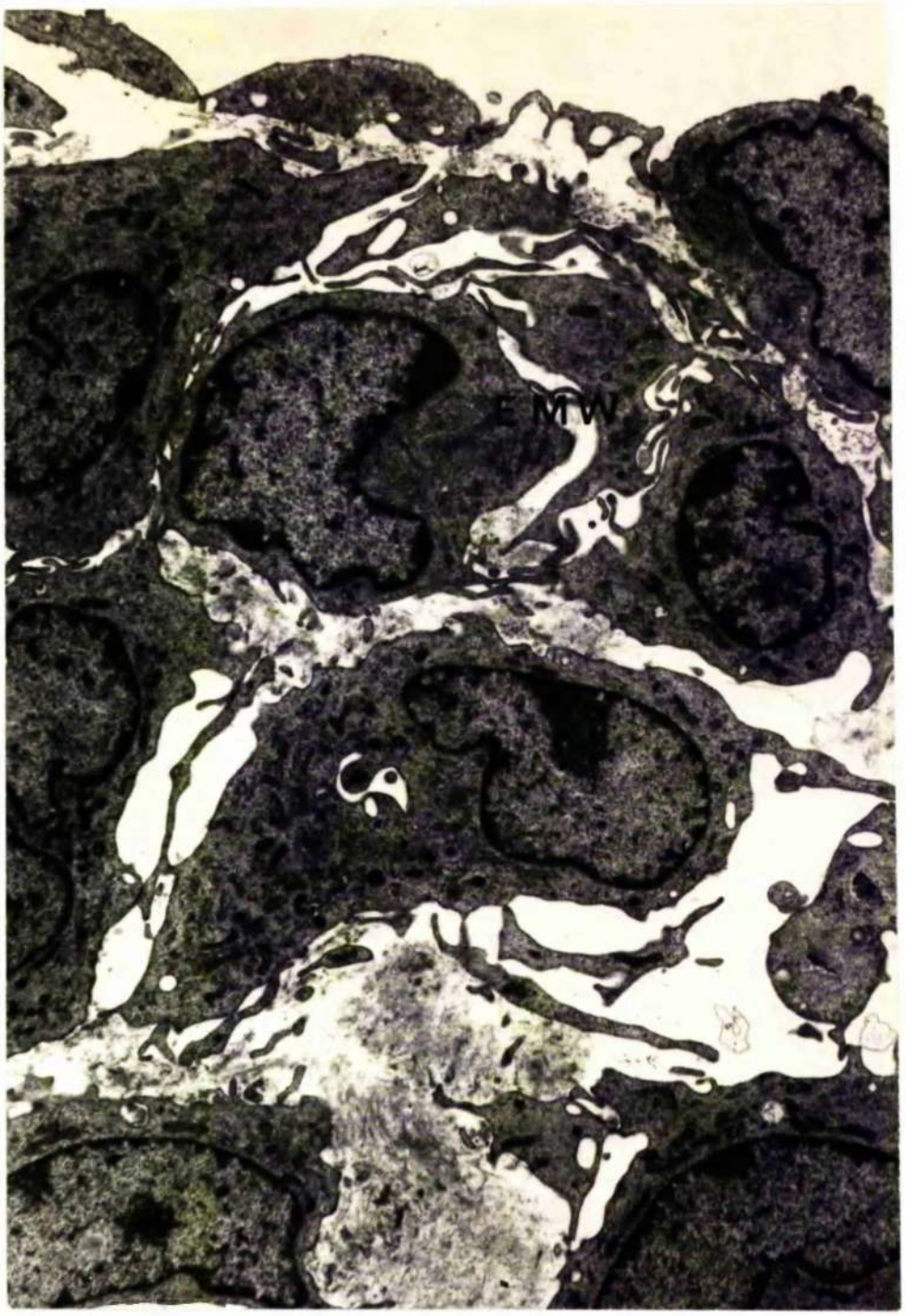

Fig.9.3 Part of the endothelial meshwork (EMW) at 15 mm Hg where cell orientation is more random. T.E.M. (x7,400).

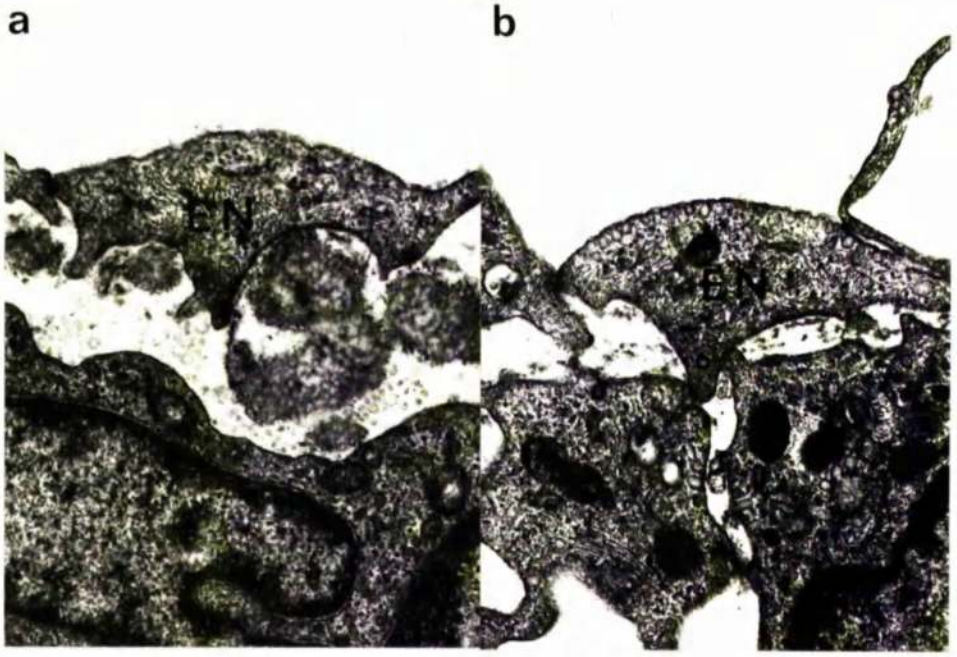

Fig.9.4 At I5 mm Hg short processes from the endothelial cells (EN) of Schlemm's canal insert into the underlying meshwork and come into contact with either a) extracellular material or b) meshwork cells. T.E.M. (x25,000).

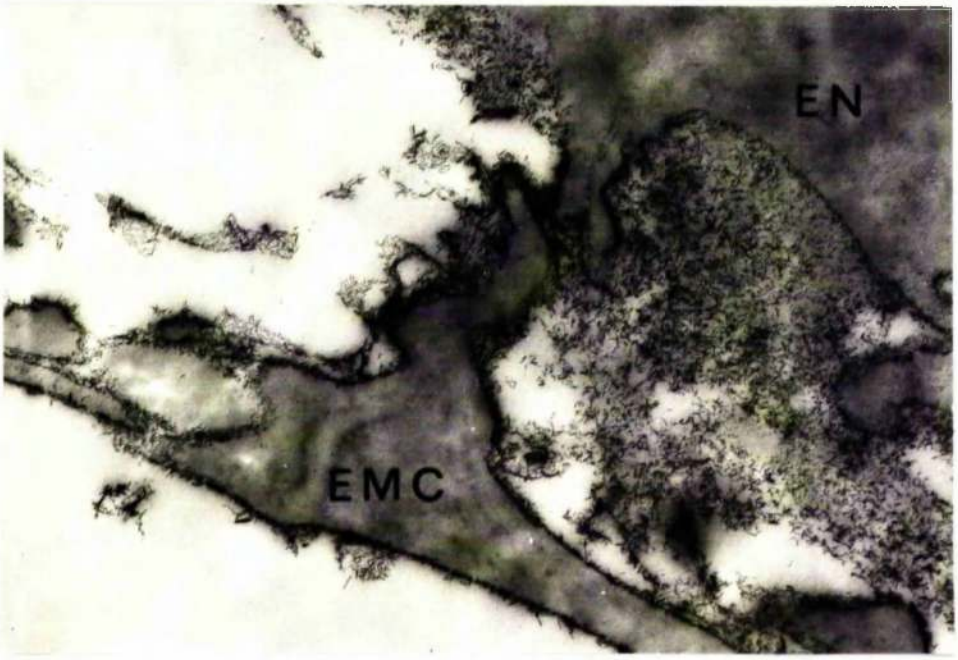

Fig.9.5 Process association between the canal endothelium (EN) and an endothelial meshwork cell (EMC) after iron staining. Colloidal iron is particularly concentrated around the processes at I5 mm Hg. T.E.M., no section staining (x56,000).

(Fig. 9.6) and of these, process-to-process apposition was the most common (Fig. 9.7) (the assessment was based on the examination of 1,000 regions of contact). After staining for mucopolysaccharides, colloidal particles were prominent on the surface of the meshwork cells (Fig. 9.8), in the trabecular cores (Fig. 9.8), in the endothelial meshwork (Fig. 9.5) and on the endothelial cells lining the canal (Fig. 9.28b). Mucopolysaccharides were particularly prevalent at the sites of canal endothelium/meshwork cell apposition and may, therefore, contribute to tissue adhesion (Fig. 9.5).

9.3.2 8 mm Hg

In the outer corneoscleral meshwork, the intertrabecular spaces were contracted and in some places almost eliminated. The compact endothelial meshwork was reduced to less than 10 μm in thickness and the native cells were arranged in 2 or 3 irregular layers usually lying parallel to the endothelium lining Schlemm's canal. The narrow and tortuous extracellular spaces, which were sites of particularly intense colloidal thorium and iron staining, were filled with extracellular material similar to that described in the control tissue. In addition the extracellular spaces in some areas contained granular plasmoid material identical to that present in the lumen of Schlemm's canal (Fig. 9.9).

The cells lining the trabecular wall of Schlemm's canal were narrow in cross section and the nuclei were often infolded, so that the cells appeared to be more compressed than those in the control tissue (Fig. 9.10). Junctional modifications were apparent in the typically tortuous zones of contact between neighbouring cells (Figs 9.9 and 9.10).

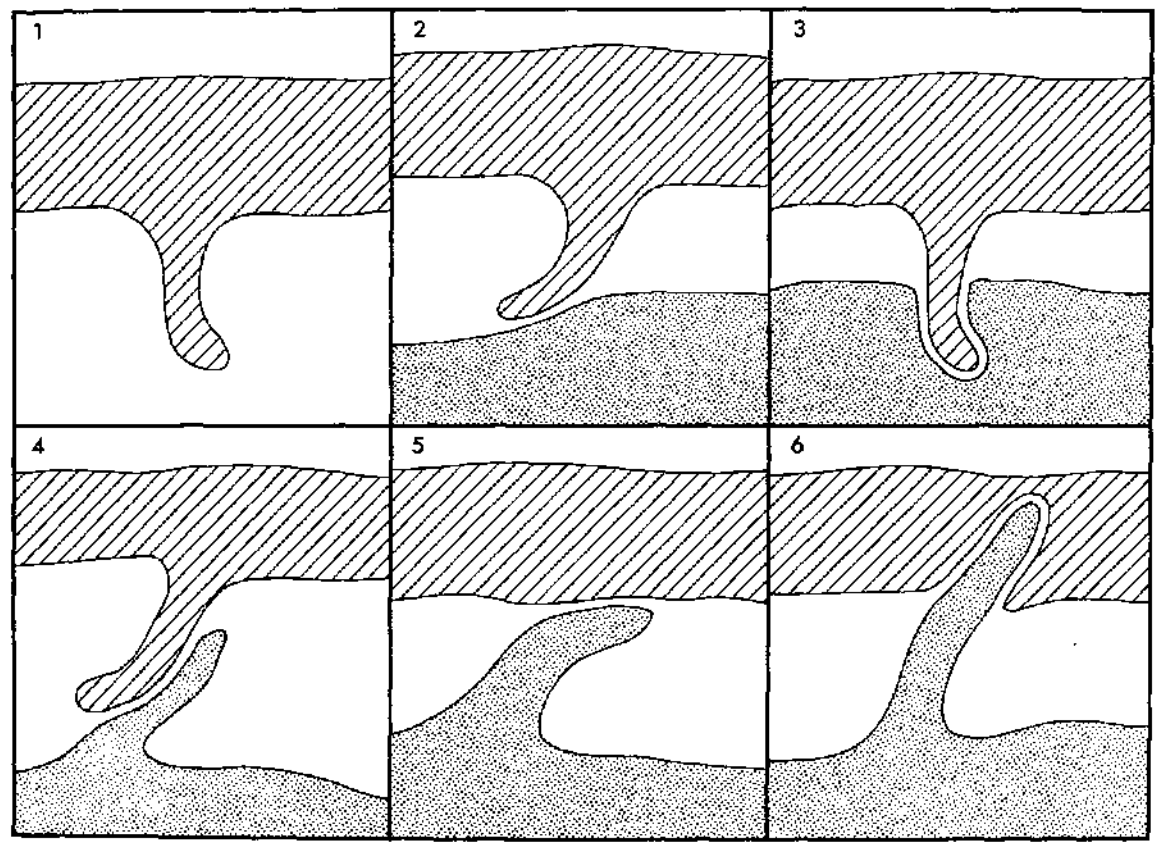

Fig.9.6 Diagram showing the various types of canal endothelial (diagonal lines) processes (I to 4) and endothelial meshwork cell (dots) processes (4 to 6) with their associations. In all, 5 types of canal endothelium/meshwork cell apposition were identified at I5 mm Hg (2 to 6).

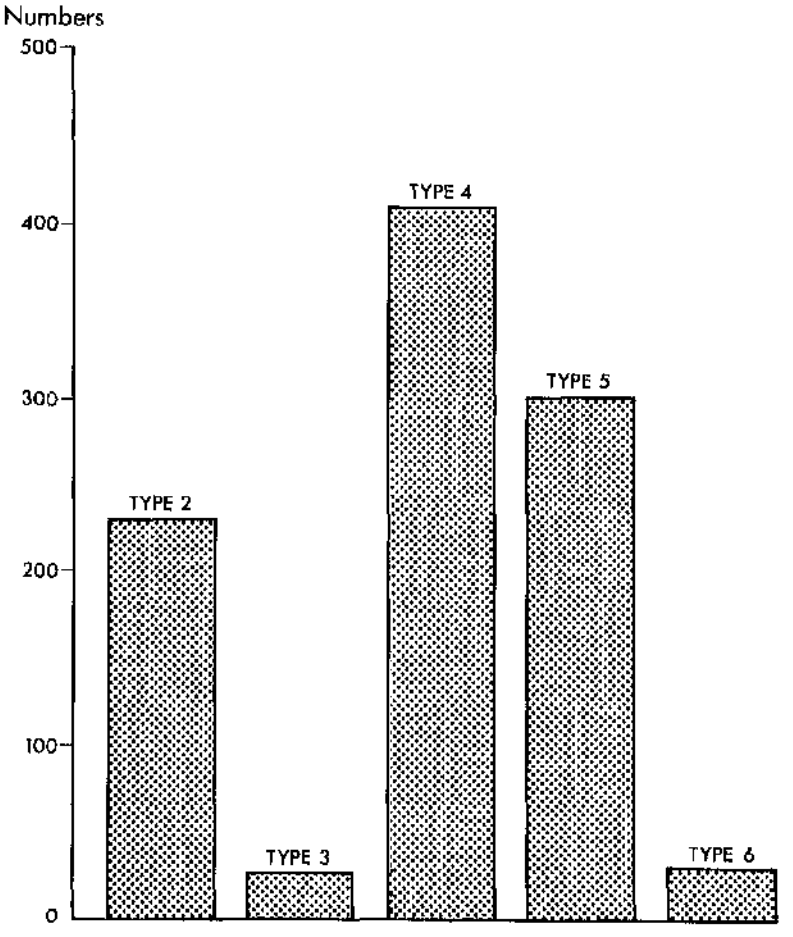

Fig.9.7 Histograms to show the frequency of the five types of canal endothelium/meshwork cell association at 15 mm Hg. The assessment was based on the examination of 1,000 regions of contact.

Fig.9.8 Corneoscleral trabeculae at I5 mm Hg treated with colloidal iron. Iron particles are prominent on the apical surface of the endothelial cells and within the trabecular cores. T.E.M., no section staining (xI4,750).

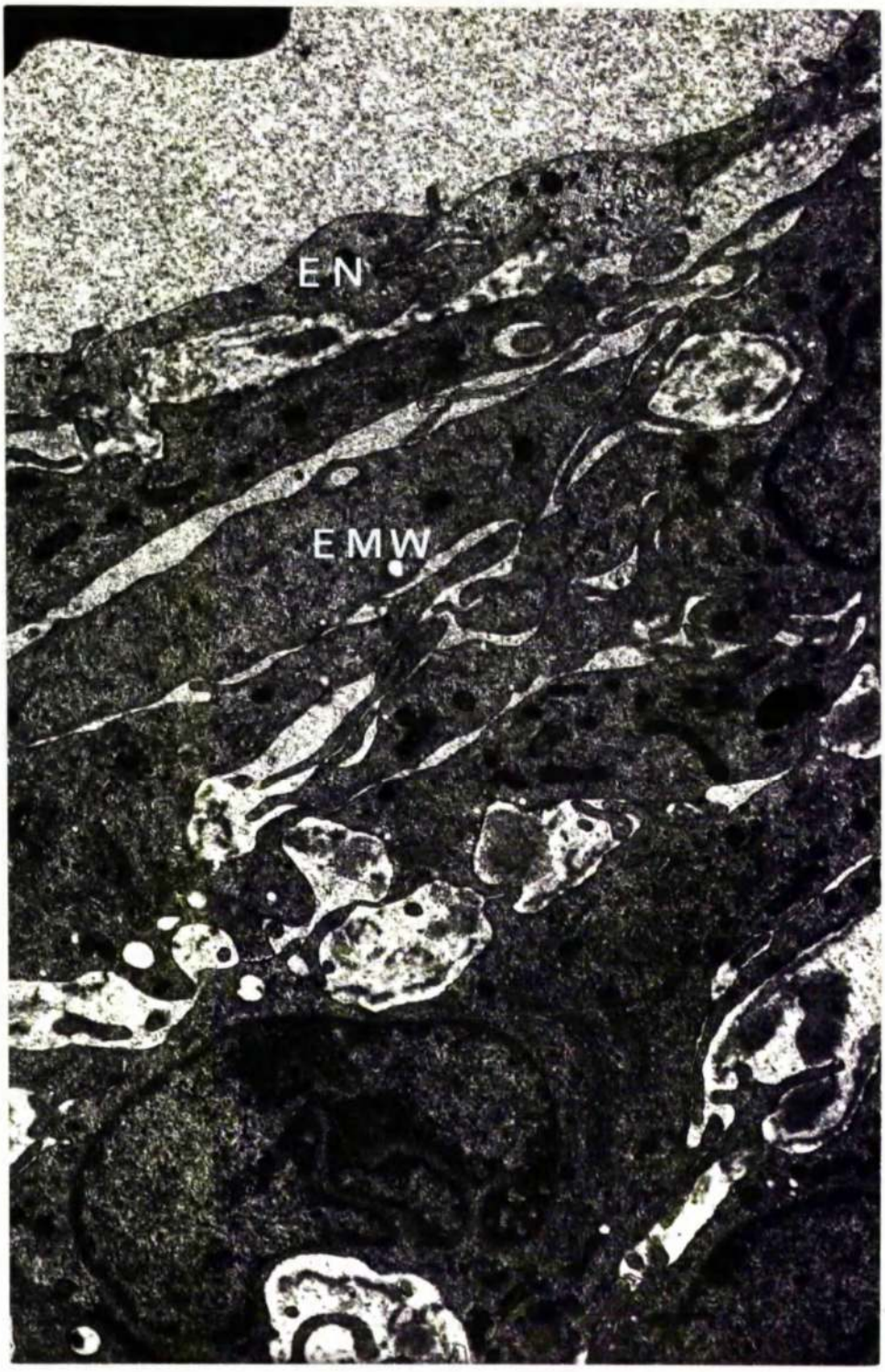

Fig.9.9 The endothelial meshwork (EMW) at 8 mm Hg is compact and the native cells are arranged with their long axes parallel to the endothelial monolayer (EN). Some granular plasmoid material is present in the narrow extracellular spaces. T.E.M. (x16,000).

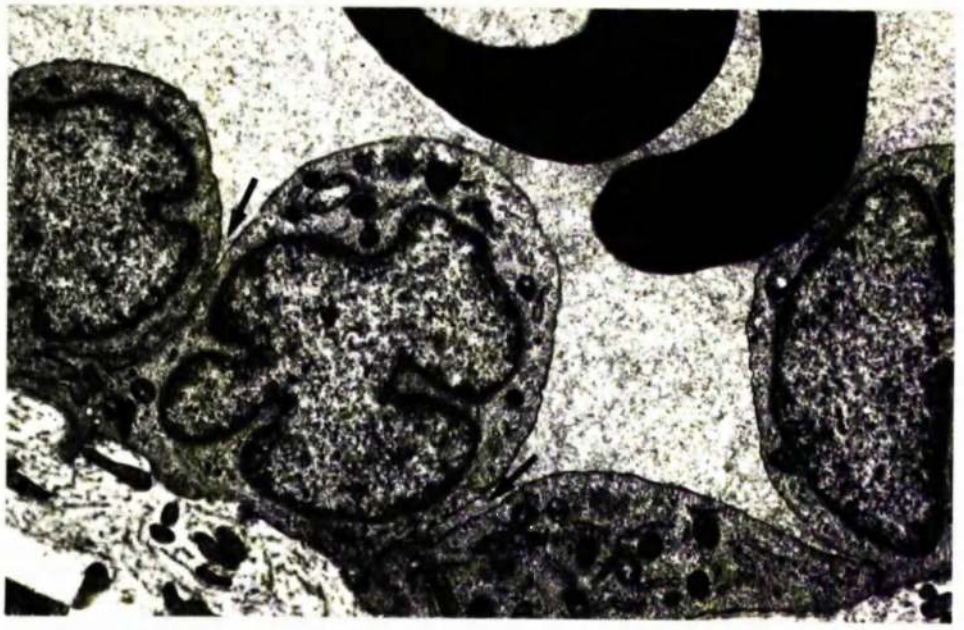

Fig.9.IO At 8 mm Hg many of the cells in the endothelium lining the trabecular aspect of Schlemm's canal have a squat appearance, invaginated lateral borders (arrows) and prominent infoldings in their nuclei. A wide diffuse basement material is present under the endothelial monolayer. T.E.M. (xI2,500).

9.3.3 22 mm Hg

By comparison with the tissue at lower pressures, the inter-trabecular spaces in the outer corneoscleral meshwork were wide but process attachments remained and junctions were still obvious and intact at the region of contact. The processes were thin and extended (4 - 7 μm in length) and the longitudinal microfilament organisation was pronounced (Fig. 9.11).

The endothelial meshwork was distended (in excess of 20 μm) and the distension produced a reorientation of the endothelial cells so that their long axes tended to lie at right angles, rather than parallel, to the canal endothelial monolayer. Although the cells were more separate, and hence the extracellular spaces were larger, cell-to-cell contacts were still present and the integrity of the tissue was maintained. The extracellular material was focally aggregated and was usually found in limited regions close to the endothelium lining Schlemm's canal. Elsewhere, wide electron-lucent extracellular spaces, with a poor affinity for the mucopoly-saccharide stains, were a prominent feature (Fig. 9.12).

At this pressure, the endothelium lining the trabecular wall of the canal was usually in close contact with the underlying endothelial meshwork, but limited regions of separation were seen occasionally.

9.3.4 30 mm Hg

The outer corneoscleral meshwork was more distended at this pressure than at 22 mm Hg. The widely separated trabeculae were bridged by delicate cell processes which often reached a length of 10 μm. Intracytoplasmic microfilaments were orientated along the

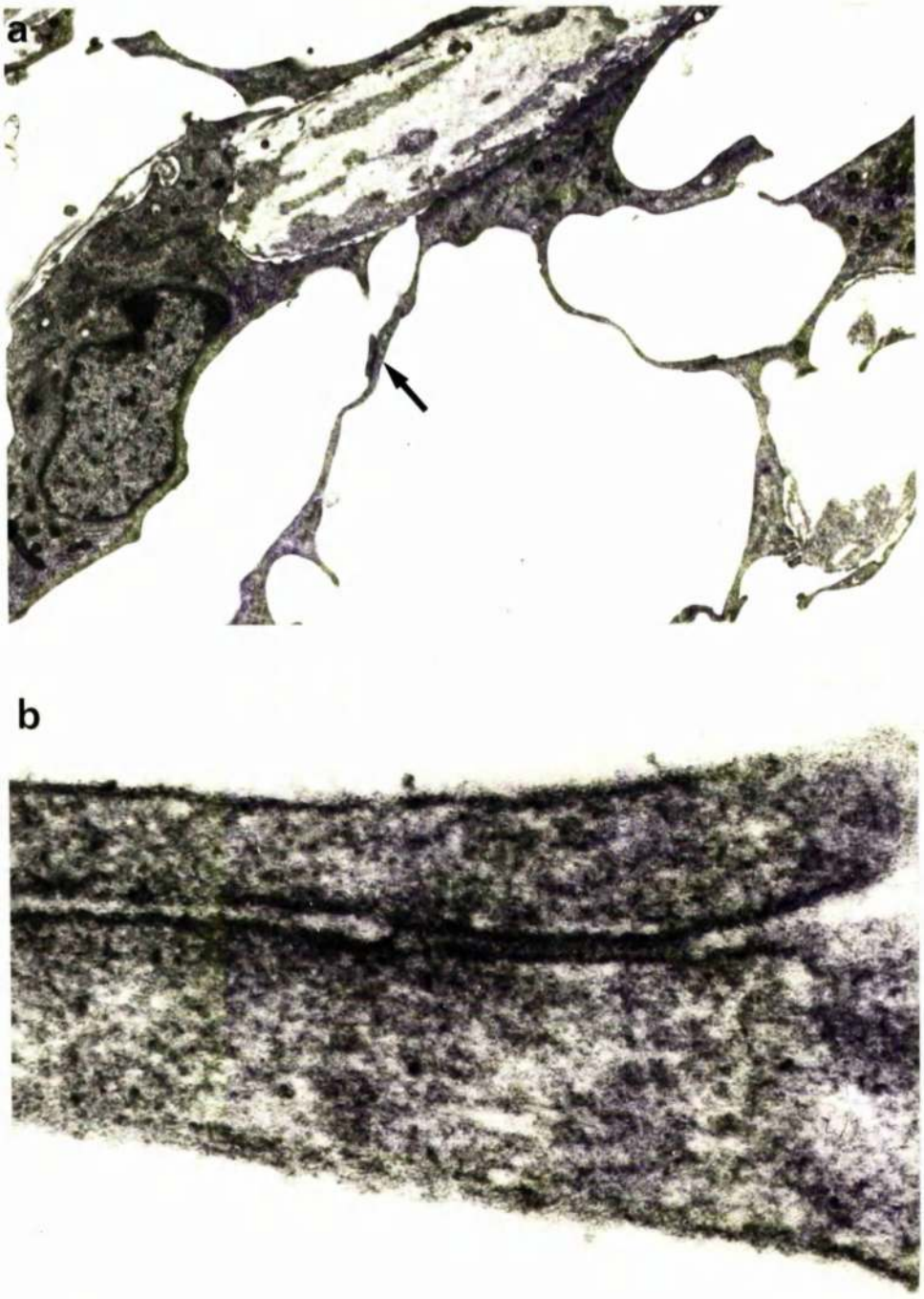

Fig.9.II a) The outer corneoscleral trabeculae at 22 mm Hg are separated by wide intertrabecular spaces. The wide spaces are crossed by long thin processes. Junctions, where identified (arrow), were seen at high magnification b) to be intact. T.E.M. (a x9,000; b x230,000).

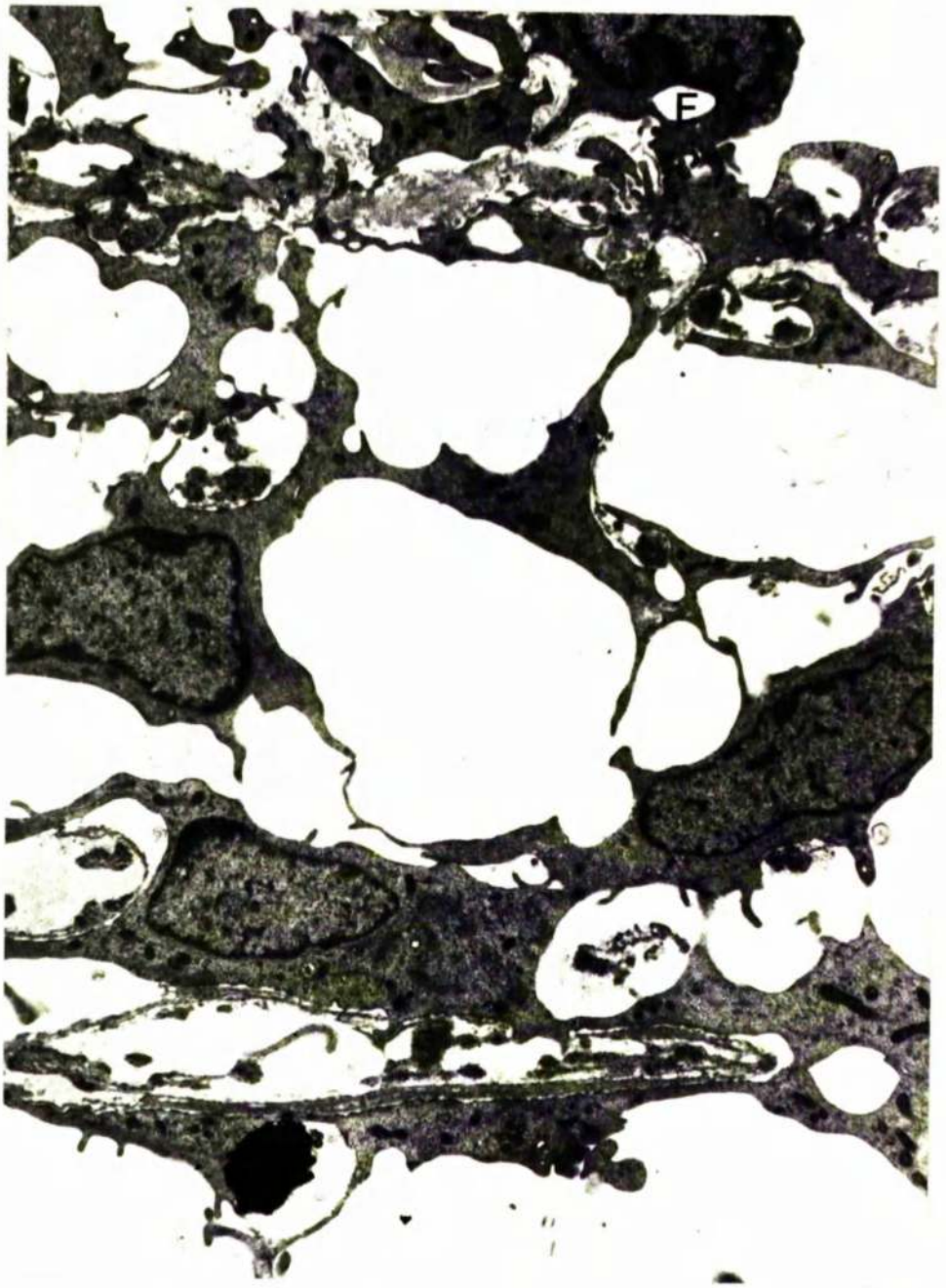

Fig.9.I2 Part of the endothelial meshwork at 22 mm Hg. Wide electron lucent spaces are evident. The cells tend to be orientated at 90° to the endothelial monolayer (EN) and cell-to-cell contacts are maintained by long thin processes. T.E.M. (x8,000).

long axes of the cell processes and the junctional modifications apparently were unaltered. There was evidence of cellular separation from some of the trabecular cores and at these foci, the basement membrane was diminished or absent and the underlying matrix was either disorganised or diminished. By way of contrast, where cellular attachment persisted, focal segments of basement material were thickened (Fig. 9.13).

Distension of the endothelial meshwork was striking and the thickness of this layer varied between 15 and 35 μm. The most advanced distension occurred in the posterior portion where loss of cell-to-cell contact was prevalent in the most severely affected areas (Fig. 9.14). On the other hand, process contacts persisted elsewhere, not only between native meshwork cells, but also between the meshwork cells and processes from the endothelium lining Schlemm's canal (Fig. 9.15). Extracellular material was reduced in quantity throughout the endothelial meshwork (Figs 9.14 and 9.15) and in some areas it could not be detected in the wide spaces.

Despite the fact that the cells lining the trabecular aspect of Schlemm's canal were attenuated and the basement membrane material was absent, there was no extensive loss of cell-to-cell adhesion. The endothelial cell nuclei were elongated and had a smooth outline.

After colloidal thorium and iron staining, the meshwork cells were seen to have a reduced surface coat (Figs 9.16 and 9.17) and staining in the endothelial meshwork was sparse. On the other hand, the trabecular cores showed more intense staining than at lower pressures (Fig. 9.17) and the surface coat on the luminal aspect of the canal's endothelial monolayer was pronounced.

A general qualitative assessment of the effects of change in intraocular pressure on the fine structure of the meshwork cells

Fig.9.I3 At 30 mm Hg the intertrabecular spaces in the corneoscleral meshwork are wide and there is some evidence of cellular separation from the trabeculae (arrows). Despite the separation process contacts are still obvious. T.E.M. (x6,500).

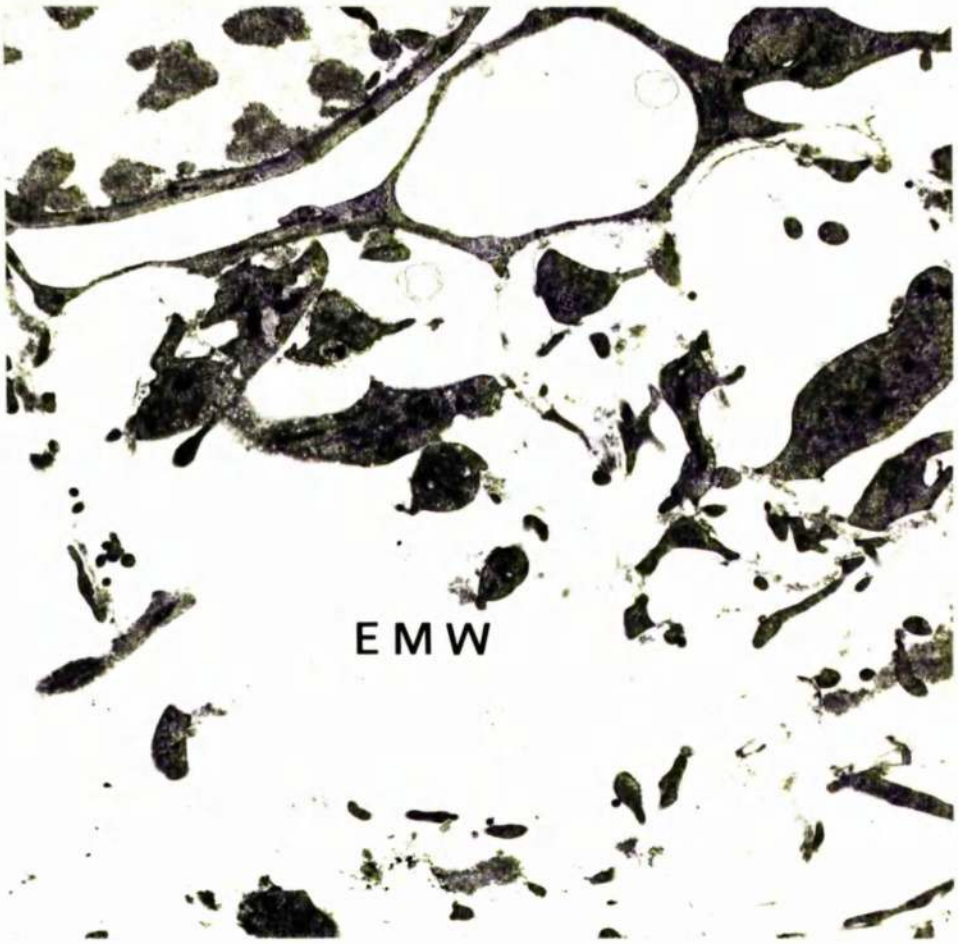

Fig.9.I4 Advanced distension in the endothelial meshwork (EMW) at 30 mm Hg with loss of cell-to-cell contact. T.E.M. (x4,200).

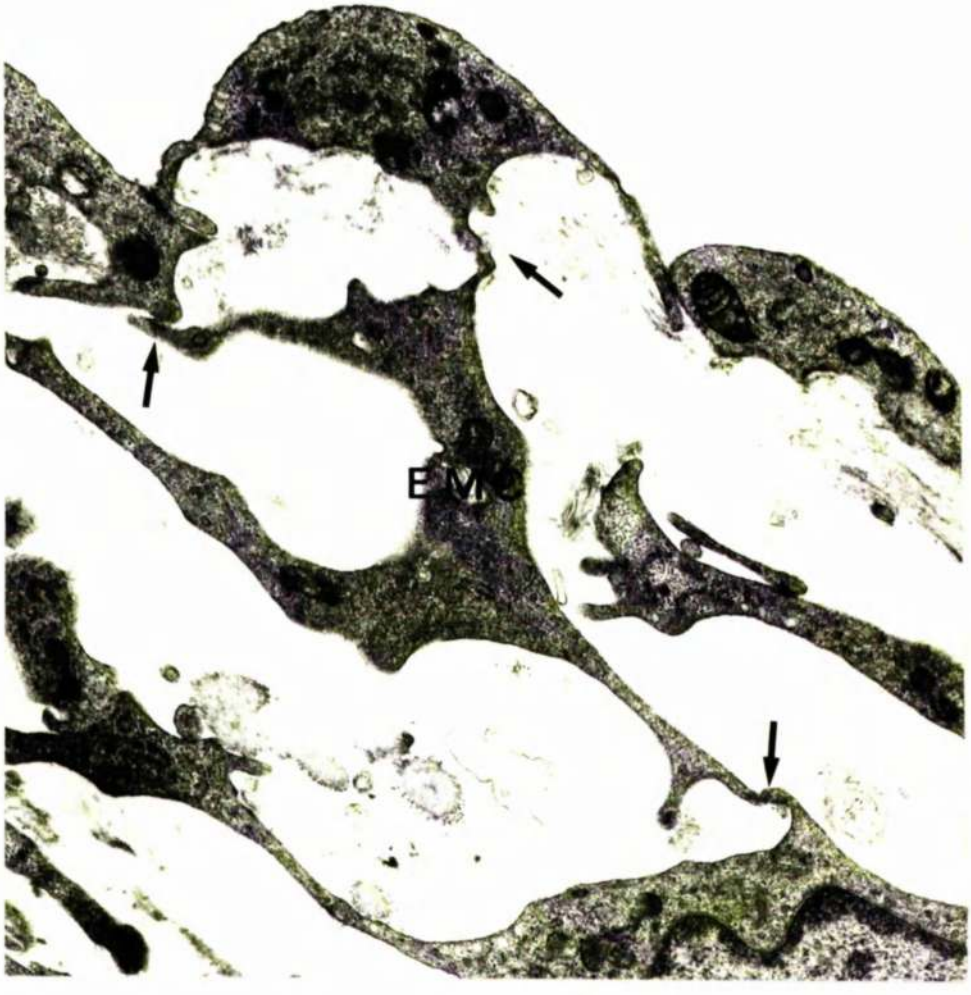

Fig.9.I5 An endothelial meshwork cell (EMC) in the endothelial meshwork at 30 mm Hg which makes process contacts with the canal endothelium and a neighbouring meshwork cell (arrows). T.E.M. (x2I,000).

Fig. 9.16 Corneoscleral trabeculae at 30 mm Hg stained with colloidal iron. The surface coat on the apical border of the endothelial cells is reduced from that seen at 15 mm Hg. T.E.M., no section staining (x6,000).

Fig.9.I7 Part of a corneoscleral trabecula at 30 mm Hg stained with colloidal iron. A rich deposit of iron particles has collected in the trabecular core. T.E.M., no section staining (x47,000).

(for canal endothelial cells see next chapter) showed no obvious variation in the number of mitochondria or the amount of rough endoplasmic reticulum. Similarly, significant variations in micropinocytosis could not be detected. By contrast there appeared to be an increase in the number of lysosomes, lysosomal complexes, multivesicular bodies and lipid vesicles (Fig. 9.18) in the meshwork cells at 30 mm Hg when compared with the appropriate 15 mm Hg controls. The results of the quantitative analysis at the two pressures are summarised in Figs 9.19a - d and they show, for each animal, an increase in organelle counts at 30 mm Hg in both the endothelial meshwork cells and the cells lining the trabeculae. The increase was variable however and, for example, was about 100% in the lipid vesicle count and about 500% for secondary lysosomes. When the total counts for the five animals were compared statistically, the differences in organelle counts were significant ($P < 0.01$).

9.3.5 0 mm Hg

Intertrabecular spaces were of normal width in the uveal and inner corneoscleral meshwork but the outer corneoscleral trabeculae and the elements of the endothelial meshwork formed a compact zone. The compact zone was particularly thick in the central region forming a layer 30 µm wide in which the endothelial meshwork cells were arranged in parallel layers (Fig. 9.20). The narrow spaces between the cells were rich in extracellular material and had a strongly positive reaction with the mucopolysaccharide stains (Fig. 9.21). The endothelium lining the trabecular wall of the canal was attenuated (probably because the canal lumen was dilated and filled with blood) but intact. The surface coat on the luminal aspect of these cells, which was so prominent at higher pressures, was reduced (Fig. 9.28a).

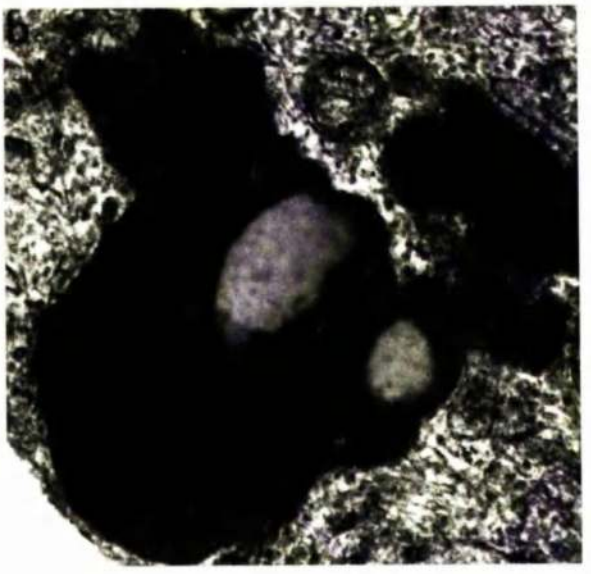

Fig.9.I8 Various cell organelles in trabecular meshwork cells at 30 mm Hg. a) A lysosome above 2 lipid vesicles, b) a lysosomal complex and c) a multivesicular body. T.E.M. (x60,000).

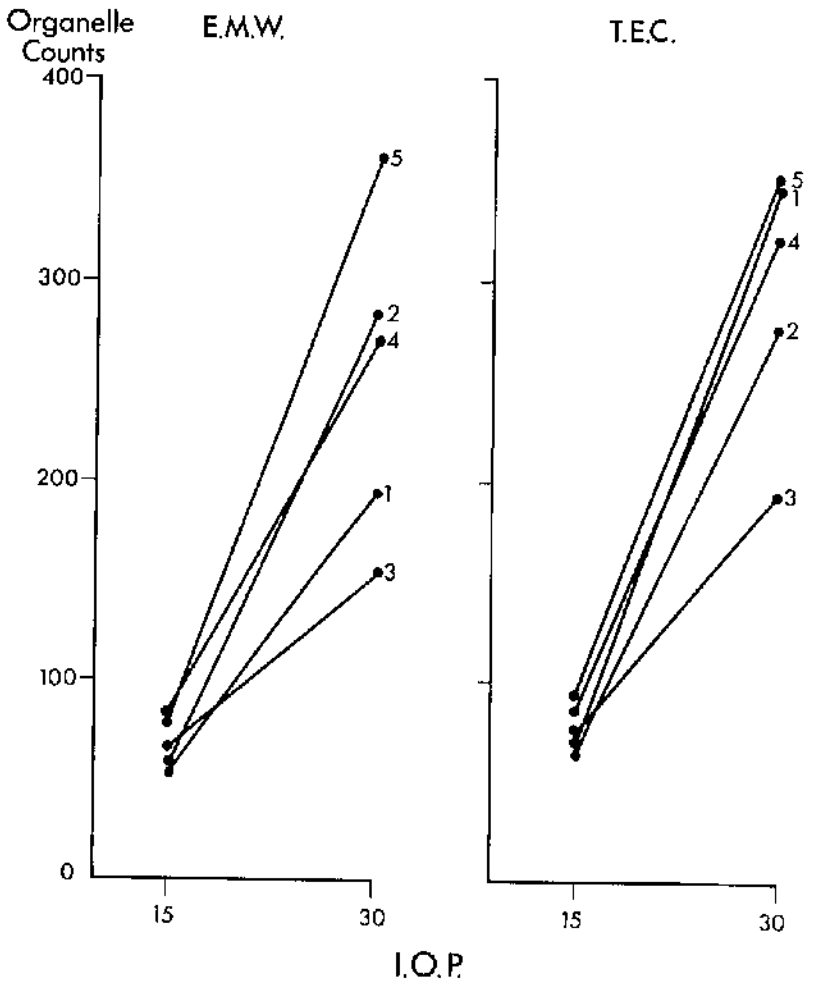

Fig.9.I9a Counts of lysosomes.

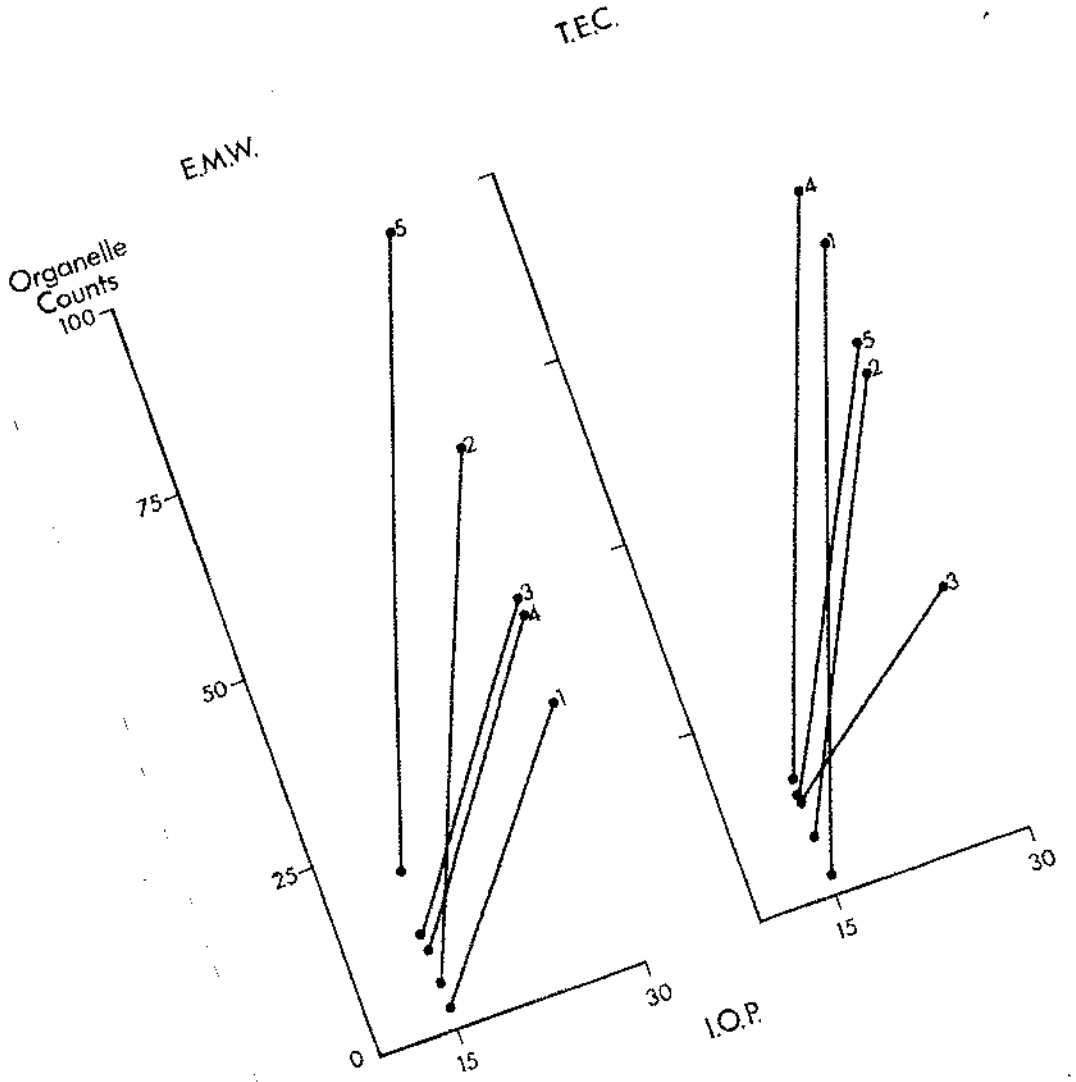

Fig.9.19b Counts of lysosomal complexes.

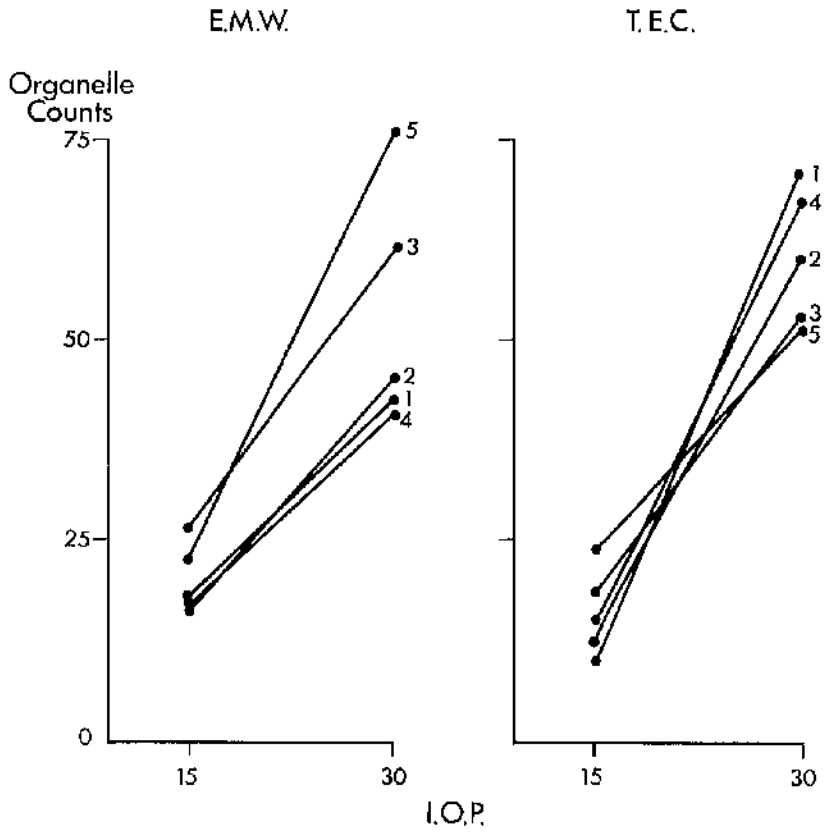

Fig.9.I9c Counts of multivesicular bodies.

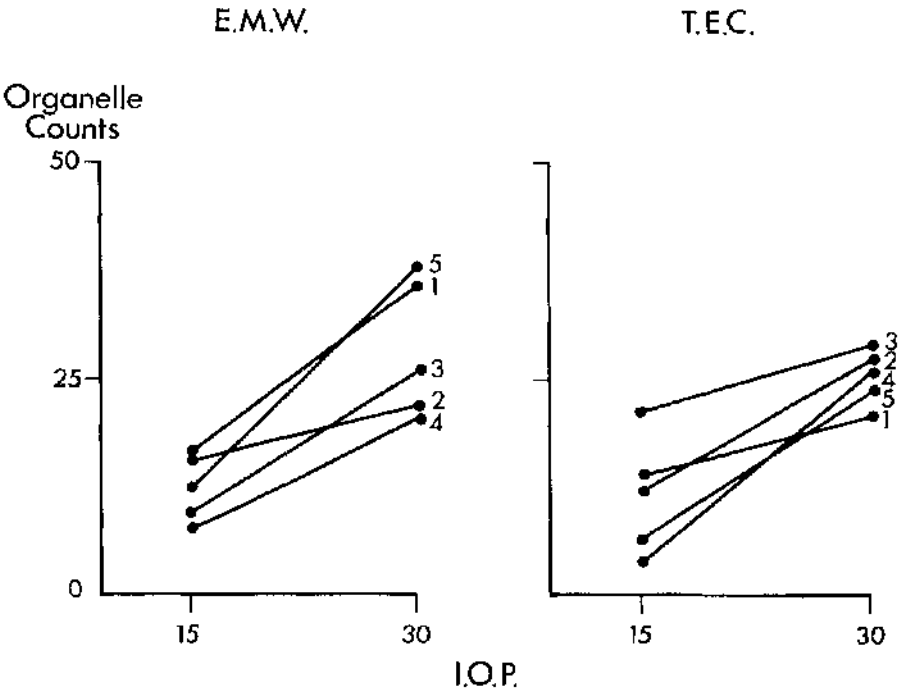

Fig.9.I9d Counts of lipid vesicles.

Fig.9.I9a - d Show the results of the a) lysosome, b) lysosomal complex, c) multivesicular body and d) lipid vesicle counts from I00 cell sections in the endothelial meshwork (E.M.W.) and trabecular endothelial cells (T.E.C.). A line connects the control (I5 mm Hg) and the experimental (30 mm Hg) counts for each animal and the animal number for each individual is the same in all four figures (in animals I - 3 fixation was by anterior chamber infusion and in 4 and 5 by carotid perfusion).

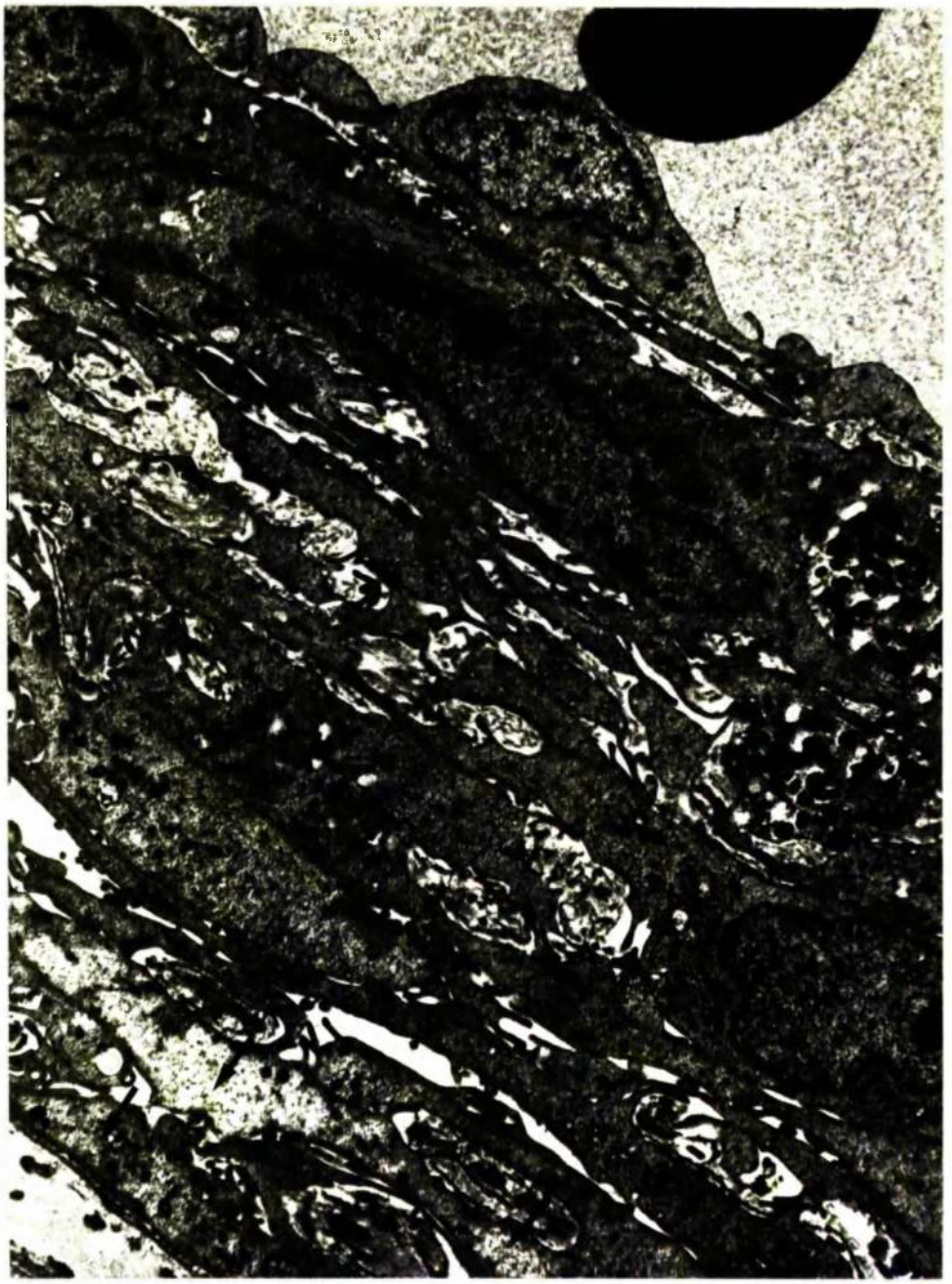

Fig.9.20 At 0 mm Hg the endothelial and outer corneoscleral meshwork form a compact zone. Regions of cytoplasmic rarefaction and vesiculation in corneoscleral trabecular cells are marked by arrows. T.E.M. (x6,600).

Fig.9.2I Part of the endothelial meshwork at 0 mm Hg stained with colloidal iron. The canal endothelium is indicated (EN). A rich deposit of iron particles obliterates the narrow extracellular spaces. T.E.M., no section staining (x30,000).

Cellular degeneration was a consistent finding in all three animals used in the experiment. The endothelial cells lining the uveal cords (Fig. 9.22) were in an advanced stage of ultrastructural degradation which, in its most severe degree, included disruption of the plasma membrane and extrusion of the cytoplasm and organelles. Adjacent to the degenerate cells, there were membraneous profiles which were either empty or contained small electron dense particles and vesicles.

The degenerative changes were less severe, but still marked, in the inner corneoscleral meshwork and were associated with an apparent reduction in the cytoplasmic microfilament content and the micropinocytotic activity at the cell membrane. Focal groups of trabecular cells exhibited dilatation of the cisternae of the rough endoplasmic reticulum; lipid vesicles, lysosomes and lysosomal complexes were prevalent in the cytoplasm (Fig. 9.23). The cell nuclei and the relationships of the stacks of Golgi apparatus were unaffected and in the majority of cells, the plasma membranes were intact. In some of the trabeculae, the basement membrane was either focally thickened or multilayered. Beneath the basement membrane the trabecular cores contained disorganised and swollen collagen fibre bundles and prominent clumps of elastic material. After mucopolysaccharide staining, colloidal deposits were abundant in the trabecular cores of the uveal and inner corneoscleral meshwork and the cytoplasm of the endothelial cells contained stain particles. The presence of intracytoplasmic stain was a further indication that some plasma membranes had ruptured.

The changes in the endothelial meshwork were minimal and confined to occasional foci of cytoplasmic rarefaction but in the compressed outer corneoscleral region, the cytoplasmic rarefaction,

Fig.9.22 A uveal trabecula at 0 mm Hg in an advanced state of structural and cellular degradation. T.E.M. (xI3,000).

Fig.9.23 At 0 mm Hg the endothelial cells on the trabeculae of the inner corneoscleral meshwork had extensive cytoplasmic rarefaction and vesiculation, T.E.M. (x7,500).

although patchy, was more pronounced and was accompanied by the appearance of intracytoplasmic membrane bound vesicles of various sizes.

The peripheral corneal endothelium contained intracytoplasmic vesicles and showed organelle degeneration similar to, although less pronounced than, that seen in the cells of the inner meshwork. Examination of the structures adjacent to the meshwork e.g. the ciliary muscle and the iris stroma failed to demonstrate comparable degenerative changes.

9.3.6 50 mm Hg

In the distended meshwork at 50 mm Hg the intertrabecular spaces in the corneoscleral meshwork were wide and were crossed by thin delicate processes (Fig. 9.24a). When examined closely, there was no evidence of excessive damage to these processes and often junctions could be identified at the narrow sites of process apposition.

In many areas, the trabecular cores of both the uveal and corneoscleral parts of the meshwork were not lined by endothelial cells. Where endothelial separation and stripping had occurred there was evidence of depletion of the constituents of the trabecular cores (Fig. 9.24b). The endothelial cells throughout the meshwork contained an abnormally large number of lysosomes, lysosomal complexes, multivesicular bodies and lipid vesicles.

When mucopolysaccharide stains were applied to this tissue, the surface staining on the luminal aspect of the meshwork cells was found to be further reduced from that seen at 30 mm Hg whereas in the trabecular matrices colloidal particles were plentiful.

Distension of the outer meshwork was pronounced so that, in the anterior (Fig. 9.25a) and central (Fig. 9.25b) portions, the canal lumen

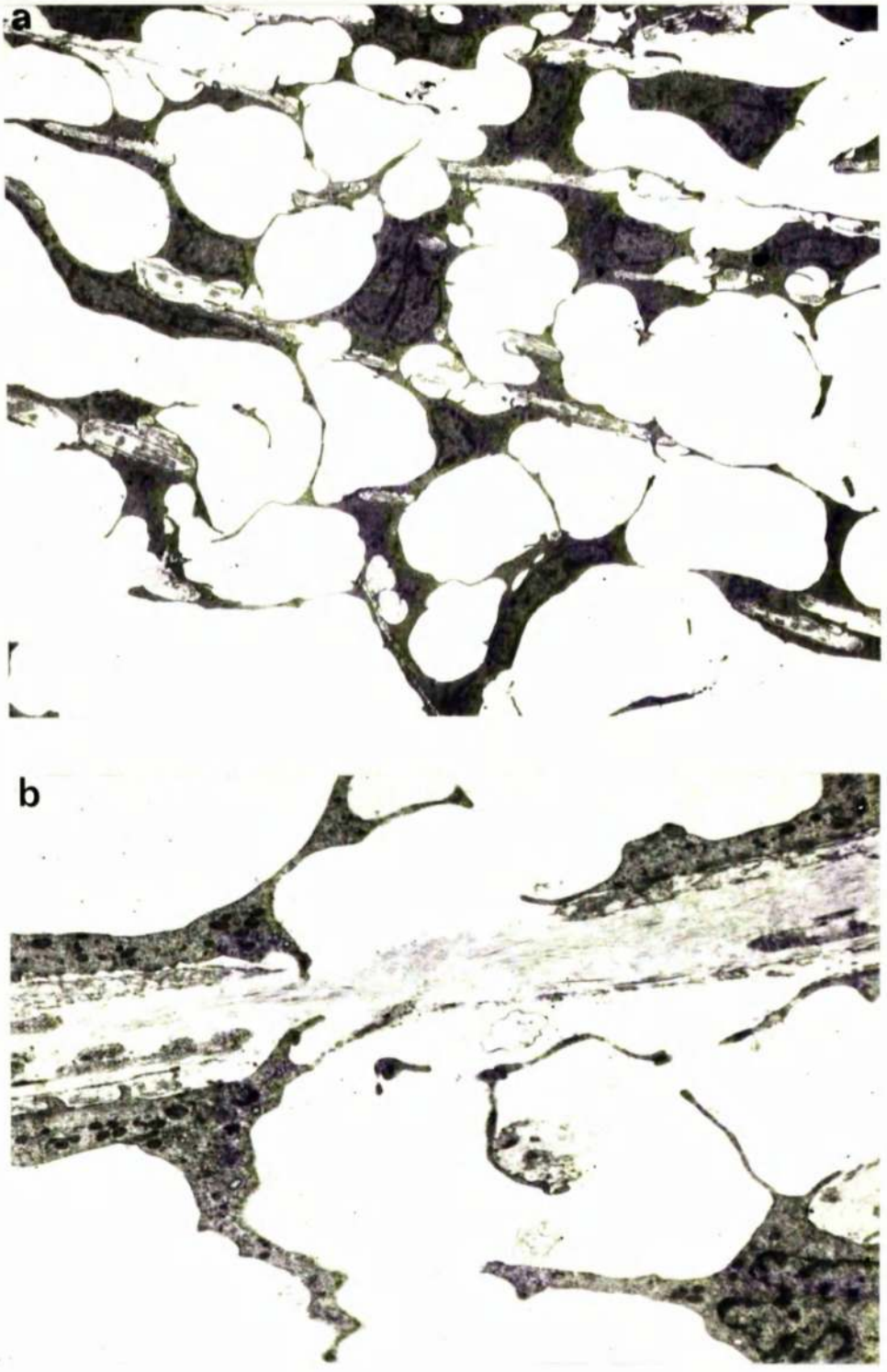

Fig.9.24 a) At 50 mm Hg many trabeculae had an incomplete endothelial cover and b) at these sites there was depletion of the core constituents. T.E.M. (a x2,500; b x8,000).

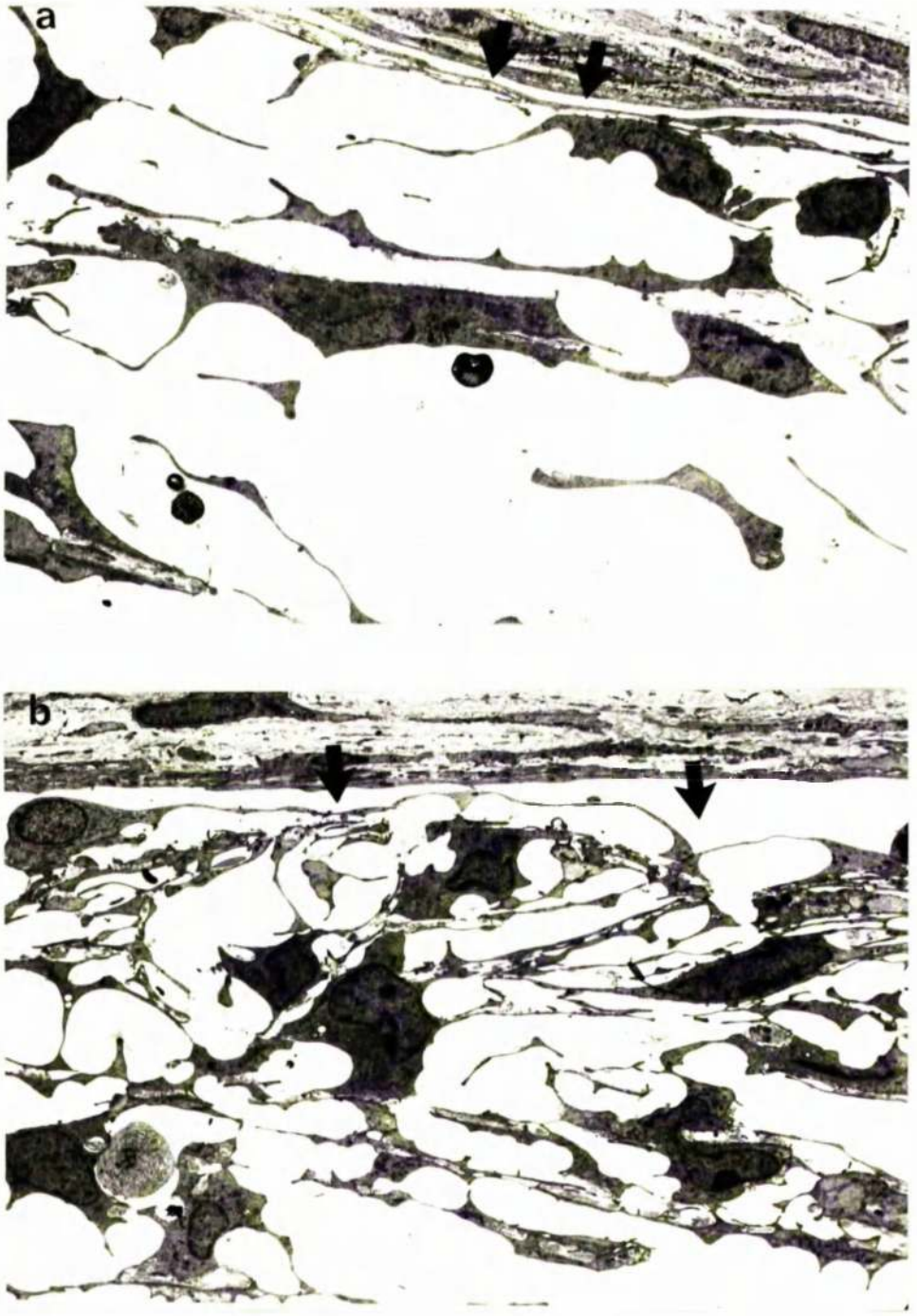

Fig.9.25 a) An anterior and b) a central portion of Schlemm's canal (arrows) and the underlying meshwork at 50 mm Hg. T.E.M. (x2,000).

was either reduced to a narrow slit or was totally occluded. The endothelium lining the trabecular wall of Schlemm's canal was extended and junctions were intact where the cells were in contact. In the posterior part of the canal, there were gaps between the cells of the endothelial monolayer on the trabecular aspect of the canal and the cells were often contracted and rounded (Fig. 9.26a) but in some segments continuity persisted and here the cells were markedly elongated (Fig. 9.26b). The elongated cells had restricted zones of apposition which were occupied by at least one junction. In the anterior part of the endothelial meshwork the vertical cell process connections were usually absent but the horizontal connections remained; extracellular material was reduced in quantity (Fig. 9.25a). In the posterior part, the endothelial meshwork contained isolated cellular elements and fragmented and disorganised extracellular material (Fig. 9.26). Perforations were detected in the cytoplasm of some of the native cells.

Predictably, colloidal thorium and iron were sparsely distributed in the endothelial meshwork and there was reduced surface staining on the native meshwork cells (Fig. 9.27). Where the endothelial monolayer was perforated, the luminal coat was unremarkable (Fig. 9.27) but where the canal endothelium was intact, very thick, and often irregular, coat of colloidal particles was adherent to the luminal surface of the cells (Fig. 9.28a) - the antithesis of the situation in the 0 mm Hg eyes (see Fig. 9.28c).

9.4 Discussion

It is evident from the findings presented in this chapter that up to a pressure of 30 mm Hg, progressive distension in the meshwork can occur without causing extensive cellular damage and loss of cell

Fig.9.26 Posterior portions of Schlemm's canal at 50 mm Hg where the endothelium on the canal's trabecular wall is a) perforated (arrows) and b) intact. T.E.M. (a x9,000; b x4,600).

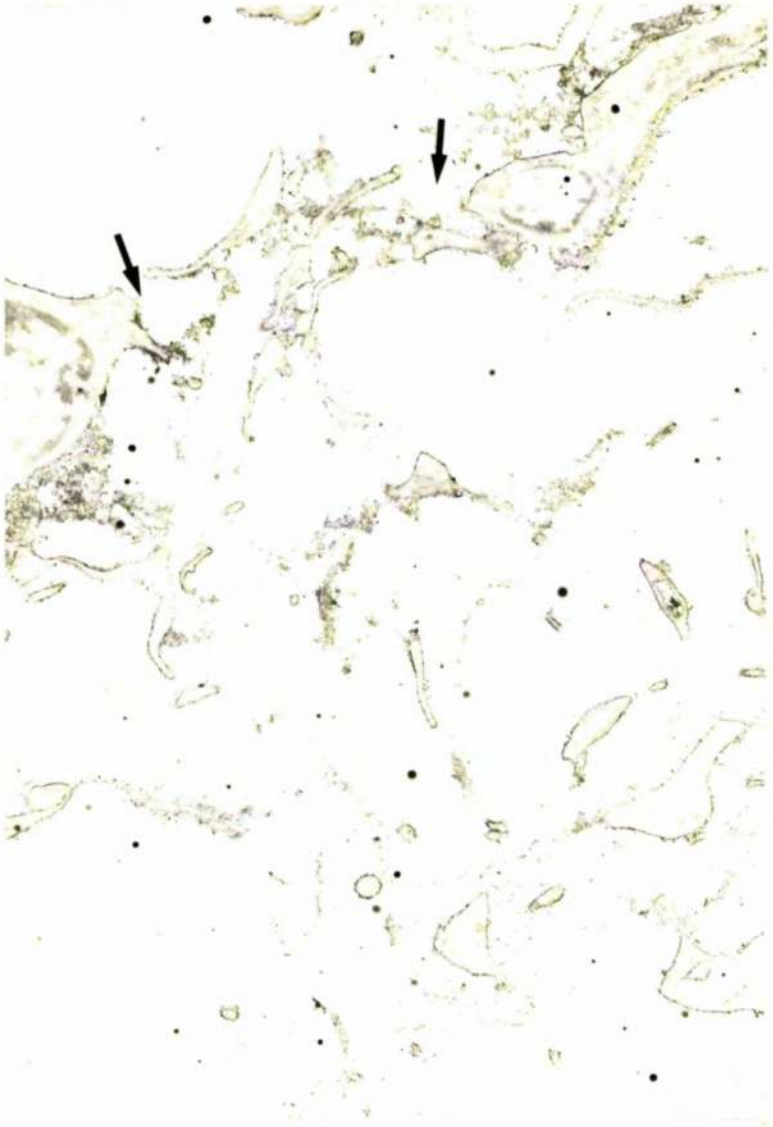

Fig.9.27 Part of the trabecular wall of Schlemm's canal at 50 mm Hg stained with colloidal iron and no subsequent section staining. The canal endothelium is disrupted (arrows). T.E.M. (x5,000).

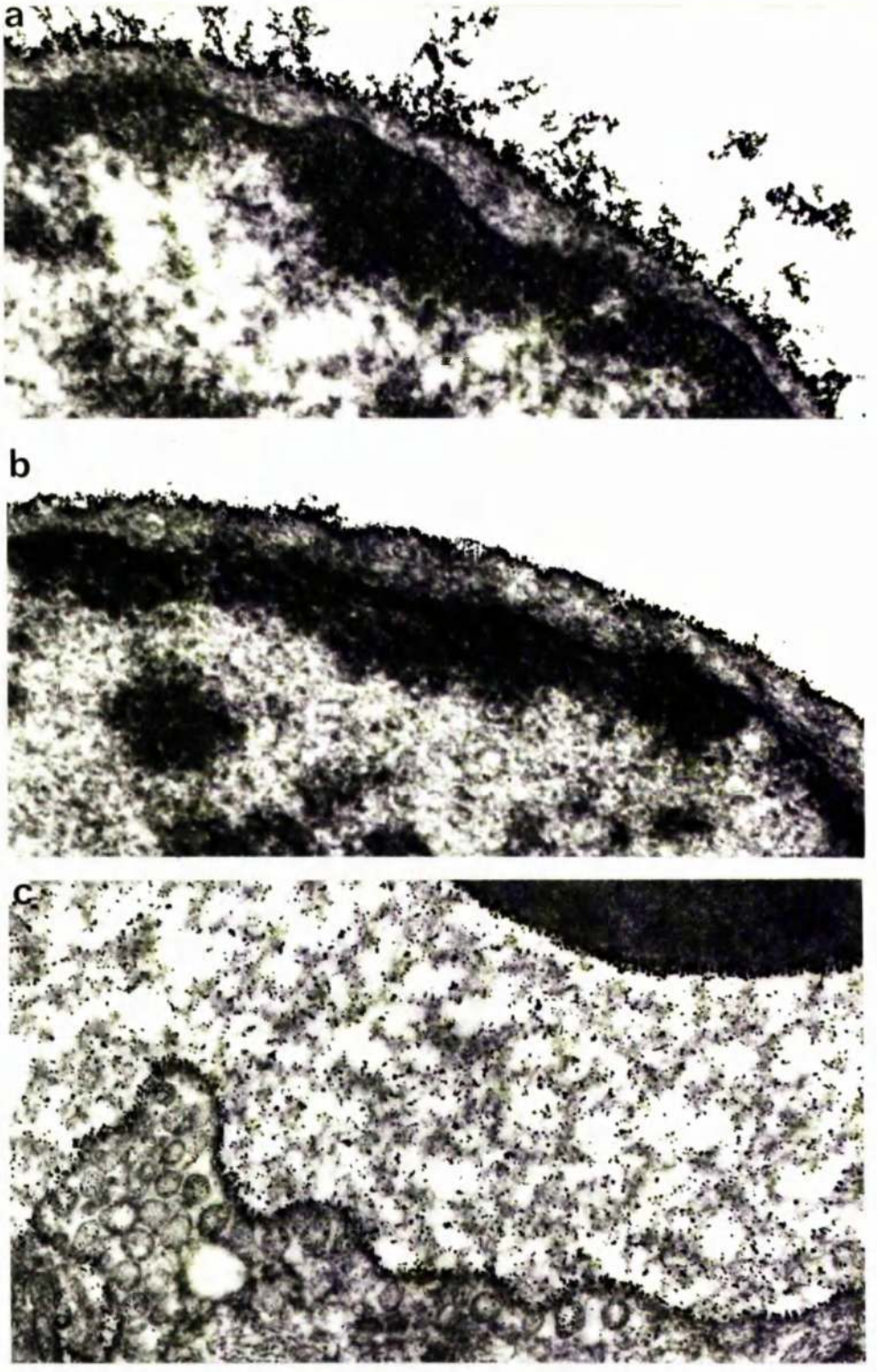

Fig.9.28 The apical surface of endothelial cells on the trabecular aspect of Schlemm's canal after colloidal thorium staining with conventional section staining at a) 50 mm Hg, b) I5 mm Hg and c) 0 mm Hg. T.E.M. (x55,000).

contacts in either the endothelium on the canal's trabecular aspect or the underlying meshwork. The native cells can adapt their morphology partly becuase of their inherent elasticity and partly because of effective intercellular adhesion. The elasticity probably depends on the presence of cytoplasmic microfilaments which have certain similarities to the contractile elements in smooth muscle cells (see Tripathi, 1974). It is of interest to note that when cellular attenuation involves the whole cell as in the canal endothelium (rather than the cell processes as in the meshwork cells) changes are observed in nuclear outline which are remarkably similar to those described by Majno, Shea and Leventhal (1969) in contractile vascular endothelium which also has a prominent microfilament content. The changes in nuclear outline are shown diagrammatically in Fig. 9.29 and using the criteria outlined by Majno et al (1969) it can be seen from Fig. 9.30 that at 8 mm Hg when the monolayer was constricted over 96% of the nuclei examined had infolds whereas at 30 mm Hg only about 33% had infoldings.

The small junctions between the endothelial cells on the canal's trabecular aspect provide sufficient cell-to-cell adhesion to maintain the integrity of the monolayer up to 30 mm Hg but are unable to withstand an acute elevation of the intraocular pressure to 50 mm Hg. It can therefore be concluded that facility calculations which involve stepwise increase in pressure outwith near-physiological limits are of dubious merit.

In the trabecular meshwork, the anchorage provided by the gap junctions and maculae adherentes provide a probable explanation for the ability of the meshwork cells to maintain intercellular contact in spite of deformation in the distended tissue. Cellular adhesion to the basement substance of the trabeculae is probably enhanced by

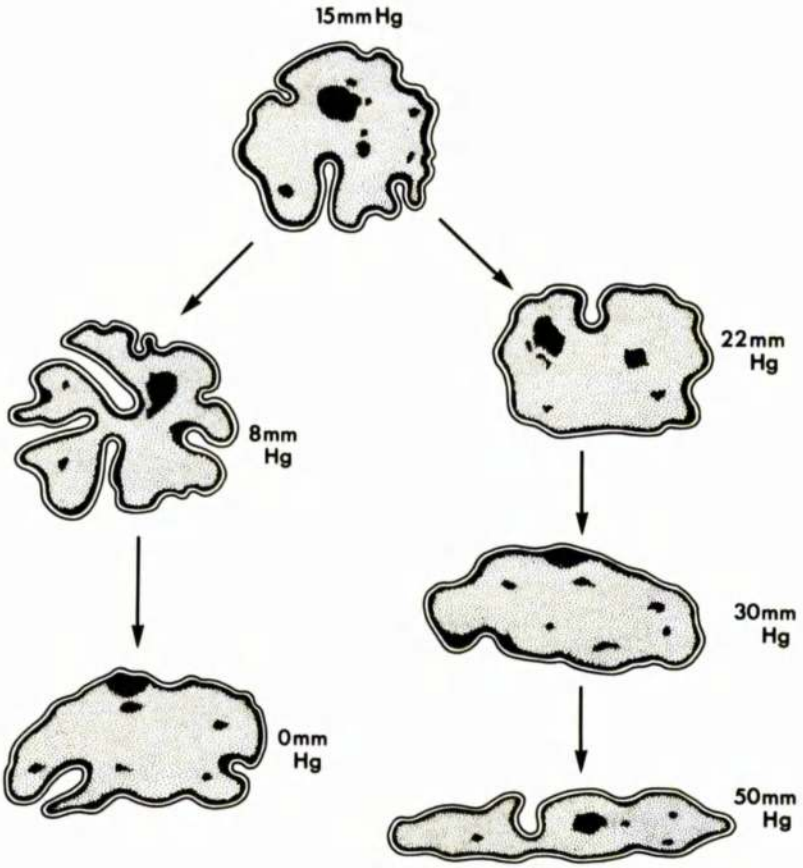

Fig.9.29 Diagram which shows the typical appearance of the nuclei in the endothelial cells on the canal's trabecular aspect at the various levels of intraocular pressure.

Intraocular Pressure (mm Hg)	Nuclei Without Folds (% of total)	Nuclei With Folds (% of total)	Number of Nuclei Examined
50	61 (53.0%)	54 (47.0%)	115
30	122 (67.4%)	59 (32.6%)	181
22	25 (24.5%)	77 (75.5%)	102
15	17 (15.3%)	94 (84.7%)	111
8	4 (3.7%)	104 (96.3%)	108
0	38 (36.2%)	67 (63.8%)	105

Fig.9.30 Frequency of nuclei with and without membrane infoldings in the endothelium lining the trabecular aspect of Schlemm's canal.

basal processes and close association with mucopolysaccharide material. However at 50 mm Hg, it appeared that cellular attachments were more resilient than cellular adhesion to the trabeculae.

Although the endothelium lining the trabecular aspect of Schlemm's canal does not have a distinctive basement membrane it is maintained against a pressure gradient and therefore requires some form of anchorage to prevent detachment from the underlying meshwork. Extracellular material e.g. fine fibrillar material, ground substance and elastic-like concentrations, lies close to the monolayer in the 15 mm Hg tissue and this material may have adhesive properties. Also the projection of small cell processes into the ground substance, described in this chapter and by Inomata, Bill and Smelser (1972a) and Tripathi (1974), would provide stability. However at 30 mm Hg, when presumably the pressure gradient is increased and the forces acting on the endothelial monolayer are greater, the endothelium remains in close contact with the underlying meshwork even though much of the extracellular material is diminished in this area. Since endothelial cell contacts with the endothelial monolayer are intact (and are still intact in some regions at 50 mm Hg), it is considered that cellular and not extracellular elements play the major part in maintaining the position of the trabecular wall lining endothelium.

At 50 mm Hg the pattern of cell stress and trabecular disruption is similar to that described by Svedbergh (1974) in the vervet monkey meshwork subjected to pressures of 33 and 44 mm Hg for periods of several hours. In particular Svedbergh observed trabecular disruption and total detachment of complete endothelial cells. The changes described by Svedbergh were obviously more severe than those described here but could be explained by longer exposure to excessive pressure.

In several investigations using conventional staining, attention has been paid to the material present in the extracellular spaces of the endothelial meshwork (Vegge and Ringvold, 1970; Inomata, Bill and Smelser, 1972a; Lütjen-Drecoll, 1973; Tripathi, 1974). This material was considered to be of importance because changes in the nature, distribution and density of the extracellular substances may influence the rate of aqueous flow through the extracellular spaces to the canal's endothelial monolayer. In the present study it has been shown that, as intraocular pressure increases, the extracellular spaces become dilated and extracellular materials, including the mucopolysaccharides, are lost (presumably they are washed through the canal monolayer perhaps via giant vacuoles at e.g. 30 mm Hg and via deficits at 50 mm Hg). It is intriguing to speculate that the endothelial meshwork cells are in an active synthesising phase (they have the appearance of metabolically active cells see Chapter 4) and are continuously replacing small amounts of extracellular material which have been eroded from the matrix and washed through the canal endothelium with the aqueous flow.

The loss of extracellular coat from the meshwork cells with increase in pressure, like the loss of extracellular mucins from the spaces in the endothelial meshwork, is probably a washout phenomenon. Equally the more intense trabecular staining at high pressures may be due to a greater accessibility created by cellular separation. On the other hand the inverse relationship between the thickness of the luminal coat on the canal endothelium and intraocular pressure is more difficult to explain but it may be related to an alteration in pinocytotic activity (see next chapter).

The increase in the counts of lysosomes, lysosomal complexes, multivesicular bodies and lipid vesicles at 30 mm Hg, when compared

with 15 mm Hg, may be the result of two factors a) an increase in organelle size and b) an increase in organelle numbers. As the lysosomal complexes often appeared to be larger at the higher pressure, both factors probably contribute to the increased count of this organelle. With the other three organelle types there were no obvious size changes so the increased count represents a true increase in incidence.

It has been shown that, like lysosomes and lysosomal complexes, multivesicular bodies contain acid phosphatases (Smith and Farquar, 1966). An increase in these three cellular organelles may therefore be an indication of early autophagic degeneration and probably represents a cell response to a less favourable environment. Similarly, if the residue of the autolytic processes was rich in lipid, the increase in lipid vesicles could be explained. In addition to the increase in the numbers of multivesicular bodies, there appeared to be a decrease in the mean number of vesicles within the organelles (Fig. 9.31). If the vesicles contained hydrolytic enzymes, then the decrease in vesicle content could be explained by increased enzyme demand by cells involved in autophagic digestion. As would be expected, all four organelles were prominent in the meshwork cells at 50 mm Hg.

If the gradient of meshwork cell degeneration observed at 0 mm Hg was not a fixation artefact the finding may be of relevance to clinical hypotonia. That these eyes were immersion rather than perfusion fixed must make the finding suspect, but there are several reasons for casting doubt on fixation artefact. A comparable degenerative pattern was not seen in the immersion fixed tissue described in chapter 4. It would be anticipated that with poor immersion fixation the degeneration would be more advanced in the outer than the inner meshwork and this was not the case. Similarly, the adequate fixation of the ciliary

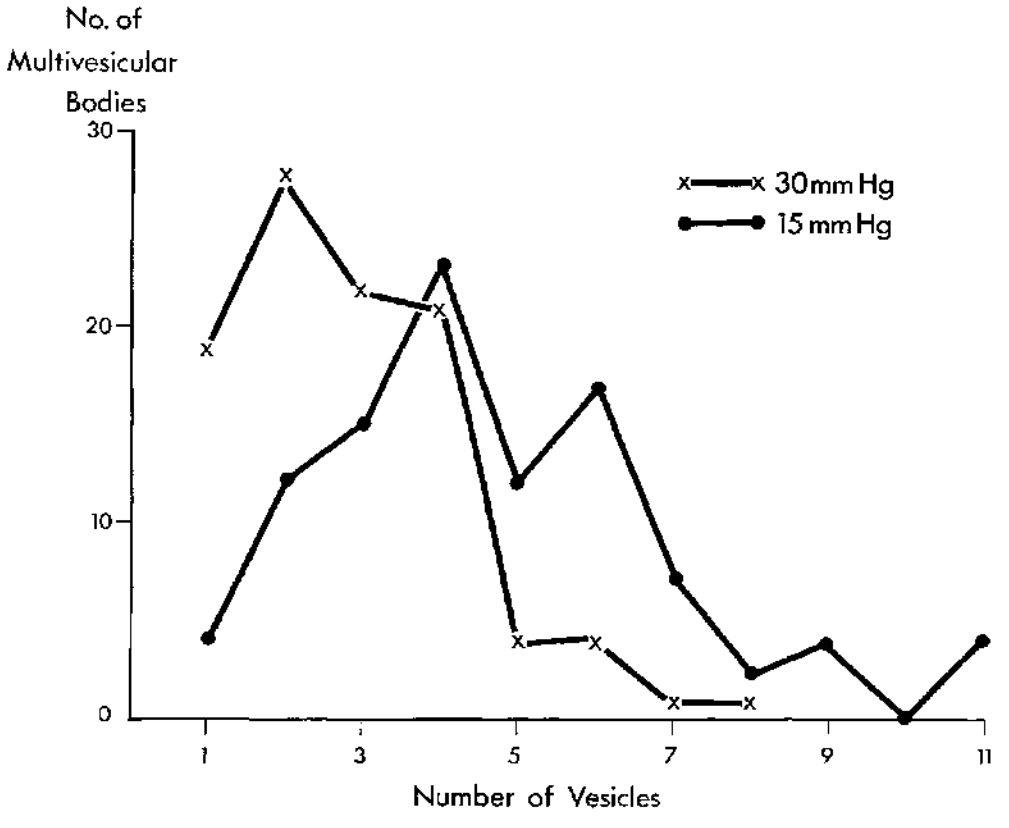

Fig.9.3I Shows the distribution of vesicles in I00 multivesicular bodies at 30 and I5 mm Hg. Significantly fewer ($P < 0.0I$) vesicles were present in the bodies at 30 mm Hg (mean 2.8 $\pm$ I.5) than at I5 mm Hg (mean 4.7 $\pm$ 2.3).

muscle and the iris makes inadequate fixative penetration seem unlikely. Post-mortem cellular degradation is a well recognised phenomenon and even after considerable fixation delay, it rarely approaches that seen in the present material.

Since the corneal endothelium was also vulnerable to the process responsible for the degeneration gradient through the meshwork, aqueous stagnation and the accumulation of toxic metabolites might be a causal process worthy of consideration. The preservation of the outer meshwork could then be explained by the presence of blood in Schlemm's canal which would protect the adjacent tissue from hypoxia and acidosis. Thus the gradient of cellular degradation could be explained.

CHAPTER 10

PRESSURE-INDUCED ALTERATIONS TO SUSPECTED OUTFLOW ROUTES THROUGH THE ENDOTHELIUM LINING SCHLEMM'S CANAL.

10.1 Introduction

This transmission electron microscopic study is concerned with the ultrastructural investigation of the pressure induced changes in the giant vacuoles described in chapters 7 and 8. It was hoped to determine a) whether or not the vacuoles were of the same type as those described in normal tissue (see Chapter 4 section 4) and b) if changes in the vacuole population could be related to changes in the metabolic or synthetic activities of the canal endothelium. In addition the pressure response of other possible routes for the passage of aqueous humour through the endothelium (see Chapter I and Fig. 1.6) was assessed.

Finally a quantitative analysis was undertaken a) to discover the significance of resolution errors which may have prejudiced the findings of the light microscopic vacuole counts and b) to determine, in as precise a manner as possible, the pressure influences on suspected endothelial flow pathways.

10.2 Materials and methods

The morphological assessment of the canal endothelium was based on tissue mapping of single thin sections and serial reconstruction of various structures within the endothelium. A quantitative analysis based on isolated thin sections was also performed.

10.2.1 Serial reconstructions

From serial sections, reconstructions were made of giant vacuoles, their meshwork and lumen pores and transcellular non-vacuolar openings. Either a complete set of sequential sections or only the most informative sections from each structure were photographed. Maximum pore and vacuole

widths were measured on the appropriate electron micrographs using a x 7 magnifier which incorporated a graticule. The plate and print magnifications were standardised with the aid of a line grating (2,160 lines per mm).

10.2.2 Single section analysis

The 2 carotid perfusion fixed animals were not used for this part of the study, thus the quantitative analysis was restricted to the 12 rhesus monkeys in which primary fixation was by intraocular infusion (the subjects of the light microscopic giant vacuoles count described in Chapter 8).

Meridional sections were cut from each of 10 tissue blocks equally distributed between the superior and inferior halves of the anterior segment. For every tissue block separate ribbons of sections were mounted on 5 grids (100 mesh) so that, 50 grids were available for each eye. One grid square was selected from each of the available grids. The grid square chosen was usually that which contained the greatest amount of canal endothelium. Section quality was taken into consideration and anatomical regions complicated by the presence of either septae or collector channels were avoided. To standardise comparison, the analysis was biased towards the endothelium of the middle third of the canal's trabecular wall.

On the selected grid squares, the numbers of nuclei, giant vacuoles and their pores, pseudovacuoles, non-vacuolar openings and minipores were counted. In this way, the numbers of each of the various structures incorporated within the endothelium lining the trabecular aspect of Schlemm's canal, on 50 grid squares, was obtained from each eye.

Simple conversion of the data to provide values per unit length

of canal was not tenable because fewer cells were present in the attenuated endothelium at higher pressure. To validate comparison between intraocular pressure levels the numbers of vacuoles with and without pores, vacuoles with pores, pseudovacuoles, non-vacuolar openings, and minipores were expressed in terms of the nuclei counted; this was considered to be a more reasonable reflection of the number of cells examined. Vacuolar pore incidence was also expressed as a percentage frequency of the number of vacuoles counted.

10.3 Qualitative assessment

10.3.1 General features of the canal endothelium

Within the endothelial cells on both sides of Schlemm's canal, the mitochondrial size and frequency, the prominence of the Golgi apparatus, the development of the rough and smooth reticular systems, the numbers of free ribosomes and the amount of glycogen remained unaltered throughout the pressure range under investigation. Therefore, within a time period of one hour, maintained intraocular pressures of various levels did not produce recognisable changes to the organelles associated with cellular metabolic and synthetic activity.

There was, on the other hand, some evidence to indicate cell stress at the extremes of intraocular pressure. At 8, 15 and 22 mm Hg the organelles involved in intracellular lytic processes, lysosomes, lysosomal complexes and multivesicular bodies, were rare but were more prevalent at the lowest (0 mm Hg) and highest (30 and 50 mm Hg) pressures.

Giant vacuoles, non-vacuolar openings, minipores, pinosomes and micropinosomes have been considered as possible routes for the passage of aqueous humour into Schlemm's canal (see Chapters 1 and 4).

As all these structures demonstrated interesting pressure related changes particular attention was paid to their ultrastructural appearance, distribution and frequency at the various pressure levels.

10.3.2 15 mm Hg

Giant vacuoles, non-vacuolar openings and minipores were restricted to the endothelium on the canal's trabecular aspect and the septae where they formed part of the canal's trabecular wall. Typically, giant vacuoles were found in association with the perinuclear regions of the squat endothelial cells (Fig. 10.1), were of variable size and were always limited by a smooth membrane. A vacuole involved the cytoplasm of one endothelial cell and cytoplasmic microfilaments came into close association with the vacuolar membrane. The microfilaments were more obvious at the apex and base than at the sides of the vesicular structures.

From single sections most of the vacuole population appeared to be intracytoplasmic but some had meshwork openings or pores (Figs. 10.1 and 10.2) and an even smaller proportion had lumen pores (Fig. 10.3). Meshwork pores were usually larger than lumen pores. Extracellular elements and cell processes from the underlying endothelial meshwork were often in close association with the vacuolar meshwork pore (Figs 10.1 and 10.2).

Serial studies revealed that most giant vacuoles were invaginations from the meshwork surface of the endothelial cells i.e. each had a meshwork pore. If a meshwork and a lumen pore were present in a vacuole, the structure constituted a vacuolar transcellular channel which made a direct communication between the meshwork and the canal. There was a paucity of vacuolar transcellular channels at 15 mm Hg (Fig.10.4

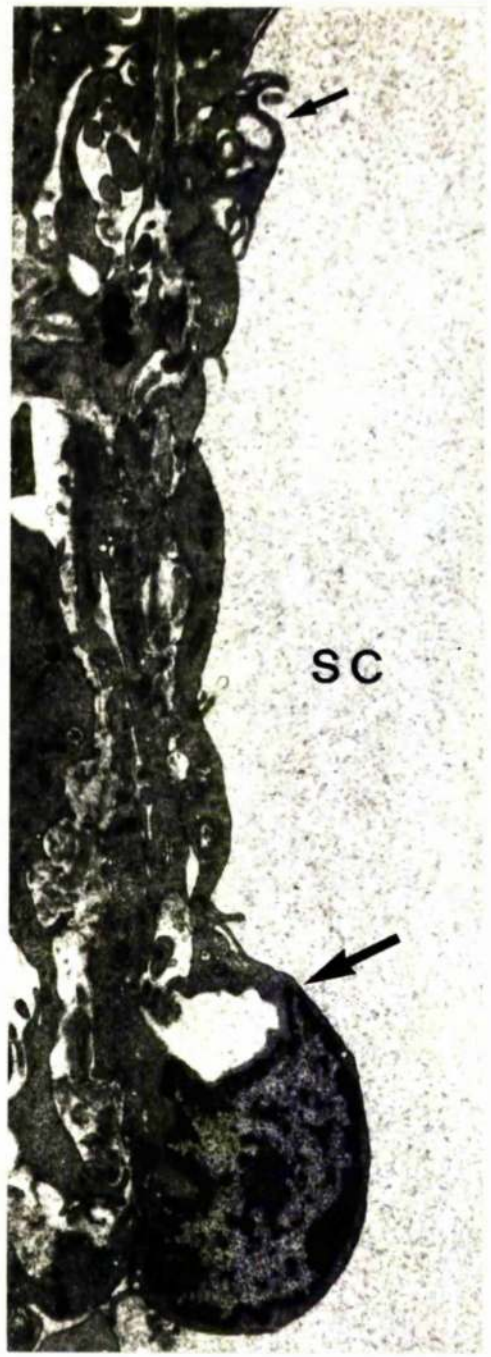

Fig.IO.I Part of the endothelium lining the trabecular aspect of Schlemm's canal (SC) at I5 mm Hg. A giant vacuole is indicated by a large arrow and a pinosome by a small arrow. T.E.M. (x6,500).

Fig.IO.2 A giant vacuole with a meshwork pore (large arrow) at I5 mm Hg. A pinosome is indicated by a small arrow. T.E.M. (x37,000).

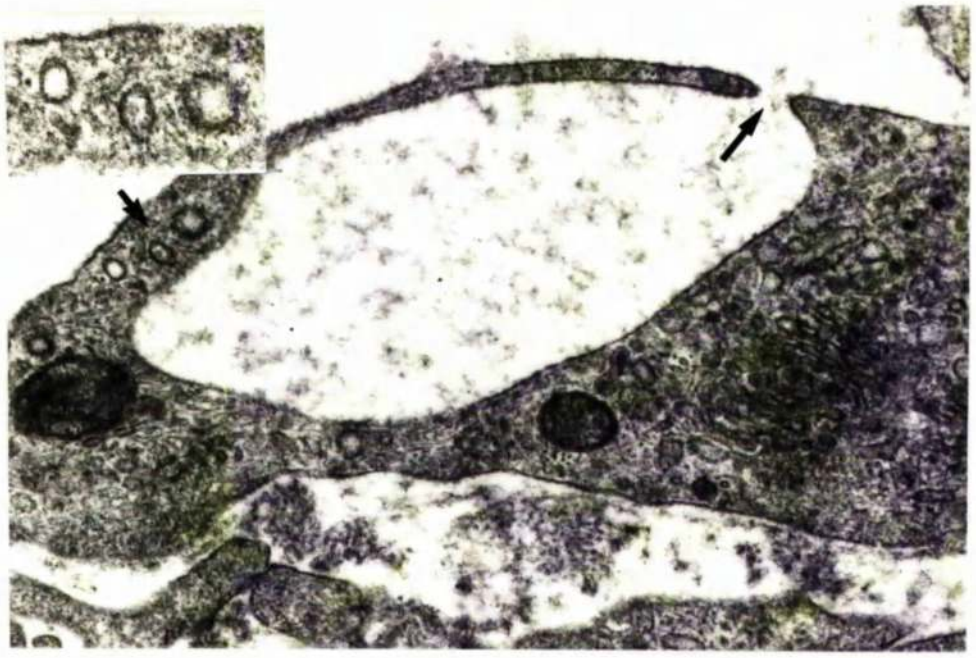

Fig.10.3 A giant vacuole with a lumen pore (arrow) at 15 mm Hg. Coated vesicles (indicated by a small arrow) are shown at higher power in the insert. T.E.M. (x44,000; insert x72,000).

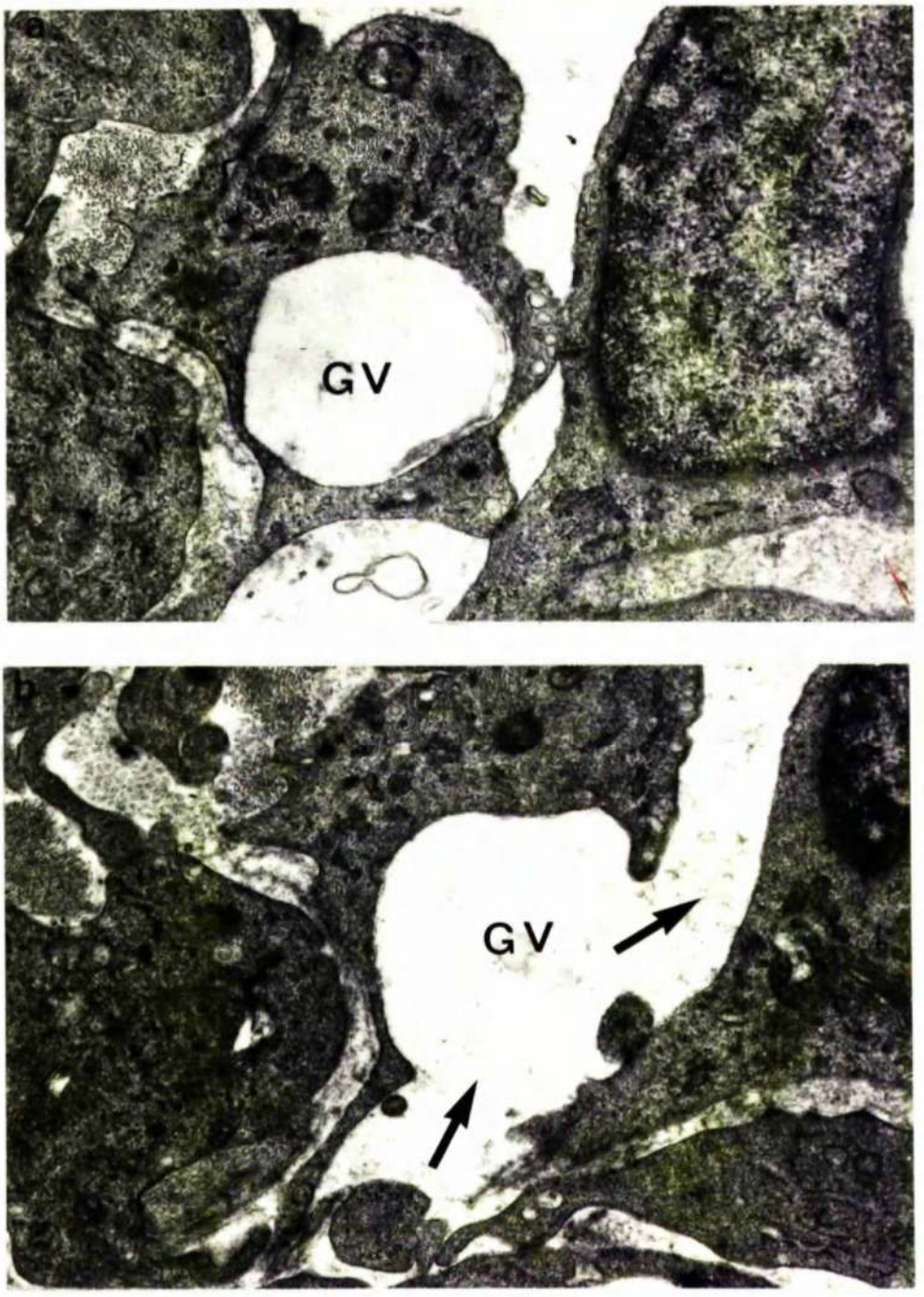

Fig.IO.4 a and b are two different levels of section through a giant vacuole (GV) at I5 mm Hg. In a) the vacuole appears as an intracellular vesicle while in b) the vacuole is seen as a transcellular channel (arrows). T.E.M. (x26,000).

Non-vacuolar openings were an infrequent finding. The openings were restricted to the narrow marginal regions of the endothelial cells (Fig. 10.5) and sometimes they contained a wandering cell which was presumed to be in transit. On the few occasions when the gaps were included in a sequential series of sections they were shown to be intra rather than intercellular structures (Fig. 10.6).

Small fenestrations (about 0.1 μm wide), referred to as minipores by Inomata, Bill and Smelser (1972a), were restricted to very narrow portions of the endothelium such as the attenuated marginal zones (Fig. 10.5) and the thin cytoplasmic shells of the largest giant vacuoles. Because the endothelial cells were fairly squat and large dilated vacuoles were uncommon at 15 mm Hg, minipores were rare.

The endothelial cells on both sides of Schlemm's canal contained pinocytotic and micropinocytotic vesicles. Fawcett (1965) considered that pinocytotic vesicles were formed at the surface of vessel endothelia by the folding over of a cytoplasmic flap (called a marginal fold) to enclose a fluid droplet within the cell. A few marginal folds were present at the lateral connections between some endothelial cells. Associated with the folds were pinosomes in various stages of formation. When completely enclosed within the cell cytoplasm, the pinosomes measured up to 0.2 μm in diameter (Figs 10.1 and 10.2).

Micropinocytotic vesicles were dispersed throughout the cell cytoplasm but were most prevalent at, or only a few Ångstroms from, the cell surface. There was a greater frequency of vesicles per unit length at the luminal than the basal surface of the canal endothelium, the ratio being approximately 3 to 1. Two distinct types of micropinosome were present, a smaller vesicle (600 to 800 Å in diameter) lined by a smooth membrane (Figs 10.2 and 10.4) and, seen only rarely, a larger coated vesicle (approximately 1,000 Å in diameter) with electron

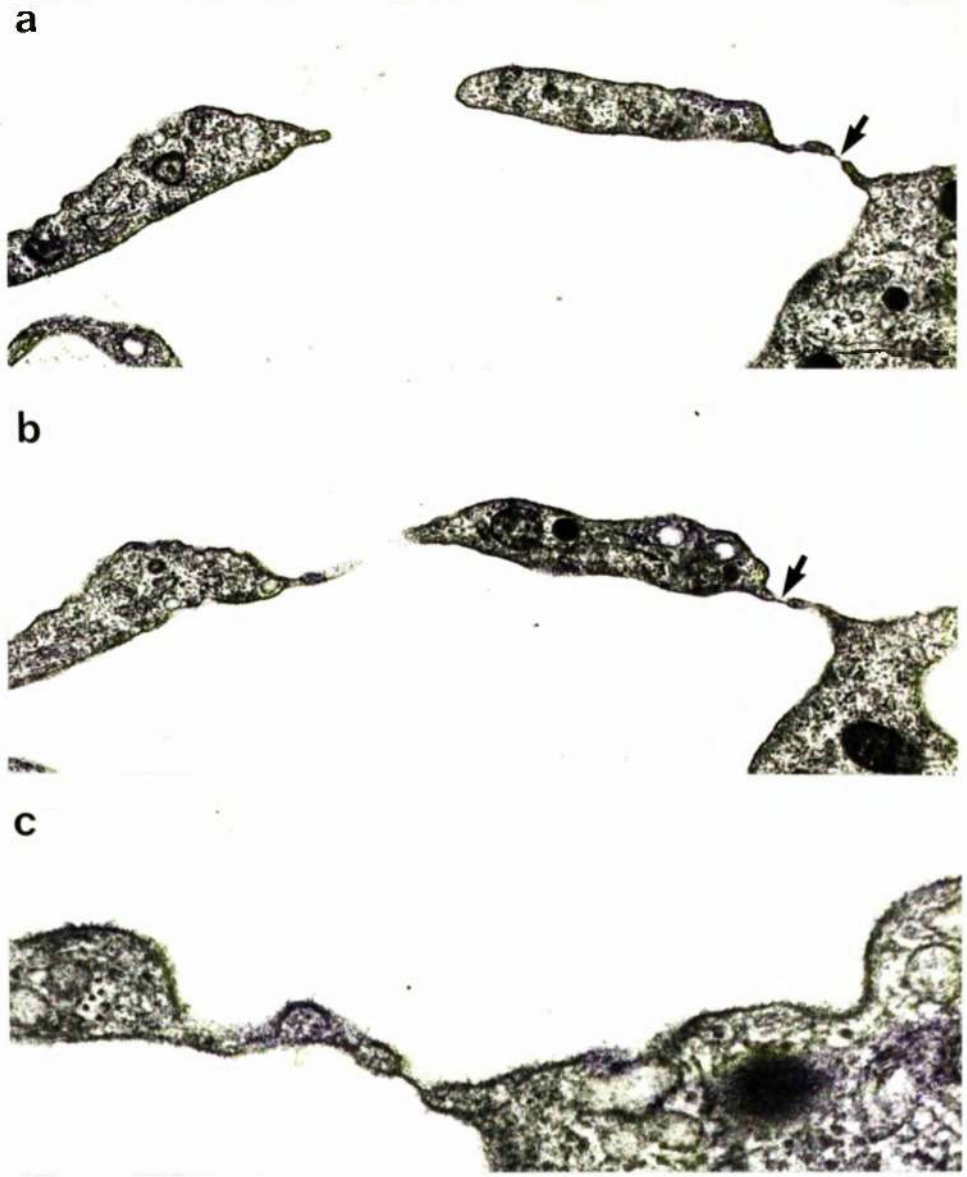

Fig.IO.5 a and b are two levels through a non-vacuolar transcellular channel. Minipores are indicated by arrows. The minipore in a) is shown at higher power in c). I5 mm Hg T.E.M. (a and b x29,000; c x73,000).

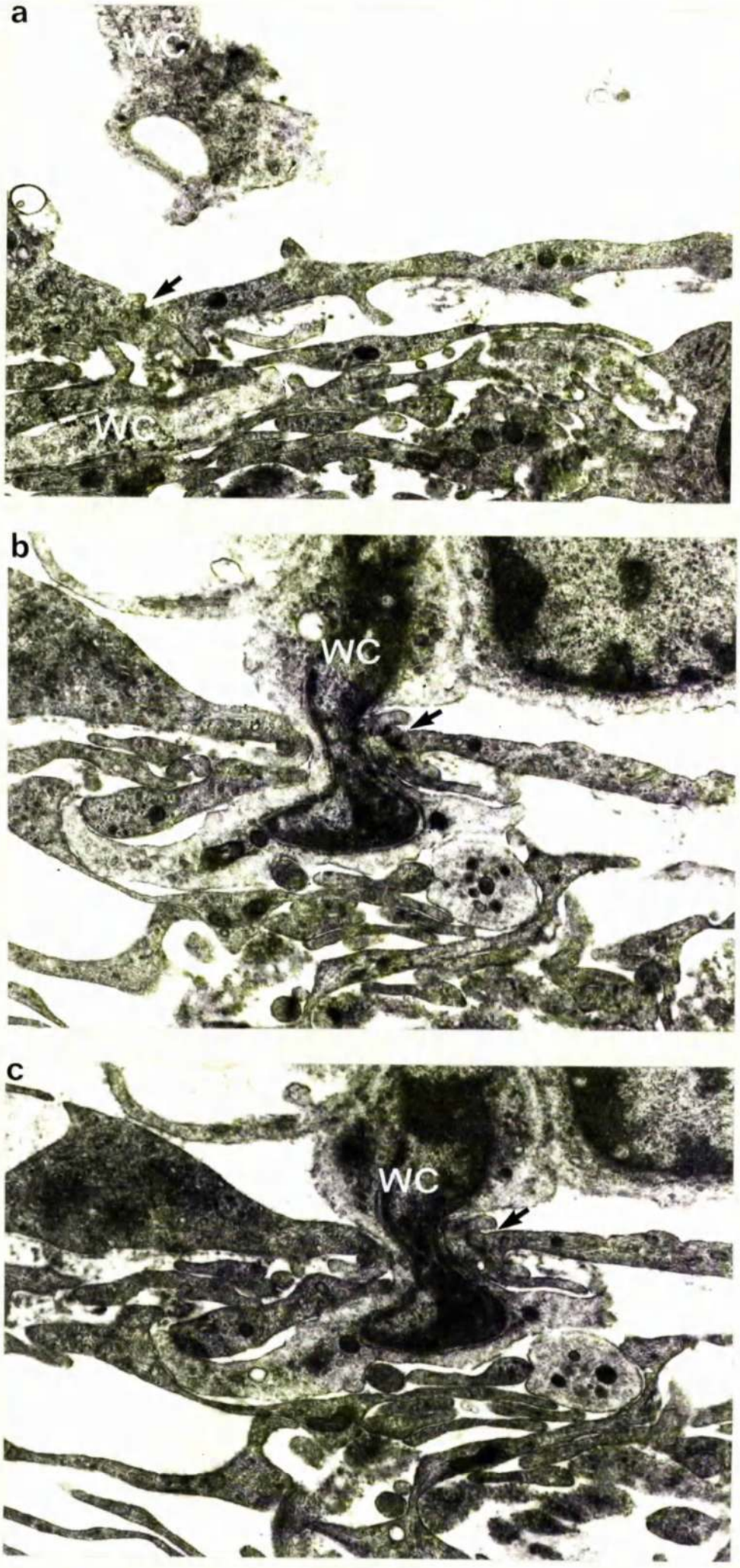
a
WC
WC
b
WC
c
WC

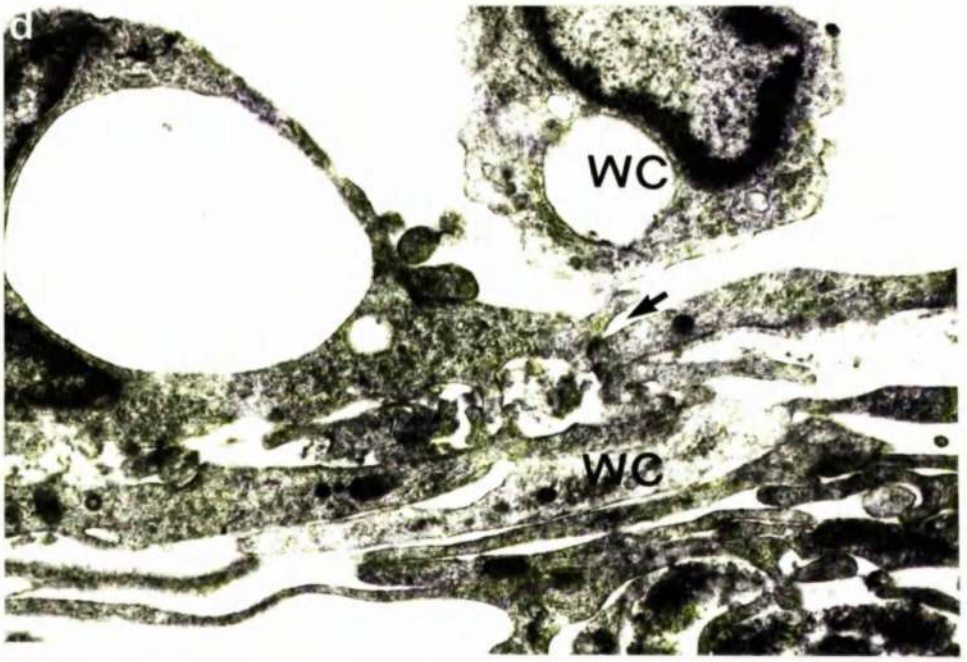

Fig.10.6 a to d show four levels through a non-vacuolar transcellular channel which contains a wandering cell (WC). The arrows indicate the intercellular cleft between adjoining endothelial cells. 15mm Hg, T.E.M. (x20,000).

opaque material on both surfaces of its limiting membrane (Fig. 10.3).

10.3.2 8 mm Hg

After close examination of the endothelium lining the trabecular aspect of Schlemm's canal, vacuolar transcellular channels, non-vacuolar openings and minipores could not be found. Giant vacuoles were sparse and poorly developed (by transmission electron microscopy the largest was only 4 μm in diameter) but invariably they were delineated by a single limiting membrane (Fig. 10.7). Fortuitous sections revealed the intimate association between the vacuolar membrane and the closely packed cytoplasmic microfilaments (Fig. 10.8). Although lumen pores were not identified, meshwork pores were shown to be present. The vacuolar meshwork pores were longer in the vertical axis and more cylindrical than their counterparts in the control (15 mm Hg) tissue (Figs 10.9 and 10.10). Ground substances from the underlying meshwork were in close association with the passageways and, in some examples, appeared to fill the pore lumen (Fig. 10.10).

The endothelium on both sides of Schlemm's canal contained more micropinosomes (both the smooth and coated forms) than at 15 mm Hg and pinocytotic folds were prominent at the cell margins. Much of the increase in micropinocytotic activity was associated with the apical surface of the cells, so that the disparity between apical and basal vesicle frequency (a ratio of approximately 8 to 1) was greater than in the control tissue (Fig. 10.11).

10.3.4 22 mm Hg

Minipores and intracellular non-vacuolar channels were identified more easily in the endothelium lining the trabecular aspect of Schlemm's canal than at lower pressures. They were, however, absent from the

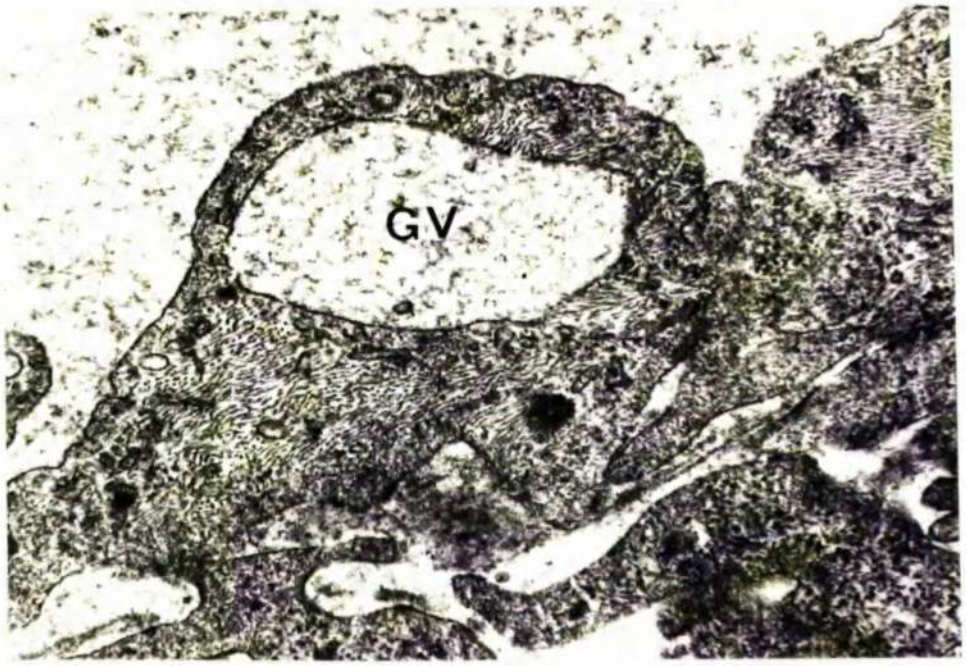

Fig.IO.7 A small giant vacuole (GV) at 8 mm Hg. T.E.M. (x35,000).

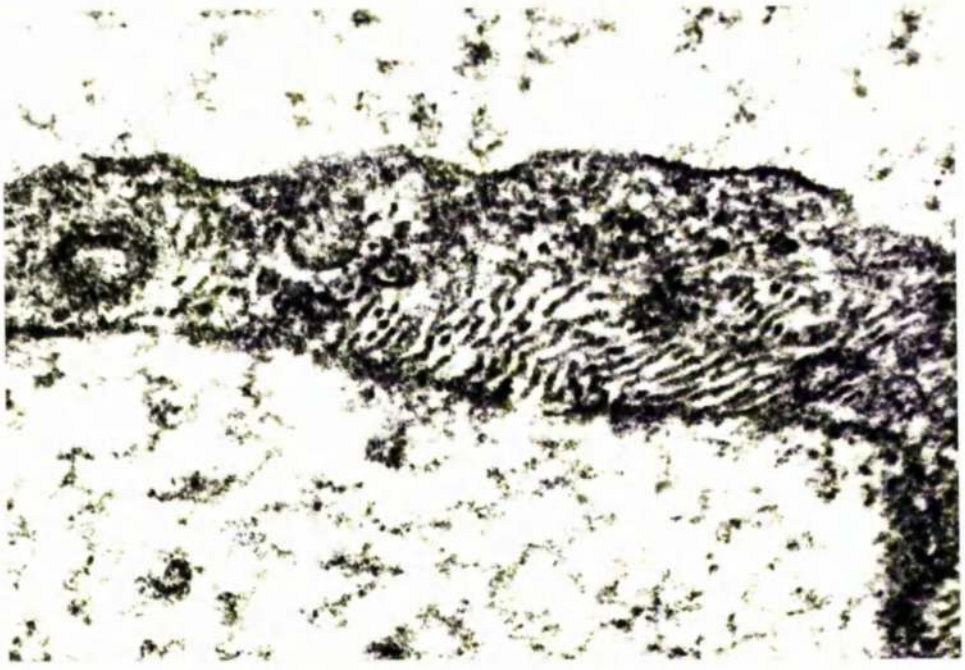

Fig.IO.8 A higher power of the giant vacuole shown in IO.7 to show the insertion of microfilaments into the vacuolar membrane. T.E.M. (xI05,000).

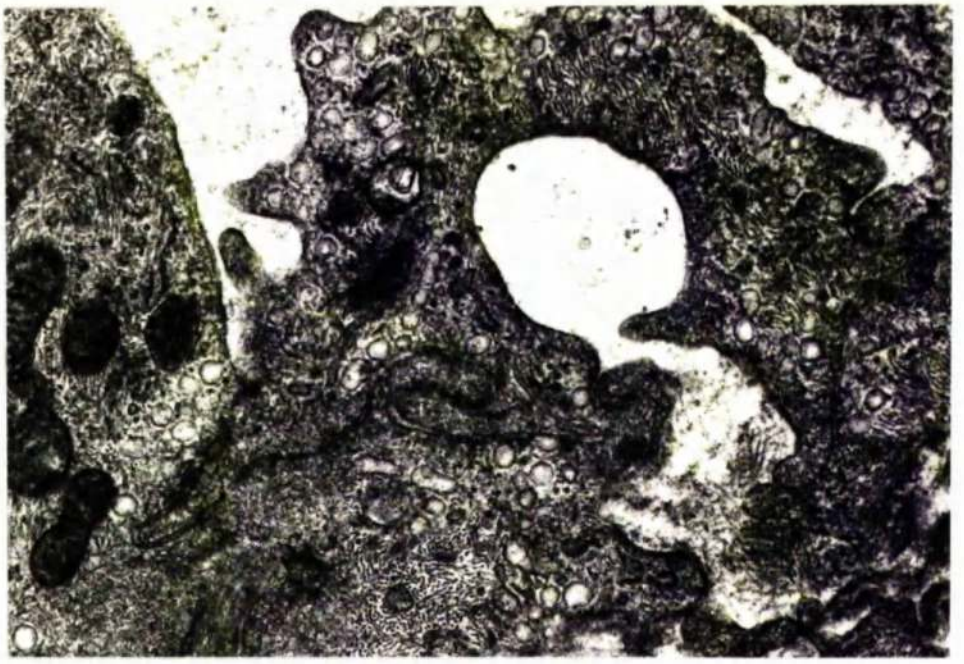

Fig.IO.9 A giant vacuole at 8 mm Hg with a typical narrow but tortuous meshwork opening. T.E.M. (x33,000).

Fig.IO.IO A giant vacuole at 8 mm Hg with a meshwork·pore plugged with extracellular material. T.E.M. (x44,000).

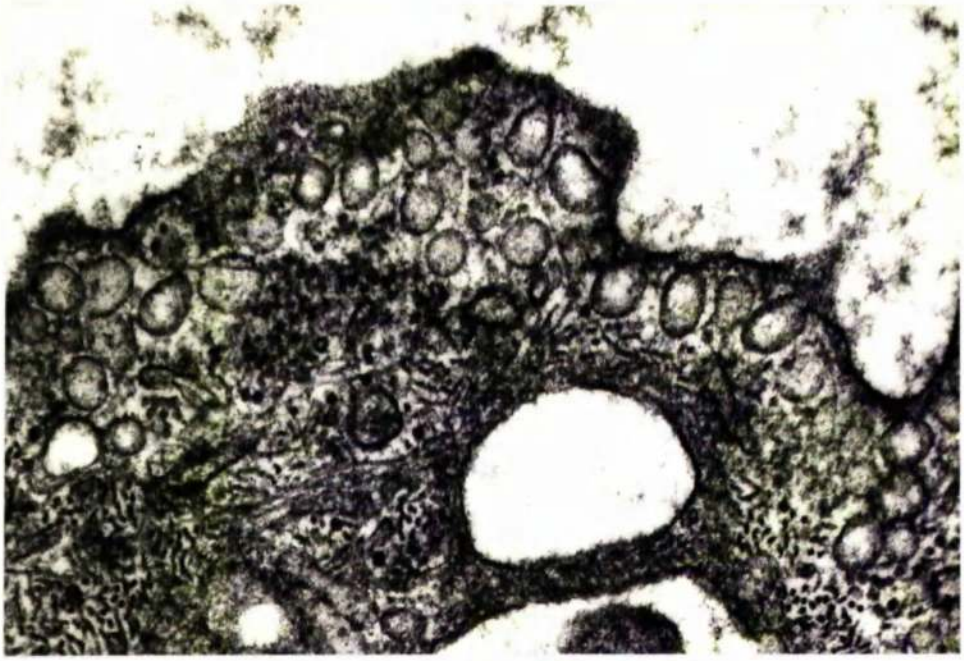

Fig.IO.II Part of an endothelial cell at 8 mm Hg in which micropinocytosis is particularly prolific at the cell's luminal surface. T.E.M. (x76,000).

endothelium lining the corneoscleral aspect of the canal.

The canal's trabecular endothelium was distinguished by the presence of numerous giant vacuoles (Fig. 10.12). Particularly large numbers of vacuoles were associated with the canal endothelium overlying focal dilatations in the endothelial meshwork (Fig. 10.13). The profusion of vacuolar structures afforded the opportunity to study greater numbers more easily by serial reconstruction. As at 15 mm Hg the bulk of the population had meshwork pores only, but a small proportion existed as vacuolar transcellular channels (Figs 10.14 and 10.15). Some small vacuoles had lumen pores but no meshwork pores and thus they represented luminal invaginations (Fig. 10.16). Luminal invaginations, like vacuolar transcellular channels, made up a small proportion of the total vacuole population.

10.3.5 30 mm Hg

At 30 mm Hg, in common with all other pressures, minipores and intracellular non-vacuolar openings were absent from the corneoscleral aspect of Schlemm's canal. Both structures were, however, prominent in the endothelium on the trabecular aspect of the canal.

The vacuoles, which abounded in the trabecular wall endothelium, were membrane lined and were enclosed by the cytoplasm of one endothelial cell thus they were essentially similar to the vacuoles described at lower pressures (Fig. 10.17). The vacuoles were often very large and some endothelial cells contained multilocular structures with intercommunicating compartments. Many vacuoles were associated with the endothelium lining the septae and an occasional vacuole was present on the corneoscleral aspect of the canal.

Giant vacuoles which had meshwork pores but were without lumen pores comprised the bulk of the population. Although vacuolar

Fig.IO.I2 Part of the endothelium lining the trabecular aspect of Schlemm's canal (SC) at 22 mm Hg in which giant vacuoles are a prominent feature of many of the cells. A meshwork pore is indicated by an arrow. T.E.M. (x2,800).

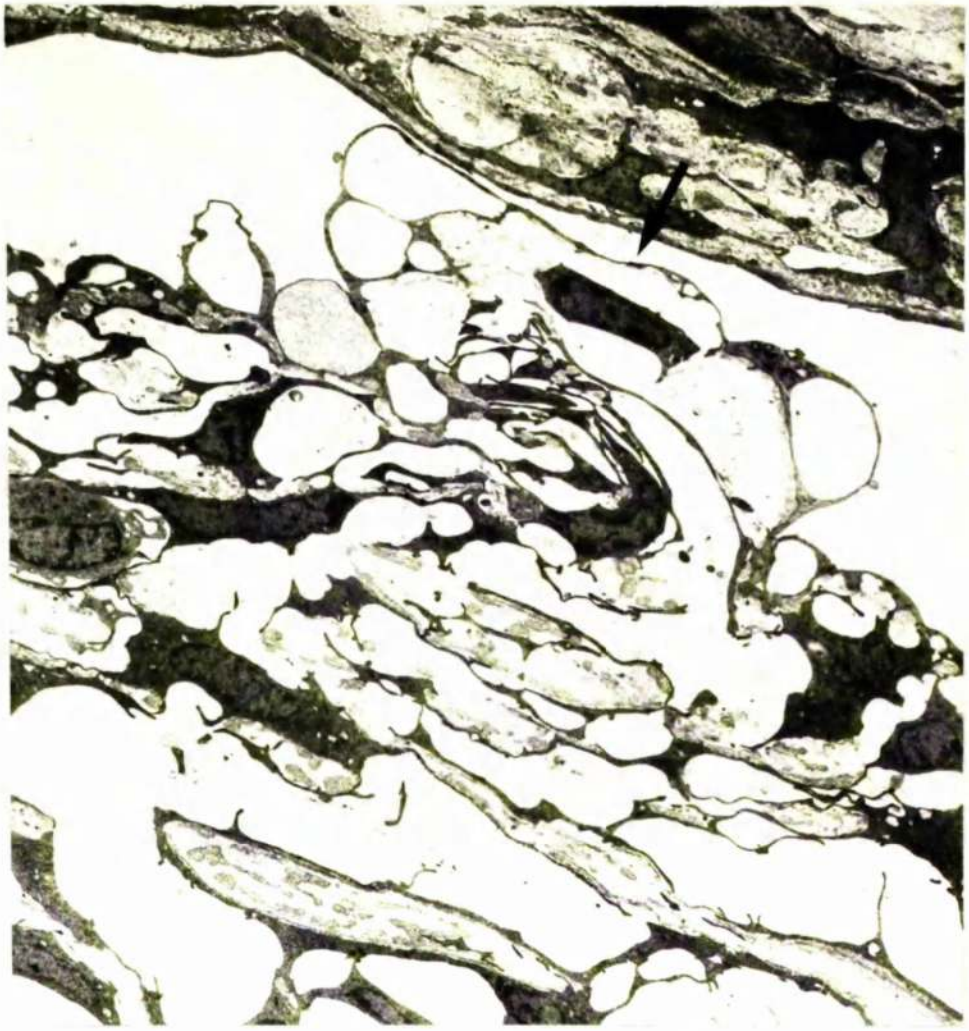

Fig.IO.I3 A prominent dilatation of the endothelial meshwork (arrow) at 22 mm Hg. Giant vacuoles are conspicuous in the overlying endothelial monolayer. T.E.M. (x3,000).

a

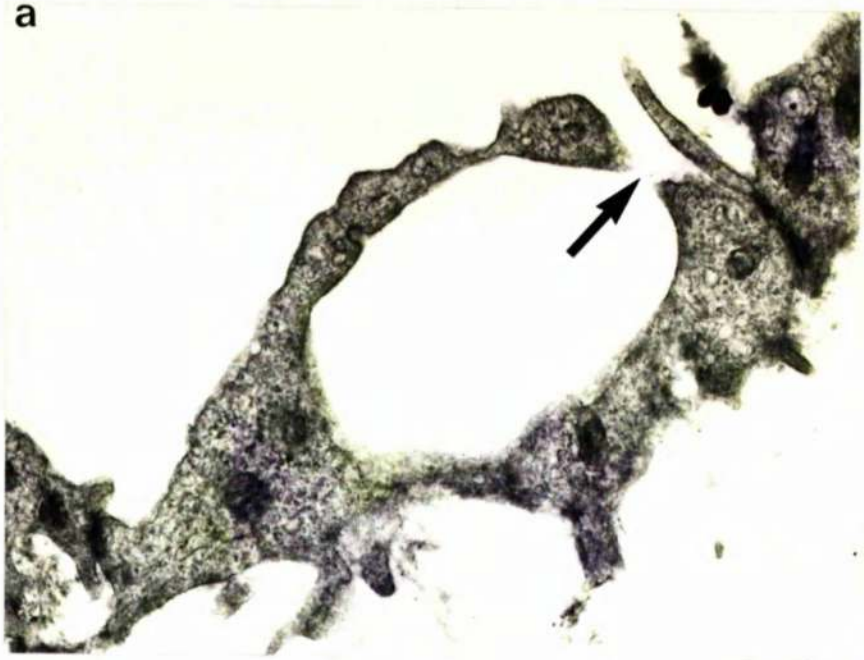

b

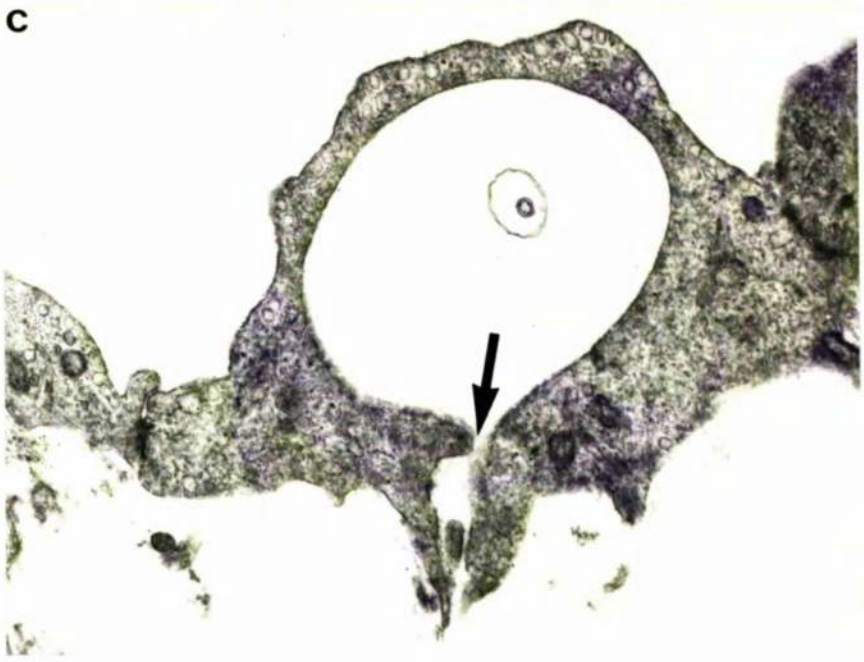

Fig.IO.I4a - c Three levels of section through a giant vacuole in the endothelium lining the trabecular wall of Schlemm's canal at 22 mm Hg. The vacuole constitutes a transcellular channel having both a canal and a meshwork opening. The canal opening in a) and the meshwork opening in c) are indicated by arrows. T.E.M. (x25,000).

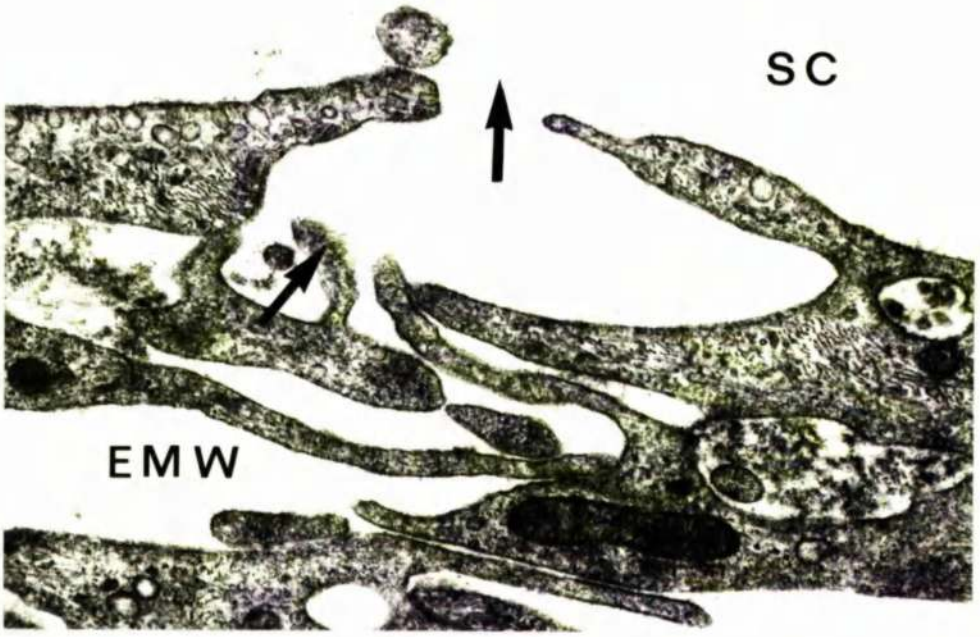

Fig.IO.I5 A vacuolar transcellular channel (arrows) at 22 mm Hg which makes a direct communication between the endothelial meshwork(EMW) and Schlemm's canal (SC). T.E.M. (x2I,000).

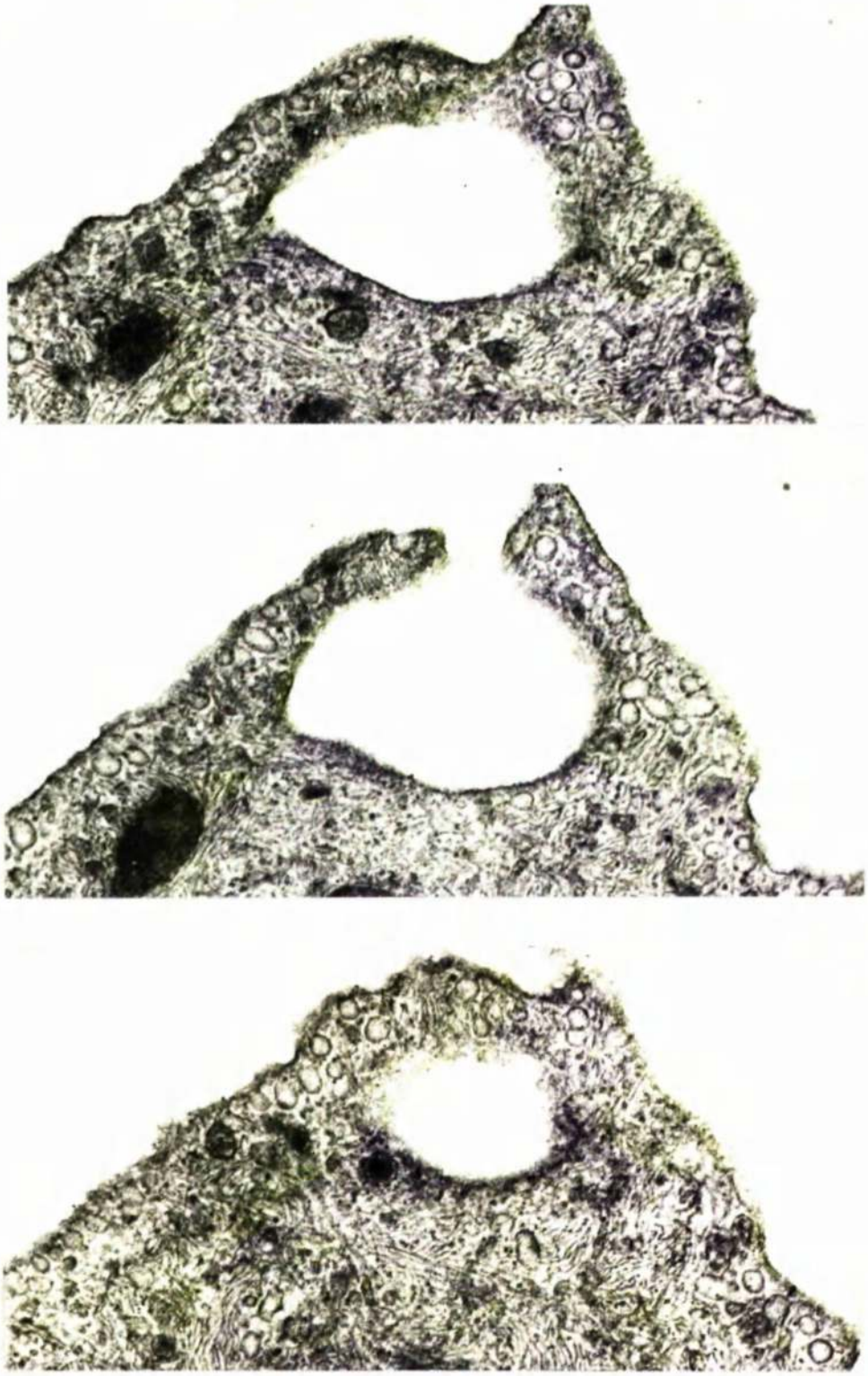

Fig.IO.I6 Three levels of section through a vacuole at 22 mm Hg which has a lumen pore but no meshwork pore. T.E.M. (x40,000).

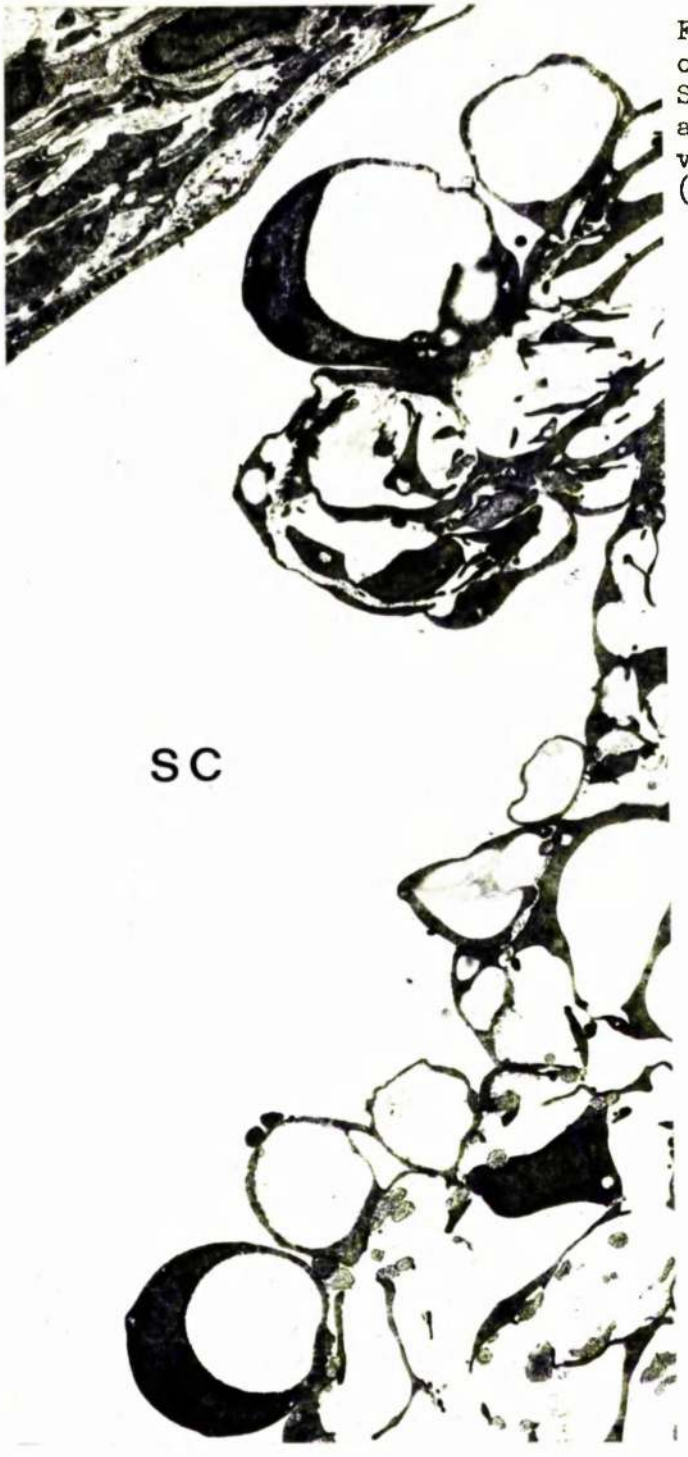

Fig.IO.I7 The endothelium on the trabecular aspect of Schlemm's canal (SC) contair a profusion of giant vacuoles at 30 mm Hg. T.E.M. (x4,000).

transcellular channels and luminal invaginations represented a small proportion of the population they were found more frequently than at lower pressures because of the overall increase in vacuolar incidence.

The meshwork pores were broad, but short in the vertical plane. Frequently more than one pore occupied the shell of a single giant vacuole. The pores were usually free from extracellular materials and cell processes, which were so closely associated with the vacuolar meshwork openings at lower pressures, were absent (Fig. 10.18). The lumen pores were smaller than meshwork pores and more than one lumen pore to a vacuole was a rarity.

On both sides of Schlemm's canal the endothelial cells had a few coated and uncoated micropinosomes. The disparity between vesicle incidence at the apical and basal surfaces was less pronounced than it had been at lower pressures (the ratio was down to only 2 to 1). Pinocytotic vesicles and marginal folds were difficult to find.

10.3.6 0 mm Hg

Giant vacuoles, non-vacuolar channels and minipores were absent from all the samples of tissue examined at this pressure (Fig. 10.19).

The endothelium lining the canal (including the corneoscleral aspect) exhibited prolific micropinocytotic activity. The coated and uncoated micropinosomes were most prominent immediately beneath the apical surface of the endothelium, to the extent that the ratio of apical to basal vesicle incidence approached 10 to 1 (Figs 10.20 and 10.21b). The coated vesicles were larger (up to 1,500 Å in diameter) and of more complex ultrastructure than those previously described. By conventional staining, the vesicles had a thin but regular luminal coat. The cytoplasmic coat was thicker and consisted

Fig.IO.I8 A giant vacuole with a meshwork pore at 30 mm Hg. T.E.M. (x22,000).

Fig.IO.I9 At O mm Hg the endothelium on the trabecular aspect of Schlemm's canal is attenuated and contains no giant vacuoles. Only the occasional perinuclear bulge (arrows) protrudes into Schlemm's canal. T.E.M. (x5,000).

Fig.IO.20 At O mm Hg the endothelial cells in the monolayer on the trabecular aspect of Schlemm's canal have abundant micropinosomes (arrow) beneath their apical surfaces. T.E.M. (x55,000).

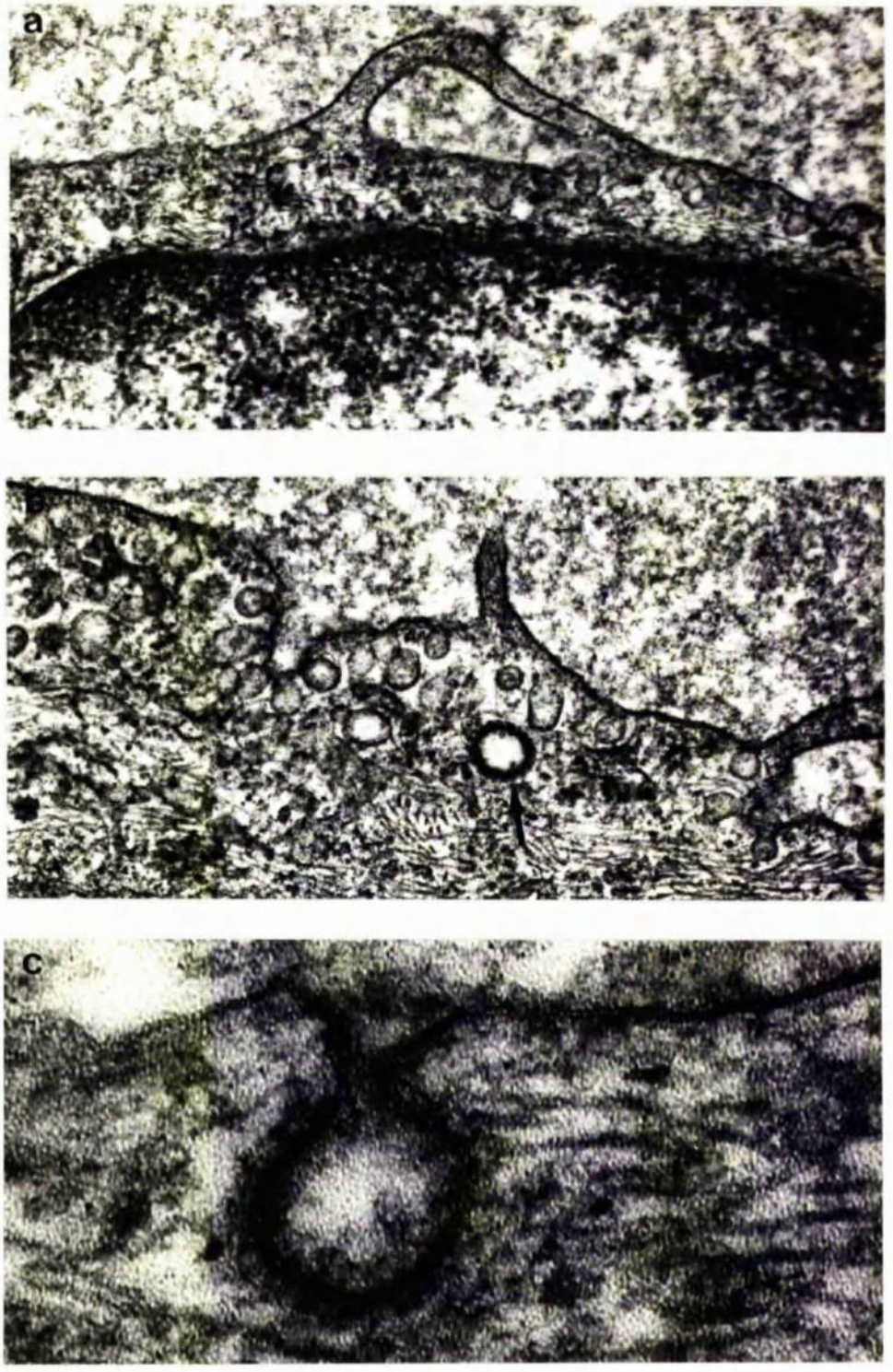

Fig.IO.2I Portions of the apical surface of endothelial cells lining the trabecular wall of Schlemm's canal at 0 mm Hg to show a) a pinosome in a perinuclear position, b) a coated vesicle (arrow) and smooth micropinosomes and c) a coated vesicle stained "en bloc" with uranyl acid and no section staining. T.E.M. (a x32,000; b x64,000; c x220,000).

of many osmiophilic spoke-like strands which radiated out from the limiting membrane to give the vesicle a fuzzy appearance (Fig. 10.21b). Uranyl acetate "en bloc" staining emphasised the distinction between the luminal and cytoplasmic coats by showing that they were adherent to separate leaflets of the trilaminar limiting membrane. The material within the coated vesicles at the cell surface was similar to that in the lumen of Schlemm's canal (Fig. 10.21c).

At 0 mm Hg, cytoplasmic processes from the cell surfaces were not restricted to the marginal zones but could be found elsewhere on the cell surface (Fig. 10.21a). Therefore the pinocytotic vesicles were more evenly distributed throughout the endothelial cells at this pressure.

10.3.7 50 mm Hg

Where Schlemm's canal was patent, usually in the posterior portion, large giant vacuoles with thin cytoplasmic walls were much in evidence. The vacuoles contained many openings (Fig. 10.22) which on close examination were seen to be ragged deficits rather than regular membrane-lined pores. There were many openings through the canal's trabecular endothelial monolayer in this region. Again the openings were not pores but were mechanical separations between adjacent cells.

At the narrowed anterior portion of Schlemm's canal the attenuated endothelium on the canal's trabecular side contained minipores and a few distorted vacuoles.

A general feature of all the endothelial cells was the absence of pinosomes, the virtual absence of coated micropinosomes and the scarcity of uncoated micropinosomes (Fig. 10.23). Of the micropinosomes present, a few were scattered throughout the cell cytoplasm and the rest were at or immediately beneath the cell surface. The

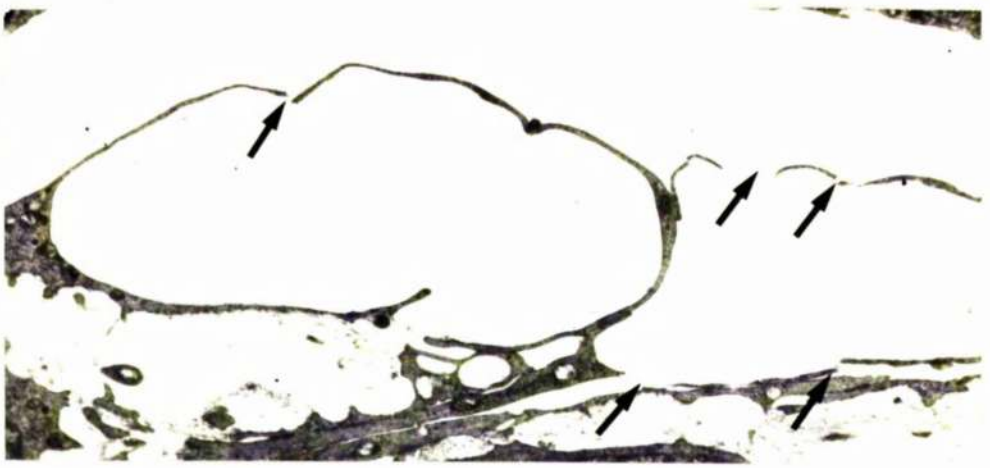

Fig.IO.22 Large giant vacuoles at 50 mm Hg with deficits (arrows) rather than pores in their shells.T.E.M. (x6,000).

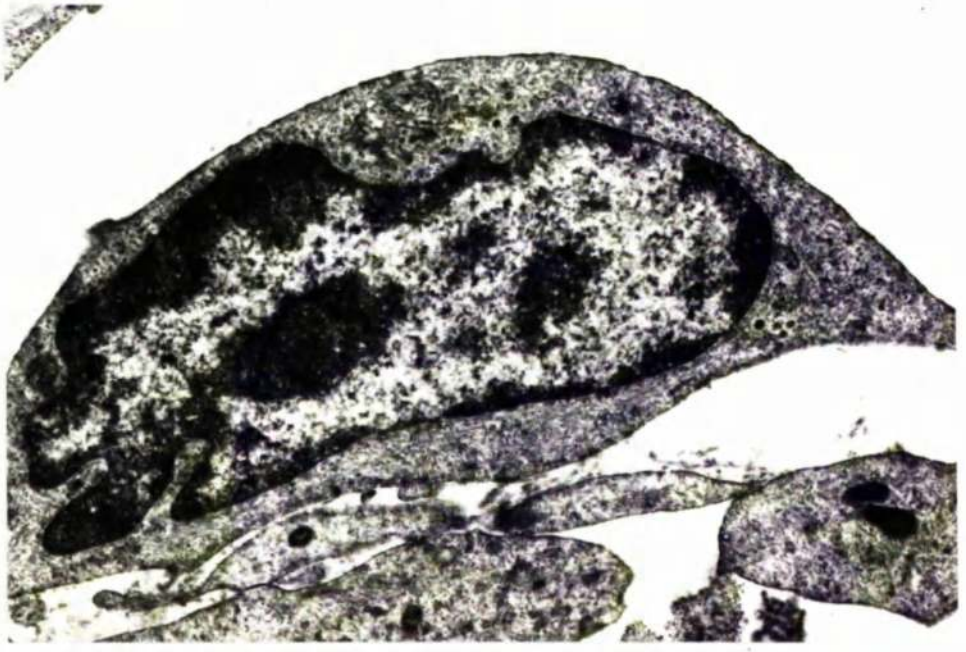

Fig.IO.23 A cell from the endothelium which lines the trabecular wall of Schlemm's canal. Micropinosomes are infrequent. T.E.M. (x25,000).

micropinosomes at the apical surface were of similar numbers to those at the basal surface.

10.4 Serial analysis

All the data from the serial investigation of vacuoles, their pores and non-vacuolar pores is listed in Fig. 10.24. The samples presented were not representative either in size or numbers of the populations at the various pressure levels. This was because a sequential series through a small vacuole was more easily obtained than through a large structure and disproportionately larger amounts of tissue had to be screened at low than high pressures to obtain worthwhile samples.

The data did show, however, that the vacuolar meshwork pore occupied a larger proportion of the vacuolar shell with increase in pressure. At 15 mm Hg the ratio of meshwork pore to vacuole maximum width was 1 to 4 whereas at 30 mm Hg the ratio had decreased to almost 1 to 2. A similar trend existed in the lumen pore/vacuole relationship because at 15 mm Hg the ratio was about 1 to 10 and was reduced to 1 to 5 at 30 mm Hg. From the available information it could be deduced that meshwork pores were larger than lumen pores, irrespective of pressure, and that non-vacuolar pore widths exhibited no pressure relationship.

In an attempt to relate individual vacuole width to pore width, the maximum width of the meshwork and lumen pores was plotted against the maximum width of their respective vacuoles. At each level within the range 8 to 30 mm Hg the relationship between meshwork pore width and vacuole width was linear ($P < 0.001$). A representative scatter diagram (22 mm Hg) is shown in Fig. 10.25a. Each regression line had a positive slope (Fig. 10.26) and the gradient of the line (b)

I.O.P mm.Hg.	MAXIMUM VACUOLE WIDTH µm	MAXIMUM MESHWORK PORE WIDTH µm	NO.	MAXIMUM VACUOLE WIDTH µm	MAXIMUM LUMEN PORE WIDTH µm	NO.
30	3.9 ± 2.3	1.7 ± 1.0	96	4.5 ± 2.6	0.9 ± 0.6	40
22	3.1 ± 1.7	0.9 ± 0.6	57	3.5 ± 2.1	0.5 ± 0.3	28
15	2.0 ± 1.3	0.5 ± 0.5	57	1.9 ± 1.1	0.2 ± 0.1	12
8	2.0 ± 1.0	0.3 ± 0.2	9	*	*	*

* No Data Available

Fig.10.24 Pore and vacuole sizes at the various pressure levels between 8 and 30 mm Hg.

a

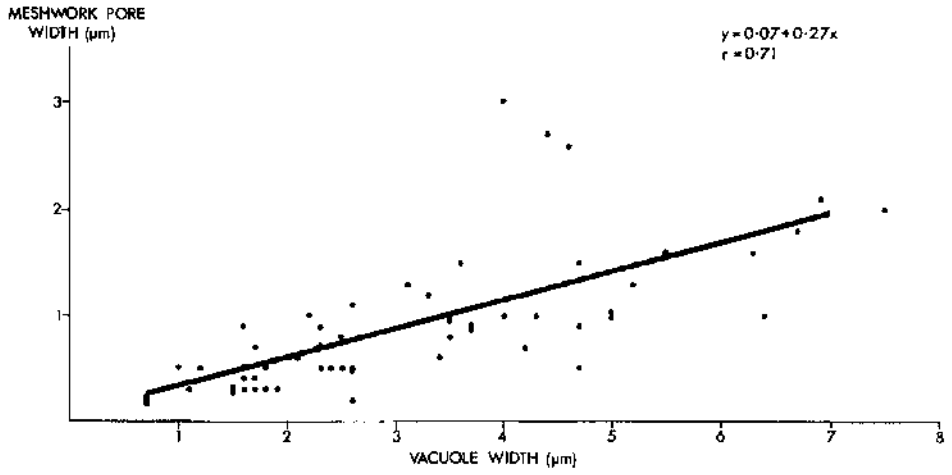

b

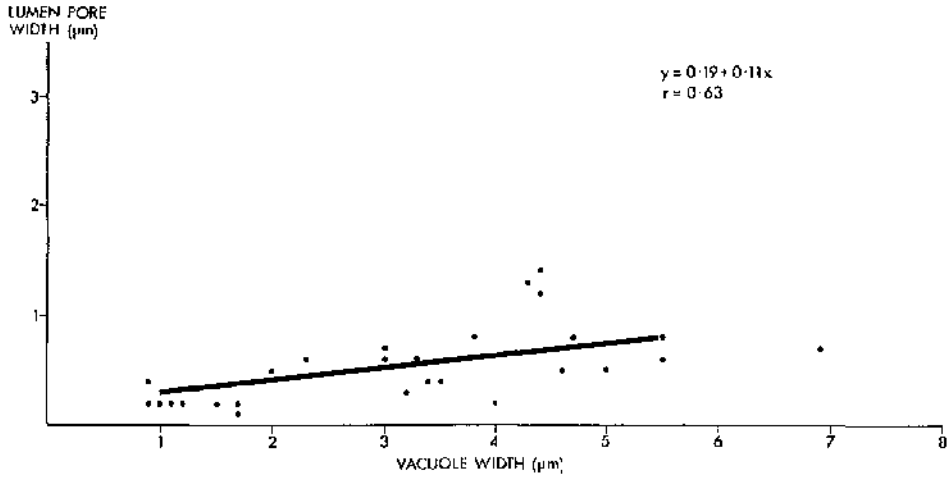

Fig.IO.25 Correlations between a) meshwork pore maximum width, b) lumen pore maximum width and the maximum widths of the appropriate vacuoles at 22 mm Hg.

VACUOLE MAXIMUM WIDTH VS MESHWORK PORE MAXIMUM WIDTH				VACUOLE MAXIMUM WIDTH VS LUMEN PORE MAXIMUM WIDTH			
I.O.P. (mm Hg)	NO. OF VACUOLES SERIAL SECTIONED	THE SLOPE OF THE LINE (b)	CORRELATION COEFFICIENT (r)	I.O.P. (mm Hg)	NO. OF VACUOLES SERIAL SECTIONED	THE SLOPE OF THE LINE (b)	CORRELATION COEFFICIENT (r)
30	96	0.36	0.81	30	40	0.10	0.44
22	57	0.27	0.71	22	28	0.11	0.63
15	57	0.26	0.71	15	12	0.04	0.32
8	9	0.15	0.89	8	0	*	*

* No Data Available

Fig.IO.26 Correlations between meshwork pores, lumen pores and their appropriate vacuoles at the various pressure levels between 8 and 30 mm Hg.

increased with increasing pressure.

The increase in lumen pore width was significant at 30 mm Hg ($P < 0.01$) and 22 mm Hg ($P < 0.001$) (Fig. 10.25b), but at 15 mm Hg, perhaps because of the limited sample, a relationship could not be established. The slope of the regression lines (b) did not increase with pressure rise (Fig. 10.26).

10.5 The quantitative investigation of single sections

For the purposes of quantitation it was impractical to make distinction between what may have been either pinocytotic vesicles or small giant vacuoles, therefore vesicular structures smaller than 0.3 μm in diameter were excluded from the vacuole count. Also no distinction could be made between non-vacuolar transcellular channels and separations between neighbouring endothelial cells in this part of the investigation.

Certain structures in the endothelial monolayer superficially resembled giant vacuoles and could have been a source of error in previous light microscopic quantitation (Chapter 8). By transmission electron microscopy three types of structure were identified which were sufficiently similar that they may have been mistaken for giant vacuoles at the light microscopic level.

The three types of structure were called pseudovacuoles and referred to as types a, b and c.

Pseudovacuoles type a, were regions of dilatation of the intercellular cleft which resembled small giant vacuoles but which had junctional modifications above and usually below the dilatation (Fig. 10.27).

Pseudovacuoles type b, were regions formed by zones of apposition between neighbouring endothelial cells and downward projections from

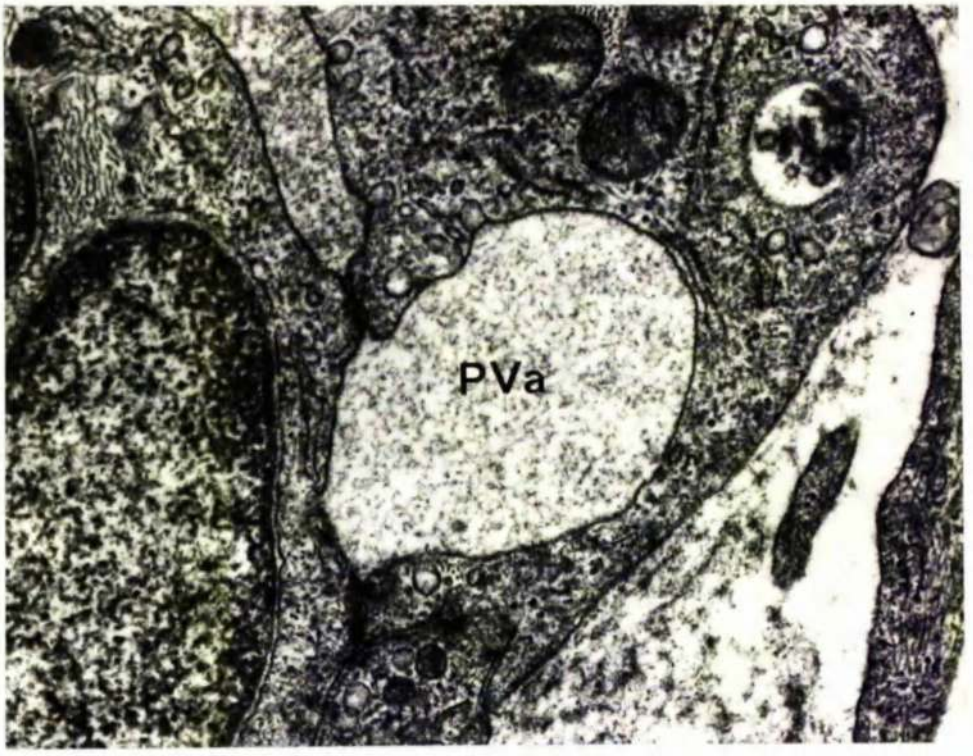

Fig.IO.27 A pseudovacuole type a (PVa) in the endothelium lining the trabecular aspect of Schlemm's canal at 8 mm Hg. The pseudovacuole represents a dilatation of the intercellular cleft. T.E.M. (x45,000).

each of the adjacent cells. They resembled vacuoles with meshwork pores (Fig. 10.28).

Pseudovacuoles type c, were structures which resembled relatively large giant vacuoles with meshwork pores but were, instead, bulges of the endothelial monolayer involving several endothelial cells (Fig. 10.29).

The total counts of the specified structures under investigation from each eye, at the various pressure levels, are shown in Fig. 10.30. When the vacuole counts were expressed as an incidence per 100 nuclei the vacuoles were shown to be approximately 8 times as frequent at 30 than at 8 mm Hg, and there were similar vacuole incidences at 15 and 50 mm Hg (Fig. 10.31). Vacuoles with meshwork pores increased throughout the pressure range 8 to 30 mm Hg, but decreased at 50 mm Hg to a value which approximated that at 22 mm Hg. On the other hand, vacuoles with lumen pores were not found at 8 mm Hg, but thereafter became progressively more numerous as the pressure was increased (Fig. 10.32). Thus at 30 mm Hg vacuoles with lumen pores were about 8 times as frequent than at 15 mm Hg.

Comparison of the percentage incidence of vacuoles with meshwork pores and those with lumen pores in the total vacuole populations demonstrated a distinct increase in both types over the pressure range. At each pressure level, it was evident that the percentage incidence of vacuoles with meshwork pores was higher than that for vacuoles with lumen pores (Fig. 10.33).

Pseudovacuoles were infrequent at all pressures. Pseudovacuoles type c were not found at 0 and 8 mm Hg, but were present at the higher pressures whereas the pseudovacuole type a and b showed no pressure relationship (Fig. 10.34a). When the total pseudovacuole count was expressed as a percentage of the total giant vacuole plus pseudovacuole

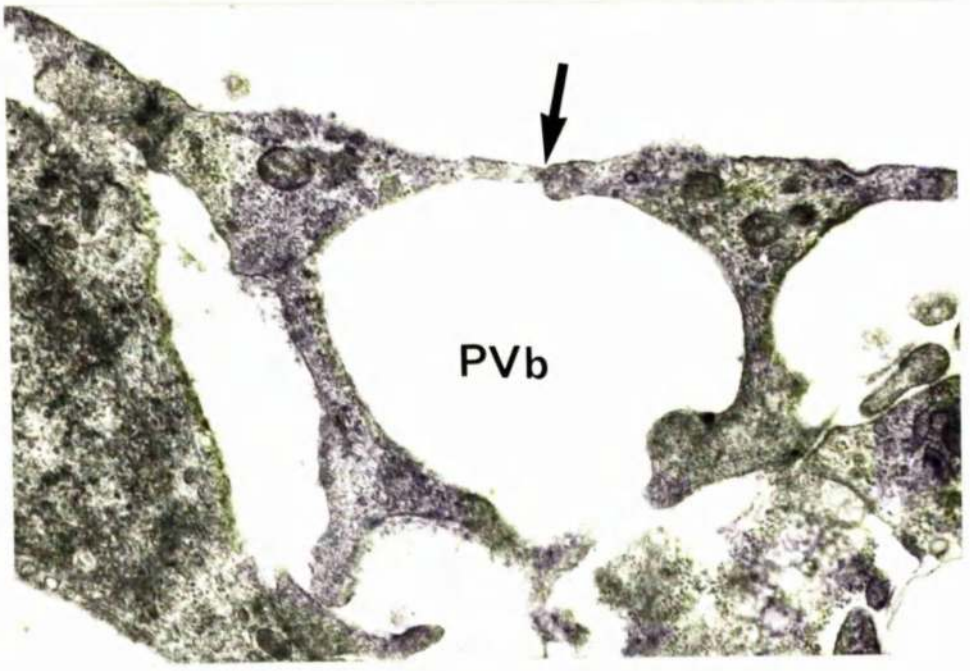

Fig.IO.28 A pseudovacuole type b (PVb) in the endothelium lining the trabecular aspect of Schlemm's canal at 30 mm Hg. The arrow indicates the region of contact between adjacent cells. T.E.M. (x27,000).

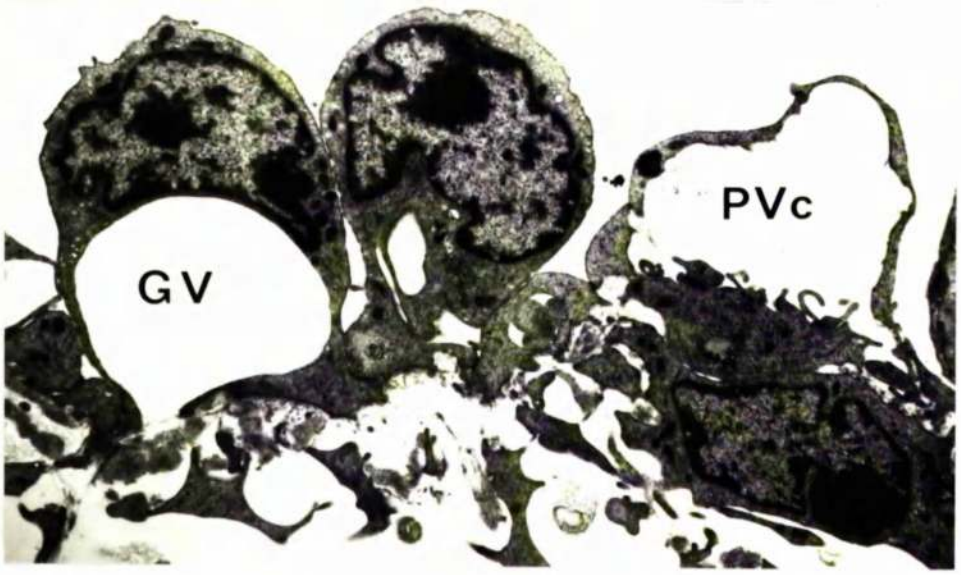

Fig.IO.29 A pseudovacuole type c (PVc) in the endothelium lining the trabecular aspect of Schlemm's canal at 22 mm Hg. It involves several endothelial cells and attachments are indicated by arrows. The pseudovacuole can be compared with a giant vacuole (GV) which has a meshwork pore. T.E.M. (x20,000).

Animal No.	I.O.P. (mm.Hg.)	Nuclei	Giant Vacuoles	Meshwork Pores	Lumen Pores	Pseudo Vacuoles Type C	Pseudo Vacuoles Types a & b	Non Vacuolar Openings	Mini Pores
81/73	50	134	130	58	26	4	1	73	15
140/73	50	144	196	57	23	9	6	27	11
141/73	50	199	149	83	26	13	6	44	16
58/72	30	171	384	135	21	8	4	18	7
119/72	30	182	390	151	28	7	6	16	9
125/72	30	167	372	144	18	8	8	13	7
50/73	22	144	241	56	8	8	4	7	6
51/73	22	150	297	94	11	11	6	7	8
52/73	22	194	267	68	8	5	3	5	4
58/72	15	223	191	32	3	4	4	6	2
119/72	15	130	135	23	4	2	2	2	2
125/72	15	165	149	31	0	0	2	4	1
50/73	15	147	123	20	1	0	2	2	2
51/73	15	156	137	32	3	0	4	0	1
52/73	15	121	156	28	4	1	3	4	4
74/73	15	167	128	24	1	3	4	1	1
75/73	15	157	172	28	2	3	6	2	2
76/73	15	172	170	30	4	1	6	5	2
74/73	8	141	53	7	0	0	5	0	0
75/73	8	162	20	1	0	0	5	0	0
76/73	8	189	64	9	0	0	7	0	0
81/73	0	144	0	0	0	0	3	0	0
140/73	0	126	0	0	0	0	2	0	0
141/73	0	112	0	0	0	0	2	0	0

Fig.10.30 Total counts of the various structures in the endothelium lining the trabecular aspect of Schlemm's canal for each eye at the various pressures under investigation.

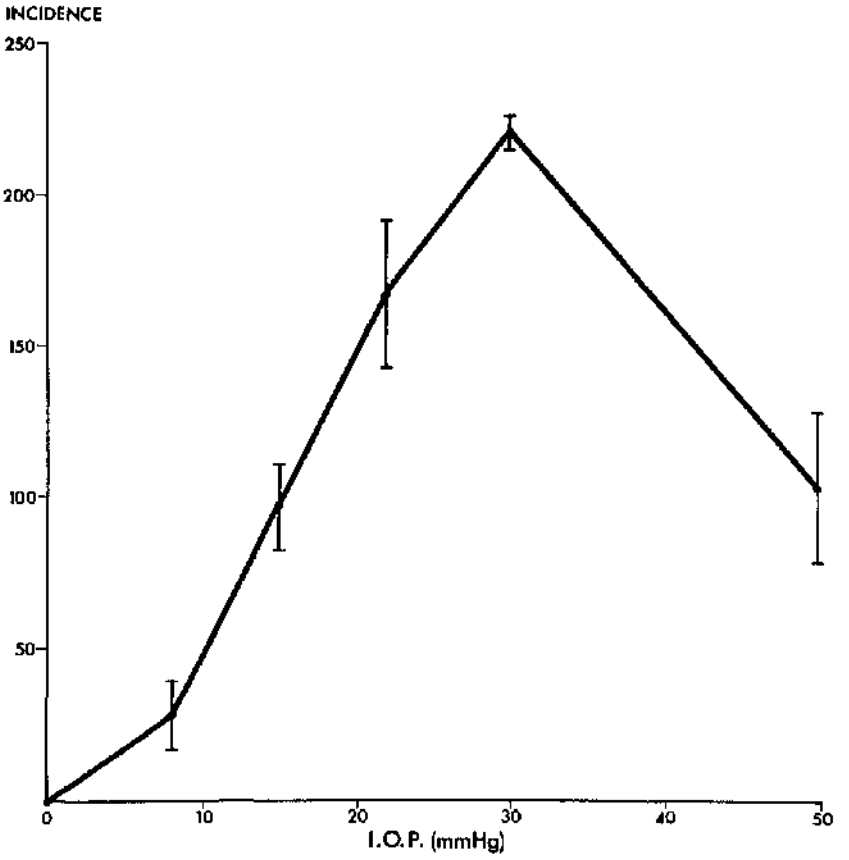

Fig.IO.3I The incidence of giant vacuoles per I00 nuclei counted at each of the various pressure levels.

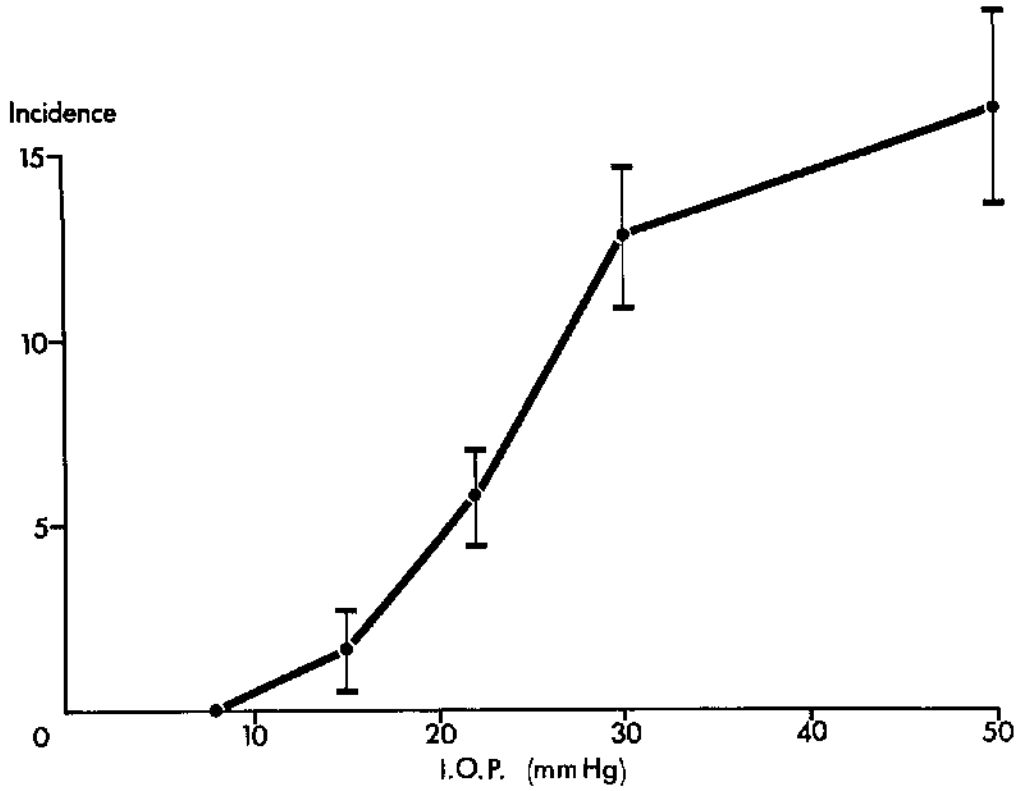

Fig.IO.32 The incidence of vacuoles with lumen pores per IOO nuclei counted at the various pressure levels.

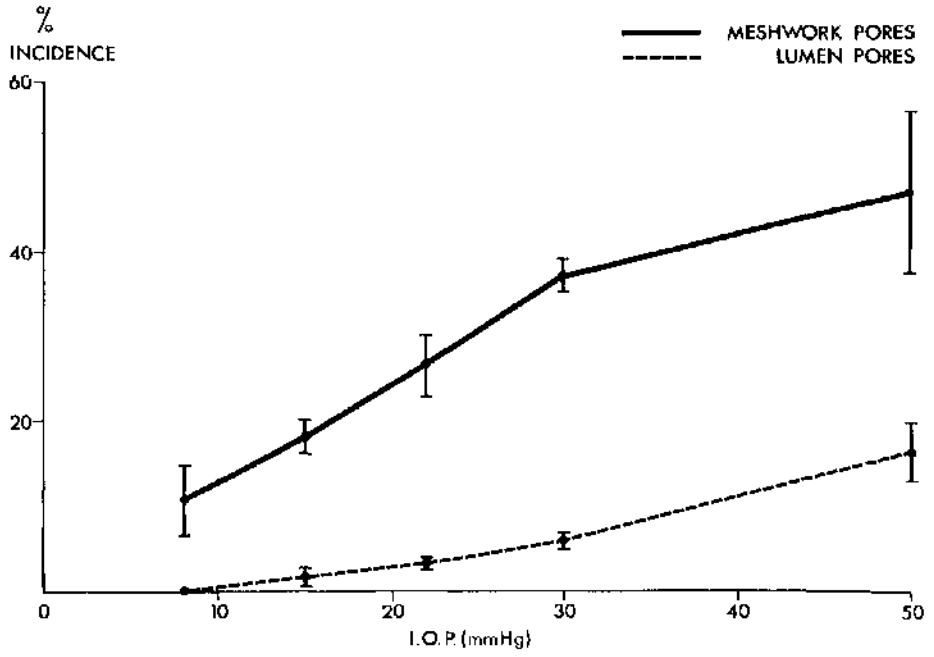

Fig.IO.33 Vacuole pore frequency in the total vacuole sample from each pressure level.

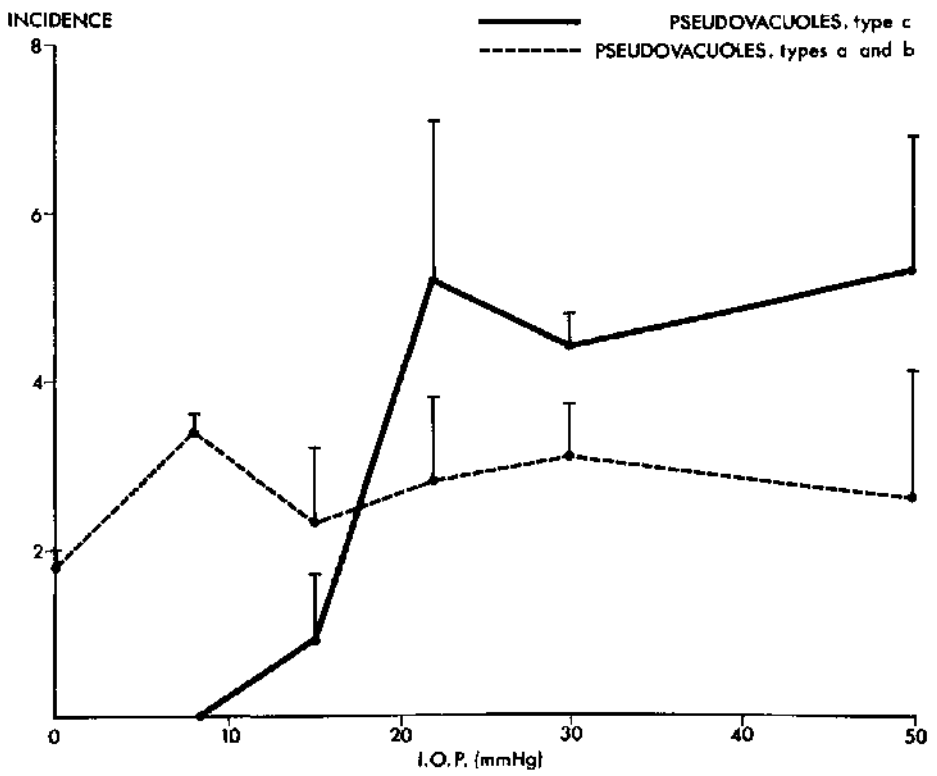

Fig.IO.34a The pseudovacuole incidence per IOO nuclei counted at each pressure level.

count it could be seen that pseudovacuoles were a much more significant factor at low than high pressures (Fig. 10.34b).

Non-vacuolar openings and minipores were absent at 0 and 8 mm Hg, they were identified at 15 mm Hg and, thereafter, their frequency increased at each pressure level to the highest pressure in the series. Of particular interest was the sharp rise in the incidence of non-vacuolar openings from 30 to 50 mm Hg and the large standard deviation about the mean value at 50 mm Hg (Fig. 10.35).

10.6 Discussion

The study of the fine structure of the endothelium lining Schlemm's canal, at the various intraocular pressure levels, revealed that interesting pressure related changes occurred to the giant vacuoles, non-vacuolar openings, minipores, pinosomes and micropinosomes all of which, at one time or another, have been proposed as mechanisms for the transfer of aqueous humour across the endothelium on the canal's trabecular aspect.

10.6.1 Giant vacuoles

By comparison with the light microscopic analysis (Chapter 8), the amount of tissue sampled for the transmission electron microscopic quantitative study was small. On the other hand, giant vacuoles could be identified with more precision, so that the present quantitation provided data which both supported and augmented previous light microscopic findings. It was apparent that the frequency of what were considered to be "true" giant vacuoles at the various pressure levels closely approximated that found in the light microscopic study. Giant vacuoles were absent at 0 mm Hg, their incidence increased progressively over the range 8 to 30 mm Hg and, thereafter, decreased

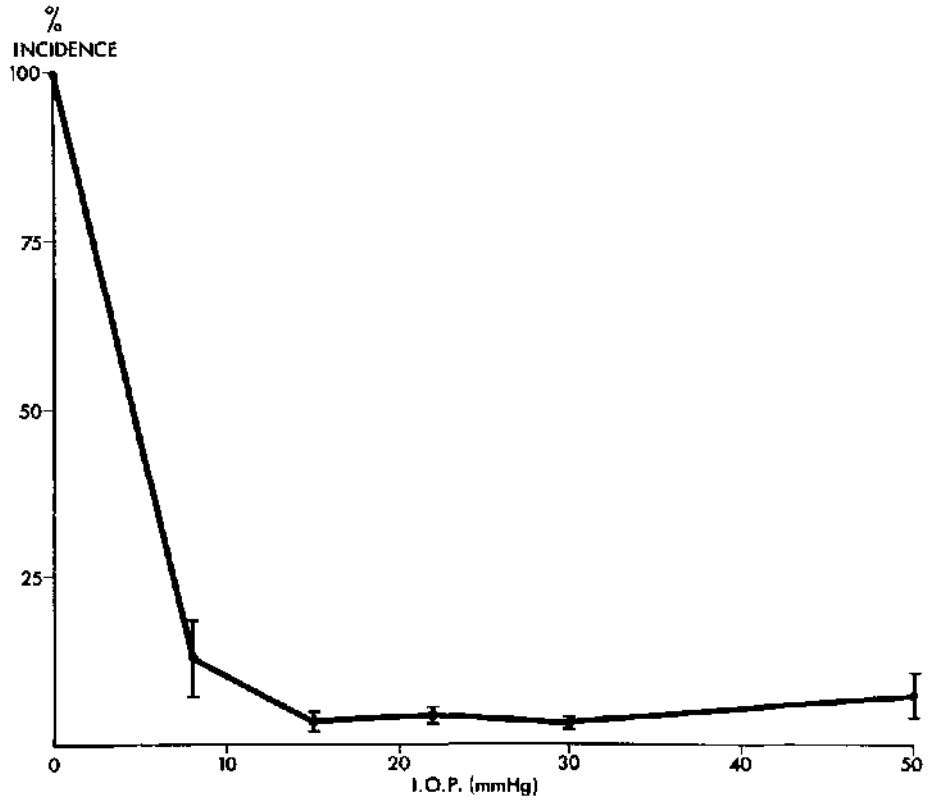

Fig.IO.34b The % incidence of pseudovacuoles in the total giant vacuole plus pseudovacuole population at the various pressure levels.

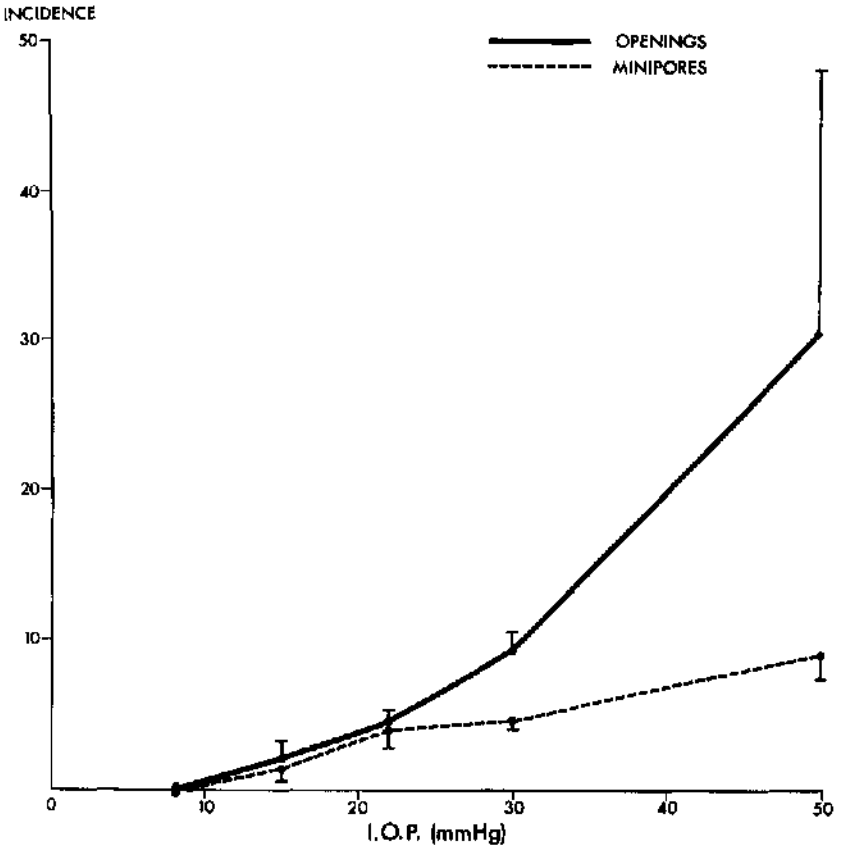

Fig.10.35 The incidence of non-vacuolar openings and minipores per 100 nuclei counted at each of the various pressure levels.

at 50 mm Hg.

In addition, an assessment was made of the significance of false positives (pseudovacuoles) as an error in the previous, more comprehensive light microscopic vacuole quantitation. The structures classified as types a and b pseudovacuoles were recognised by Fink, Felix and Fletcher (1971) who did not distinguish between these structures and "true" giant vacuoles. Types a and b pseudovacuoles were rare and their incidence showed no pressure relationship, so that their frequency in relation to the giant vacuole population was greatest at low pressure (1% of the count at 30 mm Hg but 11% at 8 mm Hg). However, since vacuolar structures were not observed by light microscopy at 0 mm Hg it seems likely that the pseudovacuoles were excluded by the criteria adopted for the light microscopic investigation.

Pseudovacuoles type c have been described by Rohen (1969) who noted an increase in their numbers after the administration of atropine. In the present study, they were present only at the higher pressures but their numbers were very low. Although some may have been included in the light microscopic vacuole count, like pseudovacuoles types a and b, they would constitute only a minor error.

When isolated sections were examined some of the giant vacuoles were seen to have membrane lined pores. Pores on the meshwork aspect of the vacuolar structures were larger and more frequent than lumen pores. When vacuoles were particularly prevalent, as at 22 and 30 mm Hg, three types of vacuole were identified from serial analysis (1) those which had a meshwork pore only (the bulk of the population), (2) those which had lumen pores only and (3) those which had both. The latter could be considered to constitute transcellular channels through which

aqueous humour may pass from the meshwork to Schlemm's canal. Vacuolar transcellular channels, and vacuoles with lumen pores only, represented a small proportion of the vacuole populations at the higher pressures so it was not surprising that at low pressures, where vacuoles were rare and there were sampling problems, these types were found only occasionally (15 mm Hg) or not at all (8 mm Hg). A truly intracytoplasmic structure (a vacuole without an opening) was never found, an observation which was in agreement with previous authors who considered that the term "giant vacuole" was erroneous and "invaginations" would be more applicable (Segawa, 1968, 1971a and b; Inomata, Bill and Smelser, 1972a).

The results of the vacuole and vacuolar pore counts, from the investigations of lengths of canal endothelium at the various pressure levels between 8 and 30 mm Hg, showed that the percentage of the vacuole sample which had meshwork pores increased from 9 to 37% and the percentage with lumen pores from 0 to 6%. Thus, raising the intraocular pressure caused the vacuole population not only to become more enlarged but more porous.

Counts from flat sections provided two dimentional information and, as such, did not distinguish between an increase in actual pore frequency and a disproportional enlargement of the pores relative to the giant vacuoles. That the pores occupied an increasingly greater proportion of the vacuolar shells, as pressure increased, was evident from serial analysis (Fig. 10.24). By multiplying the ratio of vacuole to pore width given in Fig. 10.24 by the percentage incidence of vacuoles with pores in the total vacuole sample from the two dimentional analysis (Fig. 10.33), a crude estimate of actual pore incidence was made for each pressure level (Fig. 10.36).

I.O.P. (mm Hg)	Meshwork pore incidence	Lumen pore incidence	Estimated incidence of vacuolar transcellular channels	Estimated incidence of vacuolar transcellular channels Per mm length of canal
30	86%	29%	14%	752
22	92%	23%	11%	407
15	77%	17%	8%	179
8	71%	0%	0%	0

Fig.10.36 Estimated incidence of vacuolar pores and transcellular channels from T.E.M.

If it was assumed that there were approximately equal numbers of transcellular channels and luminal invaginations, about 8% of the vacuole population at 15 mm Hg and 14% at 30 mm Hg would constitute transcellular channels. The control value of 8% was considerably higher than that estimated by Kayes (1967) and Tripathi (1968) from their transmission electron microscopic studies of normotensive primates (1 and 2% respectively) but less than the values obtained in scanning electron microscopic investigations (see Chapter 11).

When the percentage incidence of transcellular channels was multiplied by vacuole numbers per mm of length of canal (from the regression equation calculated in chapter 8, see page 111) approximate but useful values for the frequency of transcellular flow pathways were available for the various pressure levels. Based on these assumptions and somewhat limited information, the absolute values had little credence but a trend was obvious. There were about four times as many vacuolar transcellular channels at 30 than at 15 mm Hg. This finding, coupled with the very obvious quantitative and qualitative changes in the giant vacuole population, indicated that the potential for aqueous outflow by the vacuolar route increased quite dramatically with pressure increase up to 30 mm Hg.

Tripathi (1968, 1969a and b, 1971a, 1973b , 1974), based on his investigations of the normotensive primate outflow system, proposed that the vacuolar transcellular channel was a stage in a cyclical process whereby the vacuole formed, developed and eventually collapsed. He hypothesised that the driving force for vacuolation was the pressure gradient across the canal endothelium. Energy consumption was thought not to play a major role in the vacuole cycle but there must be a distinctive or particular property of the endothelial cells which allowed them to vacuolate.

The increase in the percentage of trancellular channels in the vacuole population with intraocular pressure elevation could be explained by the hypothesised vacuole cycle as a prolongation of the "life-span" of the transcellular stage during vacuolation. The 8% frequency of transcellular channels at 15 mm Hg would represent approximately 1/12th of the cycle and the 14% frequency at 30 mm Hg 1/7th of the cycle.

The present investigation provided an opportunity to test some of the assumptions which were fundamental to Tripathi's model. It was established that giant vacuoles were temporary pressure-dependent structures which, by the formation of transcellular channels, may serve as a pressure-sensitive outflow route for aqueous humour. Further, there was no obvious change in the glycogen content, the ribosomal content, the reticular systems or the numbers and size of the mitochondria within the endothelium between 0 mm Hg (where there were no vacuoles) and 30 mm Hg (where vacuoles were prolific). Thus there was no indication that either extensive energy consumption or protein production was necessary for vacuolation.

Indeed that Johnstone and Grant (1973) demonstrated pressure-dependent vacuolation in post-mortem eyes argued against the involvement of cellular metabolism in endothelial vacuolation. However, there is no reason why the vacuole cycle should not operate in cells with questionable viability provided the cells retained those properties (Tripathi, 1968, 1969a and b, 1971a, 1973a , 1974) which allow vacuolation to occur. Certainly, if pressure-induced vacuolation did not occur in vitro it would be a less plausible outflow route, given similarities in outflow dynamics between living and post-mortem eyes (Grant and Trotter, 1955; Becker and Constant, 1956; Grant, 1963).

While Tripathi's hypothesised vacuolation cycle cannot be accepted entirely without reservation, it would appear to be a useful working model which can be applied to the findings in the present study. The possible sequence of anatomical and physiological events which leads to the formation of a vacuolar transcellular channel and a more detailed assessment of Tripathi's proposed endothelial vacuolation cycle is presented in chapter 12.

At this point it should be stated that several authors did not accept that vacuoles were involved in aqueous transfer, but instead they were thought to be degenerative vesicles of one form or another.

Both Speakman (1959) and Ashton (1960) entertained the possibility that the giant vacuoles of Schlemm's canal may be similar to vesicles which form very rapidly in corneal endothelial cells due to post-mortem hydrophic degeneration. Although, on reconsideration, Speakman reverted to his initial opinion that the giant vacuole were flow pathways for aqueous humour (Speakman, 1960, 1961), later investigators noted that vacuoles were more prevalent in the canal endothelium of post-mortem eyes than fresh, rapidly fixed eyes (Fine, 1966; Segawa, 1971b).

Recently Shabo, Reese and Gaasterland, (1973) demonstrated that spontaneous vacuolation occurred when primary fixation was postponed for 30 minutes after death. Shabo and co-workers suggested that all giant vacuoles were a post-mortem artefact produced by poor or delayed fixation, because vacuoles were rare if immediate fixation via the episcleral veins was employed.

In the light of the pressure dependent nature of "true" giant vacuoles Shabo's findings are not surprising since retrograde perfusion would reverse the natural direction of fluid flow through the outflow

system.

The present author is of the opinion that vacuoles are neither artefactual nor degenerative structures. The pressure sensitivity of the endothelial vacuole population was demonstrated both in carotid and anterior chamber perfusion fixed tissue so that the appearance of the canal endothelium did not depend on a particular mode of fixation. Equally, the fact that giant vacuoles were absent at 0 mm Hg is in direct contradiction to their being degenerative structures since this was an experimental situation in which the primary fixation technique was least satisfactory and autolytic changes were most likely to occur.

"True" giant vacuoles are membrane lined structures which have been demonstrated by many authors (see Chapter I) in endothelial cells with an acceptable morphological appearance. The possibility that giant vacuoles are artefacts was made even more unlikely by demonstrations, using tracer materials (Feeney and Wissig, 1966; MacRae and Sears, 1970; Tripathi, 1971a, 1974; Inomata, Bill and Smelser, 1972a), that the vacuolar lumen was a viable space in vivo.

It is not disputed that post-mortem vacuolation does occur when there is considerable delay before fixation, but "true" pressure-dependent vacuoles and post-mortem vacuoles are probably separate entities. Post-mortem vacuoles are as frequent on the corneoscleral as the trabecular aspect of the canal (Fine, 1966; Segawa, 1971b; Shabo, Reese and Gaasterland, 1973), they appear to be pressure independent (Shabo, Reese and Gaasterland, 1973) and appear to be totally intracytoplasmic structures (Segawa, 1971b). The observation that spontaneous post-mortem vacuolation can occur in such a short time period as 30 minutes (Shabo, Reese and Gaasterland, 1973) has not gone unchallenged. Kayes (1975a) fixed hypotensive

rhesus monkey eyes 5 and 30 minutes post-mortem, the canal endothelium contained few giant vacuoles and there was no difference in vacuolar incidence between the two situations.

The influence of the endothelial meshwork on vacuolar distribution is worthy of emphasis. Rohen, Lütjen and Barány (1967) first put forward the proposal that hydrostatic pressure under the endothelium lining the trabecular wall of Schlemm's canal was not uniform, because there were preferential flow pathways through the outer meshwork. That this was, in fact, the case was borne out by the erratic distribution of vacuoles at 15 and 22 mm Hg. Indeed clusters of giant vacuoles were often associated with focal distensions of the endothelial meshwork. Thus, it could be considered that filtration differences in the heterogenous endothelial meshwork determine vacuolar distribution.

Increase in pressure to 30 mm Hg resulted in the opening up of more pathways and as vacuoles were abundant along the whole length of the endothelium, the system was probably close to its maximum capacity at this pressure.

At 50 mm Hg, the system was so overloaded that drainage was by non-physiological routes. The anterior portion of the canal was often occluded and where the canal was patent the endothelial cells were mechanically separated. Giant vacuoles, when found, had frequent tears (rather than membrane lined pores) in their shells.

10.6.2 Non-vacuolar transcellular channels

At pressures of 15, 22 and 30 mm Hg gaps were present in the endothelium lining the trabecular aspect of Schlemm's canal. The gaps were located in the narrow peripheral portions of the endothelial cells and were shown to be non-vacuolar transcellular channels. Non-

vacuolar channels of similar dimensions to those described in the present study have been identified in the normotensive canal endothelium by Segawa (1968, 1971a); Fink, Felix and Fletcher (1972); Inomata, Bill and Smelser (1972a) and Tripathi (1974).

Counts of the transcellular channels at the various pressure levels revealed their absence at 8 mm Hg and, thereafter, a progressive increase in frequency to 30 mm Hg. Some of the channels contained migrating wandering cells, an indication that the passageways were patent in vivo. Thus the non-vacuolar transcellular channels were temporary pressure sensitive structures which could serve as auxiliary drainage pathways augmenting the vacuolar drainage route.

At 50 mm Hg counts were particularly high but, as stated previously, these were mechanical separations of adjacent cells and not intracellular pathways.

10.6.3 Minipores

The small intracellular fenestrations, called minipores by Inomata, Bill and Smelser (1972a) were of comparable diameter to the abundant fenestrations of the choriocapillaris and the vessels of the ciliary processes (Taniguchi, 1962). Minipores were associated with the attenuated endothelium of large giant vacuoles and cell peripheries. Therefore, the endothelium lining the trabecular wall of Schlemm's canal became more fenestrated with increase in pressure, because of vacuolar abundance and endothelial stretching at elevated pressures.

To some extent, the ability of the endothelium to form minipores must be a property of the particular cell type and not just the inevitability of extreme cellular thinning. The endothelium on the corneoscleral aspect of the canal was very narrow and, indeed, except

for the highest pressures these cells were more elongated than their counterparts on the opposing wall. Despite the attenuation, minipores were never found on the corneoscleral side of Schlemm's canal.

10.6.4 Pinocytosis and micropinocytosis

The canal endothelial cells contained pinosomes, coated micropinosomes and uncoated micropinosomes. It has been proposed that uncoated micropinosomes (Fine, 1964; Feeney and Wissig, 1966; Rohen and Van der Zyphen, 1968; Van der Zyphen, 1971) and also pinosomes, formed from marginal cytoplasmic folds, (Fine, 1964, 1966) may transfer aqueous humour across the endothelium of Schlemm's canal so functioning as a respiratory dependent component of bulk outflow. Although, both uncoated micropinosomes (Palade, 1961) and the larger pinosomes (Fawcett, 1965) have been implicated in the active transport of fluid across the endothelium lining blood vessels, respiratory dependent vesiculation does not appear to be an important mechanism for the transfer of aqueous humour into Schlemm's canal given that metabolic poisons do not have a significant influence on bulk drainage (Barány, 1953).

In the present experiment, the inverse relationship between the frequency of all three types of vesicle and intraocular pressure was unexpected. A possible explanation may be that vesicle formation was influenced by the chemical composition of the fluid which bathed the cells. At 0 mm Hg the canal was filled with refluxed blood and there were numerous pinosomes and micropinosomes in the endothelial cells. Thereafter, with pressure elevation and the consequential removal of blood elements, the vesicles become progressively less frequent up to the highest pressure of the series (50 mm Hg).

Certainly, in other tissues, it has been shown that all three processes can be affected by the nature and composition of the surrounding environment. The formation of large pinocytotic vesicles can be induced in peritoneal macrophages by the presence of calf serum, and many other organic molecules, outside the cells (Cohn and Parks, 1967; Cohn, 1968; Cohn and Ehrenreich, 1969).

A close relationship appears to exist between the presence of macromolecules on the cell surface and the formation of uncoated micropinosomes (Shirahama and Cohen, 1972) and their primary function, in capillary endothelia, may be the transcellular transport of complex substances (Bruns and Palade, 1968; Shirahama and Cohen, 1972; Simionescu, Simionescu and Palade, 1973). Finally coated micropinosomes also take up macromolecules (Roth and Porter, 1964; Fawcett, 1965 and 1969; Bowers, 1965) and vesicle formation by the mosquito-oocyte can be stimulated by an increase in the protein content of the surrounding medium (Roth and Porter, 1964).

Although the findings indicated that there was a relationship between plasma concentration in Schlemm's canal and the incidence of endothelial pinocytotic and micropinocytotic vesicles, uncertainties remain about their significance, function(s) and directional movement.

Kayes (1975a) conducted an investigation somewhat comparable to the present study. He made no reference to pinocytotic activity, but found that the canal endothelial micropinosomes were usually coated at high pressure, whereas the uncoated form predominated at low pressure. Despite the fact that Kayes' findings and the current observations were not complementary, and further experimentation will be necessary to resolve the differences, both investigations indicated that endothelial vesiculation was affected by alterations to intraocular pressure.

CHAPTER 11

PRESSURE EFFECTS ON THE TOPOGRAPHY OF THE ENDOTHELIUM LINING THE TRABECULAR ASPECT OF SCHLEMM'S CANAL

11.1 Introduction

The scanning electron microscope made a useful contribution to the study of pressure effects on the endothelium lining the trabecular aspect of Schlemm's canal because the image from the instrument conveyed three dimensional spatial information and eliminated the need for tedious serial reconstruction which handicaped both light microscopic and transmission electron microscopic investigations. Since a) large areas of tissue could be screened with relative ease and b) the resolving power was sufficient for the identification of vacuolar and non-vacuolar pores (see Chapters 1 and 4), a quantitative assessment of pressure induced changes in the numbers and size of endothelial pores was attempted.

11.2 Materials and methods

The examination of dissected specimens (see Chapter 3 for details of the dissection procedure) was restricted to the three animals in which the experimental eye was maintained at 8 mm Hg and one in which the experimental eye was maintained at 22 mm Hg. At 30 and 50 mm Hg the canal lumen was narrow, which prohibited successful dissection, while at 0 mm Hg the endothelial monolayer was obscured by the blood which filled Schlemm's canal. All the tissue in this series was prepared by freeze-drying.

A quantitative analysis of endothelial porosity was conducted on the three 8 mm Hg eyes and their corresponding 15 mm Hg control eyes. For the quantitative analysis, coded pieces of tissue from the experimental and control eyes were processed in parallel to minimise preparatory variation between subjects. Mapping photographs of the endothelial monolayer were taken at a magnification of x 3,000

and enlarged to a print size which corresponded to an area of 2,500 μm^2. The prints were coded and the number of cellular bulges and surface openings, both on and off the bulges, were recorded on matching sets of prints by two observers (the present author and Dr. W. R. Lee, see acknowledgements). The total area of the trabecular wall endothelium examined for each of the eyes was between 130,000 and 300,000 μm^2. Maximum pore widths were measured, with a x 7 magnifying eye piece which incorporated a graticule, by one observer (the present author) from sets of prints which corresponded to a surface area of 100,000 μm^2 for each eye. On each print bulge and non-bulge pores had been indicated by a second observer (W. R. Lee).

11.3 Results

11.3.1 General considerations

At each pressure level the monolayer consisted of a mosaic of closely packed spindle-shaped endothelial cells whose long axes, in general, were aligned in the coronal plane. The cells had discrete bulges which were thought to house either the cell nucleus, a giant vacuole or both. Pores were found both on the bulges (the lumen pores of giant vacuoles) and away from the bulges (either non-vacuolar pores or the pores of small giant vacuoles which did not indent the cell surface). As such, the tissue at the various pressure levels conformed to the general appearance of normal primate trabecular wall endothelium which was outlined in chapter 4.

11.3.2 15 mm Hg

There was often considerable regional variation in the trabecular

wall within the dissections. In the anterior portion, the wall was usually flat, whereas in the posterior portion, there were distinctive ridges, projections and convolutions (Fig. 11.1a).

At 15 mm Hg it was difficult to identify cell borders with any degree of precision therefore accurate measurement of cell length was impractical, nevertheless the impression gained was that the individual cells were extremely long. On the other hand the cellular bulges could be identified easily, even at relatively low magnifications (Fig. 11.1b). The bulges in some areas were plump and, on occasion, almost spherical (Fig. 11.2a) but typically they were flatter and more extended (measuring up to 20 µm in length) (Fig. 11.2b). In limited zones, usually towards the anterior portion of the canal the bulges were scarce and the cells were particularly elongated (Fig. 11.2c).

Openings with a smooth outline were found on and off the bulges. The openings were considered to correspond to the pores observed by transmission electron microscopy (Figs. 11.2b and 11.3a, b and c). It was often difficult to distinguish "true pores" from small tears and ragged deficits produced either during the drying procedure or from dissection. The largest deficits revealed cystic spaces in the bulges which were the lumina of giant vacuoles. Where there had been extensive disruption to the vacuolar shell the meshwork pore could be identified.

Surface pitting (Fig. 11.2b) was found, to a greater or lesser extent, both on and off the bulges. This was an artefact which may have been produced by the crystallisation of surface deposits (plasma) during the freeze drying and was troublesome because the largest pits could be mistaken for pores. Therefore the identification of true pores was not always clear cut but, with care and critical evaluation,

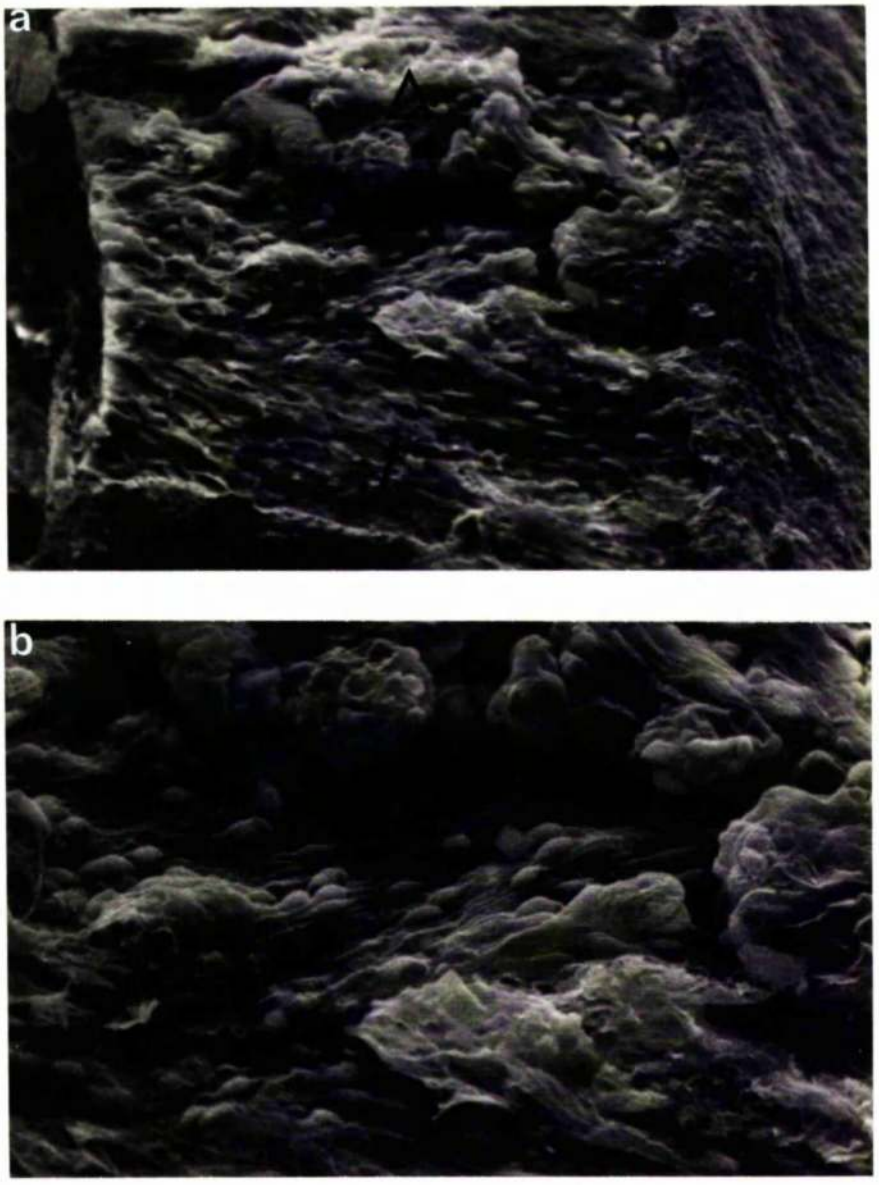

Fig.II.I Part of the endothelial monolayer on the trabecular aspect of Schlemm's canal a) at low and b) at higher magnification. In a) the flat anterior portion of the wall is seen in the foreground (arrow). The posterior portion is more convoluted (triangle). In b) the endothelial cells can be seen to be spindle shaped with an ovoid central bulge. I5 mm Hg, S.E.M. (a x230; b x500).

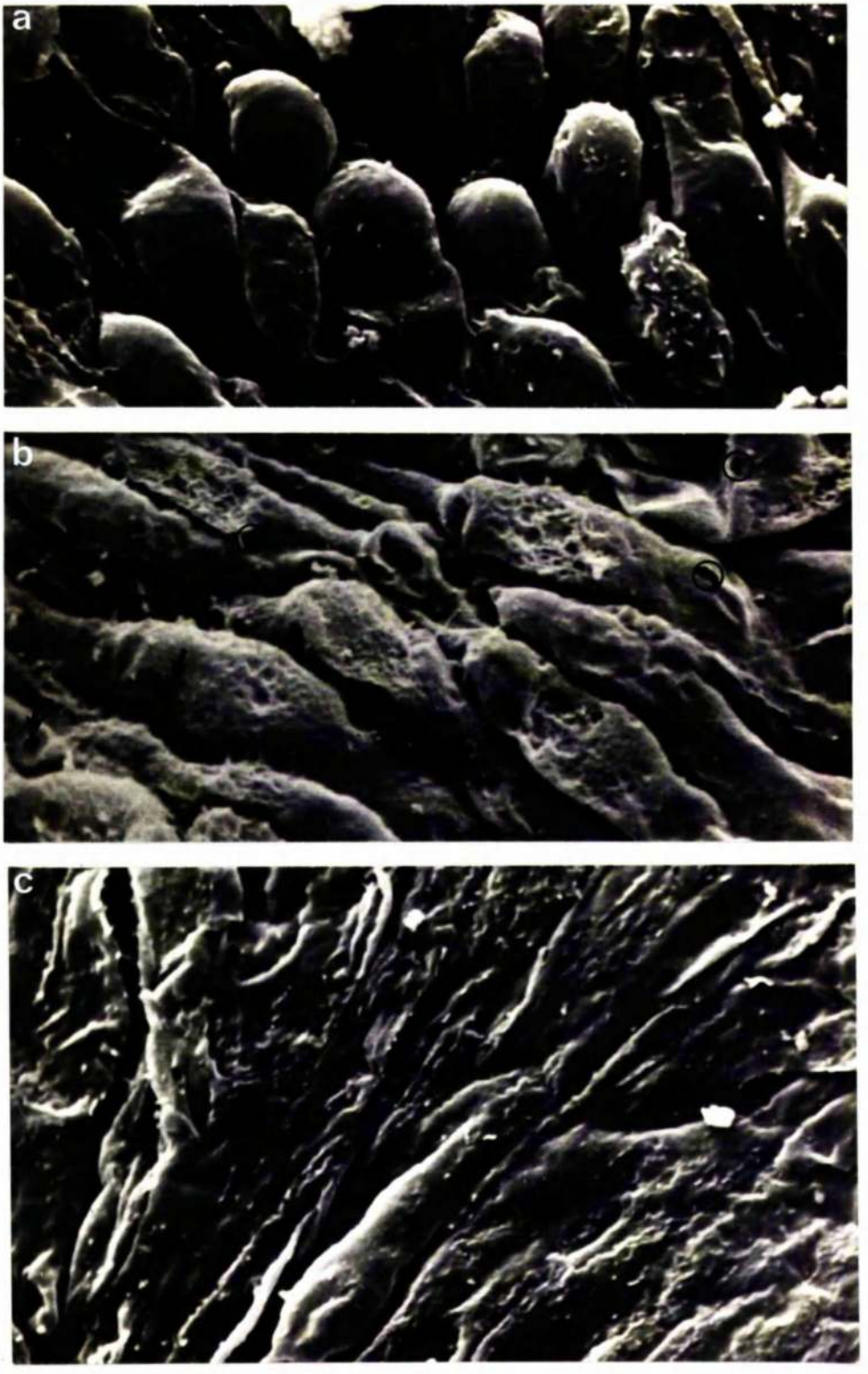

Fig.II.2 Endothelial bulges at different sites in the endothelial monolayer (15 mm Hg). Areas can be found where the bulges are a) plump, b) elongated or c) scarce. In b) some pores are indicated by arrows and some tears by circles. S.E.M. (x2,000).

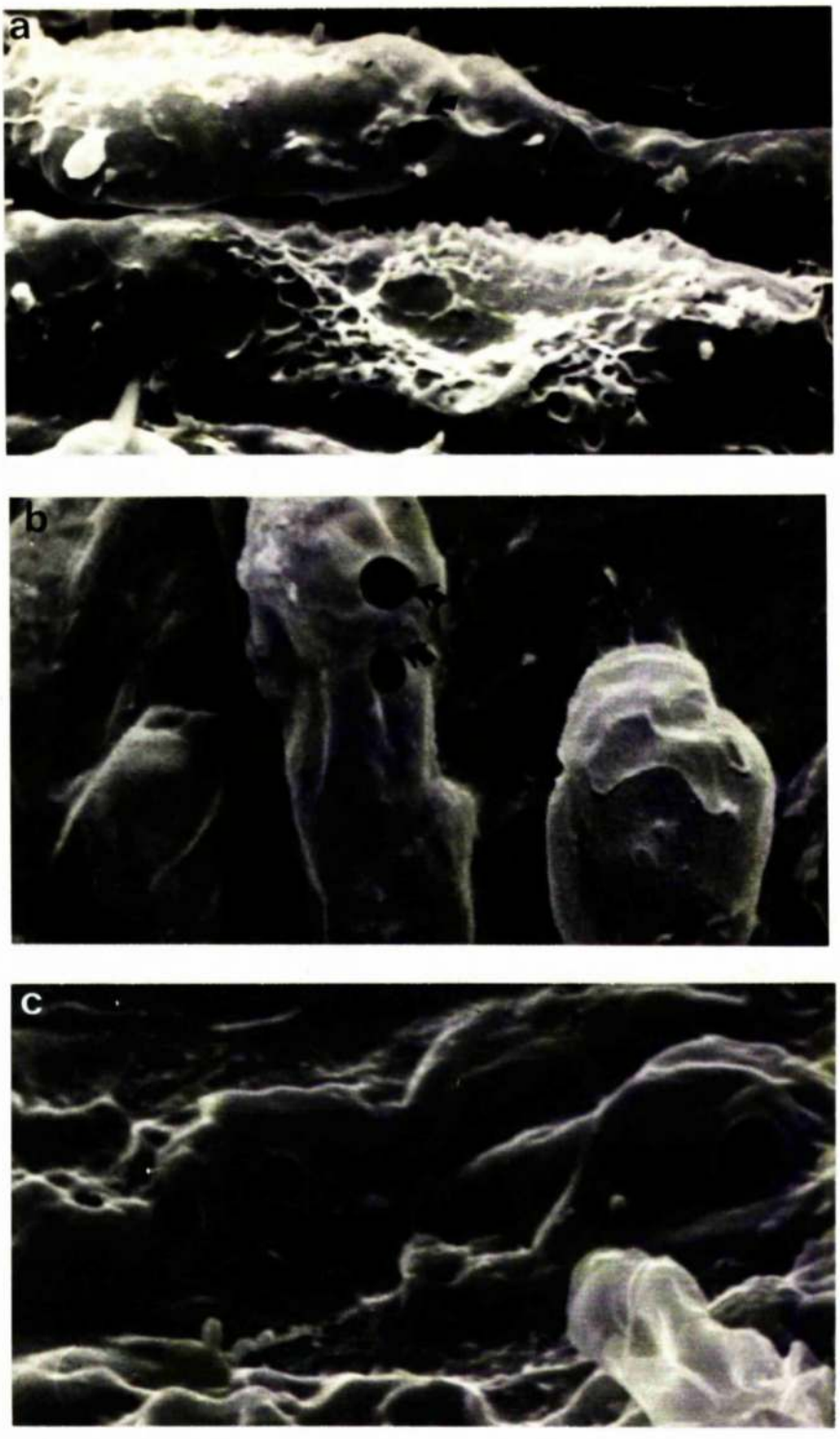

Fig.II.3 Pores in the endothelial monolayer at I5 mm Hg indicated by arrows. a) Pores were present both on and off the bulges, b) sometimes two pores occupied the same endothelial bulge and c) some pores had a raised lip. S.E.M. (a x6,000; b x6,800; c x7,I00).

most of the artefacts could be eliminated.

The pores were either ovoid or circular and some had a lip which protruded above the cell surface (Fig. 11.3c). Bulge pores were usually single (Figs 11.2b and 11.3a and c) but, on occasion, two pores occupied the same bulge (Fig. 11.3b). The distribution of both types of pore was not uniform, areas of abundance were called "active zones" and areas where there was a deficiency were called "inactive zones".

11.3.3 8 mm Hg

At 8 mm Hg there were distinctive grooves or furrows between the adjacent endothelial cells and the cells were more compressed than at 15 mm Hg. The furrows could be seen quite clearly at low magnification and the overall appearance of the endothelial monolayer was reminiscent of a ploughed field (Fig. 11.4). Cellular bulges were less obtrusive and had either a crenated (Figs 11.4 and 11.5a) or a smooth (Fig. 11.5b) outline. Pores were identified both on and off the bulges but they were rather difficult to find at this pressure. Proteinaceous material and red cells obscured significant portions of the surface of the endothelial monolayer.

11.3.4 22 mm Hg

At 22 mm Hg the cellular bulges occupied a large proportion of the endothelium and were seen as smooth walled, spherical grape-like structures protruding from the surface of the monolayer (Fig. 11.6). Pores were very obvious at this pressure and, on the bulges, they were usually single but multiple pores were more in evidence than at 15 mm Hg (Fig. 11.7a). The bulges were more prone to total or partial collapse (the action of surface tension forces during the drying process)

Fig.II.4 Part of the endothelial monolayer on the trabecular aspect of Schlemm's canal at 8 mm Hg. The cell bulges are less obtrusive than at I5 mm Hg and there are distinctive grooves between neighbouring endothelial cells. S.E.M. (x775).

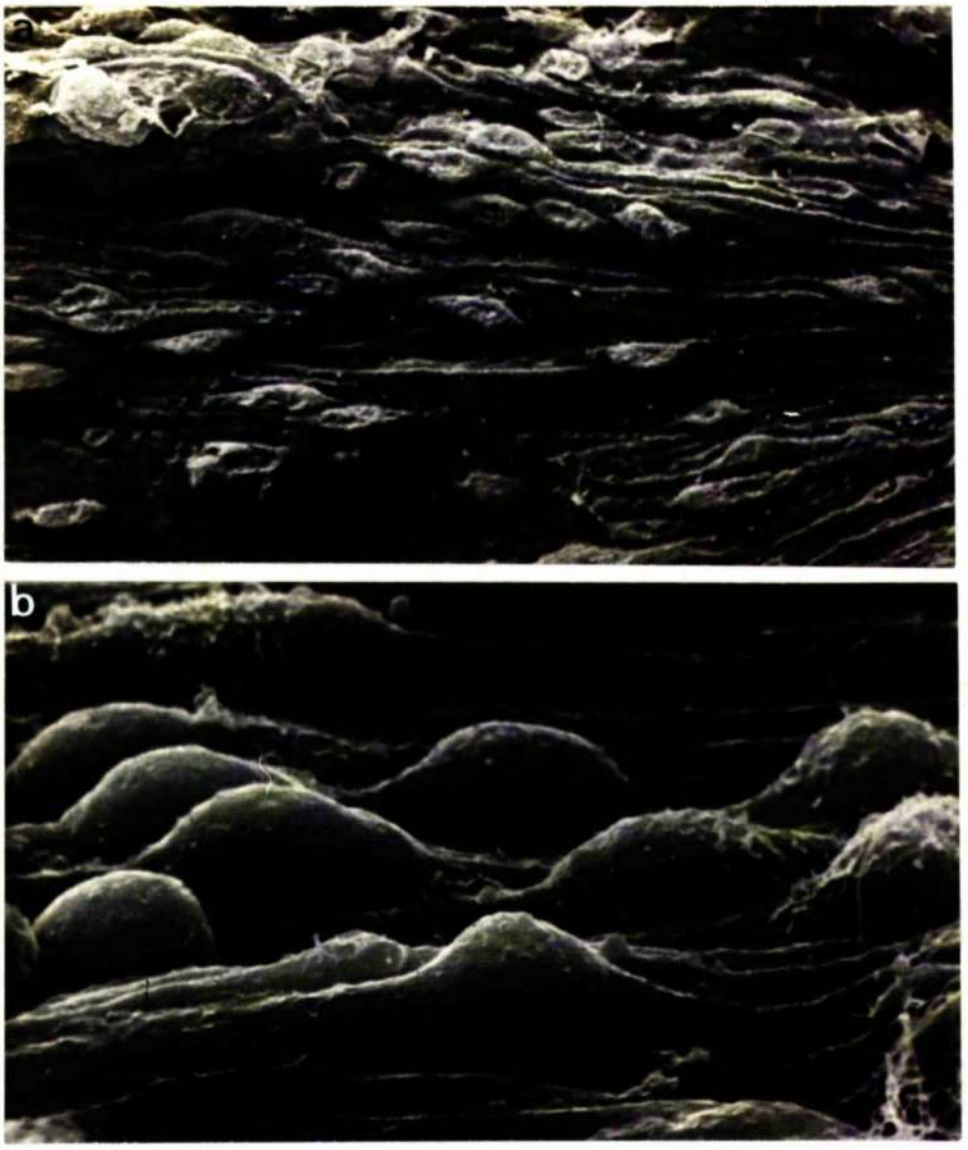

Fig.II.5 At 8 mm Hg the endothelial bulges had either a) a crenated or b) a smooth outline. S.E.M. (a x875; b x2,500).

Fig.II.6 Ovoid bulges were particularly prominent in the endothelial monolayer at 22 mm Hg. S.E.M. (xI,I00).

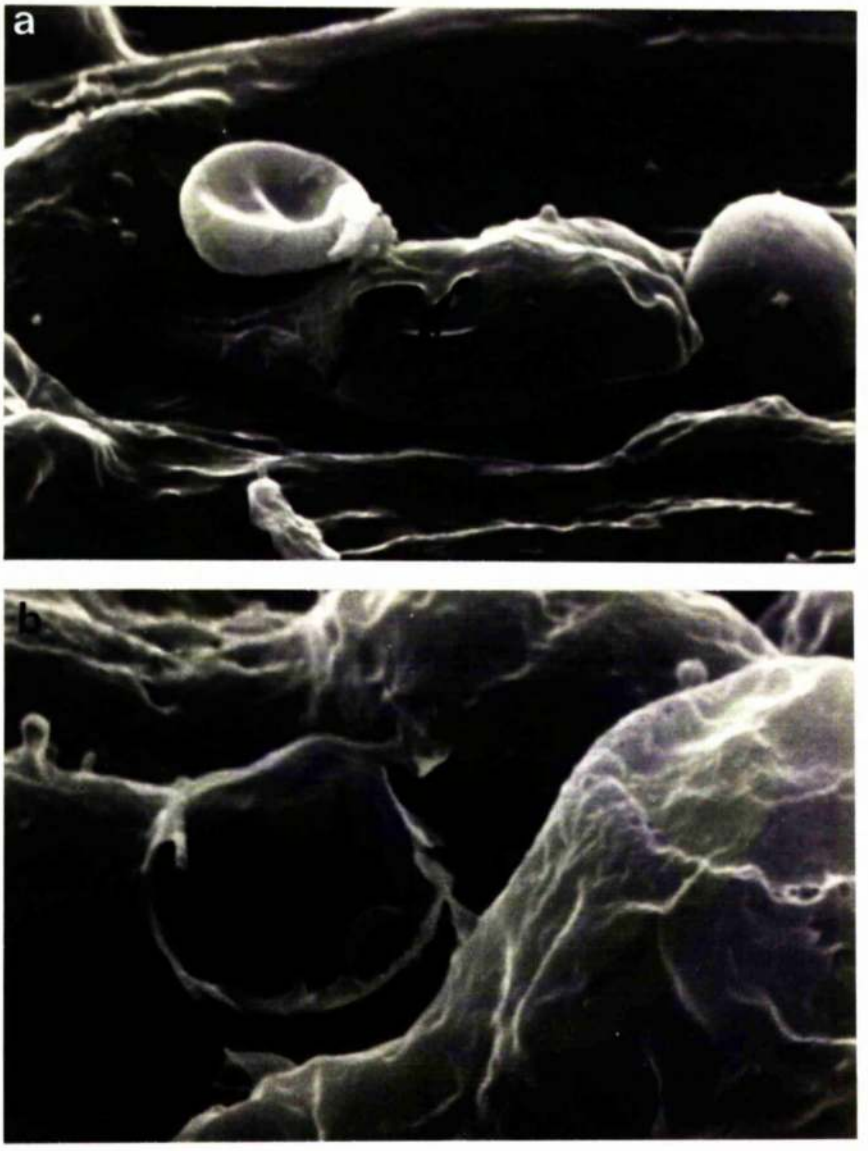

Fig.II.7 The endothelial bulge shown in a) has 2 pores (arrows). The relative sizes of the pores and bulges can be compared with that of a nearby red blood cell. A torn bulge is shown in b) and a meshwork pore (arrow) can be seen at the base of the cavity. 22 mm Hg, S.E.M. (a x5,000; b x5,500).

and to artefactual tearing than those at the lower pressures. Presumably this was due to the presence of particularly large giant vacuoles with delicate, and therefore vulnerable, cytoplasmic shells. Artefactual tears were occasionally large enough to reveal the cystic cavities within the bulges and the meshwork pores (Fig. 11.7b).

11.3.5 30 mm Hg

Although dissection was impractical at this pressure, in some of the meridional tissue slices the canal was sufficiently wide to observe part of the trabecular wall (Fig. 11.8). From this limited sample, the topography of the endothelium appeared to progress from that seen at 22 mm Hg. The endothelial bulges were often very large, ovoid, even pear-shaped structures projecting up to 15 μm from the surface of the monolayer and, where sectioned, they were seen to be giant vacuoles surrounded by a very thin endothelial shell (Fig. 11.8). Pores were very prominent in the endothelial bulges.

11.3.6 Quantitative analysis

Three structural features were counted in the 8 mm Hg eyes and their corresponding 15 mm Hg controls, a) bulges (since some contained giant vacuoles), b) openings on the bulges and c) openings elsewhere on the endothelial cells.

There were three major sources of error or inaccuracy in the quantitative analysis.

1) True pores were defined as openings with a regular and smooth outline to distinguish them from ragged deficits. However the distinction was not always clear cut and therefore an over count was possible. Equally, true pores may have been damaged and thus eliminated from the count.

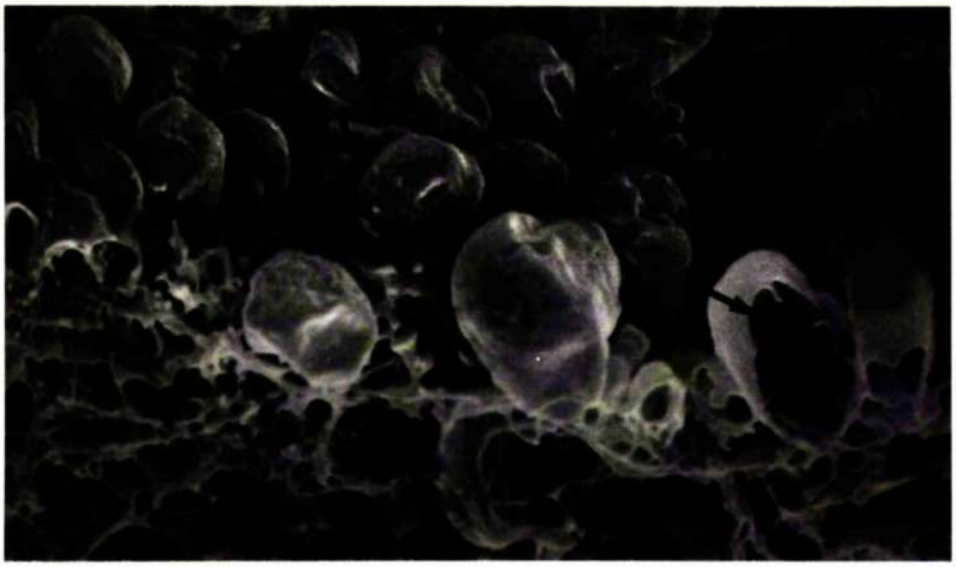

Fig.II.8 Part of the trabecular wall of Schlemm's canal at 30 mm Hg. The arrow indicates an opened vacuole. S.E.M. (x2,000).

2) Particular difficulty was encountered with pores outwith the endothelial bulges because the openings could have been obscured by grooves and ridges in the monolayer.

3) The analysis was based on viewing from one angle only, so that inevitably a proportion of the openings would have been missed.

Comparison of the results obtained by the present author and another (W. R. Lee) on duplicate sets of micrographs showed that interobserver error was lowest for cellular bulges (5%) and highest for non-bulge pores (12%). Despite interobserver variation the statistical trends were the same in both sets of figures. Fig.11.9 shows my values for bulges, pores on bulges, non-bulge pores and total pores per unit area for each animal at the two pressure levels. The values for each structure are expressed as an incidence in an area of 10,000 μm^2 ("n" equals 4 print areas of 2,500 μm^2) to avoid, where possible, presenting pore counts at 8 mm Hg as fractions.

Taking into consideration the various forms of error associated with the analysis, the pore counts in the three 8 mm Hg were remarkably consistent. On the other hand, the differences in pore incidence in the three 15 mm Hg control eyes were quite substantial. For each animal there were more bulge pores, non-bulge pores and therefore total pores in the 15 mm Hg than the 8 mm Hg endothelial monolayer. The differences were either significant or highly significant for each comparison with the exception of non-bulge pores in animal number 74/73. Pores were found in approximately 4% of the endothelial bulges at 8 mm Hg and in 15% at 15 mm Hg, while there were about 4 times as many total pores at the higher pressure. The difference in the numbers of cellular bulges was significant in only one animal. The large standard deviation for each of the structures counted was probably a reflection of regional variation.

ANIMAL NO.	I.O.P. Mm.Hg.	BULGES	PORES IN BULGES	% INCIDENCE OF PORES IN BULGES	PORES OFF BULGES	TOTAL PORES	N
74/73	8	27.5 ± 8.3	1.1 ± 1.0	4.0%	1.0 ± 1.2	2.1 ± 1.5	16
	15	30.0 ± 13.6	3.5 ± 3.1 **	11.7%	2.1 ± 1.9	5.6 ± 4.2 **	30
75/73	8	28.4 ± 9.4	1.4 ± 1.4	4.9%	1.0 ± 0.8	2.4 ± 2.1	13
	15	40.1 ± 13.2 *	5.9 ± 3.0 ***	14.7%	3.3 ± 2.0 ***	9.2 ± 4.6 ***	18
76/73	8	42.2 ± 9.6	1.7 ± 1.7	4.0%	0.9 ± 1.1	2.6 ± 2.6	16
	15	43.8 ± 13.3	8.8 ± 5.1 ***	20.1%	4.6 ± 3.2 ***	13.4 ± 7.7 ***	29

* $p < 0.05$

** $p < 0.01$

*** $p < 0.001$

Fig.II.9 The mean counts of bulges, pores in bulges, pores off bulges and total pores at 8 and 15 mm Hg.

Measurements of maximum pore widths (Fig. 11.10) were made without stereoscopic correction. Without correction a pore will appear erroneously larger or smaller than its "true" size, depending on the inclination of the pore relative to the viewing angle and the direction of its long axis relative to the viewing direction. Since this error was common to the measurements of pore sizes at both pressures, comparison of maximum pore widths at 8 and 15 mm Hg could be justified.

It can be seen in Fig. 11.10 that there was a smaller pore population in the 8 mm Hg than the 15 mm Hg sample of the endothelial monolayer. In each population, the histogram shows a skew distribution, there being more small than large pores. The most important finding was that, for each of the three comparisons, the 15 mm Hg population had a significantly larger mean width than the 8 mm Hg population ($P < 0.01$). Despite the differences in the mean values, the size ranges covered by the 8 mm Hg populations were similar to the appropriate control range.

11.4 Discussion

The instantaneous three dimensional image of the scanning electron microscope helped to highlight the topographical differences in the endothelial monolayer at the various levels of intraocular pressure. In particular, it was shown that bulges became more prominent and the porosity of the endothelium was increased with stepwise elevation of the intraocular pressure up to 30 mm Hg. At each pressure level, the distribution of pores was non-uniform and this was considered to be evidence for preferential flow pathways through the underlying meshwork.

A much larger tissue sample could be examined by scanning than by transmission electron microscopy so that the former technique was

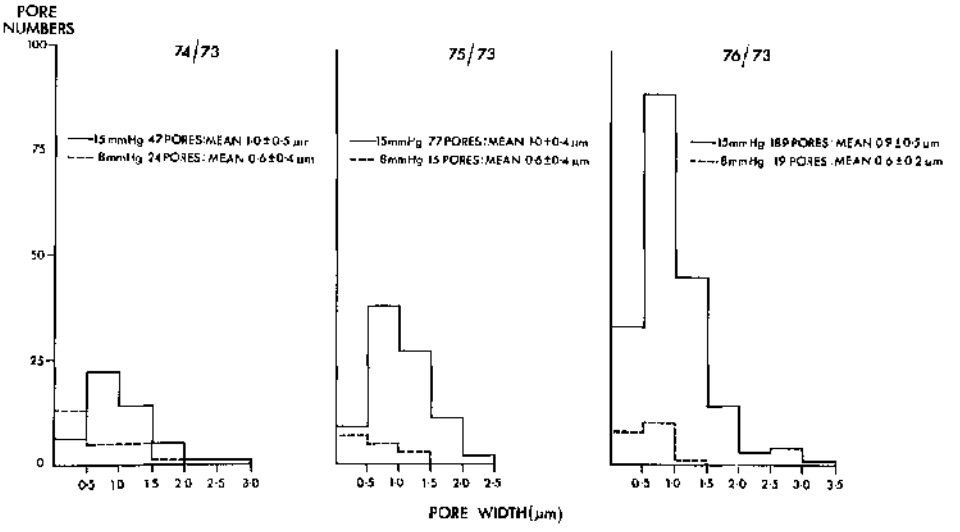

Fig.II.IO The distribution of pore widths in the populations at 8 and I5 mm Hg.

more suited to the study of the relatively rare and sporadically distributed endothelial pores. That pores were found at 8 mm Hg with the scanning but not with the transmission electron microscope (see previous chapter) served to illustrate the point.

In the pore analyses with the scanning electron microscope it was found that for each animal the total pore count and the average pore size was significantly greater at 15 than at 8 mm Hg a trend which, from the transmission electron microscopic investigation, was shown to continue at 22 and 30 mm Hg. However the results must be interpreted with caution since pore analysis by scanning electron microscopy was not without hazard. Several factors may have had a preferential influence either by accentuating or supressing the difference in pore counts between the two pressure levels. At 15 mm Hg the canal was usually narrower than at 8 mm Hg, thus the endothelial monolayer was more prone to dissection damage. Dissection damage may have artificially elevated the pore count because of the presence of artefactual holes or suppressed the pore count because of damage to "true" pores. At 8 mm Hg there was plasma in the lumen of Schlemm's canal which tended to form a surface layer on portions of the endothelial monolayer. Protein masking would tend to reduce the pore count whereas, in some regions, coagulated protein produced surface pitting which may have artificially boosted the count. In the investigation care was taken to identify and eliminate the various artefacts where possible and, as can be seen, the influences of these artefacts were, to some extent, self-cancelling so that statistical comparisons between the experimental and control tissue were not invalid.

Further information could be gained by a comparison of the quantitative information obtained from the same animals by the three

microscopic systems (Fig. 11.11). It was apparent that at 8 mm Hg the transmission quantitation was ineffectual whereas the total pore counts per mm^2 at 15 mm Hg by transmission and scanning electron microscopy were reasonably comparable. However, in reality, the pore difference between the two techniques at the higher pressure was probably much greater because the scanning counts were restricted to viewing from one angle only. The pore incidence based on transmission electron microscopy was, of necessity, a crude estimate so that it would be inadvisable to be too critical of the difference between the two results. Indeed it was somewhat encouraging that both the transmission and scanning estimates fell within the 230 - 2,000 pores per mm^2 range used by Cole and Tripathi (1971) in their theoretical paper on the outflow mechanism in the normal primate eye.

Comparison of bulge incidence at 15 mm Hg with the light microscopic values for the numbers of vacuoles and nuclei was illuminating. The frequency of endothelial bulges compared quite favourably with the incidence of cell nuclei but was considerably lower than the number of giant vacuoles. Thus it would seem that, in the normotensive tissue, the bulges corresponded to perinuclear zones and, in agreement with the findings from chapter 8, most of the giant vacuoles were too small to produce additional indentations on the surface of the monolayer. Only at the higher pressures of 22 and 30 mm Hg were large giant vacuoles sufficiently numerous to have a substantial influence on the shape and frequency of the endothelial bulges.

In the light of the problems associated with tissue preparation for the scanning electron microscope, it was of interest to make comparisons between the data obtained at 15 mm Hg with that in the

MICROSCOPE	I.O.P.	BULGES PER MM^2.	TOTAL PORES PER MM^2.	AVERAGE PORE SIZE μM.	VACUOLES PER MM^2.	NUCLEI PER MM^2.
SEM	8	3,300	250	0.6	*	*
	15	3,800	950	1.0	*	*
TEM	8	*	0	*	*	*
	15	*	750	0.5	*	*
LM	8	*	*	*	2,100	*
	15	*	*	*	6,400	4,000

Fig.II.II Comparable data from counts of various structures in the trabecular wall endothelium of Schlemm's canal by scanning electron microscopy, transmission electron microscopy and light microscopy.

literature for normotensive primates (Fig. 11.12). The size range for endothelial pores and bulge frequency was in good agreement with previous findings. Although the total pore frequency and pore frequency on bulges was lower than previous estimates, the difference was minimal and could be explained by the fact that, as has been said earlier, for the present count viewing was from one angle only so that pores behind bulges were missed.

Only in one other scanning electron microscopic investigation did the authors (Bill and Svedbergh, 1972) try to determine the distribution of sizes in the pore population. In the four human eyes examined the population graphs had skew distributions, there being far more small than large pores, a finding which was consistent with the present results.

AUTHOR	SPECIES	I.O.P.	BULGES PER MM^2.	PORE FREQUENCY ON BULGES.	TOTAL PORES PER MM^2.	PORE SIZE IN μ M.
Bill (1970)	Vervet and Rhesus Monkeys.	Normal	4,000	29%	1,200	0.3 - 2.0
Lee (1971)	Rhesus Monkey	18-20mm.Hg.	6,000	*	*	0.2 - 1.0
Hoffman and Dumitrescu (1971)	Human	Normal	*	*	*	up to 2.0
Bill and Svedbergh (1972)	Human	Normal	2,000	*	1,800	up to 3.0
Segawa (1973)	Human	Normal	5,000	20%	1,000	0.5 - 1.5
Present Study	Rhesus Monkey	15mm.Hg.	3,800	15%	950	0.1 - 3.2

Fig.II.I2 Scanning electron microscopic data: comparison between the present study and the previous literature.

CHAPTER 12

GENERAL DISCUSSION

12.1 The valve-action of the outflow apparatus

It has been shown in the present investigation of the rhesus monkey outflow apparatus that the configuration of the trabecular meshwork and the appearance of the trabecular wall of Schlemm's canal was remarkably dissimilar at different levels of intraocular pressure. In the hypotensive eye, the outer corneoscleral meshwork and the endothelial meshwork were compressed while the canal's trabecular endothelium showed a paucity of giant vacuoles and transcellular channels. Conversely, in the hypertensive eye, the outer meshwork was distended and the canal endothelium, if the pressure level was beneath that necessary to produce extensive disruption, contained large numbers of giant vacuoles and transcellular channels. To illustrate the point Fig. 12.1 shows three dimensional drawings of the trabecular wall of Schlemm's canal and the adjacent tissues at high and low intraocular pressure. The results confirm previous findings in both the living (Kayes, 1975a) and post-mortem (Johnstone and Grant, 1973) primate eyes with respect to meshwork distension and endothelial vacuolation. The current study has gone further than the earlier investigations, as it is the first investigation in which a relationship between intraocular pressure and the porosity of the canal's trabecular endothelium has been established.

With a silicone analogue of the outflow apparatus Allen and Burian (1965) demonstrated that distension of the drainage tissues and widening of the intertrabecular spaces increased the rate of aqueous outflow. Since, in the present study, the meshwork opens up in a situation of increased pressure differential across the outflow apparatus and collapses when the pressure head is reduced, this action

Fig.I2.Ia A three dimensional drawing of the trabecular wall of Schlemm's canal when intraocular pressure is high.

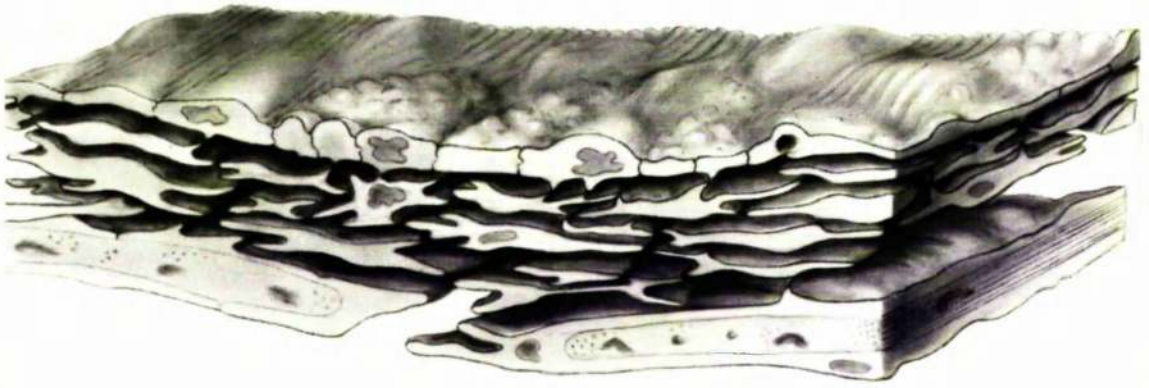

Fig.I2.Ib A three dimensional drawing of the trabecular wall of Schlemm's canal and the adjacent tissues when intraocular pressure is low.

can be compared to that of a one-way valve (see Johnstone and Grant, 1973). By adopting a configuration which is conducive to rapid flow during ocular hypertension (thus tending to reduce intraocular pressure) and a low flow configuration during hypotension (which would tend to stabilise intraocular pressure) the drainage tissues can be considered to function in a homeostatic manner.

A feature of normal aqueous dynamics is a demonstrable diurnal variation in intraocular pressure (Drance, 1960; deVenecia and Davis, 1963; Newell and Krill, 1965; Henkind, Leitman and Weitzman, 1973; Kitazawa and Hore, 1975 and others) which is thought to result from rhythmical fluctuations to the rate of aqueous production (Ericson, 1958). The valve-like action of the meshwork and the trabecular wall of Schlemm's canal would serve as a "dampening device" on intraocular pressure variation to maintain the amplitude of the pressure oscillations within strict limits. It is therefore of some interest that patients with chronic simple glaucoma, who would be expected to have a defective "dampening device", have more extreme pressure fluctuations than normal individuals (Langley and Swanljung, 1951; Duke-Elder, 1952; Goldmann, 1959; Drance, 1960; Katavisto, 1964; Newell and Krill, 1965; Kimura, 1965; Kitazawa and Horie, 1975 among others). Further, it has been shown that intraocular pressure variation is greater in patients with established chronic simple glaucoma than ocular hypertensives without trabecular pathology (Kitazawa and Horie, 1975).

Thus the facility of aqueous outflow, defined by Grant (1950) as "the extra volume of fluid driven out of the eye in unit time when the intraocular pressure is raised 1 mm Hg above normal", can be considered to be a measurement of functional competence of the meshwork valve action. In other words, facility is an index of a) meshwork

pliability and b) the ease by which temporary transcellular channels can arise in the endothelium on the trabecular aspect of Schlemm's canal. For a given increase or decrease of the pressure gradient, an outflow system with a high facility should be more capable of changing its configuration to either the hyper or hypotensive appearance (Fig. 12.1a and b) than one with a low facility of outflow.

The importance of the pliability of cells and extracellular elements to the outflow system is highlighted by flow studies through aldehyde fixed tissue. Aldehyde fixation reduces the pliability of the meshwork cells, turns the ground substances of the endothelial meshwork into a cross-linked immobile network (Bowes and Carter, 1968) and presumably "freezes" the vacuole and pore populations of the canal endothelium. Under such circumstances it has been shown that the rate of aqueous outflow and facility (Grant, 1963; Johnstone and Grant, 1973) and small particle (0.1 μm) penetration of the endothelial meshwork (Inomata, Bill and Smelser, 1972a) are drastically reduced.

In the post-mortem eye, the valve-like action of the trabecular meshwork and endothelial vacuolation could only be a mechanical response to pressure alteration (Johnstone and Grant, 1973). Given the similarity of the response produced in vivo then, by implication, it would seem reasonable that this is also a passive action. However it remains to be determined whether a) changes in trabecular configuration can be induced to effect, as opposed to their being the result of, pressure alteration, b) neurological or hormonal influences can modify the valve action of the outflow apparatus and c) there are nervous feedback mechanisms sensitive to, for example, changes to the spatial relationships between the various meshwork components.

Undoubtedly reduced resistance and increased outflow can be produced by the contraction of the ciliary muscle during accommodation

or under the influence of parasympathominetics (Armaly and Burian, 1958; Armaly and Jepson, 1962; Barány, 1962; Harris, 1968 and others). This is probably the result of alterations to the flow pathways by the action of the muscle on the pliable meshwork (Burian and Allen, 1955; Flocks and Zweng, 1957; Allen and Burian, 1965; Rohen, Lütjen and Barány, 1967).

Apart from the action of the ciliary muscle, which has been thought to act as a pump to assist the removal of aqueous humour (Hogan, Alvarado and Weddell, 1971), other effector mechanisms which alter spatial relationships are more speculative.

In this context François (1975) proposed that acid mucopolysaccharides may help to regulate intraocular pressure. He considered that when intraocular pressure drops, mucopolysaccharides in the trabecular cores are further polymerised to increase their hydration capacity. The hydration produces trabecular swelling and narrowing of intertrabecular spaces so that resistance is increased and fluid outflow decreased. When pressure is high, liberation of catabolic enzymes from the endothelial cells causes depolymerisation and trabecular shrinkage so that outflow will increase.

Although, from the present study, carbohydrate-rich complexes were demonstrated throughout the drainage tissues of four species, the appearance of the rhesus monkey outflow apparatus after either ocular hyper or hypotension was not consistent with François' hypothesis. Trabecular thickness remained constant throughout the pressure range and, at high pressures, the trabecular cores had a more pronounced rather than a reduced colloidal staining. However, there were more primary lysosomes in the trabecular endothelial cells of the hypertensive than the normotensive outflow system which could

be taken as evidence for the build up of the catabolic enzymes necessary for the depolymerisation of mucopolysaccharides. On the other hand, the finding that lysosomal complexes and lipid vesicles also became more prevalent at high pressure would indicate that intracellular (probably autolytic) rather than extracellular catabolism had been evoked.

Considerable research has centered around the identification of nerve terminals in the meshwork (see Chapter 4 and Tripathi, 1974 for a review of the literature). The nature of meshwork innervation is unsettled, but Tripathi (1974) concluded that both sensory and autonomic nerve fibres were present. It is conceivable that the terminals may serve as mechanoreceptors sensitive to change in meshwork configuration and thus have an indirect influence on the valve action of the drainage system through a feedback mechanism. As an alternative, nervous action may have a direct influence on the outflow tissues by controlling for example, vacuolation (Tripathi and Tripathi, 1972) or the size of trabecular endothelial cells [since their swelling and shrinking would narrow and widen inter-trabecular spaces (Tripathi, 1974)]. The present study has not helped to identify a particular neuronal controlling mechanism but has, by the identification of gap junctions (electrotonic coupling devices) in the canal endothelium and between meshwork cells (Chapter 5), made nervous control a more attractive proposition.

12.2 The giant vacuoles and transcellular channels

It is considered, on the basis of the findings from this thesis, that the bulk of aqueous passage through the endothelium lining the trabecular wall of Schlemm's canal is by way of a system of temporary pressure-sensitive vacuolar and non-vacuolar transcellular channels.

The precise sequence of events which results in the formation and the eventual elimination of the channels remains unknown. However, from the morphological findings listed below (a - h), a developmental progression can be proposed.

a) Vacuole and pore formation did not appear to depend, to any significant extent, on cellular energy and protein production.

b) The bulk of the vacuole population consisted of invaginations from the meshwork surface and only a small proportion were transcellular channels.

c) Luminal invaginations were identified.

d) The dimensions of the giant vacuoles at each pressure level within the near-physiological range were such that there were far more small than large vacuoles (a skew distribution).

e) Cytoplasmic microfilaments were found in close association with the vacuole membrane.

f) Meshwork pore widths and, to a lesser extent, lumen pore widths had a positive correlation with the appropriate vacuole widths.

g) Minipores were associated with attenuated endothelium and therefore became more prominent at elevated pressures.

h) The pressure dependent non-vacuolar transcellular channels were associated with the narrow marginal regions of the endothelial cells.

The morphological evidence suggests that extensive energy consumption or protein synthesis are not necessary for vacuolar development so it would appear that the process does not involve membrane production. Substantial membrane production is not essential if the vacuoles are considered as deep invaginations of the cell surface rather than cytoplasmic organelles. The vacuolation process

would then be a progressive distortion of the cell. Thus the factors controlling the rate of vacuole development would be the pressure gradient across the cell opposed by the natural elasticity of the endothelial cell cytoplasm. Cytoplasmic microfilaments may contribute to endothelial pliability and, conceivably, if the microfilaments have contractile properties these structures may be involved in the initial invagination process.

The enlarging vacuole causes attenuation of the cytoplasm towards the canal surface. Cytoplasmic attenuation eventually results in the formation of an opening or pore. It is not easy to explain or demonstrate the exact mechanism by which a pore is formed. A possible precursor of the lumen pore may be the fenestration or minipore, previously described in vacuolar shells by Wulle (1972) and Inomata, Bill and Smelser (1972a), which the present study has shown to become increasingly prevalent in attenuated endothelium. It would seem likely that a minipore appears after the vacuolar endothelium has reached a critical degree of attenuation. A minipore would constitute a region of weakness in the stretched vacuolar shell. The subsequent rupture of the fenestration could result in the production of the vacuolar lumen pore. When such a stage is reached, the vacuole constitutes a transcellular channel through which aqueous, particulate material and cells may pass (see Chapter I for details of particle passage through the outflow apparatus).

The process by which a non-vacuolar transcellular channel develops may be essentially similar to that of the vacuolar transcellular channel. At a thicker part of the endothelium, aqueous transfer necessitates vacuole formation but at narrower marginal regions (where less thinning is needed to produce a fenestration and then an opening), a smaller non-vacuolar channel is sufficient.

When intraocular pressure is stable it has been suggested that the various vacuolar and non-vacuolar channels are in a "fluid" state of continual formation, collapse and reformation at the same or a different site. This is implicit in Tripathi's theory of the "dynamic" endothelial vacuolation cycle (Tripathi, 1968, 1969a and b, 1971a, 1973a and b, 1974; Cole and Tripathi, 1971). If the Tripathi model of cyclical vacuolation is to be accepted an explanation must be provided for the collapse of the vacuolar transcellular channel.

Presumably vacuolar collapse results when the inflow of fluid into the channel is reduced below a level necessary to maintain its patency. Vacuolar collapse, therefore, may be produced by the active constriction of the meshwork pore but, as this would involve the expenditure of cellular energy, the explanation is not easily acceptable.

It is more likely that the collapse is achieved by a passive process. For example, the effective diameter of the meshwork pore could be reduced by a mechanical valve-like action of the cellular and extracellular elements in the endothelial meshwork immediately adjacent to the giant vacuole. If the meshwork elements are drawn towards the meshwork pore with the general flow of aqueous to and then through the transcellular channel, transendothelial flow would diminish as the pathway into the vacuole becomes occluded. As an alternative, the collapse could be initiated by changes in flow characteristics rather than by alterations to vacuolar morphology. With a faster transendothelial flow than that through the part of the endothelial meshwork which "services" the vacuole, the pressure differential across the channel would decrease due to insufficient filling of the subvacuolar space. After a while, the pressure

differential would reach a critical level and be insufficient to maintain a viable channel.

The end stage or residual vacuole would appear to be an invagination from the canal surface of the endothelium, a vesicle with a lumen pore but no meshwork pore. The mechanisms which have been proposed to explain how the vacuolar transcellular channel would collapse are also applicable to the non-vacuolar channel.

It has been shown that small vacuoles made up the bulk of the vacuole population irrespective of pressure. In terms of the vacuole cycle, the preponderance of small vacuoles would be explained if vacuole development becomes progressively faster with increase in vacuole size. A positive correlation between the size of the meshwork pores and the size of the corresponding giant vacuoles indicates that such is the case, since the larger the meshwork pore the greater the amount of fluid which can enter the vacuole.

The vacuolation cycle theory proposes that vacuolar transcellular channels are short lived, temporary structures. It is therefore necessary to postulate that there is a continual reformation of transcellular channels from "fresh" vacuoles to provide the requisite number of flow pathways for transendothelial drainage into Schlemm's canal. From the available information, it is equally possible that, at steady-state intraocular pressure, the vacuole population is stable. In other words, once there are sufficient numbers to account for drainage the transcellular channels do not collapse and no more are formed until there is a change in flow dynamics. Therefore, it could be argued that at normotensive pressure the vast majority of the vacuoles remain as blind pockets. Factors which could determine why a few vacuoles develop into flow pathways, and why the majority do not, are probably regional differences in the flow pattern through

the endothelial meshwork (preferential flow pathways were discussed in Chapter 10) and localised variation in endothelial resilience.

Although much still remains unclear about vacuolar morphogenisis, a weight of evidence now exists to implicate giant vacuoles in aqueous transfer. Not only are giant vacuoles associated with the endothelium of Schlemm's canal but they are found in the endothelial cells lining the angular aqueous plexus of a great variety of vertebrate species. Thus vacuoles represent a common mechanism for aqueous drainage in a diversity of animals from primates to dogfish (Tripathi, 1974).

Giant vacuoles are not peculiar to the outflow system of the eye but are also associated with the mesothelium lining the arachnoid granulations of the brain (Van der Zypher, 1971; Tripathi, 1973a; Tripathi and Tripathi, 1974). Tripathi proposed that a mesothelial vacuolation cycle provides the requisite number of transcellular channels for the passage of cerebrospinal fluid into the superior sagittal sinus. As the dynamics and characteristics of aqueous humour and cerebrospinal fluid outflow compare favourably (Davson, 1972), it would be expected that the drainage pathways of the eye and brain are morphologically and functionally similar.

12.3 The resistance to aqueous outflow

The obstruction or hindrance to aqueous passage offered by the outflow pathways will depend on the size, length and complexity of the functional flow routes. In the case of the endothelial meshwork the density and nature of the extracellular materials through which the aqueous passes must also be taken into consideration. The general concensus of opinion is that the bulk of the resistance to aqueous

outflow lies between the anterior chamber angle and the lumen of Schlemm's canal (see Chapter I).

On anatomical grounds it would seem reasonable that the narrow extracellular spaces of the endothelial meshwork and the small transcellular channels through the endothelium lining the trabecular aspect of Schlemm's canal have a relatively lower conductance than the pathways through the trabecular portion of the meshwork. That the trabecular wall of Schlemm's canal is a region of high resistance to aqueous outflow has been accepted by many morphologists (Rohen, 1960; Tripathi, 1968, 1969a, 1969b, 1971a, 1972, 1974; Segawa, 1970a, 1973; Inomata, Bill and Smelser, 1972a; Bill and Svedbergh, 1972) but it is of some importance to distinguish between the relative contributions made by the component layers which comprise the wall. Tripathi (1971a) entertained the possibility that the hypothetical vacuolation cycle (during which transendothelial pores are formed) may be responsible for the maintenance of intraocular pressure. Such a possibility would only remain attractive if the endothelial monolayer made a particularly large contribution to the total resistance.

Evidence to the contrary has been provided by Bill and Svedbergh (1972) who conducted a pore analysis of the normal human canalicular endothelium by scanning electron microscopy. The authors considered that the total pore numbers in the endothelial cells of the trabecular wall of Schlemm's canal approached 20,000 and maximum pore diameter was in the region of 3.0 μm. The total conductance was estimated from calculations

based on Poiseuille's law* and found to be high. It was concluded that only about 10% of the total resistance was located in the flow pathways through the monolayer. By implication, the narrow spaces of the endothelial meshwork were thought to be the predominant rate limiting region in the outflow route.

The pore frequencies and size distribution profiles outlined by Bill and Svedbergh were somewhat similar to those found by scanning electron microscopy in the 15 mm Hg tissue of the present study (see Chapter 11, Figs 11 10 to 12). However, it is not necessarily substantiated that the canal endothelium makes a relatively unimportant contribution to flow impedance by either the current results or those of Bill and Svedbergh.

Calculations of conductance from scanning electron microscopic observations by means of Poiseuille's equations must be interpreted with some caution becuase of the following considerations:-

---

*FOOTNOTE: Poiseuille's law was used by McEwen (1958) to determine the numbers of pores at various sizes which would be necessary to account for aqueous outflow. Cole and Tripathi (1971) applied Poiseuille's flow equations to vacuolar transcellular channels to find if their incidence was sufficient to account for bulk drainage of aqueous humour. The law relates flow through a channel as a function of pressure drop, viscosity of the fluid passing through and the radius of the channel. Transendothelial channels are too short for the direct application of Poiseuille's law and certain corrections have to be made.

a) The preparation and drying procedures for scanning electron microscopy are not without hazard. Shrinking or flattening of the delicate canal monolayer could either produce artifactual pores or increase the size of "true" pores. Thus, from my own results, both pore size and incidence at 15 mm Hg was greater by scanning than transmission electron microscopy (Chapter 11, Fig. 11.11). The difference being such that, while the scanning electron microscopic findings indicate that the canal endothelium has a relatively high conductance, the transmission electron microscopic data indicate that the endothelium could make an important contribution to the maintenance of intraocular pressure.

b) Of the "true" pores identified under the scanning electron microscope a proportion will be flask shaped invaginations from the canal surface of the endothelium and, therefore, will not be functional (see Chapter 10).

c) Flow calculations based on Poiseuille's law assume that the passageways are rigid uniform channels. The actual passageways are temporary, pliable structures of unknown morphogenesis and duration so that resistance, far from being a property of a static system, can be considered as the ability of the pores to adjust their configuration and incidence in response to an altered flow pattern.

d) Bill and Svedbergh (1972) assumed that the transcellular channels were smooth, but they have been shown (see Chapter 6) to have a coating of complex polysaccharides and are therefore sticky. The coat will reduce the effective diameter of the pathways (see Chapter 6, Fig. 6.17) and this may have a considerable influence on flow characteristics through these channels (McEwen, 1958).

To quote Duke-Elder (1968) "an obvious objection to this mathematical treatment is that Poiseuille's law is concerned with flow through straight rigid tubes arranged in a simple system, while the channels of drainage in the angle of the anterior chamber are not rigid but complex, ...". Undoubtedly the endothelial meshwork is an important aqueous flow rate limiting region however the significance of the other component of the canal's trabecular wall, the endothelial monolayer, has not as yet been satisfactorily assessed.

12.4 Final comments

A limitation of this investigation was that the rates of aqueous outflow and facilities were not determined in the eyes maintained at various levels of intraocular pressure. Clearly, the physiological data would have provided the necessary information to correlate the hydrodynamics of aqueous outflow with the anatomical appearance of the outflow system. It was, however, valid to keep experimentation as simple as possible because the manipulations involved in facility determinations may have predjudiced the findings. Forearmed with the results of the present study, allowance can now be made for manipulative effects on the delicate outflow tissues and a combined physiological and anatomical study of the outflow apparatus at graded levels of intraocular pressure would be a logical projection of the current work.

The important contribution made by the endothelial meshwork to outflow dynamics has been emphasised throughout this thesis and a fruitful line of future research would be to undertake a careful cytochemical analysis of its extracellular constituents. Preliminary observations made in the present thesis, by Segawa (1971b)

and by Armaly and Wang (1975) indicate the presence of a matrix of mucopolysaccharides. As yet, the influence of this matrix on the rate of fluid passage is speculative because attempts to demonstrate a hyaluronidase effect on aqueous outflow have provided variable results (see Chapter 6). Obviously, combined physiological and anatomical research involving perfusion of various enzymes (for example hyaluronidase, neuraminidase and chondroitinases) and colloidal staining may reveal more about the characteristics and properties of the matrix and help to resolve some of the controversy.

From autoradiographic procedures, it may be possible to determine whether the native cells of the endothelial meshwork are in an active synthesising phase and so discover if the collagenous and mucopolysaccharide ground substances represent a stagnant pool of material or are continually being reformed and replaced. The results may have significance to primary open angle glaucoma where the abnormal accumulation of fibrous and amorphous material within the endothelial meshwork is a feature of the diseased outflow system (Rohen and Witmer, 1972; Tripathi, 1972).

An important source of pathological tissue is the segments of trabecular meshwork removed in the surgical treatment of glaucoma (trabeculectomy and other related operative procedures). As yet, the material has been of limited histological value (see Yanoff and Fine, 1975). Major problems are that trabeculectomy specimens must be subject to the hazards of handling artefact and pressure alteration prior to immersion fixation. As indicated by the present study, the spatial relationships of the trabecular meshwork components and the incidence of temporary pressure dependent flow pathways will bear little relationship to their in vivo condition.

Although purely anatomical studies of trabeculectomy segments are fraught with interpretational difficulties, the biochemical analysis of the extracellular component of trabeculectomy specimens and the culture of glaucomatous meshwork cells may be more rewarding.

Culture of trabecular meshwork elements, of which there are only preliminary accounts (François and Troncoso, 1974; François, 1975), affords the opportunity to investigate cellular responses and properties in a biologically controlled environment. Comparison could be made between for example the phagocytic activity*, synthetic activity, pharmacological responses and mechanical properties (pliability) of normal and diseased meshwork cells and provide a significant contribution to glaucoma research.

Clearly, much remains obscure about the primary pathology associated with chronic simple glaucoma and the nature of aqueous transfer across the normal and diseased outflow system. The present study has underlined the need for intraocular pressure control during tissue fixation. Future anatomical studies must take into account the pliability of the meshwork tissues and the pressure-sensitivity of transendothelial flow pathways. The author considers that anterior chamber infusion is the primary fixation technique of choice for the investigation of the drainage system. In my hands, tissue appearance was more satisfactory by anterior chamber infusion

---

*FOOTNOTE: Trabecular meshwork cells have a considerable phagocytic capability (Rohen and Van der Zyphen, Shabo and Maxwell, 1972a and b; Grierson and Lee, 1973; Tripathi, 1974) and the meshwork has been described as a biological filter (see Tripathi, 1974). Bill (1975) proposed that phagocytic dysfunction may be a primary factor in chronic simple glaucoma.

than vascular perfusion or immersion fixation. Fixative penetration may be slower by the anterior chamber route than by retrograde perfusion via the aqueous veins (a system used by Shabo, Reese and Gaasterland, 1973 but not in the present study) but the passage of fixative solution follows the direction of aqueous flow at physiological rates.

Where pressure regulated fixation is not always practical, as with human tissue, great care must be taken if misleading conclusions are to be avoided. However, with a better understanding of the valve-action of the normal outflow system, progress may follow in the understanding of those disease processes which make the action defective.

A P P E N D I C E S

Tissue blocks from all the specimens listed in the following appendices were processed conventionally for transmission electron microscopy. Appropriate symbols indicate whether additional tissue blocks were treated "en bloc" with uranyl acetate, stained with colloidal thorium and iron or used for scanning electron microscopy.

KEY

●	-	tissue blocks treated "en bloc" with uranyl acetate.
✡	-	tissue blocks treated with colloidal thorium.
✶	-	tissue blocks treated with colloidal iron (with and without subsequent conversion to prussian blue).
▲	-	tissue used for scanning electron microscopy.

APPENDIX

I

THE NORMAL OUTFLOW APPARATUS (HUMAN)

	CASE NO.	SEX	AGE YEARS	MODE OF I^{ry} FIXATION	HISTORY
1)	03/71	M	54	Immersion	Choroidal melanoma ▲
2)	04/71	F	45	Immersion	Choroidal melanoma ▲
3)	13/72	F	21	Immersion	Choroidal melanoma ●☆✶▲
4)	67/72	F	57	Immersion	Choroidal melanoma ●☆✶
5)	94/72	M	53	Immersion	Choroidal melanoma ●☆✶▲
6)	32/73	F	75	Immersion	Choroidal melanoma ●
7)	36/73	F	64	Immersion	Choroidal melanoma
8)	43/73	F	76	Immersion	Choroidal melanoma ●☆✶▲
9)	47/73	M	57	Immersion	Choroidal melanoma ☆✶
10)	79/73	F	68	Immersion	Choroidal melanoma ●
11)	146/73	M	1	Immersion	Pseudoglioma of optic disc ●☆✶▲
12)	51/74	F	63	Immersion	Choroidal melanoma ▲
13)	54/74	F	63	Immersion	Choroidal melanoma ●✶▲
14)	76/74	F	38	Immersion	Choroidal melanoma ●✶▲
15)	81/74	M	37	Immersion	Choroidal melanoma ●▲

APPENDIX

2

THE NORMAL OUTFLOW APPARATUS (BABOON)

	ANIMAL NO.	SEX	WEIGHT (IN KILOS)	EYE	MODE OF I^{TY} FIXATION
1)	14/71	F	12	R●▲ L●▲	Immersion
2)	16/72	F	11	R✶▲ L●☆✶▲	Anterior Chamber Infusion Arterial perfusion
3)	84/72	F	13	R☆✶▲ L▲	Arterial Perfusion
4)	85/72	M	12.5	R●☆✶▲ L☆✶▲	Anterior Chamber Infusion
5)	86/72	M	11	R☆✶▲ L●▲	Anterior Chamber Infusion
6)	93/72	F	12	R●▲ L☆✶▲	Immersion
7)	63/73	F	15	R✶▲ L●☆✶	Immersion
8)	148/73	M	14	R●☆✶ L●	Immersion
9)	202/73	F	9	R●☆✶▲	Immersion

APPENDIX

3

THE NORMAL OUTFLOW APPARATUS (RHESUS MONKEY)

	ANIMAL NO.	SEX	WEIGHT (IN KILOS)	EYE	MODE OF I^{ry} FIXATION
1)	19/71	F	5.2	R●✡✶	Arterial Perfusion
2)	20/71	M	6.0	R●✡✶ L●▲	Arterial Perfusion
3)	28/71	F	5.5	R●✡✶▲ L●✡✶▲	Immersion
4)	30/71	F	5.4	R●✡✶▲ L●✡✶▲	Immersion
5)	2/72	F	4.3	R●✡✶▲ L●✡✶▲	Immersion
6)	28/72	F	3.0	R●✡✶▲	Anterior Chamber Infusion
7)	29/72	F	3.0	R●✡✶	Anterior Chamber Infusion
8)	31/72	F	3.0	R●✡✶▲	Anterior Chamber Infusion

APPENDIX

4

THE NORMAL OUTFLOW APPARATUS (RABBIT)

	ANIMAL NO.	SEX	WEIGHT (IN KILOS)	EYE	MODE OF I^{ry} FIXATION
1)	27/71	M	2.4	R● L●✡✶▲	Arterial Perfusion
2)	31/71	M	2.2	R●✡✶ L●✡✶▲	Arterial Perfusion
3)	1/72	M	2.1	R●✡✶ L●✡✶	Arterial Perfusion
4)	56/72	F	2.2	R●✡✶ L●✡✶	Arterial Perfusion
5)	96/72	F	2.0	R L	Anterior Chamber Infusion
6)	108/72	F	1.7	R▲ L	Anterior Chamber Infusion Immersion
7)	117/72	F	1.8	R▲ L●	Anterior Chamber Infusion Immersion
8)	118/72	F	3.0	R▲ L●	Anterior Chamber Infusion Immersion
9)	10/73	F	1.0	L●✡✶▲	Immersion
10)	15/73	F	0.9	L●✡✶▲	Immersion
11)	17/73	M	1.2	L●✡✶▲	Immersion

APPENDIX 4

(CONTINUED)

THE NORMAL OUTFLOW APPARATUS (RABBIT)

	ANIMAL NO.	SEX	WEIGHT (IN KILOS)	EYE	MODE OF I^{ry} FIXATION
12)	24/73	F	1.5	$L_{\bullet}$	Immersion
13)	35/73	F	1.7	$L_{\bullet\star\star\blacktriangle}$	Immersion
14)	49/73	F	2.2	$L_{\bullet\star\star\blacktriangle}$	Immersion
15)	24/74	F	1.8	$L_{\bullet\star\star\blacktriangle}$	Immersion
16)	25/74	F	1.1	$L_{\bullet\star\star\blacktriangle}$	Immersion

APPENDIX

5

A - RUTHENIUM RED TREATED BABOON TISSUE

	ANIMAL NO.	SEX	WEIGHT (IN KILOS)	EYE	MODE OF I^{ry} FIXATION
1)	170/73	M	20.0	R L	Immersion
2)	176/73	F	18.0	R L	Immersion
3)	178/73	F	17.0	R L	Immersion
4)	58/74	F	16.5	R L	Immersion
5)	157/74	M	25.0	R L	Immersion

B - RUTHENIUM RED TREATED RABBIT TISSUE

	ANIMAL NO.	SEX	WEIGHT (IN KILOS)	EYE	MODE OF I^{ry} FIXATION
1)	151/73	F	1.8	R L	Immersion
2)	360/73	F	2.3	L	Immersion
3)	59/74	F	2.0	R L	Immersion
4)	113/74	F	2.0	R L	Immersion

APPENDIX

6

EXPERIMENTS TO INVESTIGATE INTRAOCULAR PRESSURE EFFECTS ON THE RHESUS MONKEY OUTFLOW APPARATUS.

	ANIMAL NO.	SEX	WEIGHT (IN KILOS)	EYE	I.O.P. (mm.Hg.)	MODE OF I^{ry} FIXATION
1)	28/72	F	3.0	R ●✡✶▲ L ●✡✶▲	Not Regulated	Anterior Chamber Infusion
2)	29/72	F	3.0	R ●✡✶ L ●✡	Not Regulated	Anterior Chamber Infusion
3)	31/72	F	3.0	R ●✡✶▲ L ●✡✶▲	Not Regulated	Anterior Chamber Infusion
4)	58/72	M	4.5	R ●✡✶▲ L ●▲	30 15	Anterior Chamber Infusion
5)	119/72	F	3.0	R ●▲ L ●	30 15	Anterior Chamber Infusion
6)	125/72	M	3.5	R ●✡✶▲ L ●	15 30	Anterior Chamber Infusion
7)	163/72	M	3.0	R ✡✶ L ✡✶	15 30	Carotid Perfusion
8)	19/73	M	3.1	R ●✡✶▲ L ●✡✶▲	30 15	Carotid Perfusion

APPENDIX 6

(CONTINUED)

EXPERIMENTS TO INVESTIGATE INTRAOCULAR PRESSURE EFFECTS ON THE RHESUS MONKEY OUTFLOW APPARATUS.

	ANIMAL NO.	SEX	WEIGHT (IN KILOS)	EYE	I.O.P. (mm.Hg.)	MODE OF I^{ry} FIXATION
9)	50/73	F	3.2	R●✲✶▲ L●✲✶▲	15 22	Anterior Chamber Infusion
10)	51/73	F	3.3	R●✲✶▲ L●▲	15 22	Anterior Chamber Infusion
11)	52/73	F	3.2	R●✲✶▲ L●✲✶	15 22	Anterior Chamber Infusion
12)	74/73	F	3.5	R●✲✶▲ L●✲✶▲	8 15	Anterior Chamber Infusion
13)	75/73	F	5.0	R●✲✶▲ L●✲✶▲	15 8	Anterior Chamber Infusion
14)	76/73	F	5.0	R●✲✶▲ L●✲✶▲	15 8	Anterior Chamber Infusion
15)	81/73	F	4.8	R●✲✶▲ L●✲✶▲	50 0	Anterior Chamber Infusion Immersion

APPENDIX 6

(CONTINUED)

EXPERIMENTS TO INVESTIGATE INTRAOCULAR PRESSURE EFFECTS ON THE RHESUS MONKEY OUTFLOW APPARATUS

	ANIMAL NO.	SEX	WEIGHT (IN KILOS)	EYE	I.O.P. (mm.Hg.)	MODE OF I^{ry} FIXATION
16)	140/73	M	4.5	R●☆✶▲	50	Anterior Chamber Infusion
				L☆✶▲	0	Immersion
17)	141/73	F	3.8	R●☆✶▲	50	Anterior Chamber Infusion
				L●☆✶▲	0	Immersion

APPENDICES 7a - f.

The following appendices show the vacuole distributions from 100 serial thick sections (150µm) of canal endothelium according to maximum length (in sections) and maximum width (in µm). The samples of canal endothelium came from rhesus monkey eyes maintained at intraocular pressures between 8 and 30mm.Hg. All measurements were made directly from light micrographs. (see chapter 8 for further details).

APPENDIX

7a

DISTRIBUTION OF GIANT VACUOLES

ACCORDING TO THEIR LENGTH

FROM EYES MAINTAINED AT 30 and 15mm.Hg.

VACUOLE LENGTH IN SECTIONS	ANIMAL 58/72 VACUOLE NOS.		ANIMAL 119/72 VACUOLE NOS.		ANIMAL 125/72 VACUOLE NOS.	
	30mm.Hg. Eye	15mm.Hg. Eye	30mm.Hg. Eye	15mm.Hg. Eye	30mm.Hg. Eye	15mm.Hg. Eye
1	64	45	85	33	63	32
2	144	81	87	56	129	58
3	153	87	135	64	132	45
4	171	60	73	34	99	25
5	126	39	59	20	84	14
6	93	30	36	8	33	9
7	90	12	31	4	36	6
8	43	7	22	2	27	3
9	18	9	10	2	18	1
10		3	15	1	15	5
11	19	4	3		6	2
12	27		5		3	1
13	10		6		5	
14	6	1	3		4	
15	16		6		1	
16	5		1		3	
17	4		2		2	
18			2			
19	7					
20	5					

APPENDIX 7a

CONTINUED

DISTRIBUTION OF GIANT VACUOLES

ACCORDING TO THEIR LENGTH

FROM EYES MAINTAINED AT 30 and 15mm.Hg.

VACUOLE LENGTH IN SECTIONS	ANIMAL 58/72 VACUOLE NOS.		ANIMAL 119/72 VACUOLE NOS.		ANIMAL 125/72 VACUOLE NOS.	
	30mm.Hg. Eye	15mm.Hg. Eye	30mm.Hg. Eye	15mm.Hg. Eye	30mm.Hg. Eye	15mm.Hg. Eye
21	1		3		1	
22	2				2	
23					1	
24			2			
25	4		1			
26	2					
27	3					
28	2				1	
29	1					
30	1					
Over 30	7		1			

APPENDIX

7b

DISTRIBUTION OF GIANT VACUOLES

ACCORDING TO THEIR WIDTH

FROM EYES MAINTAINED AT 30 and 15mm.Hg.

VACUOLE WIDTH IN µM	ANIMAL 58/72 VACUOLE NOS.		ANIMAL 119/72 VACUOLE NOS.		ANIMAL 125/72 VACUOLE NOS.	
	30mm.Hg. Eye	15mm.Hg. Eye	30mm.Hg. Eye	15mm.Hg. Eye	30mm.Hg. Eye	15mm.H Eye
Less than 1.1	75	82	25	24	42	57
2.1	128	64	101	78	123	69
3.1	141	136	155	70	63	37
4.1	180	31	35	17	132	9
5.1	71	36	66	23	54	9
6.1	98	21	75	11	81	1
7.1	81	1	23	1	30	7
8.1	72	6	36		66	
9.1	49	2	30		12	1
10.1	26	1	6		30	
11.1	13		12		6	
12.1	10		19		12	
13.1	15				3	
14.1	11		6		3	
15.1	17		7		3	
16.1	12		1		6	

APPENDIX 7b

CONTINUED

DISTRIBUTION OF GIANT VACUOLES

ACCORDING TO THEIR WIDTH

FROM EYES MAINTAINED AT 30 and 15mm.Hg.

VACUOLE WIDTH IN µM	ANIMAL 58/72 VACUOLE NOS.		ANIMAL 119/72 VACUOLE NOS.		ANIMAL 125/72 VACUOLE NOS.	
	30mm.Hg. Eye	15mm.Hg. Eye	30mm.Hg. Eye	15mm.Hg. Eye	30mm.Hg. Eye	15mm.Hg. Eye
17.1	12		1		2	
18.1	6		2		1	
19.1	2					
20.1	2		1			
21.1	2					
22.1	1					
Less than 35.1			1			

APPENDIX

7c

DISTRIBUTION OF GIANT VACUOLES ACCORDING TO THEIR LENGTH FROM EYES MAINTAINED AT 22 and 15mm.Hg.

VACUOLE LENGTH IN SECTIONS	ANIMAL 50/73 VACUOLE NOS.		ANIMAL 51/73 VACUOLE NOS.		ANIMAL 52/73 VACUOLE NOS.	
	22mm.Hg. Eye	15mm.Hg. Eye	22mm.Hg. Eye	15mm.Hg. Eye	22mm.Hg. Eye	15mm.H, Eye
1	24	39	84	33	75	42
2	64	51	153	69	101	57
3	88	45	93	42	89	69
4	60	37	58	21	56	30
5	45	8	39	25	28	7
6	31	5	21	16	13	12
7	21	7	24	4	22	10
8	20	1	24	5	21	3
9	12	2	15	2	8	6
10	4		12	2	14	6
11	7	3	15		8	2
12	3		1	1	3	1
13	8	1	3	4	7	1
14	2	1	2	2	4	2
15		1		1	1	
16	1		1	1	1	1
17						

APPENDIX 7c

CONTINUED

DISTRIBUTION OF GIANT VACUOLES

ACCORDING TO THEIR LENGTH

FROM EYES MAINTAINED AT 22 and 15mm.Hg.

VACUOLE LENGTH IN SECTIONS	ANIMAL 50/73 VACUOLE NOS.		ANIMAL 51/73 VACUOLE NOS.		ANIMAL 52/73 VACUOLE NOS.	
	22mm.Hg. Eye	15mm.Hg. Eye	22mm.Hg. Eye	15mm.Hg. Eye	22mm.Hg. Eye	15mm.Hg. Eye
18		1				1
19						2
20	1	1				
21						
22		1				

APPENDIX

7d

DISTRIBUTION OF GIANT VACUOLES

ACCORDING TO THEIR WIDTH

FROM EYES MAINTAINED AT 22 and 15mm.Hg.

VACUOLE WIDTH IN µM	ANIMAL 50/73 VACUOLE NOS.		ANIMAL 51/73 VACUOLE NOS.		ANIMAL 52/73 VACUOLE NOS	
	22mm.Hg. Eye	15mm.Hg. Eye	22mm.Hg. Eye	15mm.Hg. Eye	22mm.Hg. Eye	15mm.Hg Eye
Less than 1.1	52	69	91	39	132	110
2.1	87	60	162	72	69	34
3.1	80	39	124	49	90	33
4.1	16	6	50	21	21	9
5.1	48	15	28	19	48	13
6.1	80	9	20	16	39	1
7.1	4	3	19	5	18	1
8.1	13		18	4	2	
9.1	7		10	9	5	
10.1	1		6	4	2	
11.1	1	1	3			
12.1	2	1	3			
13.1		1				

APPENDIX

7e

DISTRIBUTION OF GIANT VACUOLES

ACCORDING TO THEIR LENGTH

FROM EYES MAINTAINED AT 8 and 15mm.Hg.

VACUOLE LENGTH IN SECTIONS	ANIMAL 74/73 VACUOLE NOS.		ANIMAL 75/73 VACUOLE NOS.		ANIMAL 76/73 VACUOLE NOS.	
	8mm.Hg. Eye	15mm.Hg. Eye	8mm.Hg. Eye	15mm.Hg. Eye	8mm.Hg. Eye	15mm.Hg. Eye
1	12	52	15	30	20	52
2	27	104	12	57	34	75
3	24	44	8	72	13	38
4	4	20	1	42	9	23
5	4	20	1	21	11	17
6	5	8	1	9	2	12
7	1	9		10	1	3
8	1	2	1	4		9
9		2		1		7
10		2		1		4
11		1				2
12		4		1		5
13						1
14		1		1		1
15						1
16		2		1		
17				1		
18		1				

APPENDIX

7f

DISTRIBUTION OF GIANT VACUOLES

ACCORDING TO THEIR WIDTH

FROM EYES MAINTAINED AT 8 and 15mm.Hg.

VACUOLE WIDTH IN µM	ANIMAL 74/73 VACUOLE NOS.		ANIMAL 75/73 VACUOLE NOS.		ANIMAL 76/73 VACUOLE NOS.	
	8mm.Hg. Eye	15mm.Hg. Eye	8mm.Hg. Eye	15mm.Hg. Eye	8mm.Hg. Eye	15mm.Hg Eye
Less than 1.1	21	76	22	45	14	12
2.1	39	104	5	78	48	79
3.1	10	44	9	33	13	46
4.1	6	20	3	50	9	33
5.1	2	4		16	5	9
6.1		3		16	1	1
7.1		10		4		12
8.1		7		3		3
9.1				4		5
10.1				1		4
11.1				1		1
12.1		3				2
13.1		1				

REFERENCES

Agarwal, L.P., Singh, I.V.N., Mishra, R.K., and Khosla, P.K., (1972)
Light and electron-microscopic studies of the "presumed elastic" component of the trabeculae and scleral spur of the human eye.
Orient. Arch. Ophth., 10, 151.

Allen, L., and Burian, H.M., (1965)
The valve action of the trabecular meshwork studies with functional silicone models.
Amer. J. Ophth., 59, 382.

Allen, L., Burian, H.M., Braley, A.E., (1955)
The anterior border ring of Schwalbe and the pectinate ligament.
Arch. Ophth., 53, 799.

Anderson, D.R., (1971)
Scanning electron microscopy of primate trabecular meshwork.
Amer. J. Ophth., 71, 91.

Armaly, M.F., and Burian, H.M., (1958)
Changes in the tonogram during accommodation.
Arch. Ophth., 60, 60.

Armaly, M.F., and Jepson, N.C., (1962)
Accommodation and the dynamics of steady-state intraocular pressure.
Invest. Ophth., 1, 480.

Armaly, M.F., and Wang, Y., (1975)
Demonstration of acid mucopolysaccharides in the trabecular meshwork of the rhesus monkey.
Invest. Ophth., 14, 507.

Asayama, J., (1901)

Zur anatomie des ligamentum pectinatum.

v. Graefes Arch. klin. exp. Ophth., 53, 113.

Ascher, K.W., (1942)

Aqueous veins. Preliminary note

Amer. J. Ophth., 25, 31.

Ashton, N., (1951)

Anatomical study of Schlemm's canal and aqueous veins by means of neoprene casts. I. Aqueous veins.

Brit. J. Ophth., 35, 291.

Ashton, N., (1952)

Anatomical study of Schlemm's canal and aqueous veins by means of neoprene casts. II. Aqueous veins.

Brit. J. Ophth., 36, 265.

Ashton, N., (1958)

Discussion on the trabecular structure in relation to the problem of glaucoma.

Proc. Roy. Soc. Med., 52, 69.

Ashton, N., (1959)

The role of the trabecular structure in the problem of simple glaucoma, particularly with regard to the significance of mucopolysaccharides.

In "Proceedings of the 4th Macy Conference on Glaucoma" (ed. F.W. Newell), p.89. Princeton, N.J.

Ashton, N., (1960)

The exit pathway of the aqueous.

Trans. Ophth. Soc. U.K., 80, 397.

Ashton, N., Brini, A., and Smith, R., (1956)

Anatomical studies of the trabecular meshwork of the normal human eye.

Brit. J. Ophth., 36, 257.

Barány, E.H., (1953)

In vitro studies of the resistance to flow through the angle of the anterior chamber.

Acta Soc. Med., 59, 260.

Barány, E.H., (1956)

The action of different kinds of hyaluronidase on the resistance to flow through the angle of the anterior chamber.

Acta Ophth., 34, 397.

Barány, E.H., (1962)

The mode of action of pilocarpine on outflow resistance in the eye of a primate (Cercopithecus ethiops).

Invest. Ophth., 1, 712.

Barány, E.H., (1963)

A mathematical formulation of intraocular pressure as dependent on secretion, ultrafiltration, bulk outflow, and osmotic reabsorption of fluid.

Invest. Ophth., 2, 584.

Barány, E.H., (1964)

Simultaneous measurement of changing intraocular pressure and outflow facility in the vervet monkey by constant pressure infusion.

Invest. Ophth., 3, 135.

Bárány, E.H., and Kinsey, V.E., (1949a)

The rate of flow of aqueous humour I.

Amer. J. Ophth., 32, 177.

Bárány, E.H., and Kinsey, V.E., (1949b)

The rate of flow of aqueous humour II.

Amer. J. Ophth., 32, 189.

Bárány, E.H., and Scotchbrook, S., (1954)

Influence of testicular hyaluronidase on the resistance to flow through the angle of the anterior chamber.

Acta Physiol. Scand., 30, 240.

Becker, B., and Constant, M.A., (1956)

The facility of aqueous outflow.

Arch. Ophth., 55, 305.

Berggren, L., and Vrabec, F., (1957)

Demonstration of a coating substance in the trabecular meshwork of the eye.

Amer. J. Ophth., 44, 200.

Bill, A., (1965)

The aqueous humour drainage mechanism in the cynomologus monkey (Macaca irus) with evidence for unconventional routes.

Invest. Ophth., 4, 911.

Bill, A., (1966a)

Conventional and uveoscleral drainage of aqueous humour in the cynomologus monkey (Macaca irus) at normal and high intraocular pressures.

Exp. Eye Res., 5, 45.

Bill, A., (1966b)

The routes for bulk drainage of aqueous humour in the vervet monkey (Cercopithecus ethiops).

Exp. Eye Res., 5, 55.

Bill, A., (1966c)

Formation and drainage of aqueous humour in cats.

Exp. Eye Res., 5, 185.

Bill, A., (1966d)

The routes for bulk drainage of aqueous humour in rabbits with and without cyclodialysis.

Doc. Ophth., 20, 157.

Bill, A., (1970)

Scanning electron microscopic studies of the canal of Schlemm.

Exp. Eye Res., 10, 214.

Bill, A., (1971)

Aqueous dynamics in monkeys (Macaca irus and Cercopithecus ethiops).

Exp. Eye Res., 11, 195.

Bill, A., (1973)

The role of ciliary blood flow and ultrafiltration in aqueous humour formation.

Exp. Eye Res., 16, 287.

Bill, A., (1975)

The drainage of aquecus humour.

Invest. Ophth., 14, 1.

Bill, A., and Barány, E.H., (1966)

Gross facility, facility of conventional routes and pseudo-facility of aqueous humour outflow in the cynomolgus monkey.

Arch. Ophth., 75, 665.

Bill, A., and Hellsing, K., (1965)

Production and drainage of aqueous humour in the cynomolgus monkey (Macaca irus).

Invest. Ophth., 4, 920.

Bill, A., and Phillips, C.I., (1971)

Uveoscleral drainage of aqueous humour in human eyes.

Exp. Eye Res., 12, 275.

Bill, A., and Svedbergh, B., (1972)

Scanning electron microscopic studies of the trabecular meshwork and the canal of Schlemm - an attempt to localize the main resistance to outflow of aqueous humour in man.

Acta Ophth., 50, 295.

Bill, A., and Walinder, P.E., (1966)

The effects of pilocarpine on the dynamics of aqueous humour in a primate (Macaca irus).

Invest. Ophth., 5, 170.

Bowers, B., (1965)

Coated vesicles in the perecardial cells of the aphid (Myzus persicae sulz).

Protoplasma, 59, 351.

Bowes, J.M., and Carter, C.W., (1968)

The interaction of aldehydes with collagen.

Biochem. Biophys. Acta, 168, 341.

Boyde, A., and Wood, C., (1969)

Preparation of animal tissues for surface-scanning electron microscopy.

J. Microscopy, 90, 221.

Brightman, M.W., and Reese, T.S., (1969)

Junctions between intimately apposed cell membranes in the vertebrate brain.

J. Cell Biol., 40, 648.

Bruns, R.R., and Palade, G.E., (1968)

Studies on blood capillaries.

I. General organisation of blood capillaries in muscle.

J. Cell Biol., 37, 244.

Burian, H.M., and Allen, L., (1955)

Mechanical changes during accommodation observed by gonioscopy.

Arch. Ophth., 54, 66.

Burian, H.M., Braley, A., and Allen, L., (1954)

External and gonioscopic visibility of the ring of Schwalbe and the trabecular zones: an interpretation of the posterior corneal embryotoxon and the so-called congenital hyaline membranes on the posterior corneal surface.

Trans. Amer. Ophth. Soc., 52, 389.

Carpenter, R.L., (1958)

In "Transaction of the 3rd Macy Conference on Glaucoma". (ed. F.W. Newell), p.67, Princeton, N.J.

Chalcroft, J.P., and Bullivant, S., (1970)

An interpretation of liver cell membrane and junction structure based on observation of freeze-fracture replicas of both sides of the fracture.

J. Cell Biol., 47, 49.

Cibis, P.A., and Yamashita, T., (1959)

Experimental aspects of ocular siderosis and haemosiderosis.

Amer. J. Ophth., 48, 465.

Clark, A.E., and Curran, R.C., (1964)

Staining reactions of collagen in "Epon" sections.

Nature, 202, 912.

Cohn, Z. A., (1968)

The structure and function of monocytes and macrophages.

Acta Immunol., 9, 163.

Cohn, Z.A., and Parks, E., (1967)

The regulation of pinocytosis in mouse macrophages. IV. The immunoligical induction of pinocytotic vesicles, secondary lysosomes, and hydrolytic enzymes.

J. Exp. Med., 125, 1091.

Cohn, Z.A., and Ehrenreich, B.A., (1969)

The uptake, storage and intracellular hydrolysis of carbohydrates by macrophages.

J. Exp. Med., 129, 201.

Cole, D.F., (1966)

Aqueous humour formation.

Doc. Ophth., 21, 116.

Cole, D.F., (1974)

Comparative aspects of the intraocular fluids.

In "The Eye"

(ed. H. Davson), Vol. 5, p.71.

Academic Press, N.Y., San Francisco, London.

Cole, D.F., and Tripathi, R.C., (1971)

Theoretical considerations on the mechanism of the aqueous outflow.

Exp. Eye Res., 12, 25.

Conley, F.C., and Herman, M.M., (1973)

Intracellular septate desmosome-like structures in a human acoustic schwannoma in vitro.

J. Neurocytol., 2, 457.

Curran, R.C., (1967)

Recent developments in the field of inflammation and repair.

In "Modern trends in Pathology"

(ed. T. Crawford), p.40. Butterworths, London.

Curran, R.C., Clark, A.E., and Lovell, D., (1965)

Acid mucopolysaccharides in electron microscopy; the use of the colloidal iron method.

J. Anat., 99, 427.

Davson, H., (1962)

The intra-ocular fluids.

In "The Eye"

(ed. H. Davson), Vol.1, p.67. Academic Press, N.Y. and Londo

Davson, H., (1972)

Dynamic aspects of cerebrospinal fluid.

Cerebr. Palsy Bull. 14, suppl. 27, 1.

de Venecia, G., and Davis, M.D., (1963)

Diurnal variation of intraocular pressure in the normal eye.

Arch. Ophth., 69, 752.

Drance, S.M., (1960)

The significance of the diurnal tension variations in normal and glaucomatous eyes.

Arch. Ophth., 64, 494.

Duke-Elder, S., (1952)

The phasic variation in the ocular tension in primary glaucoma.

Amer. J. Ophth., 35, 1.

Duke-Elder, S., (1968)

"System of Ophthalmology"

Vol.4. Kimpton, London.

Duke-Elder, S., (1969)

"System of Ophthalmology"

Vol. 11, p.412. Kimpton, London.

Dvorak-Theobald, G., (1934)

Schlemm's canal. Its anastomoses and anatomic relations.

Trans. Amer. Ophth. Soc., 32, 574.

Dvorak-Theobald, G., (1955)

Further studies on the canal of Schlemm; its anastomoses and anatomic relations.

Amer. J. Ophth., 39, 65.

Edwards, J., Hallman, V.L., and Perkins, E.S., (1967)

Perfusion studies in the monkey eye.

Exp. Eye Res., 6, 316.

Edwards, J., and Yerlett, A.L., (1972)

An anterior-chamber needle gun.

Exp. Eye Res., 13, 320.

Ellingsen, B.A., and Grant, W.M., (1971)

The relationship of pressure and aqueous outflow in enucleated human eyes.

Invest. Ophth., 10, 430.

Ericson, L.A., (1958)

Twenty-four hourly variations of the aqueous flow.

Acta Ophth. 50, (suppl.), 1.

Farquar, M.G., and Palade, G.E., (1963)

Junctional complexes in various epithelia.

J. Cell Biol., 17, 375.

Farquar, M.G., and Palade, G.E., (1965)

Cell junctions in amphibian skin.

J. Cell Biol., 26, 263.

Fawcett, D.W., (1965)

Surface specializations of absorbing cells.

J. Histochem. Cytochem., 13, 75.

Fawcett, D.W., (1969)

"The Cell"

W.B. Saunders Co., Philadelphia and London.

Feeney, L., (1962)

Ultrastructure of the nerves in the human trabecular region.

Invest. Ophth., 1, 462.

Feeney, M.L., and Wissig, S., (1966)

Outflow studies using an electron dense tracer.

Trans. Amer. Acad. Ophth. Otolar., 70, 791.

Fessler, J.H., (1957)

Water and mucopolysaccharide as structural components of connective tissue.

Nature, 179, 426.

Fine, B.S., (1964)

Observations on the drainage angle in man and rhesus monkey.

Invest. Ophth., 3, 609.

Fine, B.S., (1966)

Structure of the trabecular meshwork and the canal of Schlemm.

Trans. Amer. Acad. Ophth. Otolar., 70, 777.

Fink, A.I., Felix, M.D., Fletcher, R.C., (1972)

Schlemm's canal and adjacent structures in glaucomatous patients.

Amer. J. Ophth., 74, 893.

Flocks, M., (1956)

The anatomy of the trabecular meshwork as seen in tangential sections.

Arch. Ophth., 56, 708.

Flocks, M., and Zweng, H.C., (1957)

Studies in the mode of action of pilocarpine on aqueous outflow.

Amer. J. Ophth., 44, 380.

Fowlks, W.L., and Havener, V.R., (1964)

Aqueous flow into the perivascular space of the rabbit ciliary body.

Invest. Ophth., 3, 374.

François, J., (1975)

The importance of the mucopolysaccharides in intraocular pressure regulation.

Invest. Ophth., 14, 173.

François, J., Neetens, A., and Colette, J.M., (1955)

Microradiographic study of the inner wall of Schlemm's canal.

Amer. J. Ophth., 40, 491.

François, J., Neetens, A., Leroux, G., and Colette, J.M., (1967)

Concerning the posterior routes for the drainage of aqueous humour.

Ophthalmologia, 153, 215.

François, J., and Troncoso, V., (1974)

Mukopolysaccharide und pathogenese kortisonbedingter augendrucksteigerung.

Klin. Mbl. Augenheilk., 165, 5.

Friedenwald, J.S., (1936)

Circulation of the aqueous.

Arch. Ophth., 16, 65.

Friend, D.S., and Gilula, N.B., (1972)

Variations in tight and gap junctions in mammalian tissues.

J. Cell Biol., 53, 758.

Garron, L.K., (1959)

The fine structure of the normal trabecular apparatus in man.

In "Proceedings of the 4th Macy Conference on Glaucoma". (ed. F.W. Newell), p.11 Princeton, N.J.

Garron, L.K., and Feeney, M.L., (1959)

Electron microscopic studies of the human eye.

II. Study of the trabeculae by light and electron microscopy.

Arch. Ophth., 62, 966.

Garron, L., Feeney, M.L., Hogan, M.J., and McEwen, W.K., (1958)

Electron microscopic studies of the human eye.

I. Preliminary investigations of the trabeculae.

Amer. J. Ophth., 60, 523.

Garron, L., Hogan, M.J., McEwen, W.K., Feeney, M.L., and Esperson, J., (1959)

Electron microscopy of ocular tissue.

Arch. Ophth., 61, 647.

Gasic, G., and Berwick, L., (1963)

Hale's stain for sialic acid-containing mucins.

Adaptation to electron microscopy.

J. Cell Biol., 19, 223.

Gilula, N.B., Reeves, O.R., and Steinbach, A., (1972)

Metabolic coupling, ionic coupling and cell contacts.

Nature, 235, 242.

Goldman, H., (1959)

Some basic problems of simple glaucoma.

Amer. J. Ophth. 48, 213.

Goodenough, D.A., and Revel, J.P., (1970)

The fine structural analysis of intercellular junctions in the mouse liver.

J. Cell Biol., 45, 272.

Grant, W.M., (1950)

Tonographic method for measuring facility and rate of aqueous flow in human eyes.

Arch. Ophth., 44, 204.

Grant, W.M., (1958)

Further studies on facility of flow through the trabecular meshwork.

Arch. Ophth., 60, 523.

Grant, W.M., (1963)

Experimental aqueous perfusion in enucleated human eyes.

Arch. Ophth., 69, 783.

Grant, W.M., and Trotter, R.R., (1955)

Tonographic measurements in enucleated eyes.

Arch. Ophth., 53, 191.

Green, K., and Pederson, J.E., (1973)

Aqueous humour formation.

Exp. Eye Res., 16, 273.

Grierson, I., and Lee, W.R., (1973)

Erythrophagocytosis in the human meshwork.

Brit. J. Ophth., 57, 400.

Groniowski, J., Biczyskowa, W., and Walski, M., (1969)

Electron microscope studies on the surface coat of the nephron.

J. Cell Biol., 40, 585.

Harris, L.S., (1968)

Cycloplegic-induced intraocular pressure elevations.

Arch. Ophth., 79, 242.

Hayreh, S.S., (1966)

Posterior drainage of the intraocular fluid from the vitreous.

Exp. Eye Res., 5, 123.

Henderson, T., (1908)

The anatomy of the so-called ligamentum pectinatum iridis and its bearing on the physiology and pathology of the eye.

Trans. Ophth. Soc. U.K., 28, 47.

Henkind, P., Leitman, M., and Weitzman, E., (1973)

Diurnal curve in man. New observation.

Invest. Ophth., 12, 705.

Hueck, A., (1839) quoted by Tripathi, R.C., (1974)

Comparative physiology and anatomy of the aqueous outflow pathway.

In "The Eye"

(ed. H. Davson), Vol.5., p.248. Academic Press, N.Y., San Francisco, London.

Hoffmann, F., and Dumitrescu, L., (1971)

Schlemm's canal under the scanning electron microscope.

Ophth. Res., 2, 37.

Hogan, M.J., Alvarado, J.A., and Weddell, J.E., (1971)

"Histology of the Human Eye"

W.B. Saunders Co., Philadelphia and London.

Holmberg, A.S., (1959)

The fine structure of the inner wall of Schlemm's canal.

Arch. Ophth., 62, 956.

Holmberg, A.S., (1965)

Schlemm's canal and the trabecular meshwork. An electron microscopic study of the normal structure in man and monkey (Cercopithecus ethiops).

Doc. Ophth., 19, 339.

Holmberg, A.S., (1966)

Our present knowledge of the structure of the trabecular meshwork.

In "Glaucoma Tutzing Symposium".

(ed. W. Leydhecker), p.1 S. Karger, Basel and N.Y.

Hørven, I., (1964)

A radioautographic study of erythrocyte resorption from the anterior chamber of the human eye.

Acta Ophth., 42, 600.

Hudspeth, A.J., and Yee, A.G., (1973)

The intercellular junctional complexes of retinal pigment epithelia.

Invest. Ophth., 12, 354.

Huggert, A., (1955)

Pore size in the filtration angle of the eye.

Acta Ophth., 33, 271.

Huggert, A., (1957a)

An experiment in determining the pore size distribution curve to the filtration angle of the eye. Part I.

Acta Ophth., 35, 12.

Huggert, A., (1957b)

An experiment in determining the pore size distribution curve to the filtration angle of the eye. Part II.

Acta Ophth., 35, 104.

Inomata, H., Bill, A., Smelser, G.K., (1972a)

Aqueous humour pathways through the trabecular meshwork and into Schlemm's canal in the cynomolgus monkey (Macaca irus). An electron microscopic study.

Amer. J. Ophth., 73, 760.

Inomata, H., Bill,A., and Smelser, G.K., (1972b)

Unconventional routes of aqueous humour outflow in cynomolgus monkey (Macaca irus).

Amer. J. Ophth., 73, 893.

Ito, S., (1965)

The enteric surface coat on cat intestinal microvilli.

J. Cell. Biol., 16, 541.

Iwamoto, T., (1964)

Light and electron microscopy of the presumed elastic components of the trabeculae and scleral spur of the human eye.

Invest. Ophth., 3, 144.

Iwamoto, T., (1967a)

Light and electron microscopy of Sondermann's channels of the human trabecular meshwork.

v. Graefe's Arch. klin. exp. Ophth., 172, 197.

Iwamoto, T., (1967b)

Further observation on Sondermann's channels of the human trabecular meshwork.

v. Graefe's Arch. klin. exp. Ophth., 172, 213.

Jocson, V.L., and Grant, W.M., (1965)

Interconnections of blood vessels and aqueous vessels in human eyes.

Arch. Ophth., 73, 707.

Johnson, R.G., and Sheridan, J., (1971)

Junctions between cancer cells in culture; ultrastructure and permeability.

Science, 174, 717.

Johnstone, M.A., and Grant, W.M., (1973)

Pressure-dependent changes in structures of the aqueous outflow system of human and monkey eyes.

Amer. J. Ophth., 75, 365.

Johnstone, M.A., (1974)

Pressure-dependent changes in configurations of the endothelial tubules of Schlemm's canal.

Amer. J. Ophth., 78, 630.

Karg, S.J., Garron, L.K., Feeney, M.L., and McEwen, W.K., (1959)

Perfusion of human eyes with latex microspheres.

Arch. Ophth., 61, 68.

Karnovsky, M.J., (1967)

The ultrastructural basis of capillary permeability studied with peroxidase as a tracer.

J. Cell Biol., 35, 213.

Katavisto, M., (1964)

The diurnal variations of ocular tension in glaucoma.

Acta Ophth., 78 (Suppl.), 1.

Kayes, J., (1967)

Pore structure of inner wall of Schlemm's canal.

Invest. Ophth., 6, 381

Kayes, J., (1975a)

Pressure gradient changes on the trabecular meshwork of monkeys.

Amer. J. Ophth., 79, 549.

Kayes, J., (1975b)

Pressure gradient changes.

Amer. J. Ophth., 80, 307.

Kimura, R., (1966)

Clinical studies on glaucoma: The diagnostic significance of the diurnal variation of intraocular pressure.

Acta Soc. Ophth. Jap., 70, 1326.

Kitazawa, Y., and Horie, T., (1975)

Diurnal variation of intraocular pressure in primary open-angle glaucoma.

Amer. J. Ophth., 79, 557.

Kornblueth, W., and Linnér, E., (1955)

Experimental tonography in rabbits.

Arch. Ophth., 54, 717.

Kronfeld, P.C., (1949)

Further gonioscopic studies on the canal of Schlemm.

Arch. Ophth., 41, 393.

Kupfer, C., (1973)

Clinical significance of pseudofacility.

Amer. J. Ophth., 75, 193.

Langley, D., and Swanljung, H., (1951)

Ocular tension in glaucoma simplex.

Brit. J. Ophth., 35, 445.

Lee, W.R., (1971)

The study of the passage of particles through the endothelium of the outflow apparatus of the monkey eye by scanning and transmission electron microscopy.

Trans. Ophth. Soc. U.K., 91, 687.

Leuenberger, P.M., (1973)

Lanthanium hydroxide tracer studies on rat endothelium.

Exp. Eye Res., 15, 85.

Linnér, E., (1955)

The outflow pressure in normal and glaucomatous eyes.

Acta Ophth., 33, 101.

Lowenstein, A., (1951)

The anterior draining system in the human eye.

Ophthalmologica, 122, 257.

Lowenstein, W.R., (1973)

Membrane junctions in growth and differentiation.

Fed. Proc., 32, 60.

Luft, J.H., (1964)

Electron microscopy of cell extraneous coats as revealed by ruthenium red staining.

J. Cell Biol., 23, 54a.

Luft, J.H., (1971)

Ruthenium red and violet.

I. Chemistry, purification, methods of use for electron microscopy and mechanism of action.

Anat. Rec., 171, 347.

Lütjen-Drecoll, E., (1973)

Structural factors influencing outflow facility and its changeability under drugs. A study in Macaca arctoides.

Invest. Ophth., 12, 280.

MacRae, D., and Sears, M.L., (1970)

Peroxidase passage through the outflow channels of human and rhesus eyes.

Exp. Eye Res., 10, 15.

McEwen, W.K., (1958)

Application of Poiseuille's law to aqueous outflow.

Arch. Ophth., 60, 290.

Maggiore, L., (1917)

Struttura, comportamento e significato del canale di Schlemm nell' occhio umano, in condizioni normali e patologische.

Ann. Ottal. Clin. Oculist, 40, 317.

Majno, G., Shea, S.M., and Leventhal, M., (1969)

Endothelial contraction induced by histamine-type mediators, an electron microscopic study.

J. Cell Biol., 42, 647.

Masuda, K., (1974)

Pressure dependence of the aqueous humour formation in rabbit and cynomolgus monkey eyes.

Jap. J. Ophth., 16, 60.

Matsusaka, T., (1970)

Ultrastructural differences between the choriocapillaries and retinal capillaries on the human eye.

Jap. J. Ophth., 14, 59.

Mishima, A.S., and Maurice, D.M., (1961)

The effect of normal evaporation on the eye.

Exp. Eye Res., 1, 39.

Newell, F.W., and Krill, A.E.,

Diurnal tonography in normal and glaucomatous eyes.

Amer. J. Ophth., 59, 840.

Nomura, T., and Smelser, G.K., (1974)

The identification of adrenergic and cholinergic nerve endings in the trabecular meshwork.

Invest. Ophth., 13, 525.

Ogston, A.G., (1970)

The biological functions of the glycosaminoglycans.

In "Chemistry and Molecular Biology of the Intercellular Matrix".

(ed. E.A. Balazs), Vol 3, p.1231. Academic Press, London.

Palade, G.E., (1961)

Blood capillaries of the heart and other organs.

Circulation, 24, 368.

Pappas, G.D., Asada, V., and Bennett, M.V.L., (1971)

Morphological correlates of increased coupling resistance at an electrotonic synapse.

J. Cell Biol., 49, 173.

Payton, B.W., Bennett, M.V.L., and Pappas, G.D., (1969)

Permeability and structure of junctional membranes at electrotonic synapse.

Science, 166, 1641.

Pearse, A.G.E., (1972)

"Histochemistry Theoretical and Applied."

Vol.2, p.1029. Churchill Livingstone, Edinburgh and London.

Pedler, C., (1956)

The relationship of hyaluronidase to aqueous outflow resistance.

Trans. Ophth. Soc. U.K., 76, 51.

Peter, P.A., Lyda, W., and Krishna, N., (1957)

Anterior chamber perfusion studies.

II. Controlled particle size in relationship to pore size.

Amer. J. Ophth., 44, 198.

Peterson, W.S., and Jocson, V.L., (1974)

Hyaluronidase effects on aqueous outflow resistance.

Quantitative and localizing studies on the rhesus monkey eye.

Amer. J. Ophth., 77, 573.

Peterson, W.S., Jocson, V.L., and Sears, K.L., (1971)

Resistance to aqueous outflow in the rhesus monkey eye.

Amer. J. Ophth., 72, 445.

Podos, S.M., Minas, T.F., Macri, F.J., (1968)

A new instrument to measure episcleral venous pressure.

Comparison of normal eyes and eyes with primary open-angle glaucoma.

Arch. Ophth., 80, 209.

Rambourg, A., and Leblond, C.P., (1967)

Electron microscopic observations on the carbohydrate-rich cell coat present at the surface of cells in the rat.

J. Cell Biol., 32, 27.

Raviola, G., (1971)

The fine structure of the ciliary zonule and ciliary epithelium.

Invest. Ophth., 10, 851.

Raviola, G., (1974)

Effects of paracentesis on the blood-aqueous barrier: an electron microscope study on Macaca mullata using horseradish peroxidase as a tracer.

Invest. Ophth., 13, 828.

Raviola, E., and Gilula, N.B., (1973)

Gap junctions between photoreceptor cells in the vertebrate retina.

Proc. Nat. Acad. Sci., 70, 1677.

Reese, I.S., and Karnovsky, M.J., (1967)

Fine structural localization of a blood-brain barrier to exogenous peroxidase.

J. Cell Biol., 34, 207.

Revel, J., (1964)

A stain for the ultrastructural localisation of acid mucopolysaccharides.

J. Mircoscopie, 3, 535.

Revel, J., (1970)

Role of the Golgi apparatus of cartilage cells in the claboration or matrix glycosamine glycans.

In "Chemistry and Molecular Biology of the Intercellular Matrix."
(ed. E.A. Balazs), Vol.3, p.1485. Academic Press, London.

Revel, J., and Goodenough, D.A., (1970)

Cell coats and intercellular matrix.

In "Chemistry and Molecular Biology of the Intercellular Matrix."
(ed. E.A. Balazs), Vol.3, p.1361. Academic Press, London.

Revel, J.P., and Karnovsky, M.J., (1967)

Hexagonal array of subunits in intercellular junctions of the mouse heart and liver.

J. Cell Biol., 33, C7.

Revel, J.P., Yee, A.G., and Hudspeth, A., (1971)

Gap junctions between electronically coupled cells in tissue culture and in brown fat.

Proc. Nat. Acad. Sci., 68, 2924.

Ringvold, A., (1975)

An electron microscopic study of the iris stroma in monkey and rabbit with particular reference to intercellular contacts and sympathetic innervation of anterior layer cells.

Exp. Eye Res., 20, 349.

Rochon-Duvigneaud, A., (1892)

Recherches anatomiques sur l'angle de in chambre anterieure et le canal de Schlemm. I. Anatomie descriptive de l'angle de la chambre antérieure. II. Hemologie qui existe entre l'angle de la chambre anterieure de l'homme et l'espace cilio-schleral de quadrupedes.

Arch. Ophth., 12, 732.

Rochon-Duvigneaud, A., (1893)

Recherches anatomiques sur l'angle de la chambre antérieure et le canal de Schlemm. III. Anatomie microscopique et histologie du système trabeculare slero-corneen et du canal de Schlemm. IV. Devoies d'injection du canal de Schlemm.

Arch. Ophth., 13, 20.

Rohen, J.W., (1960)

On the aqueous outflow resistance.

Cphthalmologica, 139, 1.

Rohen, J.W., (1961)

Morphology and pathology of the trabecular meshwork.

In "The structure of the Eye"

(ed. G.K. Smelser), p.335. Academic Press, N.Y. and London.

Rohen, J.W., (1963)

Experimental studies on the trabecular meshwork in primates.

Arch. Ophth., 69, 335.

Rohen, J.W., (1969)

New studies on the functional morphology of the trabecular meshwork and the outflow channels.

Trans. Ophth. Soc. U.K., 89, 431.

Rohen, J.W., and Lütjen-Drecoll, E., (1971)

Age changes of the trabecular meshwork in human and monkey eye.

In "Altern and Entwicklung"

(ed. H. Brent and J.W. Rohen), Band 1, p.1.

F.K. Schattauer Verlag, Stuttgart and N.Y.

Rohen, J.W., Lütjen, E., and Barany, E., (1967)

The relation between the ciliary muscle and the trabecular meshwork and its importance for the effect of miotics in aqueous outflow resistance. A study of two contrasting monkey species, Macaca irus and Cercopithecus aethiops.

v. Graefe's Arch. klin exp. Ophth., 172, 23.

Rohen, J., and Unger, H.H., (1959)

Zur morphologie und pathologie der kammerbucht des auges.

Akad. Wiss. Lit. Mainz., Steiner-Verlag, Wiesbaden.

Rohen, J.W., and Witmer, R., (1972)

Electron microscope studies on the trabecular meshwork in glaucoma simplex.

v. Graefe's Arch. klin. exp. Ophth., 183, 251.

Rohen, J., and Zyphen, E., (1968)

The phagocytic activity of the trabecular meshwork endothelium.

v. Graefe's Arch. klin. exp. Ophth., 175, 143.

Rose, B., (1971)

Intercellular communication and some structural aspects of membrane junctions in a simple cell system.

J. Mem. Biol., 5, 1.

Roth, T.F., and Porter, K.R., (1964)

Yolk protein uptake in the oocyte of the mosquito Aedes aegypti.

J. Cell. Biol., 20, 313.

Ruskell, G.L., (1961)

Aqueous drainage paths in the rabbit. A neoprene latex cast study.

Arch. Ophth., 66, 861.

Salzmann, M., (1912)

"The Anatomy and Histology of the Human Eyeball."

(Trans. E.V.L. Brown), University Press, Chicago.

Schlemm, F.S., (1830) quoted by Holmberg, A.S., (1965)

Schlemm's canal and the trabecular meshwork. An electron microscopic of the normal structure in man and monkey (Cercopithecus ethiops).

Doc. Ophth., 19, 339.

Segawa, K., (1968)

Porosity of Schlemm's canal and Sondermann's canals.

Med. J. Shinshu Univ., 13, 57.

Segawa, K., (1970a)

Ultrastructure of Schlemm's canal studied by a replica technique.

Jap. J. Ophth., 14, 1.

Segawa, K., (1970b)

Localization of acid mucopolysaccharides in the human trabecular meshwork.

J. Clin. Ophth., (Jap), 24, 363.

Segawa, K., (1971a)

Pores of the trabecular wall of Schlemm's canal: ferritin perfusion in enucleated human eyes.

Jap. J. Ophth., 15, 1.

Segawa, K., (1971b)

Concerning the giant vacuoles of the trabecular wall of Schlemm's canal.

Jap. J. Ophth., 15, 204.

Segawa, K., (1973)

Pore structures of the endothelial cells of the aqueous outflow pathway: Scanning electron microscopy.

Jap. J. Ophth., 17, 133.

Seidel, E., (1921)

Uber den abfluss des kammerwassers aus der vorderen augenkammer.

v. Graefe's Arch. klin. exp. Ophth., 104, 357.

Shabo, A.L., and Maxwell, D.S., (1972a)

Observations on the fate of blood in the anterior chamber. A light and electron microscopic study of the monkey trabecular meshwork.

Amer. J. Ophth., 73, 25.

Shabo, A.L., and Maxwell, D.S., (1972b)

The structure of the trabecular meshwork of the primate eye. A light and electron microscopic study with peroxidase.

Microvasc. Res., 4, 384.

Shabo, A.L., Reese, T.S., and Garsterland, D., (1973)

Postmortem formation of giant endothelial vacuoles in Schlemm's canal of the monkey.

Amer. J. Ophth., 76, 896.

Sheridan, J.D., (1971)

Electrical coupling between fat cells in newt fat body and mouse brown fat.

J. Cell Biol., 50, 795.

Shirahama, T., and Cohen, A.S., (1972)

The role of mucopolysaccharides in vesicle architecture and endothelial transport.

J. Cell Biol., 52, 198.

Simionescu, N., Simionescu, M., and Palade, G.E., (1973)

Permeability of muscle capillaries to exogenous myoglobin.

J. Cell Biol., 57, 424.

Smelser, G.K., (1967)

Pore structure of the inner wall of Schlemm's canal.

Invest. Ophth., 6, 393.

Smelser, G.K., and Ozanics, V.M.S., (1971)

The development of the trabecular meshwork in primate eyes.

Amer. J. Ophth., 7, 366.

Smith, R.E., and Farquar, M.G., (1966)

Lyososome function in the regulation of the secretory process in cells of the anterior pituitary gland.

J. Cell Biol., 31, 319.

Sondermann, R., (1930)

Beitrag zur entwicklung und morphologie des Schlemm'schen kanals.

v. Graefe's Arch. klin. exp. Ophth., 124, 521.

Sondermann, R., (1931)

Beitrag zur entwicklungsgeschichte des gefasssytems in menschlichen auge.

v. Graefe's Arch. klin. exp. Ophth., 126, 341.

Sondermann, R., (1932)

Uber druck und zirkulation in menshlichen auge.

v. Graefe's Arch. klin. exp. Ophth., 106, 319.

Sondermann, R., (1933)

Uber entstehung morphologie und funcktion des Schlemm'schen kanals.

Arch. Ophth., 11, 280.

Speakman, J., (1959a)

The development and structure of the normal trabecular meshwork.

Proc. Roy. Soc. Med., 52, 72.

Speakman, J., (1959b)

Aqueous outflow channels in the trabecular meshwork in man.

Brit. J. Ophth., 43, 129.

Speakman, J.S., (1960)

Drainage channels in the trabecular wall of Schlemm's canal.

Brit. J. Ophth., 44, 513.

Speakman, J.S., (1961)

The structure of the trabecular meshwork in relation to the pathogenesis of open angle glaucoma.

Canad. Med. Ass. J., 84, 1066.

Spelsberg, W.W., and Chapman, G.B., (1962)

Fine structure of human trabeculae.

Arch. Ophth., 67, 773.

Spencer, W.H., Alvarado, J., and Hayes, T.L., (1968)

Scanning electron microscopy of human ocular tissues: trabecular meshwork.

Invest. Ophth., 7, 651.

Spitznas, M., and Reale, E., (1975)

Fracture faces of fenestrations and junctions of endothelial cells in human choroidal vessels.

Invest. Ophth., 14, 98.

Sugar, H.S., (1940)

Concerning the chamber angle. I. Gonioscopy.

Amer. J. Ophth., 23, 857.

Sugar, H.S., (1951)

"The Glaucomas."

Cassell and Co., London.

Svedbergh, B., (1974)

Effects of artificial intraocular pressure elevation on the outflow facility and the ultrastructure of the chamber angle in the vervet monkey (Cercopithecus ethiops).

Acta Ophth., 52, 829

Taniguchi, Y., (1962)

Fine structure of blood vessels in the ciliary body.

Jap. J. Ophth., 6, 93.

Tripathi, R.C., (1968)

Ultrastructure of Schlemm's canal in relation to aqueous outflow.

Exp. Eye Res., 7, 335.

Tripathi, R.C., (1969a)

Ultrastructure of the exit pathway of the aqueous.

Ph.D. Thesis., Univ. of London.

Tripathi, R.C., (1969b)

Ultrastructure of the trabecular wall of Schlemm's canal.

Trans. Ophth. Soc. U.K., 89, 449.

Tripathi, R.C., (1971a)

Mechanism of the aqueous outflow across the trabecular wall of Schlemm's canal.

Exp. Eye Res., 11, 116.

Tripathi, R.C., (1971b)

Ultrastructure of the exit pathway of the aqueous in lower mammals (A preliminary report on the "angular Aqueous Plexus").

Exp. Eye Res., 12, 311.

Tripathi, R.C., (1972)

Aqueous outflow pathway in normal and glaucomatous eyes.

Brit. J. Ophth., 56, 157.

Tripathi, R.C., (1973a)

Ultrastructure of the arachnoid mater in relation to outflow of cerebrospinal fluid. A new concept.

Lancet, 2, 8.

Tripathi, R.C., (1973b)

Pressure-dependency of aqueous outflow.

Amer. J. Ophth., 76, 402.

Tripathi, R.C., (1974)

Comparative physiology and anatomy of the aqueous outflow pathway.

In "The Eye"

(ed. H. Davson), Vol.5, p.163. Academic Press, N.Y., San Francisco, London.

Tripathi, R.C., and Tripathi, B.J., (1972)

The mechanism of aqueous outflow in lower mammals.

Exp. Eye Res., 14, 73.

Tripathi, B.J., and Tripathi, R.C., (1974)

Vacuolar transcellular channels as a drainage pathway for cerebrospinal fluid.

J. Physicl., 239, 195.

Troncoso, M.U., (1925)

Gonioscopy and its clinical application.

Amer. J. Ophth., 8, 433.

Troncoso, M.U., (1942)

The intrascleral vascular plexus and its relations to the aqueous outflow.

Amer. J. Ophth., 25, 1153.

Unger, H.H., (1959)

Anatomy of the angle of the anterior chamber.

Klin. Mbl. Augen, 135, 161.

Unger, H.H., and Rohen, J., (1959)

Studies on the histology of the inner wall of Schlemm's canal.

Amer. J. Ophth., 48, 204.

Van der Zyphen, E., (1971)

Light and electron microscopic studies on the morphology of tissues involved in circulation of aqueous humour and cerebrospinal fluid.

In "Altern und Entiwicklung"

(ed. H. Brant and J.W. Rohen), Band 2, p.1.

F.K. Schattauer Verlag, Stuttgart and N.Y.

Vegge, T., (1963)

Ultrastructure of normal human trabecular endothelium.

Acta Ophth., 41, 193.

Vegge, T., (1967)

The fine structure of the trabeculum cribriforme and the inner wall of Schlemm's canal in the normal human eye.

Z. Zellforsch., 77, 267.

Vegge, T., and Ringvold, A., (1971)

The ultrastructure of the extracellular components of the trabecular meshwork in the human eye.

Z. Zellforsch., 115, 361.

Virchow, H., (1910)

Microskopische anatomie der ausseren augenhaut und des lldapparates.

In "Graefe-Saemisch, Handbuch der Gesamten Augenheilkunde"

Vol. 1, p.280. W. Engelmann, Leipzig.

Vrabec, F., (1974)

Age changes of the inner surface of the trabecular meshwork shown by the replica technique.

Invest. Ophth., 13, 950.

Wakeley, J., (1974)

Senile changes in the fine structure of the lens in the rudd (Scardinius erycphthalmicus).

Exp. Eye Res., 18, 571.

Wetzel, M.G., Wetzel, B.K., and Spicer, S.S., (1966)

Ultrastructural location of acid mucosubstances in the mouse colon with iron-containing stains.

J. Cell Biol., 30, 299.

Wickham, M.G., and Worten, D.M., (1974)

Postmortem formation of giant endothelial vacuoles in Schlemm's canal.

Amer. J. Ophth., 77, 926.

Wolf, J., (1965)

Regulatory mechanism for the drainage of chamber fluid demonstrated by injections in the macaque.

Fol. Morph., 13, 328.

Wolff, E., (1954)

"The Anatomy of the Eye and Orbit"

4th Edn. H.K. Lewis, London.

Wulle, K.G., (1968)

Electron microscopic observations of the development of Schlemm's canal in the human eye.

Trans. Amer. Acad. Ophth. Otol., 72, 765.

Wulle, K.C., (1972)

The development of the productive and draining system of the aqueous humour in the human eye.

Advances in Ophth., 26, 296.

Yamashita, T., and Rosen, D.A., (1964)

The elastic tissue of primate trabecular meshwork. A histologic and electron microscopic study.

Invest. Ophth., 3, 85.

Yamashita, T., and Rosen, D.A., (1965)

Electron microscopic study of trabecular meshwork in clinical and experimental glaucoma with anterior chamber haemorrhage.

Amer. J. Ophth., 60, 427.

Yanoff, M., and Fine, B.S., (1975)

"Ocular Pathology: A Text and Atlas."

Harper and Row, New York.

Yardley, J.H., and Brown, G.D., (1965)

Fibroblasts in tissue culture: use of colloidal iron for ultrastructural localization of acid mucopolysaccharides.

Lab. Invest., 14, 501.